Dissertation

Submitted to the

Combined Faculty of Natural Sciences and Mathematics

Heidelberg University, Germany

for the degree of

Doctor of Natural Sciences (Dr. rer. nat.)

Presented by

M. Sc. Gaozhan Xie

Oral examination: July 23th, 2020

Synthesis and Characterization of Azaacenes and Stable Azaacene Radical Cations

Gutachter: Prof. Dr. Uwe H. F. Bunz

Prof. Dr. Milan Kivala

Acknowledgement

Studying in Heidelberg University is a dreamlike experience for me. In 2008, I read a book, *Ten Years in Germany*, written by Xianlin Ji, an outstanding Chinese linguist and writer, who had studied and worked in Gottingen University for ten years. I was totally fascinated by what he had seen and heard while living in Germany. Whereas, I never thought I would stay in Germany someday at that moment. Now I am so lucky to have been studying here, persuing my doctor degree.

At first, I would like to show my deepest gratitude to my respectful supervisor, Prof. Dr. Uwe H. F. Bunz, for giving me an opportunity to do research in the group. During these years, Prof. Bunz has offered me with the valuable guidance in every stage of the working and writing of this thesis. Without his patient instruction, insightful criticism, and expert guidance, the completion of this thesis would not have been possible. It's my great honor to be his student. I also want to express my sincere appreciation to Dr. Jan Freudenberg for his permanent guidance and kind help during the time of my research. His professional and valuable advice contributes a lot to my works. Besides, I would like to thank Prof. Dr. Milan Kivala for his kindness as my second reviewer for this dissertation.

I would like to express a special gratitude to Dr. Sebastian Hahn, who kindly took care of me for my first year in Heidelberg University. His patient guidance and fruitful discussion made me adapt to laboratory environment quickly and finish azarubrene project successfully.

I would like to take this opportunity to thank Prof. Dr. Milan Kivala, Miriam Hauschild, and Hendrik Hoffmann for their kind supports and cooperations on the project of 5,7,12,14-tetrafunctionalized 6,13-diazapentacenes. Besides, I also thank Prof. Dr. Andreas Dreuw and his Ph.D. student Jie Han, for the quantum chemical calculations on the project of 7,14-dimesityl-5,12-dihydro-5,12-diaryldiazapentacene radical cations.

I would like to thank Mrs. Kerstin Brödner, Olena Tverskoy, Kerstin Windisch, and Mr. Holger Lambert for their selfless dedication and effective organization to provide us an easeful working circumstance. I would also like to thank all staffs in Organisch-Chemisches Institut for their kind help in chemicals and measurements, including Chemikalienausgabe, X-ray crystal structure analysis, MS analysis, NMR measurement, and elemental analysis.

I am also very grateful to my intelligent colleagues, Dr. Kai Seehafer, Dr. Allan Bastos, Dr. Jinsong Han, Dr. Yury Kozhemyakin, Dr. Benhua Wang, Dr. Emanuel Smarsly, Dr. Wei Huang, Dr. Matthias Müller, Dr. Hilmar Reiß, Dr. Sebastian Intorp, Dr. Soh Kushida, Victor Brosius, Michael Ganschow, Lukas Ahrens, Steffen Maier, Thomas Wiesner, Zheyu Li, Hao Zhang, Wansheng Zong, Maximilian Bojanowski, Saskia Braun et al. for their kind advice and valuable discussion during my research. I'm so lucky to have these very great persons as my colleagues.

I deeply appreciate my good friends, Yufeng Wu, Shaoxiong Zhang, and Eugen Kotlear, who are always there to support and encourage me. With their company, I have never felt lonely.

Finally, I would like to thank my beloved family. My parents are so unselfish, lovely, and open-minded. Their constant support, care, and love make me brave when I face difficulties in my study and life.

I am very grateful to the CSC (Chinese Scholarship Council) for their financial support of my Ph.D. research.

Abstract

This thesis focuses on the synthesis and characterization of azaacenes and stable azaacene radical cations (see Figure 1):

In Chapter 2, the synthesis, properties, and solid state X-ray single crystal structures of two new rubrene derivatives, *viz* diazarubrene **DAR** and tetraazarubrene **TAR**, are reported. Both the azarubrenes are more oxidatively stable than rubrene itself and show similar optical properties but differ in their crystal packing from that of rubrene.

In Chapter 3, the synthesis, property evaluation, and single crystal X-ray structures of 5,7,12,14-tetrafunctionalized diazapentacenes (**TDAP**s) are presented. Starting from tetrabromo-*N,N'*-dihydrodiazapentacene, Pd-catalyzed coupling gave the precursors that furnished, after further redox reactions, the diazapentacenes as stable crystalline materials. The performance of the tetraphenylated compound as n-channel semiconductor was evaluated in organic field-effect transistors.

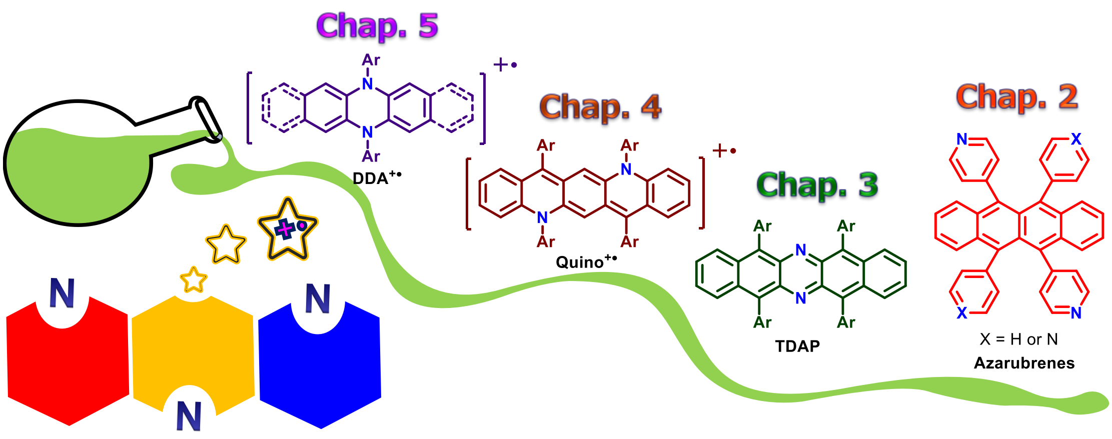

Figure 1. Target chemical structures in the thesis.

In Chapter 4, a series of quinoidal *N,N'*-diaryl-*N,N'*-dihydrodiazapentacenes (**Quino**s) were prepared in a two-step reaction, starting from quinacridone. Oxidation of **Quino**s furnished stable radical cations, isoelectronic to the radical anions of the azaacenes, whereas the dicationic species are isoelectronic to neutral azapentacenes. The spectroscopic properties of the diaryldiazapentacenes and their oxidized mono- and dications are equivalent to that of the dianion of tetraazapentacene **TAP**, its radical anion, and the neutral **TAP**.

In Chapter 5, three stable *N,N'*-diarylated dihydroazaacene radical cations (**DDA**s$^{+\bullet}$) were prepared by oxidation of neutral *N,N'*-diarylated dihydroazaacenes (**DDA**s), synthesized through Buchwald-Hartwig aminations of aryl iodides with *N,N'*-dihydroazaacenes employing a palladium catalyst. The spectroscopic properties, single crystal X-ray structures, and DFT calculations of these neutral compounds and their radical ions were systematically investigated. All the radical cations are stable and their absorption spectra in dichloromethane remained unchanged in ambient conditions for at least 24 hours.

Zusammenfassung

Diese Arbeit beschäftigt sich mit der Synthese und Charakterisierung von Azaacenen und stabilen Azaacen-Radikalkationen (siehe Abbildung 1):

In Kapitel 2 werden die Synthese, Eigenschaften, und Kristallstrukturen von zwei neuen Rubrenderivaten, nämlich Diazarubren (**DAR**) und Tetraazarubren (**TAR**), diskutiert. Beide Azarubrene sind oxidativ stabiler als Rubren, zeigen ähnliche optische Eigenschaften, unterscheiden sich jedoch in der Kristallpackung von der Rubrens.

In Kapitel 3 werden die Synthese, und Eigenschaften, sowie die Kristallstrukturen von 5,7,12,14-tetrafunktionalisierten Diazapentacenen (**TDAP**) diskutiert. Ausgehend von Tetrabrom-*N*,*N'*-dihydrodiazapentacen ergab die Pd-katalysierte Kupplung die Vorläufer, die nach weiteren Redoxreaktionen die Diazapentacene als stabile kristalline Materialien lieferten. Ferner wurde die Eignung der Tetraphenyl-substituierten Verbindung als n-Kanal-Halbleiter in organischen Feldeffekttransistoren evaluiert.

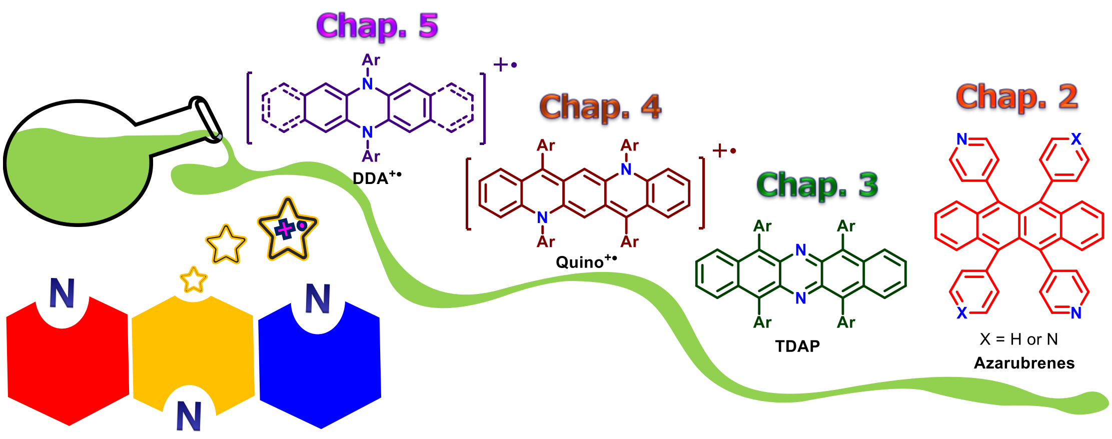

Figure 1. Chemische Zielstrukturen in der Arbeit.

In Kapitel 4 wurde eine Reihe chinoider *N*,*N'*-Diaryl-*N*,*N'*-dihydrodiazapentacene (**Quinos**) in einer zweistufigen Reaktion ausgehend von Chinacridon hergestellt. Die Oxidation des **Quinos** liefert stabile Radikalkationen, die isoelektronisch zu den Radikalanionen der Azaacene sind, während die dikationischen Spezies isoelektronisch zu neutralen Azapentacenen sind. Die spektroskopischen Eigenschaften der Diaryldiazapentacene und ihrer oxidierten Mono- und

Dikationen entsprechen denen des Dianions von Tetraazapentacen **TAP**, seines Radikalanions und des neutralen **TAP**.

In Kapitel 5 wurden drei stabile *N*,*N′*-diarylierte Dihydroazaacen-Radikalkationen (**DDA**s^{+}), durch Oxidation von neutraler *N*,*N′*-diarylierter Dihydroazaacene (**DDA**s) hergestellt. Diese wurden durch palladiumkatalysierte Buchwald-Hartwig-Aminierung von Aryliodiden mit *N*,*N′*-Dihydroazaacenen synthetisch zugänglich. Die spektroskopischen Eigenschaften, Kristallstrukturen und DFT-Berechnungen dieser neutralen Verbindungen und ihrer Radikal-Ionen wurden systematisch untersucht. Alle Radikalkationen sind stabil und ihre Absorptionsspektren in Dichlormethan bleiben unter Umgebungsbedingungen mindestens 24 Stunden unverändert.

Publications

Gaozhan Xie, Sebastian Hahn, Frank Rominger, Jan Freudenberg, and Uwe H. F. Bunz, Synthesis and Characterization of Two Different Azarubrenes. *Chem.Commun.* **2018**, *54*, 7593-7596.

Gaozhan Xie, Victor Brosius, Jie Han, Frank Rominger, Andreas Dreuw, Jan Freudenberg, and Uwe H. F. Bunz, Stable Radical Cations of *N,N'*-Diarylated Dihydrodiazapentacenes. *Chem. Eur. J.* **2020**, *26*, 160-164.

Gaozhan Xie, Miriam Hauschild, Hendrik Hoffmann, Lukas Ahrens, Frank Rominger, Michal Borkowski, Tomasz Marszalek, Jan Freudenberg, Milan Kivala, and Uwe H. F. Bunz, 5,7,12,14-Tetrafunctionalized 6,13-Diazapentacenes. *Chem. Eur. J.* **2020**, *26*, 799-803.

Abbreviations

BS	bright state
BS1	first bright state
CV	cyclic voltammetry
calcd.	calculated
Cl-TAP	2,3,9,10-tetrachloro-6,13-bisquinoxalinophenazine
DAR	5,11-di(4-pyridyl)-6,12-diphenyltetracene
DARO2	5,12-dihydro-5,11-di(4-pyridyl)-6,12-diphenyl-5,12-epidioxynaphthacene
DCM	dichloromethane
DDA	*N,N'*-diarylated dihydroazaacene
EE	ethyl acetate
EI	electron impact
ESI	electrospray ionization
ESR	electron spin resonance
FMO	frontier molecular orbital
h	hour
HOMO	highest occupied molecular orbital
HRMS	high resolution mass spectrum
KI	potassium iodide
LUMO	lowest occupied molecular orbital
MALDI	matrix-assisted laser desorption/ionization
MesCl	methanesulfonyl chloride
min	minute
MnO_2	manganese dioxide
MO	molecular orbital
Mp	melting point
NaH_2PO_2	sodium hypophosphite
NICS	nucleus-independent chemical shift
NMR	nuclear magnetic resonance
OFET	organic field-effect transistor
PE	petroleum ether

Pd_2dba_3	tris(dibenzylideneacetone)dipalladium(0)
PVD	physical vapor deposition
Quino	*N,N’*-diaryl-*N,N’*-dihydrodiazapentacene
r.t.	room temperature
rubrene	5,6,11,12-tetraphenyltetracene
SAAR	stable azaacene anionic radical
$SnCl_2$	stannous chloride
SOMO	singly occupied molecular orbital
TAP	6,13-bis(triisopropylsilylethinyl)-5,7,12,14-tetraazapentacene
TAR	5,6,11,12-tetra(4-pyridyl)tetracene
TARO2	5,12-dihydro-5,6,11,12-tetra(4-pyridyl)-5,12-epidioxynaphthacene
TDAP	5,7,12,14-tetrafunctionalized diazapentacenes
TEA	triethylamine
THF	tetrahydrofuran
TIPS	tri-*iso*-propylsilyl
TIPSPEN	tri-*iso*-propylsilylethinylpentacene
TLC	thin layer chromatography
UV-Vis	ultraviolet-visible spectrophotometry
Xphos	2-dicyclohexylphosphino-2’,4’,6’-triisopropyl-biphenyl
δ	chemical shift

Table of Contents

Chapter 1. Introduction

1.1 Acene and Azaacene Semiconductors

1.1.1 A Brief Introduction of Organic Field-Effect Transistors

Organic field-effect transistors (OFETs), a research focus over the past decades, have great potential in applications in smart labels, chemical and biological sensors, as well as large-area flexible electronic devices.[1-5] In comparison with inorganic transistors, OFETs are of low cost, low weight, and easy to prepare. As shown in Figure 2, an OFET is made up of a source electrode, a drain electrode, a semiconductor layer, a dielectric layer, and a gate electrode. The modulation of the source-drain current in transistors is realized by tuning the density of charge carriers in the thin organic semiconductor layer, generated by an electric field applied between the semiconductor and the gate electrode. The charge carrier mobility (μ, $cm^2V^{-1}s^{-1}$) of OFETs is the most important device parameter for many of their target applications, and higher carrier mobilities allow switching transistors between on and off states at higher frequencies. So far, impressive improvements have been achieved for OFET performances with the charge carrier mobilities over 10 $cm^2V^{-1}s^{-1}$,[6, 7] which have been comparable to that of polycrystalline silicon.

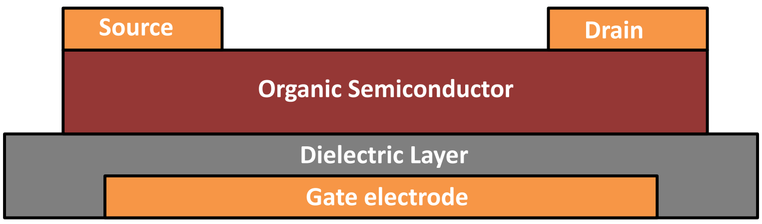

Figure 2. Schematic diagram of top contact/bottom gate OFET architecture.

There are two main families of organic semiconductors that are employed in OFETs: (i) conjugated polymers (e.g., polyphenylene,[8] poly(3-hexylthiophene) (P3HT),[9] poly(triarylamine))[10]; and (ii) small conjugated molecules (e.g., rubrene (5,6,11,12-tetraphenyltetracene),[11] pentacene,[12] oligothiophenes[13]). Compared to polymer semiconductors, small molecule semiconductors, with well-defined chemical structures, are easier to purify. They form crystalline films for the fabrication of high performance OFETs. Small conjugated molecules have no synthetic batch-to-batch variance, which provides adequate assurance of a stable device performance, thus having higher potential for commercial applications. As a result, we discuss small conjugated molecules employed in OFETs in this dissertation.

In terms of charge transport characteristics, organic semiconductors can also be divided into hole-transporting p-type materials and electron-transporting n-type materials. The typical p-type[11, 14, 15] and n-type[16-18] molecules used in OFETs are shown in Figure 3. Less n-type organic semiconductors, required to make complementary metal-oxide-like logic circuits together with p-channel OFETs,[6] have been exploited, and their mobility values are on average still lower in comparison to p-type organic semiconductors.[19-22]

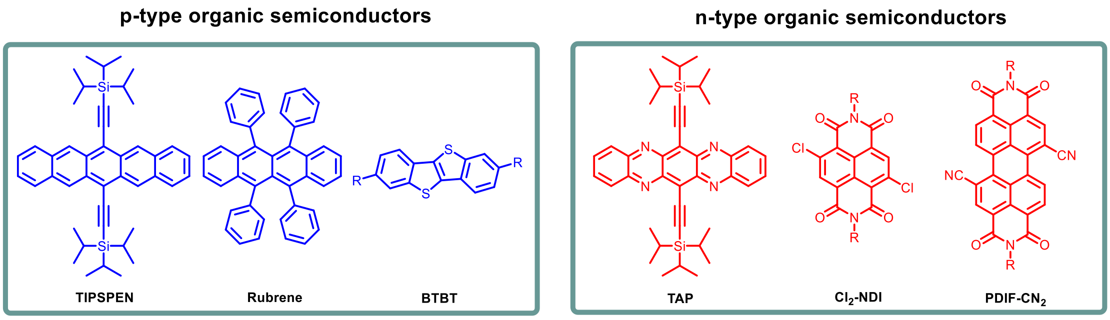

Figure 3. Representative p- and n-type organic semiconductors (**TIPSPEN**,[14] **Rubrene**,[11] **BTBT**,[15] **TAP**,[16] **Cl_2-NDI**,[17] and **PDIF-CN_2**[18]).

1.1.2 Acenes

Acenes (see Figure 4) are p-type semiconductors and show excellent transistor behaviors in OFETs. OFETs based on anthracene single crystals have been fabricated and characterized by Aleshina et al. and exhibited a mobility of 0.02 $cm^2V^{-1}s^{-1}$ at low temperatures between 170-180 K.[23] A mobility of 2.4 $cm^2V^{-1}s^{-1}$ was achieved in single crystal OFETs containing tetracene using a poly(dimethylsiloxane) polymer as the dielectric layer.[24] The OFETs of polycrystalline pentacene demonstrated mobilities as high as 5 $cm^2V^{-1}s^{-1}$ with on/off ratios over 10^6.[25] It seems that the field-effect mobilities increase from anthracene to pentacene with the extension of the π-conjugated systems, which might be ascribed to larger intermolecular π-orbit overlaps, increasing transfer integrals and reducing reorganization energies.

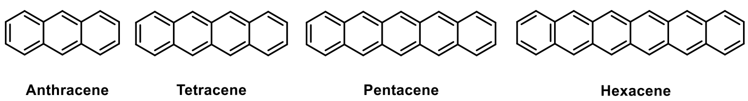

Figure 4. Representative acenes (**Anthracene**,[23] **Tetracene**,[24] **Pentacene**,[25] and **Hexacene**[26]).

However, the larger acenes are highly sensitive to oxygen and light due to their high highest occupied molecular orbital (HOMO) energy levels and narrow energy gaps between HOMO and lowest unoccupied molecular orbital (LUMO). For instance, pentacene is easily oxidized into 6,13-pentacenequinone,[27] or it forms dimers[28] under ambient conditions (see Scheme 1). In addition, extended acenes without side chains, such as hexacene, are difficult to purify because of their extremely poor solubility. Actually, pure hexacene can only be obtained by vacuum sublimation in the dark.[26] Substitution in the peri- (or side-) positions of acenes not only protects them from photooxidation, but also increases their solubility.[29] As seen in Scheme 1, tri-*iso*-propylsilylethinyl-pentacene (**TIPSPEN**) was synthesized by a double nucleophilic addition reaction of 6,13-pentacenequinone with the organolithium compound formed from tri-*iso*-propylsilyl (TIPS) acetylene and *n*-butyllithium (*n*-BuLi), followed by treatment with stannous chloride ($SnCl_2$) under acidic condition.[29] Introducing TIPS-acetylene in the 6, 13- positions makes **TIPSPEN** stable enough to be purified under ambient conditions and improves its solubility such that solution processing can be employed.

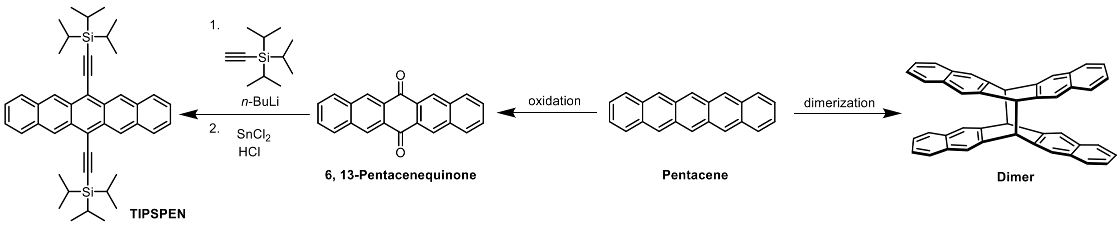

Scheme 1. Oxidation[27] and dimerization[28] of pentacene (right, middle); the synthetic route to **TIPSPEN**[29] (left).

1.1.3 Azaacenes

Azaacenes, formed from replacement of C-H by nitrogen atoms, are fascinating molecules with respect to structural and electronic properties. They have been applied in organic electronics.[30-32] Interestingly, their reduced forms, the *N,N′*-dihydro compounds (see Scheme 2a), are electron-rich and anti-aromatic, while after oxidation, the pyrazinic compounds are electron-poor aromatic species, useful as n-type semiconductors in OFETs.[33] 6,13-Bis(triisopropylsilyl-ethinyl)-5,7,12,14-tetraazapentacene (**TAP**) was first reported by Bunz et al. in 2009.[16] As shown in Scheme 2b, reacting dione **1** with the anion of TIPS-acetylene formed an intermediate diol, followed by treatment with sodium hypophosphite (NaH_2PO_2) and potassium iodide (KI) under acid condition to furnish **2**. **2** was then oxidized by manganese dioxide (MnO_2) to give **TAP** as a dark-green crystalline material. In 2011, Miao et al. reported the vacuum deposited OFETs based on **TAP**, which showed spectacular electron transporting mobilities in the range of 1.0-3.3 $cm^2V^{-1}s^{-1}$.[34, 35] In 2018, they further fabricated solution-processed OFETs containing 2,3,9,10-tetrachloro-6,13-bis[(tripropan-2-ylsilyl)ethynyl]quinoxalino[2,3-*b*]phenazine (**Cl-TAP**, see Scheme 2b), exhibiting an unprecedented electron mobility value of 27.8 $cm^2V^{-1}s^{-1}$.[36] **Cl-TAP** was obtained from reaction of **6** with the Grignard reagent of TIPS-acetylene, followed by treatment with $SnCl_2$ in the presence of HCl.[37]

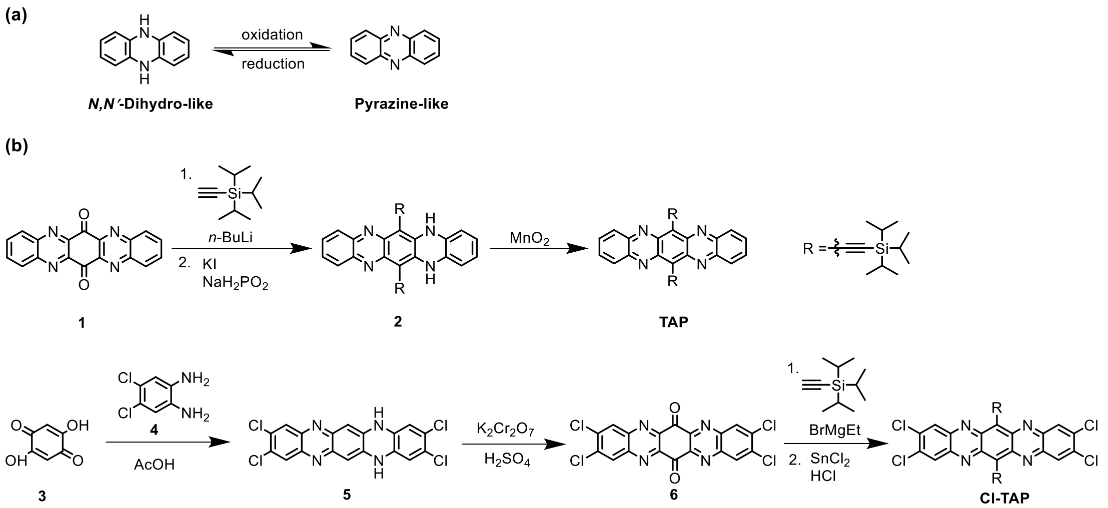

Scheme 2. a) Reduced and oxidized forms of azaacenes; b) Synthetic routes to **TAP**[16] and **Cl-TAP**[37].

1.1.4 Rubrene and Rubrene Analogues

Rubrene is a state-of-the-art semiconductor and has been studied extensively in the field of organic electronics.[38, 39] Its crystals exhibit three different polymorphs: orthorhombic, monoclinic, and triclinic.[40] Among them, the orthorhombic crystals, grown by physical vapor deposition (PVD) method, display herringbone packing (see Figure 5), exhibing the best hole-transporting ability because of large π-π overlap between adjacent molecules.[41]

Carrier mobilities between 15-40 $cm^2V^{-1}s^{-1}$ have been reported for orthorhombic rubrene crystals in different OFET device structures and measurement conditions.[11, 42] In 2007, Takeya et al. reported the fabrication of high performance OFETs with a maximum mobility value of 40 $cm^2V^{-1}s^{-1}$ by attaching purified rubrene crystals on SiO_2 gate insulators coated with a high-density self-assembled perfluorotriethoxysilane layer.[11]

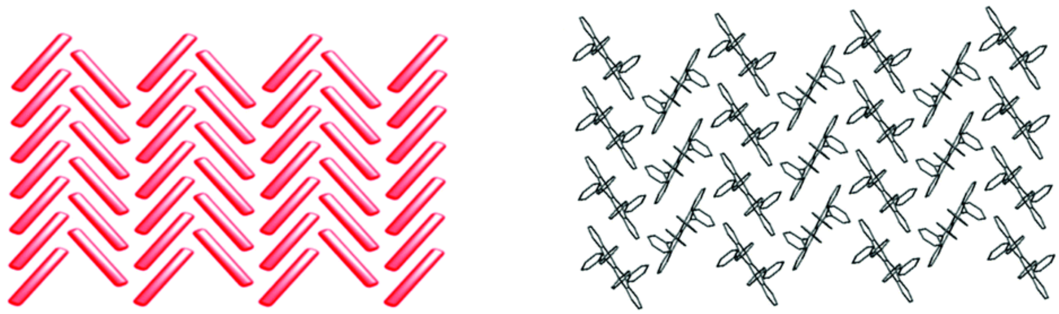

Figure 5. Herringbone packing motif of orthorhombic rubrene crystals. Adapted with permission from ref. 39 © 2018, American Chemical Society.

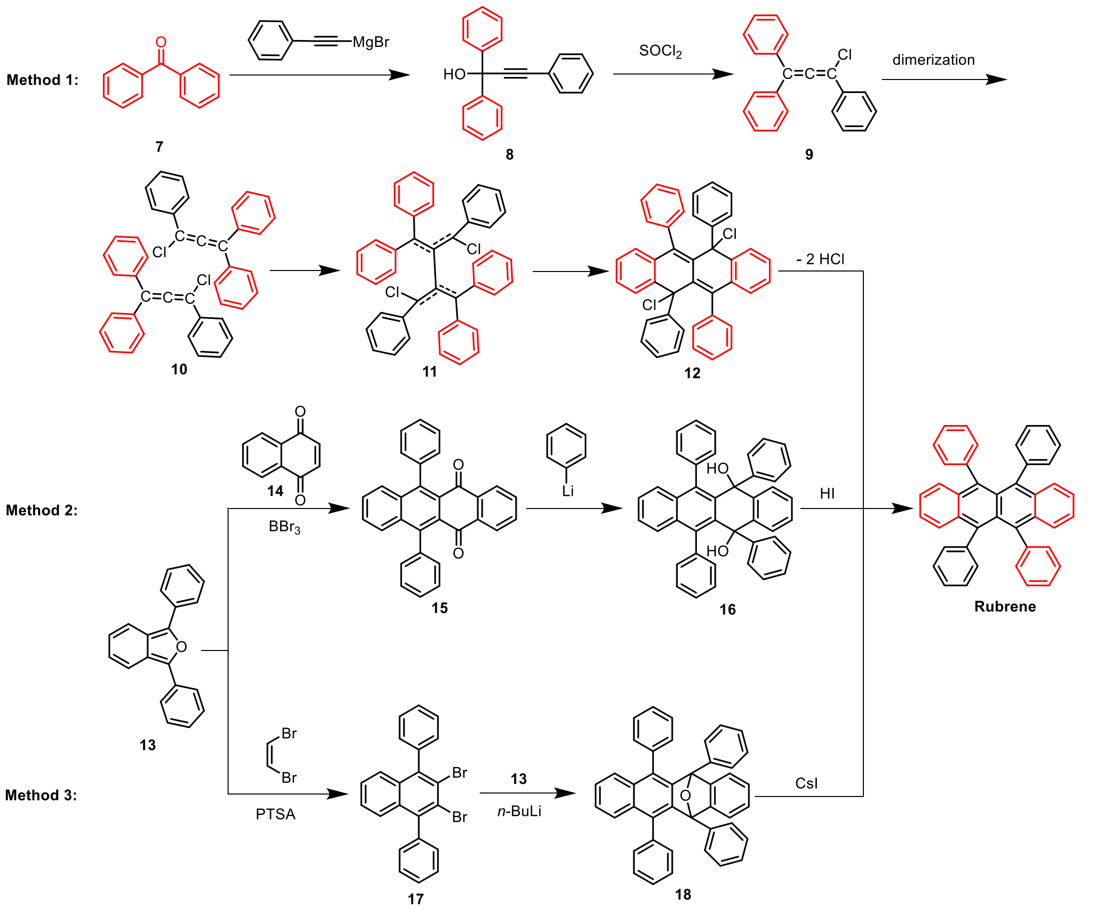

Scheme 3. Three synthetic routes to rubrene (method 1,[43] method 2,[44] and method 3[44]).

Until now, several methods have been developed for synthesizing rubrene. Commercial rubrene was prepared by treating 1,1,3-triphenylpropargyl alcohol **8** with thionyl chloride

($SOCl_2$) (see Scheme 3, method 1).[43] The resulting chloroallene **9** underwent dimerization and dehydrochlorination to give rubrene. Rubrene can also be obtained via nucleophilic addition of phenyllithium to naphthacenequinone **15** followed by hydroiodic acid (HI) mediated aromatization, and **15** was acquired from Diels-Alder cycloaddition of isobenzofuran **13** with 1,4-naphthoquinone (see Scheme 3, method 2).[44] Besides, rubrene could be prepared according to method 3 in Scheme 3.[44] Precursor **17** was obtained from **13** by [4 + 2] cycloaddition with dibromoethylene in xylene followed by *p*-toluenesulfonic acid (PTSA) catalyzed dehydration of the oxo-bridged intermediate. Treatment of **17** with *n*-BuLi initially, followed by adding isobenzofuran **13** gave the corresponding oxo-bridged adduct **18**. Rubrene formed by reducing **18** with a large excess of cesium iodide (CsI).

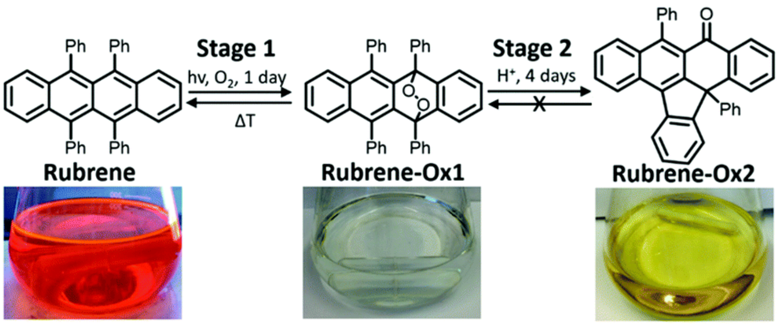

Figure 6. Molecular structures and colors in chloroform of rubrene, **rubrene-Ox1**, **rubrene-Ox2**. Adapted with permission from ref. 45 © 2018 the Royal Society of Chemistry.

Rubrene oxidizes readily in both solution and amorphous thin films, hampering its practical applications. As shown in Figure 6, rubrene in chloroform can be oxidized to **rubrene-Ox1** easily under ambient conditions, with the color changing from red to colorless.[45] Prolonged photo-oxidation in chloroform converts the endo-peroxide irreversibly to **rubrene-Ox2**.

Hence, various rubrene analogues have been prepared and investigated to exploit stable materials with excellent charge mobilities. Novel rubrene derivatives, such as **19-24** (see Scheme 4),[43, 46, 47] have been synthesized using the classic one-pot approach (similar to method 1 in Scheme 3). It seems that compounds **19-24** are more stable against oxidation in solution. Looking at Figure 7a, the integral area of characteristic absorption for rubrene solution rapidly decreases from 100% to 4% after the first 20 minutes (min) exposure to light and air, while for **19-22** solutions they decrease more slowly under the same conditions.[46] For example, the integral area reaches the same value 4% after 7.5 hours (h) for **19** (see

Figure 7b), much longer than that of rubrene. In addition, it should be mentioned that all the rubrene derivatives **19-22** display herringbone crystal structures (see Figure 8), similar to those of orthorhombic rubrene crystals, where both π-π-stacking distances and the width of herringbone angles are slightly smaller than those in rubrene, indicating they have great potential charge-transporting ability.

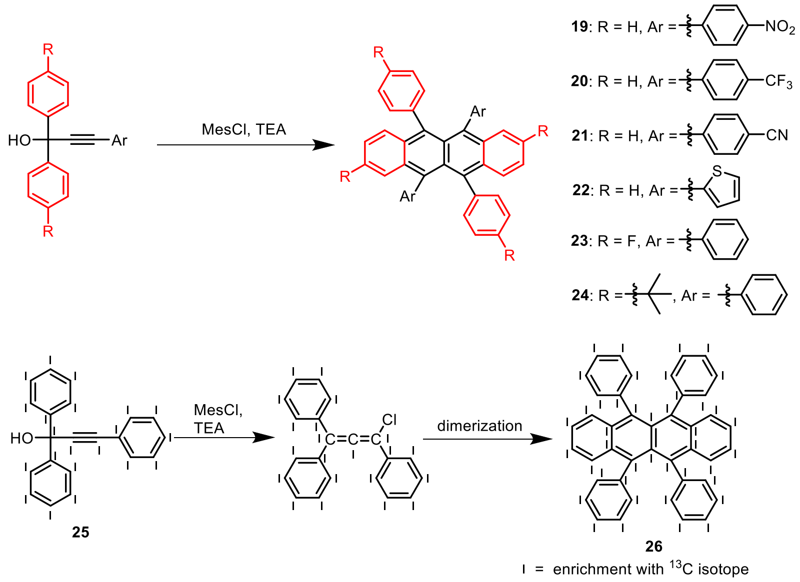

Scheme 4. Synthesis of rubrene analogues using a one-pot approach (**19-22**,[46] **23-24**,[43] and **26**[48]).

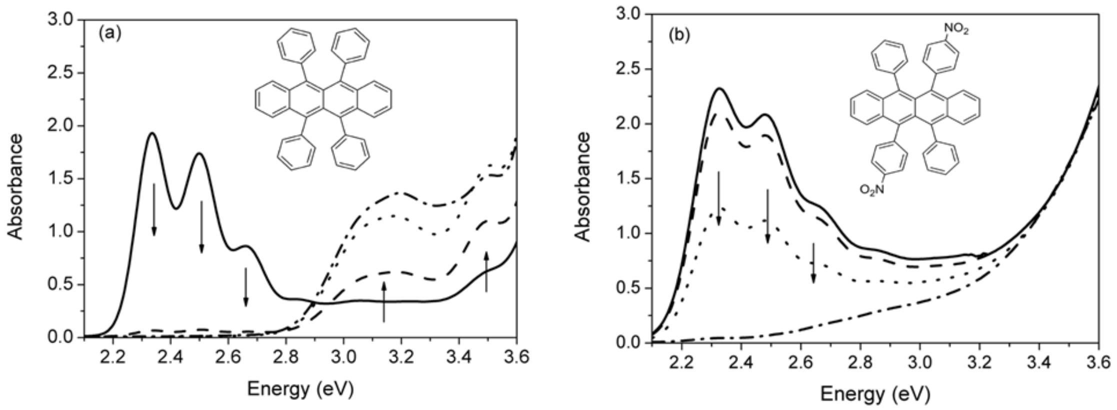

Figure 7. Absorption spectra of (a) rubrene and (b) **19** in solution. The spectra were collected immediately after preparation (continuous line), after 20 min (dashed line), after 2 h (dotted lines), and after 6 h (dash-dotted line) of exposure time under light and air. Inset: molecular structures of (a) rubrene and (b) **19**. Adapted with permission from ref. 46 © 2014 the Royal Society of Chemistry.

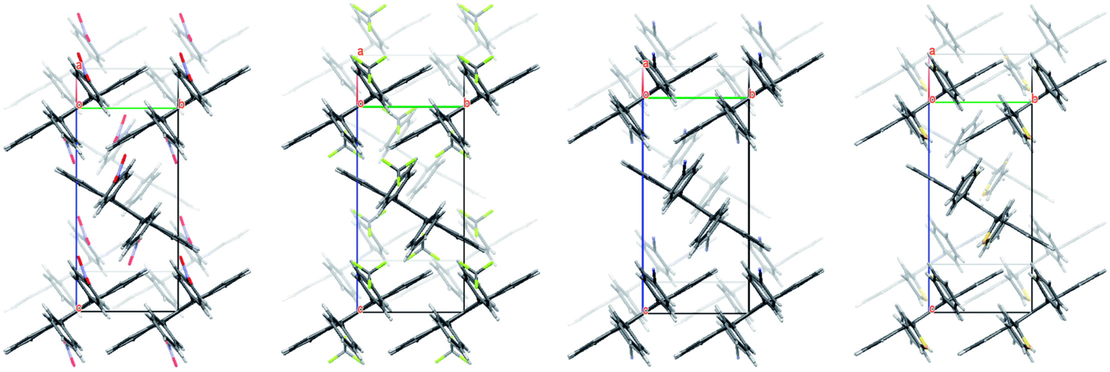

Figure 8. Packing motif of **19**, **20**, **21**, and **22**. Adapted with permission from ref. 46 © 2014 the Royal Society of Chemistry.

The fully isotope-labelled rubrene, ^{13}C-rubrene **26**, was synthesized successfully and characterized by Ren et al. in 2017.[48] As shown in Scheme 4, carbinol **25** was treated with triethylamine (TEA) and methanesulfonyl chloride (MesCl) to generate a chloroallene intermediate, which dimerized upon heating to give ($^{13}C_{42}$)-rubrene **26** in one pot. Single crystals of **26**, cultivated by the well-developed horizontal physical vapor transport, revealed an orthorhombic solid-state packing essentially identical to that of native rubrene. The OFETs based on **26** single crystals showed the average hole-transporting mobilities over 10 $cm^2V^{-1}s^{-1}$ at room temperature (r.t.) and the band-like transport was observed at very low temperature with a maximum mobility of 45 $cm^2V^{-1}s^{-1}$.

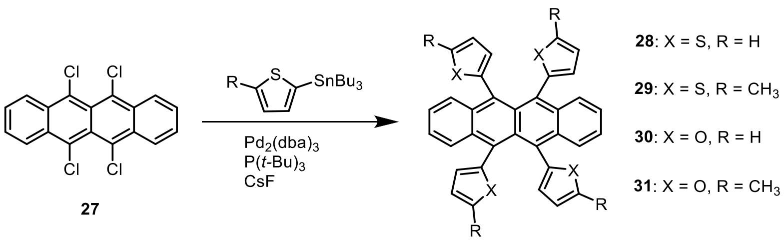

Scheme 5. Synthesis of rubrene analogues **28-31**.[49]

Rubrene analogues with the same four side groups can be synthesized based on 5,6,11,12-tetrachlorotetracene **27** by Stille coupling. As shown in Scheme 5, the straightforward C-C bond-forming cross-coupling reactions between **27** and trialkylstannyl chalcogenophenes afforded **28-31** in high yields.[49] Figure 9 shows higher photooxidation stability for **28-31** in comparison to rubrene. The absorption peaks at around 500 nm for the rubrene solution disappear after a few hours, while the absorption spectra of **28-30** remain unchanged after 24 h. There are small absorption spectra changes for **31**, which occur much more slowly than that of rubrene.

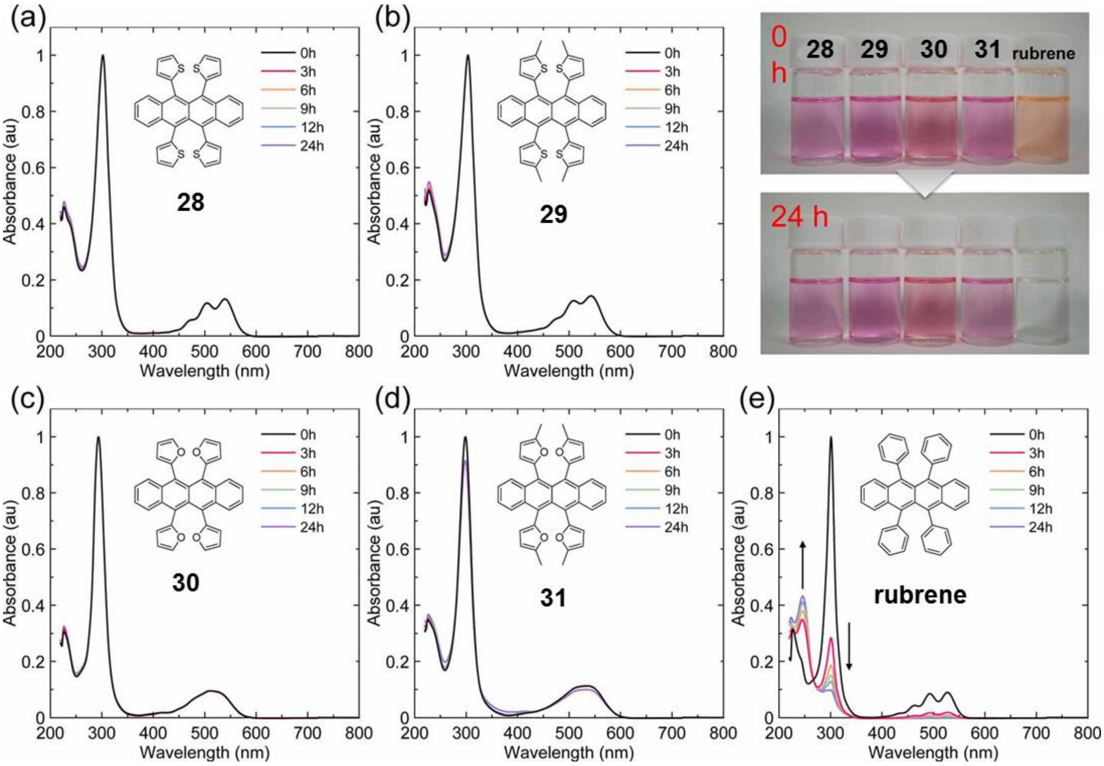

Figure 9. Ultraviolet-visible spectrophotometry (UV-vis) absorption spectra as a function of time for (a) **28**, (b) **29**, (c) **30**, (d) **31**, and (e) rubrene in dichloromethane (DCM). Adapted with permission of ref. 49 © 2015, American Chemical Society.

Douglas et al. have reported a variety of fluorinated rubrenes.[50, 51] Substitution of hydrogen by electron-withdrawing fluorine significantly impacts both the physical and chemical properties of rubrene, such as lowering the HOMO and LUMO energies of rubrene, which enhances its stability against oxidation. As shown in Scheme 6, the Suzuki-Miyaura coupling of dichloroquinone **32** with phenylboronic acids provided diarylquinones **33** in good yields. The nucleophilic addition of pentafluorophenyl lithium with **33**, followed by reduction with $SnCl_2$/HCl, gave partially fluorinated rubrene **34**.[50] The synthesis of rubrene derivative **37** with *peri*-perfluorophenyl groups required a modified synthesis because the Suzuki-Miyaura coupling of dichloride **32** with pentafluorophenyl boronic acid failed.[50] The double nucleophilic addition reactions of 6,11-dimethoxytetracene-5,12-dione **35** with pentafluorophenyl lithium, followed by treatment of the resulting diol with HCl, generated

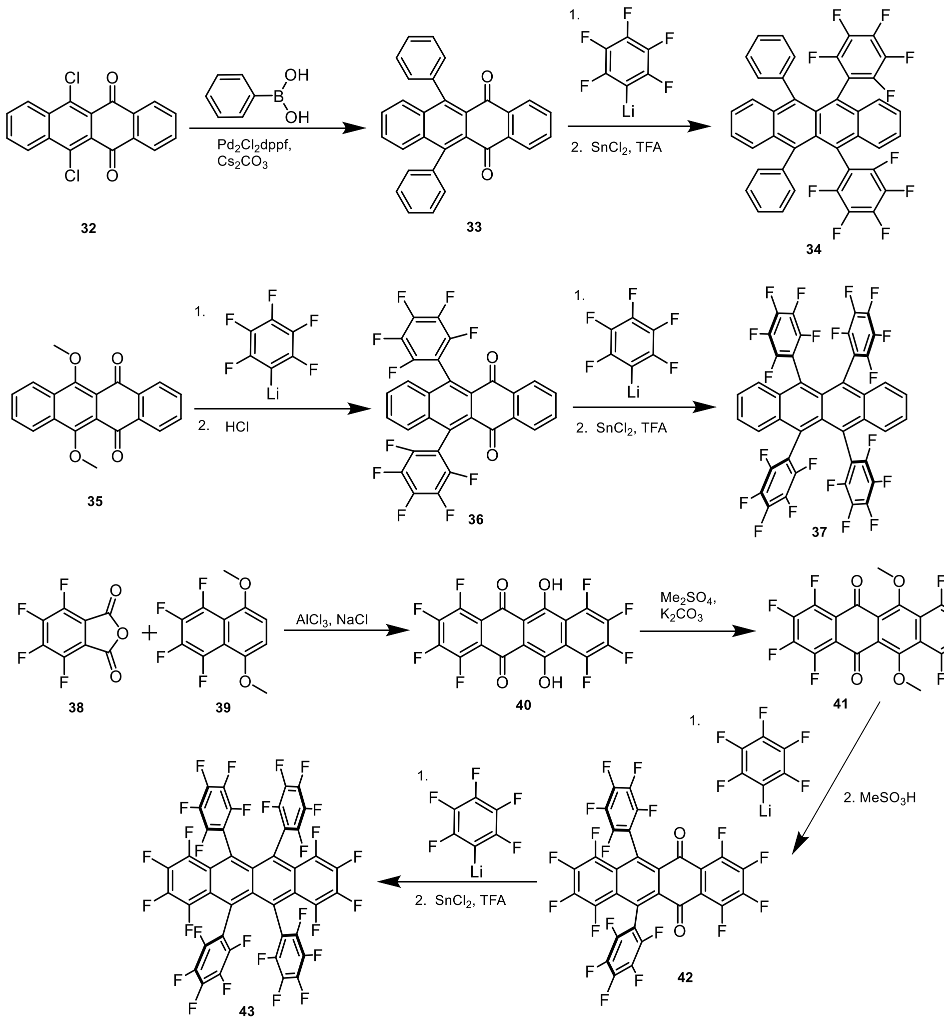

Scheme 6. Synthesis of fluoro-substituted rubrenes **34**,[50] **37**,[50] and **43**[51].

quinone **36**. Addition of the second set of perfluorophenyl rings required more strict reacting conditions. The mixture of diastereomeric diols formed by treating quinone **36** with pentafluorophenyl lithium was heated with $SnCl_2$ and trifluoroacetic acid (TFA) to yield rubrene analogue **37**. The synthesis of perfluororubrene **43** appeared more challenging since both the tetracene backbone and the peripheral phenyls of rubrene should be substituted by fluorine atoms.[51] The Friedel-Crafts acylation between tetrafluorophthalic anhydride **38** and 1,2,3,4-tetrafluoro-5,8-dimethoxy-naphthalene **39** formed naphthacenedione **40**, whose hydroxyl groups were then protected by dimethylsulfate (Me_2SO_4) under basic conditions to give the corresponding dimethoxytetracenedione **41**. Nucleophilic addition of perfluorophenyl lithium to the dione **41**, followed by treating with methanesulfonic acid ($MeSO_3H$) formed a 6,11-diaryltetracene-5,12-dione **42**. Addition of the second set of perfluorophenyl rings was the same as the procedures towards **40**. As expected, perfluororubrene **43** exhibits a much lower lying LUMO value of -4.05 eV measured in DCM in comparison with rubrene which has a LUMO value of -3.36 eV, suggesting its potential applications in n-type organic semiconductors.

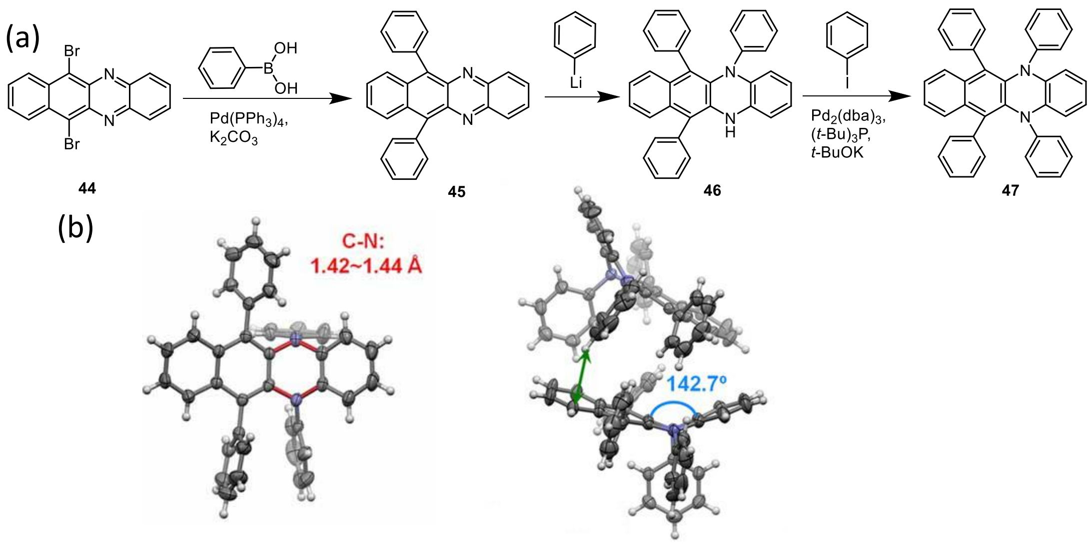

Figure 10. (a) Synthesis and (b) single crystal structures of **50**. Adapted with permission of ref. 52 © 2017, Wiley-VCH.

In 2017, Miao et al. reported the synthesis and properties of a novel N-embedded rubrene derivative, *viz* 5,6,11,12-tetraphenyl-5,12-dihydrobenzo[*b*]phenazine **50**.[52] As shown in Figure 10a, the Suzuki coupling of **47** with phenylboronic acid produced 6,11-diphenyl-5,12-diazatetracene **48**. The nucleophilic addition of phenyl lithium to **48** gave **49**, which underwent Buchwald-Hartwig coupling with iodobenzene later, affording **50** as a yellow solid. Unlike the orthorhombic rubrene crystals, the crystal structure of **50** exhibits a significantly bent backbone with a dihedral angle of 143° between the naphthalene plane and the benzene plane (see Figure 10b), in agreement with sp^3 hybridized nitrogen atoms, indicating a poor conjugation of nitrogen atoms in diazatetracene backbone. Not surprisingly, **50** behaves as an insulator in OFETs due to the lack of π-π-interactions in the solid state.

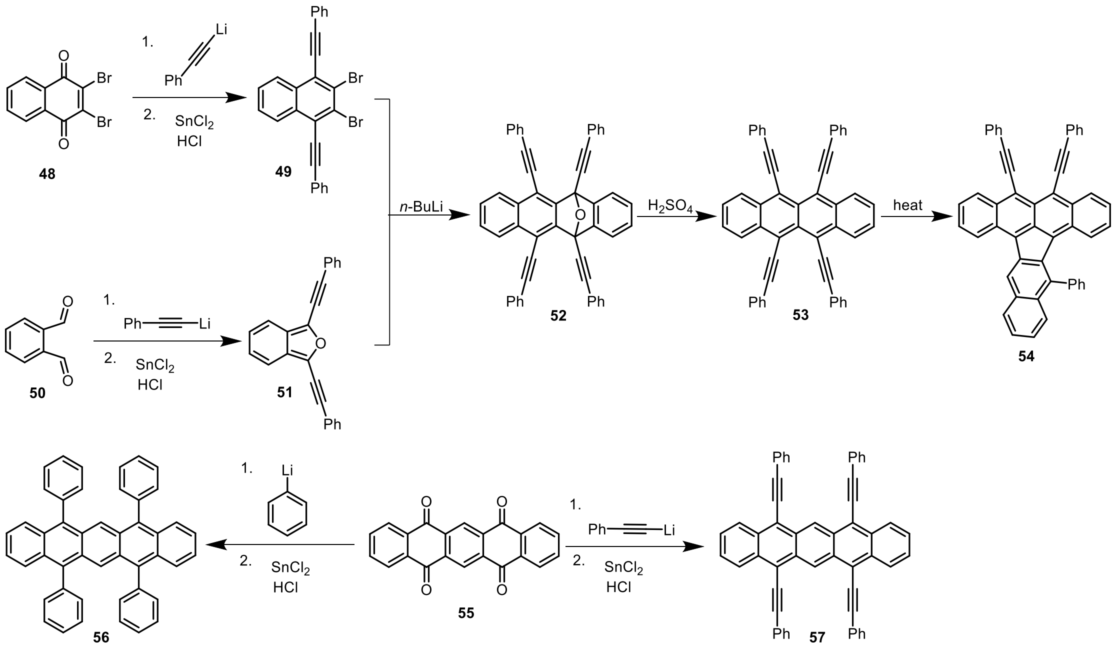

Scheme 7. Synthesis of π-extended rubrene derivatives **53**,[53] **56**,[54] and **57**[55].

5,6,11,12-Tetrakis(phenylethynyl)tetracene **53**,[53] 5,7,12,14-tetrafunctionalized pentacenes **56**,[54] and 5,7,12,14-tetrakis(phenylethynyl)pentacene **57**[55] can be regarded as π-extended rubrene derivatives in terms of chemical structures. The synthetic route to **53** is shown in Scheme 7.[53] The double nucleophilic additions of phenylethynyl lithium to naphthoquinone **48** were followed by the reduction reaction using $SnCl_2$, producing dibromodialkynylnaphthalene **49**. Another reactive precursor, bis(phenylethynyl)-isobenozofuran **51**, was synthesized by the nucleophilic additions of phenylethynyl lithium to *o*-phthalaldehyde **50**, and subsequent acid-promoted cyclization of the resulting keto-alcohol. Treatment of **49** with *n*-BuLi in the presence of **51** generated epoxytetracene **52**, which underwent aromatization after treating with H_2SO_4 to give **53**. Nevertheless, **53** was so unstable that it was subjected easily to pericyclic reactions to form **54** when heated to 80 °C. **56** and **57** were synthesized by reacting tetraone **55** with an excess of the lithium salt of benzene or phenyl acetylene and then treatment of the intermediates with $SnCl_2$.[54, 55] Neither **56** nor **57** has been employed as semiconductors in OFETs, which might be ascribed to their unstability against oxidation.

1.2 Acene-Based Radicals

1.2.1 Introduction of Organic Radicals

Organic radicals, with unpaired electrons, are open-shell electronic structures, exhibiting particular electronic, magnetic, and optical properties. They have potential applications in spintronics,[56] organic electronics,[57] energy storage and conversion devices,[58-60] etc. Generally, organic radicals are reactive and easily form closed-shell compounds by hydrogen abstraction, dimerization, or disproportionation.[61] Undoubtedly, stability is the prerequisite for the applications of organic radicals. There are several strategies to stabilize organic radicals. (i) Stable organic radicals can be obtained by introducing bulky substituents around the radical centers to disturb intermolecular interactions. The perchlorotriphenylmethyl radical **58** (see Figure 11) is an example,[62] the chlorine atoms at the *meta*-positions prevents dimerization of **58** — it's stable in solution open to air over months. (ii) Spin delocalization, e.g., enlarging π-conjugated systems, is another effective method to stabilize radicals since it leads to the decrease of reactivities by dilution of spin densities. Porphyrins and porphyrinoids exhibit superb abilities to stabilize radicals by spin delocalization.[61] In 2016, Osuka et al. developed the porphyrin-based radical **59**,[63] which is stable in air, on silica gel, in the presence of hydrogen-atom donors (such as tributyltin hydride (n-Bu_3SnH)), and concentrated H_2SO_4. (iii) Either electron-donating or electron-withdrawing groups directly connecting to radical centers contribute to stability of radicals due to their conjugative and inductive effects. Okino et al. explored the radical **60** (see Figure 11) with strong electron-withdrawing dicyano groups,[64] which is stable in spite of the absence of bulky protecting groups. Usually, the above-mentioned strategies are combined to obtain stable organic radicals. For instance, *N*-heterocyclic carbenes, possessing bulky and strong electron-donating units, have been applied intensively to synthesize stable organic radicals (e.g., radical **61** in Figure 11).[65]

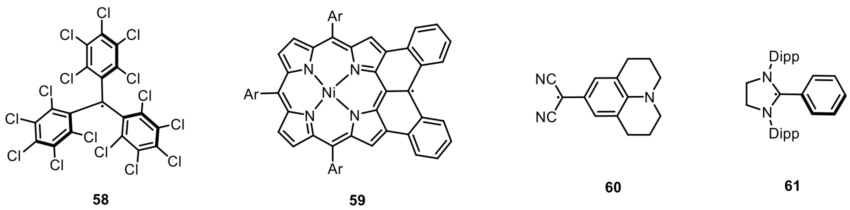

Figure 11. Representative organic radicals (**58**,[62] **59**,[63] **60**,[64] and **61**[65]).

Nowadays, diversified stable organic radicals have already been developed and characterized. In this thesis, we focus on the synthesis, properties, and applications of acene-based neutral radicals and radical ions.

1.2.2 Side-Chain Radical Acenes

As mentioned in Chapter 1.1.2, the mobility of pentacene in OFETs can reach up to 5 $cm^2V^{-1}s^{-1}$ with on/off ratios over 10^6, while the instability of pentacene in the presence of light and air prevents its practical applications. In recent years, Teki et al. reported the synthesis of three side-chain radical substituted pentacenes **66**,[66] **68**,[66] and **72**[67] (see Scheme 8) and discovered that the phenylverdazyl and phenyl nitronyl nitroxide radical side chains protected pentacene from photodegradation and enhanced its solubility in solvents. Differing from

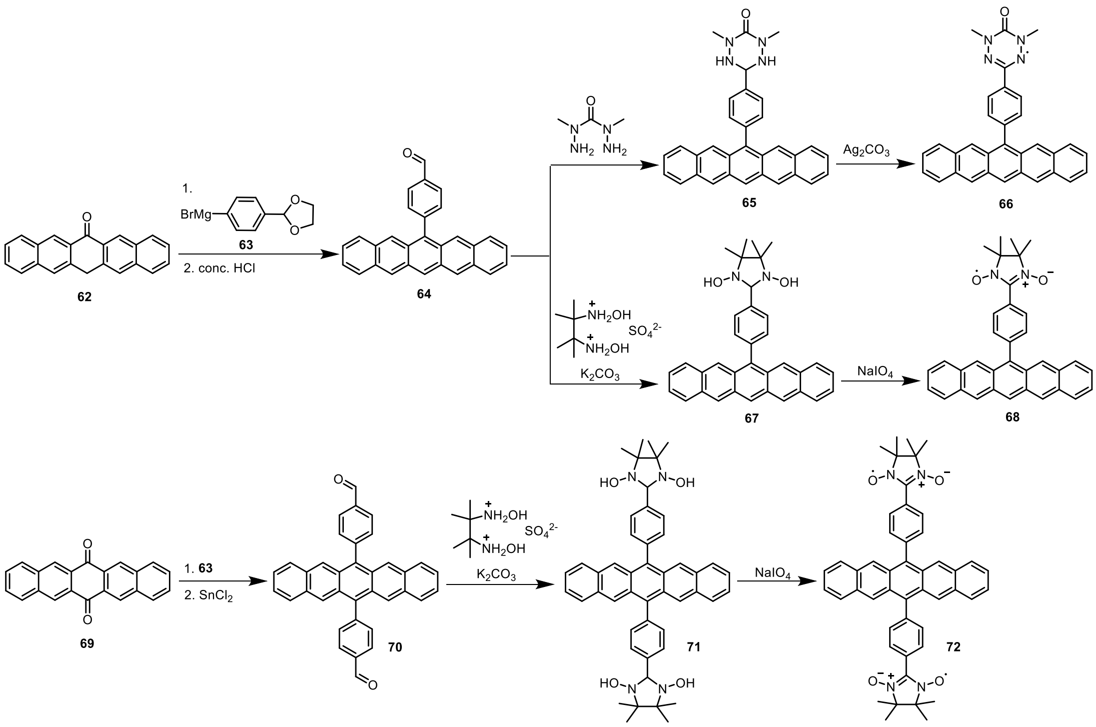

Scheme 8. Synthesis of side-chain radical pentacenes **66**,[66] **68**,[66] and **72**[67].

pentacene, insoluble in DCM, **66**, **68**, and **72** dissolve in DCM readily. The absorption bands of precursors **65**, **67**, and **71** at around 460-610 nm, the characteristic of pentacene moiety, decayed rapidly in tetrahydrofuran (THF) within a few minutes, while the corresponding absorption bands of **66**, **68**, and **72** remained unchanged under the same conditions, demonstrating remarkable protection provided by the radicals from photodegradation.

1.2.3 Fluorenyl-based Radicals

Fluorenyl radicals can be considered as a simple member of acene radicals and have been studied since they are readily synthesized and modified. Only several stable fluorenyl radicals are reported because of their high spin density at the fluorenyl center, resulting in high reactivity there. In 2012, Wu et al. reported the synthesis of stable fluorenyl radical **76** (see Scheme 9)[68] through the nucleophilic addition of fluorenone with an organolithium formed from 10-aryl-9-bromoanthracene **74** and *n*-BuLi, followed by the reduction reaction using $SnCl_2$. The bulky anthryl protecting group makes **76** stable enough to be purified by silica gel column chromatography. Benzannulation of fluorenyl radicals forms three different types π-extended dibenzofluorenyl radicals **81**, **86**, and **91** (see Scheme 11),[69]

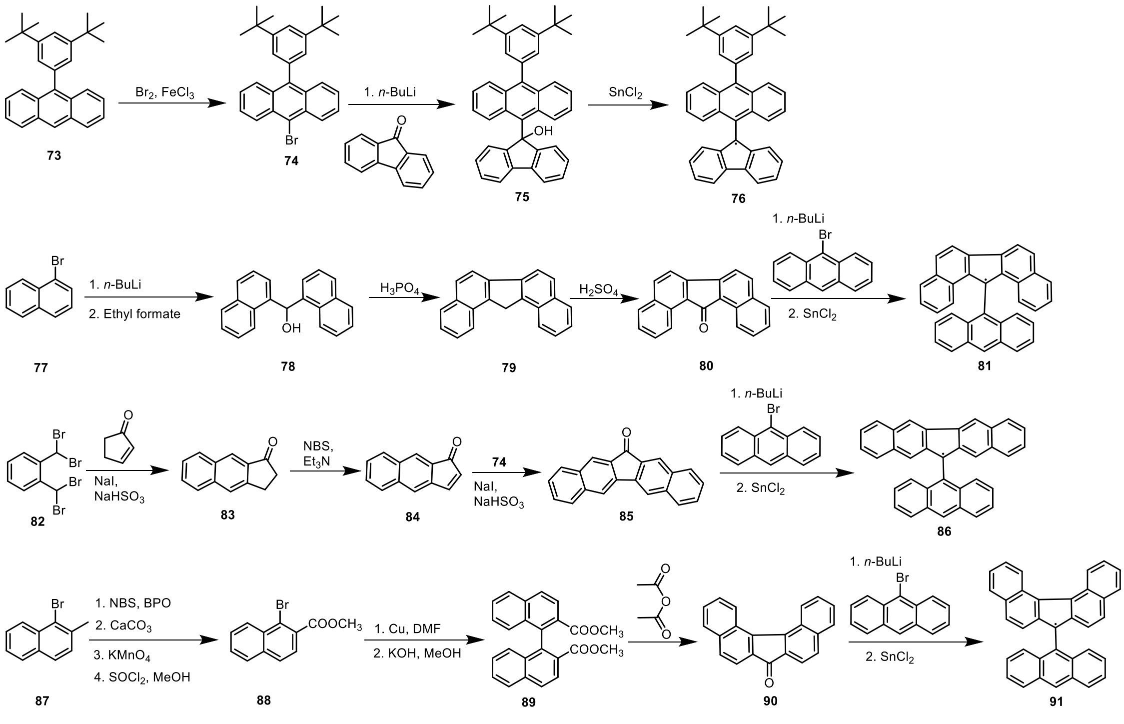

Scheme 9. Synthesis of fluorenyl-based radicals **76**,[68] **81**,[69] **86**,[69] and **91**[69].

which were reported by Kubo and co-workers in 2014. The radicals **81**, **86**, and **91** exhibited good stabilities with half-lives of 7, 3.5, and 43 days respectively in toluene under ambient conditions.

1.2.4 Azaacene Radical-Anions

Stable azaacene radical anions (SAARs) are quite rare, and so far only few SAARs have been reported. It is of interest to investigate their preparation, properties, and potential applications. **TAP**, an n-type transporting material, exhibits electron mobilities of over 11 $cm^2V^{-1}s^{-1}$ in OFETs.[73] For charge transport process in the OFETs, **TAP** reduces to **TAP**$^{-\cdot}$ at the electrode and then the injected electrons hop through adjacent molecules.[74] The synthesis of **TAP**$^{-\cdot}$ and investigating its unpaired spin density contribute to the understanding of the charge transport mechanism of n-type transporting materials in OFETs. In 2016, Marder et al. reported the synthesis of anionic radical **TAP**$^{-\cdot}$ and dianion **TAP**$^{2-}$ (see Scheme 10) by reducing **TAP** with one and two equivalent (eq.) potassium anthracenide respectively.[70] **TAP** displayed an absorption spectrum with a λ_{max} at 675 nm (See Figure 12). Upon reduction into its radical anion, a large redshift to 1400 nm was observed. The dication on the other hand displayed an absorption spectrum with a λ_{max} of 592 nm. In addition, **TAP**$^{-\cdot}$ is stable with respect to disproportionation into **TAP** and **TAP**$^{2-}$.

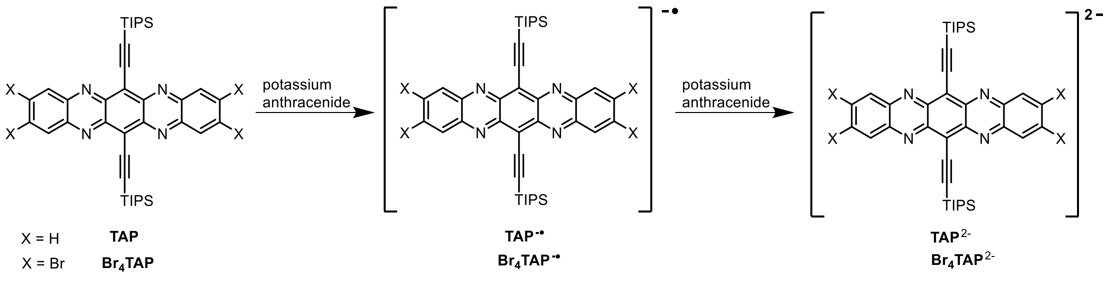

Scheme 10. Reduction of **TAP**[70, 71] and **Br_4TAP**[72] into their radical anions and dianions using potassium anthracenide.

In 2018, Bunz et al. reported an improved synthetic approach for **Br_4TAP**,[72] whose OFETs displayed electron-transporting mobilities of over 0.56 $cm^2V^{-1}s^{-1}$, around 50 times higher than those of **TAP** under the identical conditions. The authors further reduced **Br_4TAP** to its radical anion **Br_4TAP**$^{-\cdot}$ and dianion **Br_4TAP**$^{2-}$ by potassium anthracenide. The absorption spectra of **Br_4TAP**, **Br_4TAP**$^{-\cdot}$, and **Br_4TAP**$^{2-}$ (see Figure 12) are similar to those of **TAP**,

TAP$^{-\cdot}$, and **TAP**$^{2-}$ respectively. The spectrum of the radical anion is the most red-shifted while the spectrum of the dianion is opposite, that is, the most blue-shifted. Notably, **Br$_4$TAP**$^{-\cdot}$ is stable in dry diethyl ether (Et_2O) under air for at least several weeks.

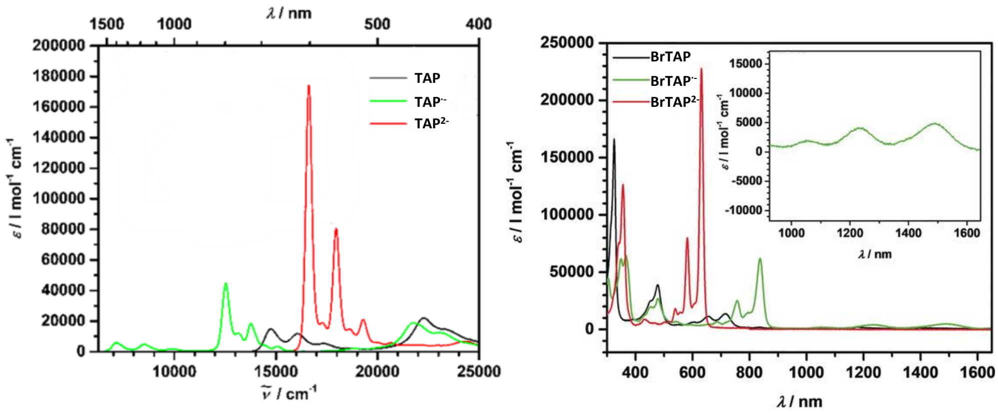

Figure 12. UV-vis spectra of the neutral (black), singly negatively charged (green), and doubly negatively charged (red) of **TAP** (left) and **Br$_4$TAP** (right). Left panel adapted with permission of ref. 71 © 2017, American Chemical Society, and right panel adapted with permission of ref. 72 © 2018, Wiley-VCH.

1.2.5 Heteroacene Radical-Cations

Stable unpaired heteroacene radical cations exhibit unique optoelectronic and electrochemical properties, inaccessible to closed shell compounds. In 2019, Chen et al. reported the synthesis and properties of **99**[75] and **104**[76]. As shown in Scheme 11, reacting **92** with *sec*-butyllithium (*sec*-BuLi)/ tetramethylethylenediamine (TMEDA), followed by adding phenalenone **93** and 2,3-dichloro-5,6-dicyano-1,4-benzoquinone (DDQ), furnished **94**. Treatment of **94** with

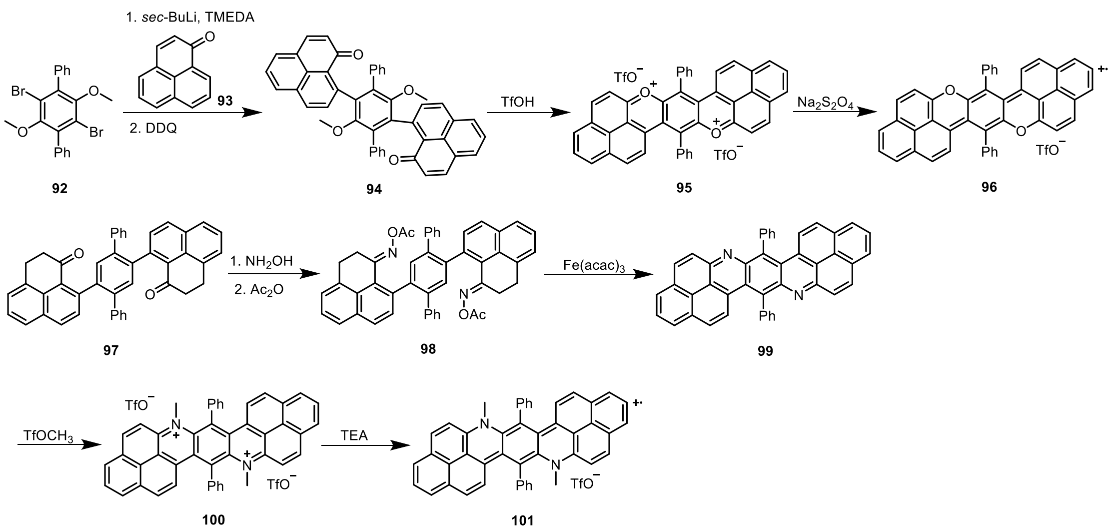

Scheme 11. Synthesis of heteroacene cationic radicals **96**[75] and **101**[76].

trifluoromethanesulfonic acid (TfOH) easily deprotected the methyl ether, which subsequently underwent dual cyclization to generate dipyrilium **95**. Reducing **95** using sodium dithionite ($Na_2S_2O_4$) furnished isolable and characterizable oxygen embedded cationic radical **96**, a dark blue solid, which was stable for multiple days in ambient conditions. On the other hand, condensation of **97** and hydroxylamine (NH_2OH), followed by acetylation, provided **98**, which was treated with tris(acetylacetonato)iron (III) ($Fe(acac)_3$) to form **99**. Then **99** was alkylated with methyl triflate ($TfOCH_3$) to afford **100**, followed by reduction with TEA to generate an air stable nitrogen-embedded cationic radical **101**. Interestingly, **101** in DCM exhibited a red emission with a λ_{max} of 592 nm, achieving a photoluminescence quantum yield of 9.3%.

1.3 Objective

Rubrene is a representative p-type semiconductor in organic electronics with carrier mobilities ranging between 15-40 $cm^2V^{-1}s^{-1}$. At the same time, it is unstable and easily oxidized. Introducing nitrogen atoms into π-system to form pyridine-like species lowers the HOMO and LUMO energies of molecules and converts the parent hydrocarbon structures from p-type to n-type heterocyclic semiconductors. Hence, in Chapter 2, we propose azarubrenes (see Scheme 12) through embedding nitrogen atoms into the phenyl peripheries of rubrene. These azarubrenes should be more stable compared to rubrene, at the same time maintaining its charge-transporting capability. To exploit more high-performance charge-transporting materials, a series of **TDAP**s (see Scheme 12) are designed and synthesized in Chapter 3. In terms of chemical structures, **TDAP**s can be seen as "homoazarubrenes" with the tetracene backbone substituted by 6,13-diazapentacene.

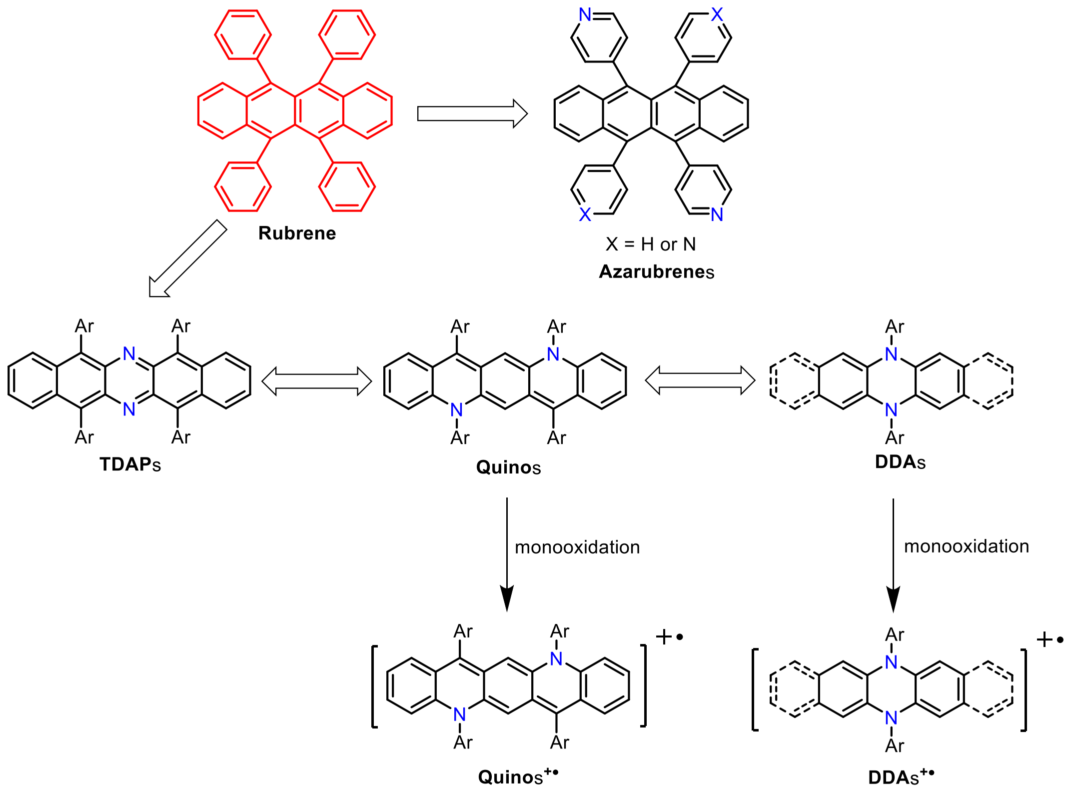

Scheme 12. Target molecular structures in this work.

In addition, quinoidal conjugated **Quino**s (see Scheme 12), the derivatives of **TDAP**s, have never been reported yet. Therefore, in Chapter 4, we are interested in investigating the synthesis and properties of **Quino**s. Moreover, their radical cations (**Quino**s$^{+\cdot}$) and dications are further prepared by oxidation. Finally, in Chapter 5, **DDA**s and their monocations (**DDA**s$^{+\cdot}$, see Scheme 12) are designed and synthesized to exploit more stable radical cations, the rare species.

Chapter 2. Synthesis and Characterization of Two Different Azarubrenes

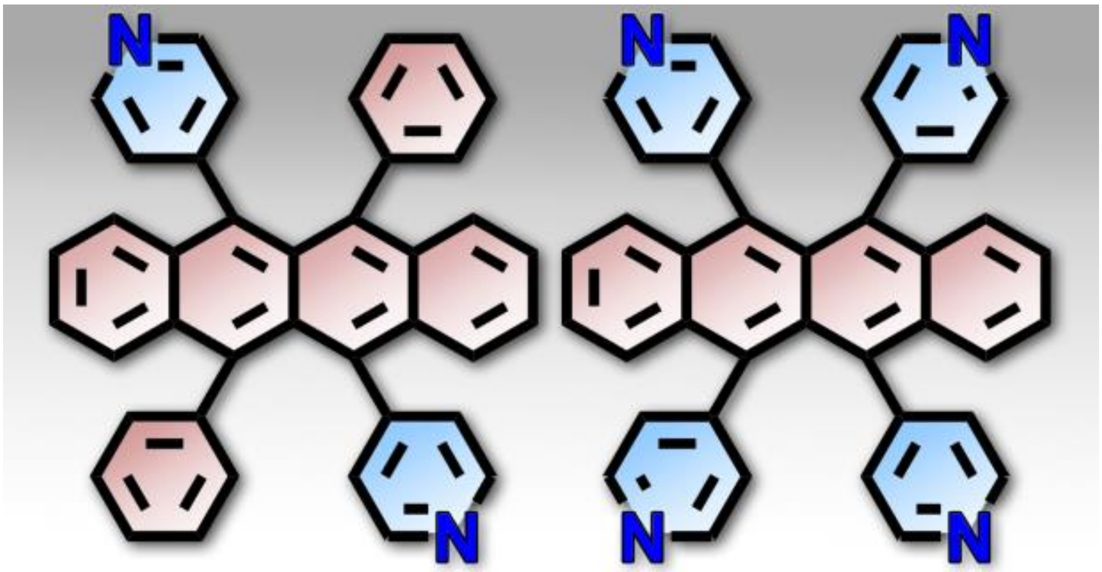

Figure 13. Molecular structures of 5,11-di(4-pyridyl)-6,12-diphenyltetracene (**DAR**) and 5,6,11,12-tetra(4-pyridyl)tetracene (**TAR**). Reproduced with permission of ref. 77 © 2018, the Royal Society of Chemistry.

2.1 Introduction and Research Purpose

Rubrene is a benchmark semiconductor and has been studied extensively in the field of organic electronics.[78-81] So far, the highest reported hole-transporting mobility for rubrene has reached 40 $cm^2V^{-1}s^{-1}$.[11] Also, rubrene promises powerful performance in next-generation solar cells with its high singlet fission quantum efficiency of nearly unity.[82] Nevertheless, rubrene oxidizes easily in ambient surroundings,[83, 84] hampering its practical applications. Thus, various substituted rubrenes have been prepared and investigated. Sakamoto and coworkers have reported half-fluorinated and perfluorinated rubrenes.[51, 85, 86] The replacement of hydrogen atoms by electron-withdrawing fluorine atoms lowers the HOMO and LUMO energies, thus enhancing stability of rubrene against oxidation. Mamada and coworkers have developed and characterized a series of rubrene analogues with thienyl or furyl substituents,[49] which show increased photooxidation stability. However, to our knowledge, azarubrenes are unknown at the present. Introducing nitrogen atoms into π-system to form pyridine-like species stabilizes the frontier molecular orbitals (FMOs) of molecules and potentially converts the parent hydrocarbon structures from p-ype to n-type heterocyclic semiconductors.[32, 87, 88] Therefore, we designed and synthesized two novel azarubrenes by introducing nitrogen atoms into the phenyl peripheries of rubrene.

2.2 Synthesis of Azarubrenes

The classic one-pot approach to synthesize rubrene using the allene protocol has been applied extensively. Some new derivatives of rubrene, such as 5,11-bis(3-thienyl)-6,12-diphenyltetracene and 5,11-bis(4-cyanophenyl)-6,12-diphenyltetracene, were synthesized using this approach.[46] To access **DAR** (see Scheme 13) we prepared the carbinol **103**. However, mesylation followed by heating in *o*-xylene to synthesize **DAR** from **103**, according to the allene method failed. Fortunately, when 1,1,2,2-tetrachloroethane was used as solvent, **DAR** was obtained in a yield of 14%. The simplicity of the synthesis rendered the poor yield acceptable, but unfortunately this scheme did not work for **TAR**, so an alternative route was developed, starting from literature known tetrachlorotetracene **27** (see Scheme 14).[89] **27** had been employed to synthesize thienyl and

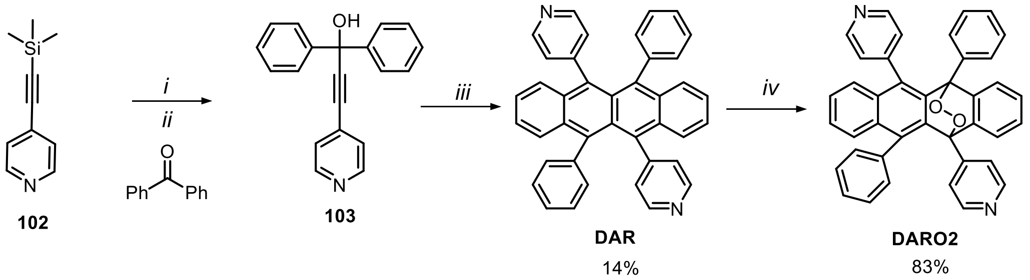

Scheme 13. Synthetic route to **DAR**. *i*) K_2CO_3, THF/CH_3OH = 1:1, r.t., 30 min; *ii*) benzophenone, *n*-BuLi, THF, 0 ℃ to r.t., 12 h; *iii*) MesCl, TEA, 1,1,2,2-tetrachloroethane, 146 ℃, 12 h; *iv*) air, DCM, r.t., 5 d. Reproduced with permission of ref. 77 © 2018, the Royal Society of Chemistry.

furyl substituted rubrene derivates by Stille coupling.[49] From **27**, **TAR** was easily obtained by the coupling of **27** to 4-pyridinylboronic acid, through a fairly efficient Suzuki reaction, employing a Buchwald-type catalyst.[90, 91] The desired **TAR** formed in 48% after column chromatography. Interestingly, in previous work, Douglas et al. found that **27** and phenyl magnesium bromide by Kumada-Tamao-Corriu cross-coupling underwent an indene annulation reaction.[92] However, similar types of transformation did not occur under our conditions.

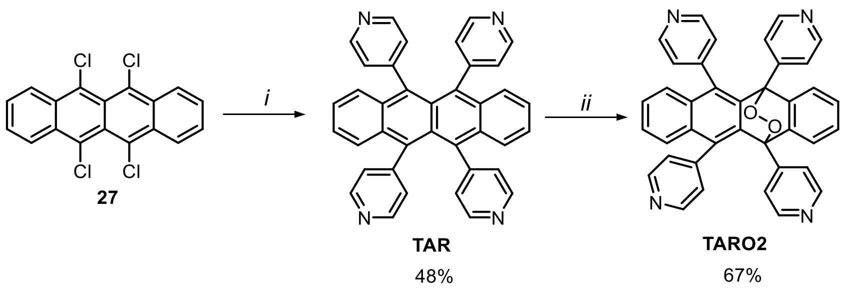

Scheme 14. Synthetic route to **TAR**. *i*) 4-Pyridinylboronic acid; tris(dibenzylideneacetone) dipalladium(0) (Pd_2dba_3), 2-dicyclohexylphosphino-2’,4’,6’-triisopropyl-biphenyl (Xphos), K_3PO_4, 1,4-dioxane, 100 ℃, 72 h; *ii*) air, DCM, r.t., 5 d. Reproduced with permission of ref. 77 © 2018, the Royal Society of Chemistry.

2.3 Results and Discussion

As shown in Figure 14, **DAR** and **TAR** exhibit absorption and emission spectra similar to each other and to those of rubrene; this result is expected, as the chromophore, tetracene, is identical in all cases. Despite the presence of two or four nitrogen atoms in the periphery, **DAR** and **TAR** are still easily oxidized in air into 5,12-dihydro-5,11-di(4-pyridyl)-6,12-diphenyl-5,12-epidioxynaphthacene (**DARO2**) and 5,12-dihydro-5,6,11,12-tetra(4-pyridyl)-5,12-

epidioxynaphthacene (**TARO2**); both emit blue-shifted as expected by the breakup of the tetracene system (see Figure 15).

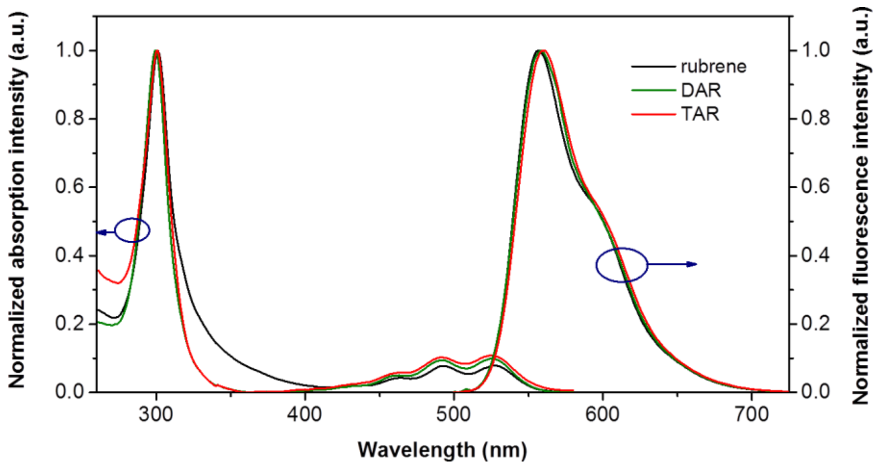

Figure 14. Normalized absorption and emission spectra of rubrene, **DAR** and **TAR** measured in DCM. Reproduced with permission of ref. 77 © 2018, the Royal Society of Chemistry.

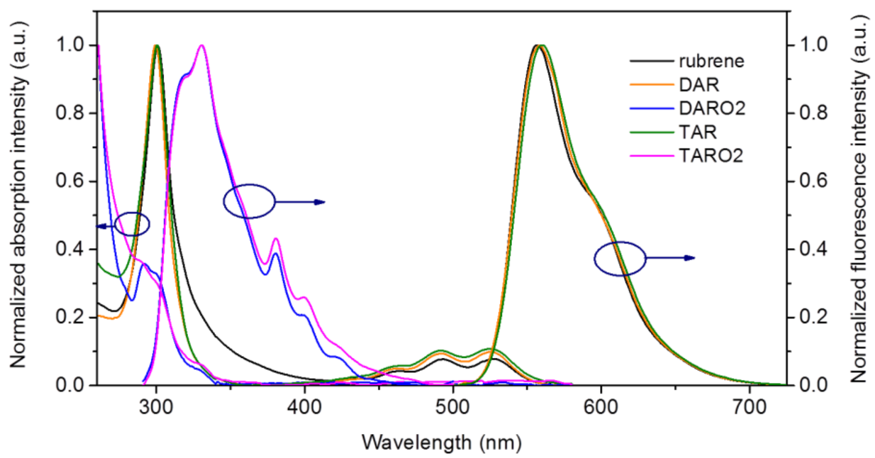

Figure 15. Normalized absorption and emission spectra of rubrene and designed compounds measured in DCM. Reproduced with permission of ref. 77 © 2018, the Royal Society of Chemistry.

Figure 16 shows a comparison of fluorescence intensity for solutions of rubrene, **DAR**, and **TAR** as a function of time in ambient air. After 24 h, the fluorescence intensity of rubrene, **DAR**, and **TAR** have decreased by 52%, 24%, and 10% respectively. Both **DAR** and **TAR** therefore are less sensitive towards oxidation in solution, but by no means air-stable for prolonged periods of time.

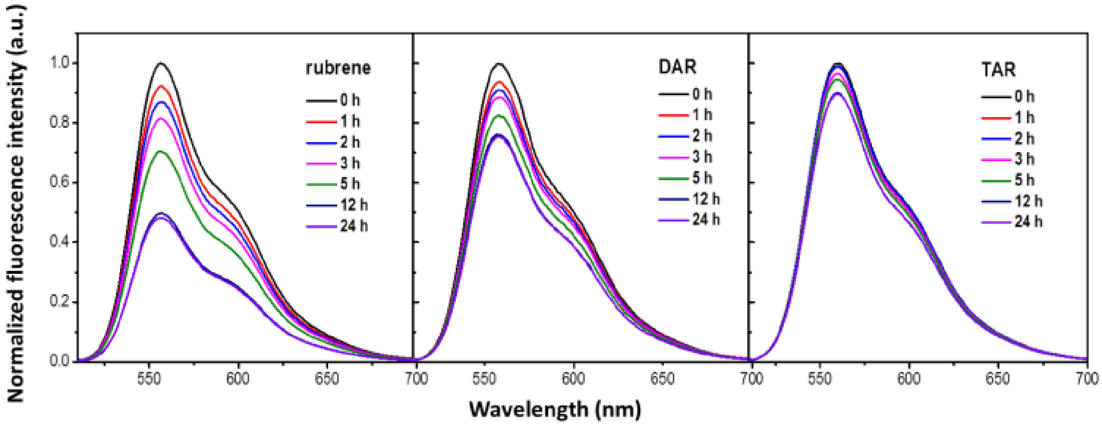

Figure 16. Normalized time-dependent emission spectra of rubrene, **DAR**, and **TAR** measured in DCM. Reproduced with permission of ref. 77 © 2018, the Royal Society of Chemistry.

Table 1. Photophysical, experimental and calculated electrochemical properties of rubrene, **DAR**, and **TAR**. Reproduced with permission of ref. 77 © 2018, the Royal Society of Chemistry.

Comp.	Abs_{max}[a] (nm)	Em_{max}[a] (nm)	E_{ox}[b] (V)	E_{red}[b] (V)	HOMO (eV) mes.[c]/cal.[d]	LUMO (eV) mes.[c]/cal.[d]	gap (eV) mes.[e]/cal.[d]
rubrene	527	556	0.37	–2.11	–5.17/–4.95	–2.69/–2.52	2.48/2.43
DAR	525	558	0.54	–1.98	–5.34/–5.24	–2.82/–2.82	2.52/2.42
TAR	525	561	0.71	–1.73	–5.51/–5.54	–3.07/–3.13	2.44/2.41

[a] Absorption peaks and maximum emissions in DCM. [b] Oxidation and reduction potentials measured in CV using ferrocene/ferrocenium as the reference redox system and internal standard (−4.8 eV). [c] Calculated from CV measurements (E_{HOMO} = –4.80 eV – E_{ox} (0/+); E_{LUMO} = –4.80 eV – E_{red} (0/–)). [d] Calculated by Gaussian 09 B3LYP/6-311++G**//BP86/def2-TZVP.[93] [e] Estimated from E_{HOMO} and E_{LUMO} ($E_{gap} = E_{LUMO} - E_{HOMO}$).

We were able to grow single crystals for XRD analysis of all of the four products, i.e. the azarubrenes but also their oxidized products. Single crystals of **DAR**, **DARO2**, and **TARO2** were obtained by slow evaporation of saturated DCM solutions under ambient conditions; **TAR** single crystals were grown by slow evaporation of THF solution in the glovebox. Rubrene displays three different polymorphs, orthorhombic (a = 26.78, b = 7.17, c = 14.26), monoclinic (a = 8.74, b = 10.13, c = 15.64, β = 91°), and triclinic (a = 7.02, b = 8.54, c = 11.95, α = 93°, β = 106°, γ = 106°).[40] As shown in Table 2, **DAR** (a = 7.07, b = 8.27, c = 11.86, α = 90°, β = 106°, γ = 98°) crystallizes in the triclinic crystal system and its molecular packing (see Figure 17a and 17e) is close to isomorphic to that of triclinic rubrene crystals, grown by the solvent diffusion method. Both of them exhibit a planar tetracene backbone with slanted stacks. Noticeably, **DAR** crystal exhibits a π-π stacking distance of 3.6

Å (0.2 Å shorter than that of rubrene[40]), a long-axis displacement of 6.1 Å, and the absence of short-axis displacement along crystal **a** direction (see Figure 17e and Figure 18), indicating it might have more efficient cofacial π-stacking interactions and electronic coupling than rubrene.[38] This is further supported by a Hirshfeld surface analysis[94] (see Figure 17g and 17h): similar to triclinic rubrene,[95] the main feature is a large, light blue colored region that corresponds to π-stacking of the tetracene core. However, the red regions on d_{norm} result exclusively from C-H···π close contacts — H···H close contacts are less prominent and N···H close contacts contribute only 5.4% to the total surface area.

More interesting is the structure and the packing of triclinic **TAR** (see Table 2). Contrary to **DAR**, the tetracene nucleus is somewhat twisted in this structure. Unfortunately, the compound crystallizes as a solvate and THF is part of the structure. As a consequence, the packing of the molecules is not rubrene-like anymore, and there is no appreciable overlap of the π-systems of different molecules. Attempts to grow single crystals from other solvents only led to very small crystals.

We could also obtain specimens of the oxidized species, which are, as expected, the oxygen adducts formed through a formal [4 + 2]-cycloaddition of **DAR** or **TAR** with O_2. The molecular packing of these species is complicated (see Figure 19).

Table 2. Unit cell data of **DAR**, **TAR**, and rubrene. Reproduced with permission of ref. 77 © 2018, the Royal Society of Chemistry.

Comp.	crystal system	space group	a (Å)	b (Å)	c (Å)	α (deg)	β (deg)	γ (deg)	V (Å3)
Rubrene[a]	triclinic	$P\bar{1}$	7.02	8.54	11.95	93	106	96	684
DAR	triclinic	$P\bar{1}$	7.07	8.27	11.86	90	106	98	660
TAR	triclinic	$P\bar{1}$	7.76	18.66	21.77	98	90	101	3068

[a] Triclinic rubrene crystal data is reported by Huang et al.[40]

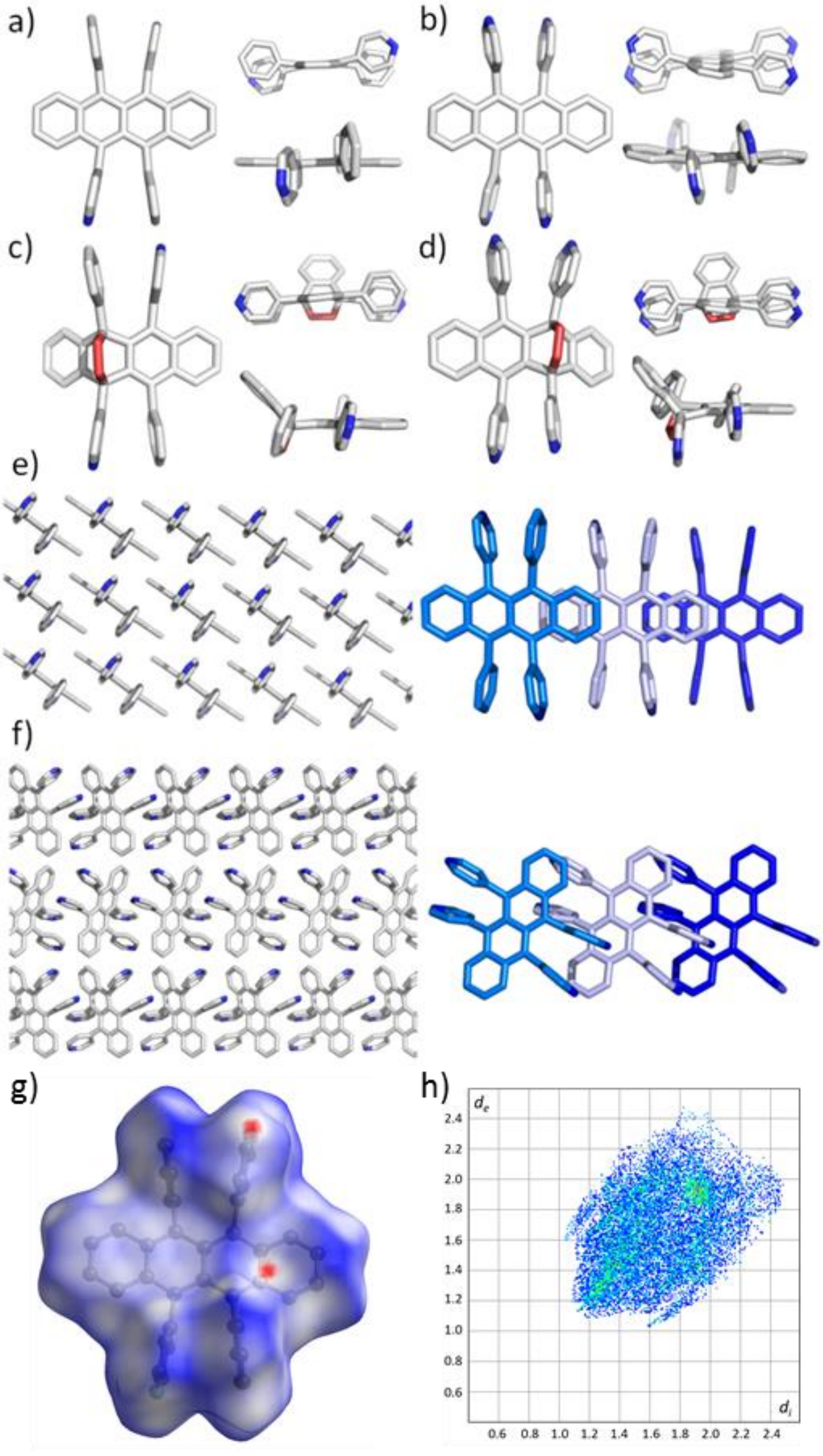

Figure 17. Different views of single crystal structures of **DAR** (a), **TAR** (b), **DARO2** (c), and **TARO2** (d). Visualization of overlap and packing of **DAR** (e) and **TAR** (f). THF molecules are omitted for clarity in the **TAR** crystal structures. g) d_{norm} Hirshfeld surface for **DAR**. h) Fingerprint plot for **DAR**. Reproduced with permission of ref. 77 © 2018, the Royal Society of Chemistry.

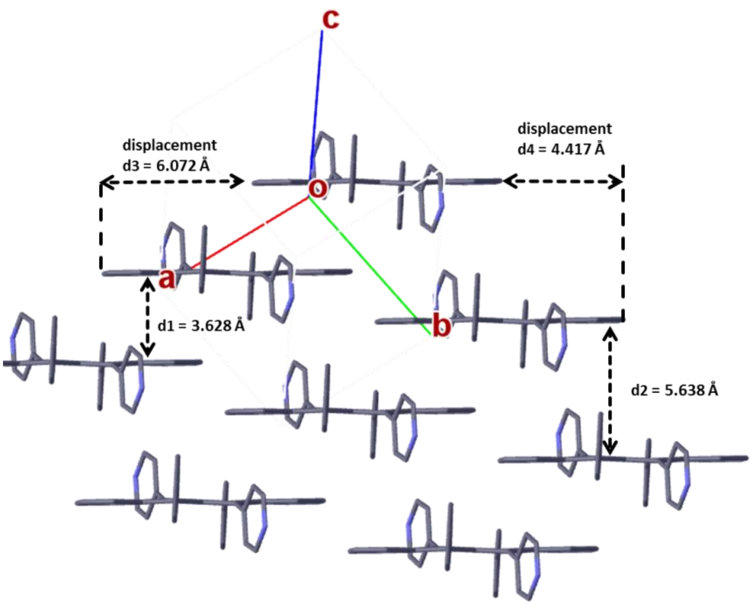

Figure 18. Illustration of the lattice parameters within **ab** layer of **DAR** crystal. The π-π stacking distances along **a** and **b** direction are estimated to be around 3.6 Å and 5.6 Å respectively; the long-axis displacements of adjacent molecule along **a** and **b** direction are estimated to be around 6.1 Å and 4.4 Å respectively. Reproduced with permission of ref. 77 © 2018, the Royal Society of Chemistry.

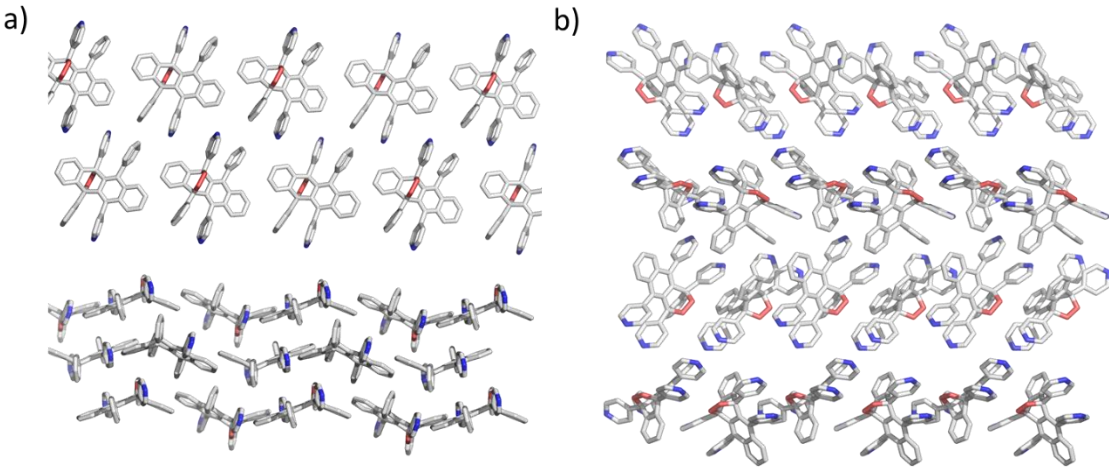

Figure 19. Examples for the visualization of packing of **DARO2** (a) and **TARO2** (b). Reproduced with permission of ref. 77 © 2018, the Royal Society of Chemistry.

Quantum chemical calculations show the influence of the pyridine units on the energetic position of HOMO and LUMO (see Figure 20). Optimized geometries of rubrene, **DAR**, and **TAR** are twisted as reported for rubrene.[96] The FMOs are stabilized by 0.3 eV (**DAR**) and 0.6 eV (**TAR**) each in comparison to rubrene, pointing to an effect of around 0.15 eV per nitrogen atom, fairly additive.

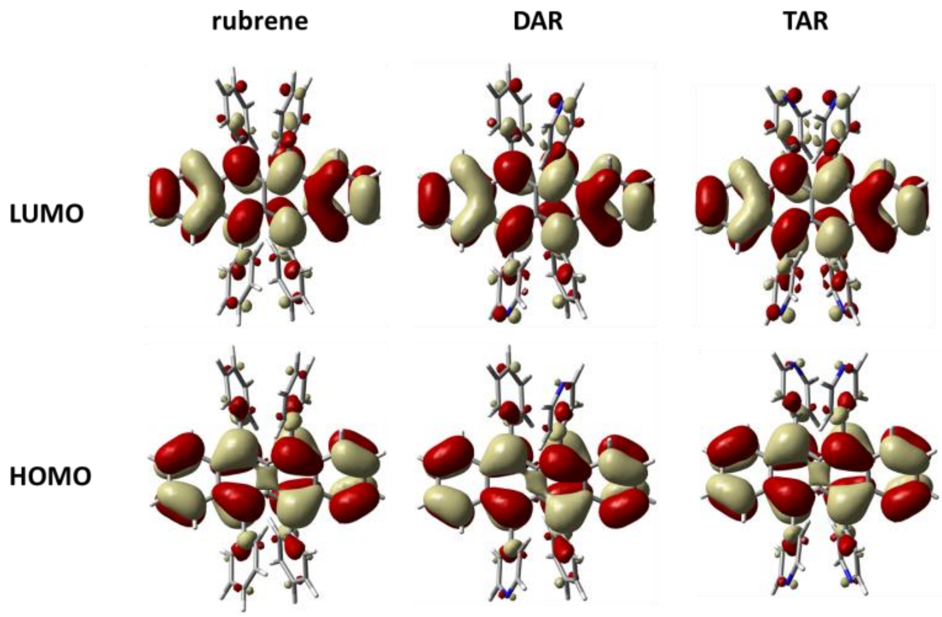

Figure 20. Quantum-chemical calculations of the FMOs (LUMOs Top, HOMOs bottom) for rubrene, **DAR**, and **TAR** (Gaussian 09 B3LYP/6-311++G**//BP86/def2-TZVP).[93] Reproduced with permission of ref. 77 © 2018, the Royal Society of Chemistry.

2.4 Conclusion

We have introduced two or four pyridine substituents to rubrene and have modulated its frontier orbital positions, without touching the tetracene unit, working on the peripheral aromatic substituents. While this concept is not new, pyridine-substituted rubrenes have to our knowledge never been prepared and **27** is a versatile starting material for the introduction of different substituents to rubrene. In future we will exploit this concept further and introduce other electron accepting substituents into the rubrene core and investigate their structure, optical and electronic properties with the final goal to develop a high mobility n-channel material based on the rubrene framework.

Chapter 3. 5,7,12,14-Tetrafunctionalized 6,13-Diazapentacenes

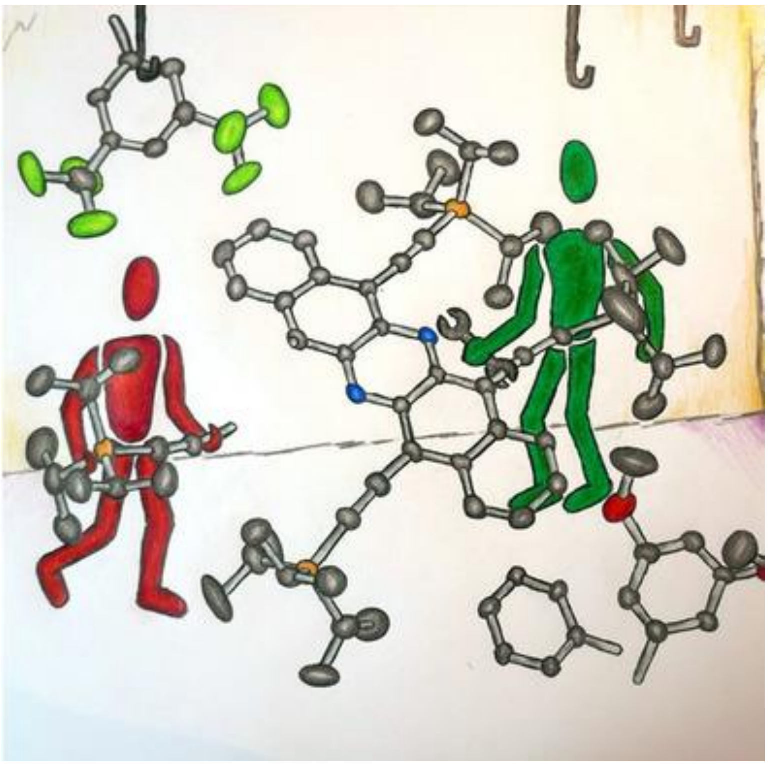

Figure 21. Chemical structures of 5,7,12,14-tetrafunctionalized diazapentacenes (**TDAP**s). Adapted with permission of ref. 97 © 2020, Wiley-VCH.

3.1 Introduction and Research Purpose

Azaacenes[98-100] have aroused great interest, starting with the synthesis of the superb n-channel semiconductor **TAP**.[16, 101] This interest was further stoked by new syntheses to construct azapentacenes[102] to azaheptacenes,[103] by Pd-catalyzed formation of embedded *N,N'*-dihydropyrazines,[104, 105] and the availability of several privileged, TIPS-substituted aromatic ortho-diamines.[102] These approaches lead to disubstituted azaacenes. The synthesis of higher substituted azaacenes (tetrasubstituted, hexasubstituted, etc.) is not common, although for their hydrocarbon analogues,[106, 107] some derivatives have recently been explored, including per-substituted species furnishing twistacenes.[108-112] Herein, we decorate the diazapentacene framework by fourfold Suzuki-Miyaura coupling.

3.2 Synthesis of 5,7,12,14-Tetrafunctionalized 6,13-Diazapentacenes

Reaction of the literature known tetrabromide **104**[113] with different boronic acids under standard palladium catalysis conditions gave the crude *N,N'*-dihydro-intermediates **2a-c**, which were not further characterized but immediately oxidized by MnO_2 into the target compounds **3a-c** (53-79% overall yield). The dihydro-species **104** is much more soluble (and does not re-oxidize the intermediately formed Pd^0 species) than its oxidized heteroacene counterpart and was employed in our coupling reactions. Attampts to synthesize **3d** from **104** through the Sonogashira reaction failed (see Scheme 16 for conditions). Fortunately, my colleague, Hendrik Hoffmann, synthesized tetrayne **3d** successfully by reacting tetraone **105** with an

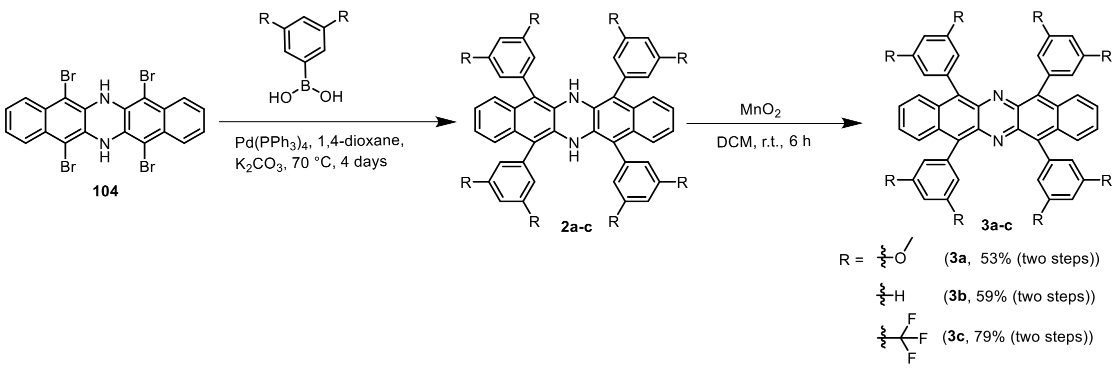

Scheme 15. Synthesis of substituted diazapentacenes **3a-c**.

excess of the lithium salt of TIPS acetylene and then treating the intermediate with $SnCl_2$ (see Scheme 17).[114, 115]

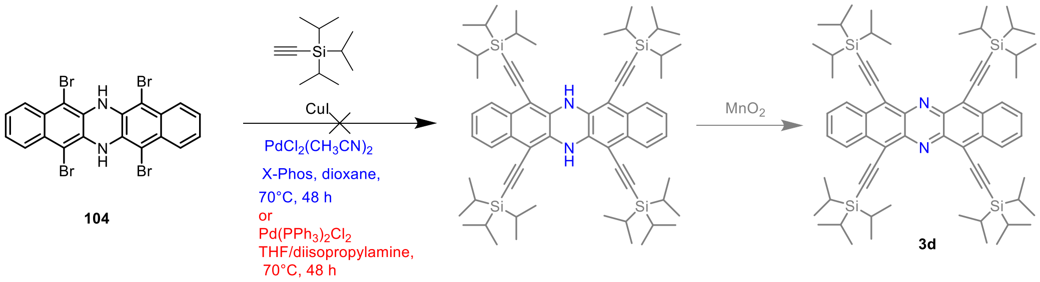

Scheme 16. Failed synthetic route to alkynylated **3d**.

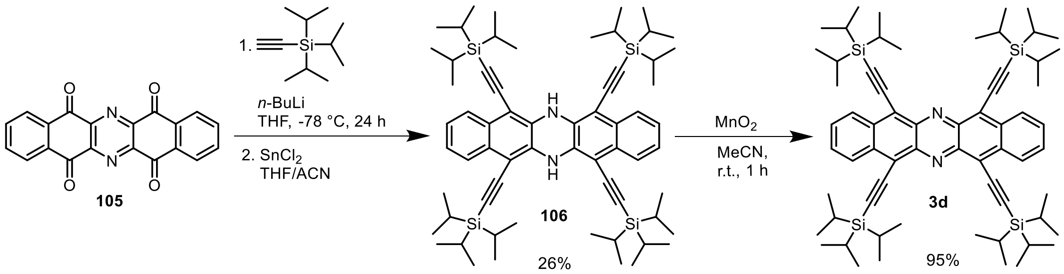

Scheme 17. Synthesis of alkynylated **3d**.

3.3 Results and Discussion

Figure 22 displays the normalized absorption spectra of nonfluorescent **3a-d** (see Table 3). We note that **3a-c** display almost identical UV-Vis spectra despite the significant electronic

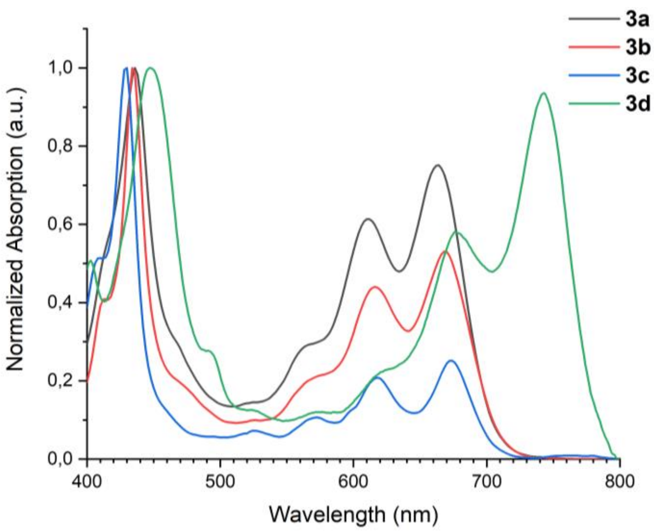

Figure 22. Normalized absorption spectra of **3a-3d** measured in DCM. Adapted with permission of ref. 97 © 2020, Wiley-VCH.

differences in the substituents of **3a-c**. The substituents only exert an inductive effect but do not increase the conjugation — not unexpected, because the arene groups are heavily twisted with respect to the diazapentacene backbone. Compound **3d** with the four alkyne groups displays a 70-80 nm red-shifted absorption at 743 nm, a consequence of the conjugation of the four alkyne groups with the diazapentacene nucleus (see Scheme 17).[116]

Table 3. Photophysical and electrochemical properties. Adapted with permission of ref. 97 © 2020, Wiley-VCH.

Comp.	Abs_{max}[a] (nm)	E_{ox1}[b] (V)	E_{red1}[b] (V)	Ionization potential (eV) meas.[c]/cal.[d]	Electron affinity (eV) meas.[c]/cal.[d]	Gap (eV) meas.[e]/cal.[e] /opt.[f]
3a	664	0.64	-1.33	-5.44/-5.08	-3.47/-2.98	1.97/2.10/1.69
3b	668	0.63	-1.32	-5.43/-5.33	-3.48/-3.25	1.95/2.08/1.68
3c	674	1.13	-1.14	-5.93/-6.27	-3.66/-4.23	2.27/2.04/1.72
3d	743	0.77	-0.96	-5.57/--	-3.84/--	1.73/--/1.59
56	621[54]	-	-	--/-4.80[54]	--/-2.59[54]	--/2.21/1.88[54]

[a] Absorption peaks in DCM; [b] The first oxidation and reduction potentials measured in CV using ferrocene/ferrocenium as the reference redox system and internal standard (−4.8 eV); [c] Calculated from CV measurements (E_{HOMO} = –4.80 eV – E_{ox1}; E_{LUMO} = –4.80 eV – E_{red1}); [d] Calculated with Gaussian 09 B3LYP/6-311++G**//DFT/B3LYP/6-31+G**;[93] [e] Estimated from E_{HOMO} and E_{LUMO} (E_{gap} = E_{LUMO} – E_{HOMO}); [f] Estimated from absorption onset measured in DCM.

Compounds **3a-d** were investigated by cyclic voltammetry (see Table 3). They can be both oxidized and reduced, suggesting ambipolar behavior.[117-119] As expected, **3c** and **3d** display the highest oxidation potentials. The effect is particularly strong for **3c**, featuring eight CF_3 groups. The same trend is observed for the reduction potentials, which are -1.14 V for **3c** and -0.96 V for **3d**. The electron affinity for **3c** and **3d** are estimated to be -3.7 and -3.8 eV, respectively. Although the alkyne substituents influence HOMO and LUMO position differently and lead to a decreased electrochemical and optical gap, electron withdrawing substituents on the aryl groups in **3c** stabilize both FMOs similarly. In comparison to 5,7,12,14-tetraphenylpentacene **56** (see Figure 23),[54] nitrogen substitutions lead to the decreased FMO energy levels, as was expected.

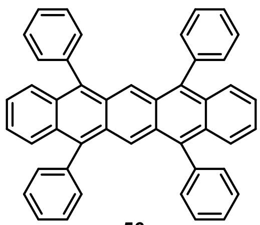

Figure 23. Chemical structures of 5,7,12,14-tetraphenylpentacene **56**.

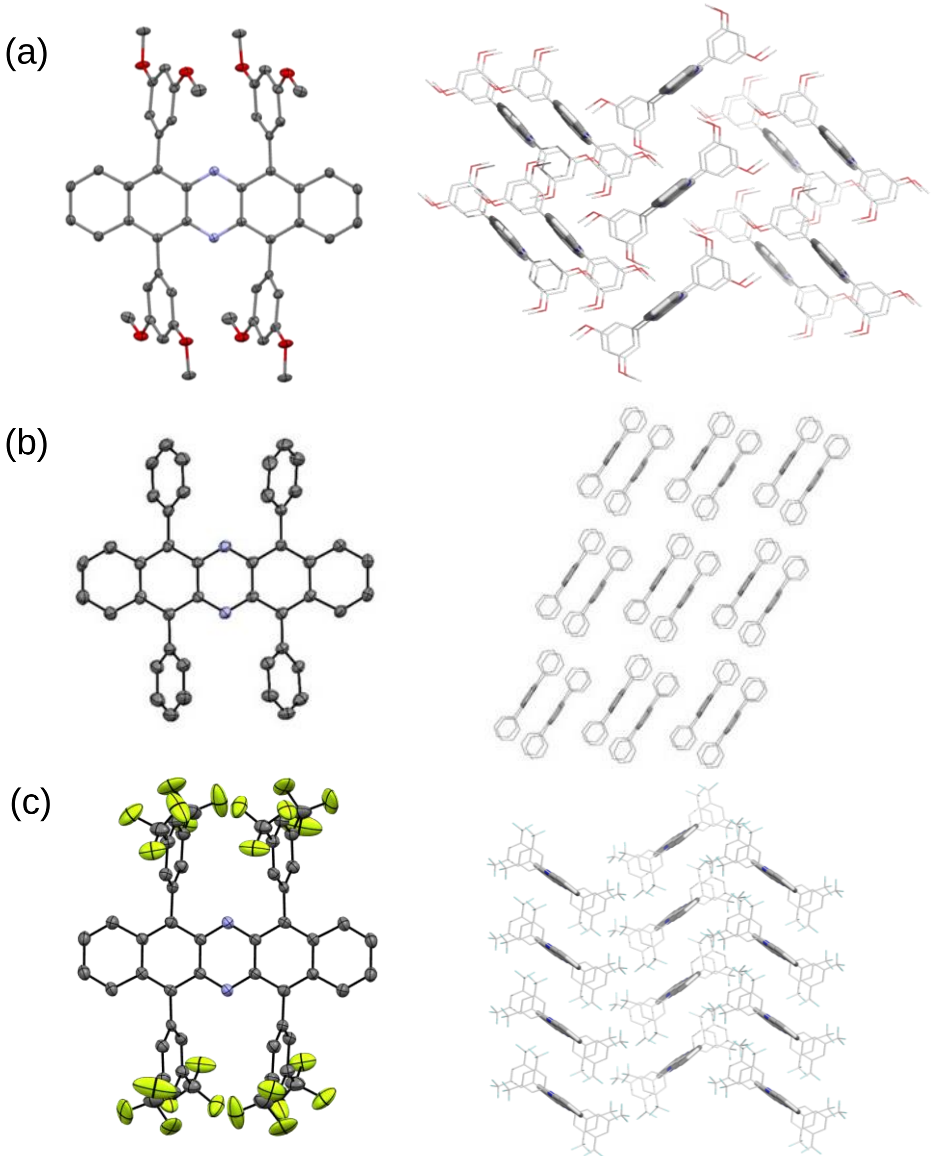

Figure 24. Molecular structures and solid-state packings of (a) **3a**, (b) **3b**, and (c) **3c**. Adapted with permission of ref. 97 © 2020, Wiley-VCH.

Compounds **3a-c** formed suitable specimens useful for X-ray single crystal analysis (see Figure 24). The diazapentacene backbone of **3a-c** is planar, and the four aryl groups are oriented parallel to each other and considerably twisted with respect to the diazapentacene (dihedral angles: 63° and 65° for **3a**; 57° and 61° for **3b** and 66° and 71° for **3c**). The molecules of **3a** and **3c** pack in a herringbone pattern with no π-π overlap between the molecules. The molecules of **3b** pack in π-π stacked dimers with an interplanar distance of 3.60 Å, which are arranged in one-dimensional slipped stacks.

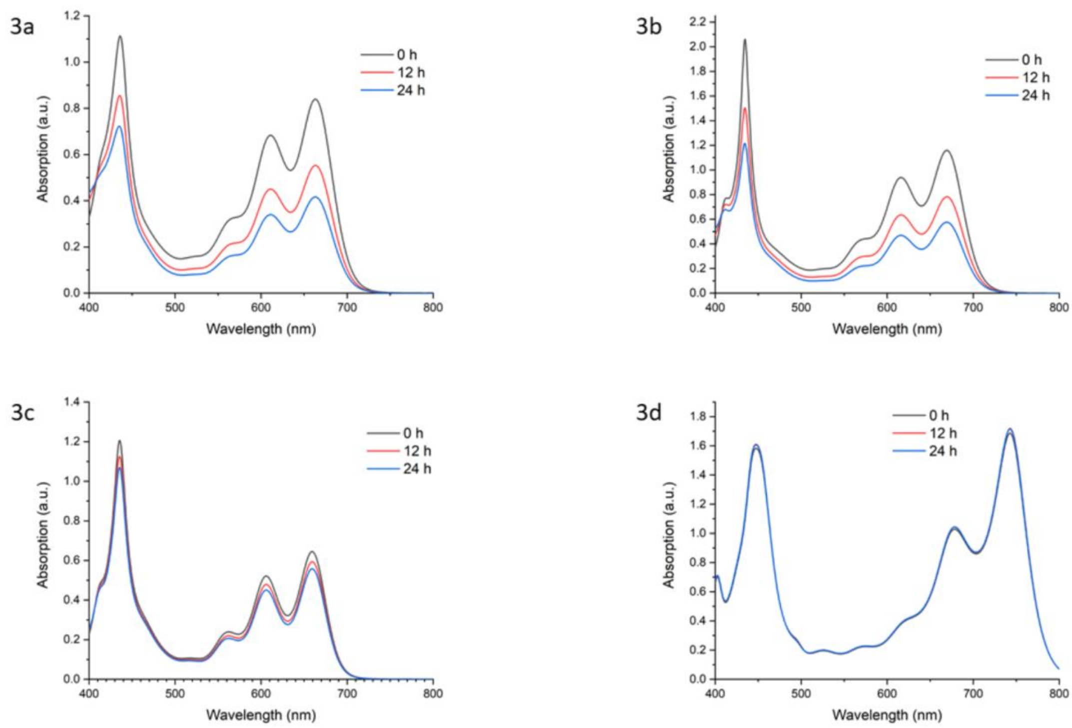

Figure 25. Normalized time-dependent absorption spectra of **3a-d** measured in DCM. Adapted with permission of ref. 97 © 2020, Wiley-VCH.

Next issue to address was stability of the diazapentacenes compared to their hydrocarbon analogues. The stability of **56** was assessed through UV-Vis measurements in dilute solution — it photooxidizes in toluene[107] or DCM[54] under ambient conditions (light and air) in less than 20 min via endo-peroxide formation. Nitrogen substitutions protect the system. As displayed in Figure 25, the absorption profile of alkynylated **3d** remains unchanged for 24 h, photooxidation of **3a-c** depends on the electronic demand of the aryl substituents. Electron-deficient trifluoromethyl groups stabilize the system most (14% absorption loss after 24 h), but even electron-rich, dimethoxy-substituted **3a** is still fairly stable (50% loss after 24 h).

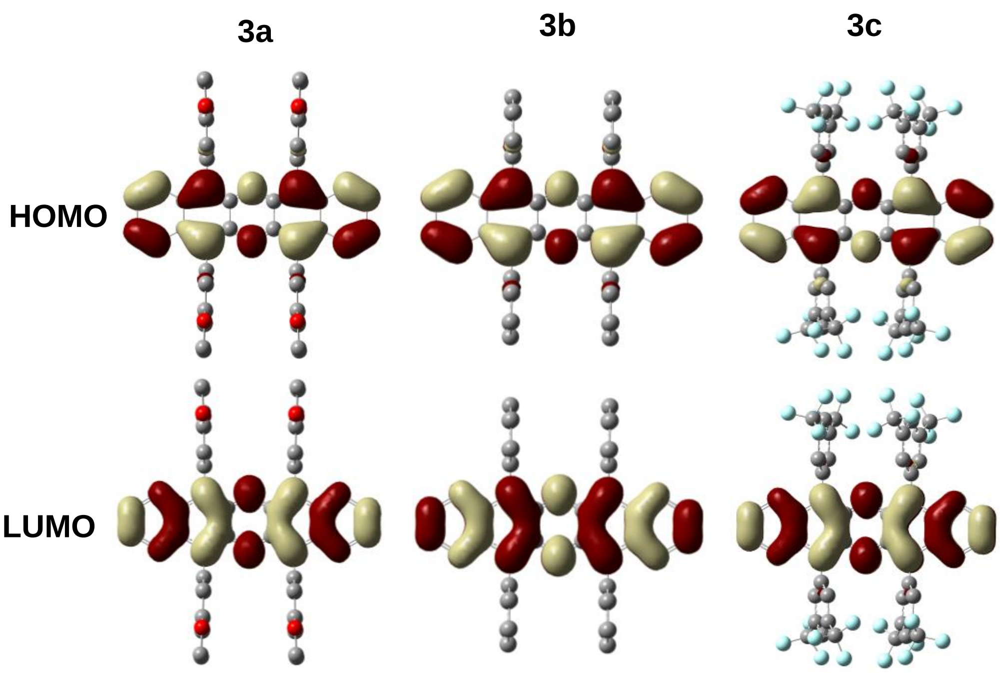

Figure 26. HOMOs and LUMOs of **3a**, **3b**, and **3c** calculated at DFT/B3LYP/6-311++G**// DFT/B3LYP/6-311+G** level of theory.[93] Adapted with permission of ref. 97 © 2020, Wiley-VCH.

Figure 26 displays the FMOs of **3a-c**. The backbones of **3a-c** are planar in computationally optimized geometries. Interestingly, similar to rubrene and azarubrenes, both HOMOs and LUMOs are distributed on the acene cores for all three compouds, regardless of their different side groups. Among three compounds, **3a** exhibits the shallowest calculated HOMO (-5.08 eV, see Table 3) and LUMO (-2.98 eV) energies due to the electron-donating ability of eight OCH_3 groups, while **3c** shows the lowest-lying HOMO (-6.27 eV) and LUMO (-4.23 eV) energies because of the strong electron-withdrawing ability of eight OCF_3 groups.

To initially evaluate the potential of the newly synthesized tetrasubstituted diazapentacenes as n-channel organic semiconductors, OFETs were fabricated by PVD method of **3b**. The compound showed n-type charge transport behavior with a maximum electron mobility of 3.2 $\times 10$ $cm^2V^{-1}s^{-1}$, a threshold voltage of 30 V and an on/off ratio on the level of 10^4. The average charge carrier mobilities calculated for twelve transistors were $1.76\times10^{-3}\pm0.51$ $cm^2V^{-1}s^{-1}$. In contrast, for the parent unsubstituted 6,13-diazapentacene hole mobilities in a range of 10^{-5} were reported.[101] This finding highlights beneficial impact of the 5,7,12,14-substitution pattern on n-channel device performance and constitutes an asset for our future efforts in this area.

3.4 Conclusion

In conclusion, we developed symmetrically tetrafunctionalized 6,13-diazapentacenes starting from the *N,N'*-dihydro-tetrabromide **104**. The compounds are stabilized with respect to photooxidation, and the tetraphenyl-substituted representative **3b** shows n-channel behavior. In the future, we will expand this concept to 6,7,14,15-tetraazahexacene and to 7,16-diazaheptacene. Herein, the solubility of the precursors might be a problem, but the prospect of stable diazaheptacenes is particularly attractive.

Chapter 4. Stable Radical Cations of 7,14-Dimesityl-5,12-Dihydro-5,12-Diaryldiazapentacenes

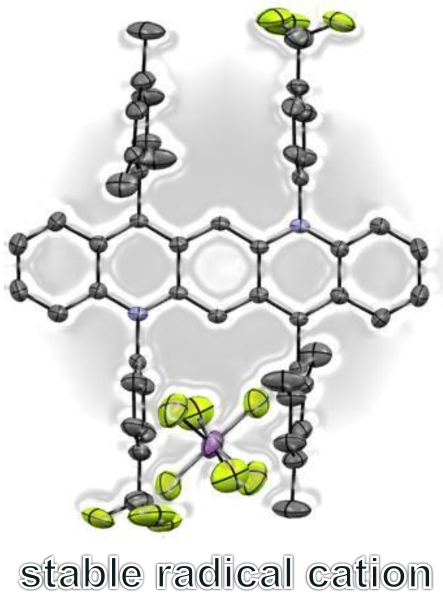

Figure 27. Single crystal structure of **Quino-CF$_3$$^{+•}$**. Adapted with permission of ref. 120 © 2020, Wiley-VCH.

4.1 Introduction and Research Purpose

Acenes and *N*-heteroacenes[98, 121-124] play a fundamental role in chemistry, material science and organic electronics, particularly as charge transport materials.[125] Larger N-heteroacenes are easily reduced into their *N,N'*-dihydro-compounds, much longer known and more stable than the *N*-acenes themselves. Yet, the chemistry of the reduced compounds is much less explored, even though some data were reported by Miao,[52, 126] Beckert,[127] and Koutentis,[128] but the redox-chemistry of these materials is surprisingly sparse.

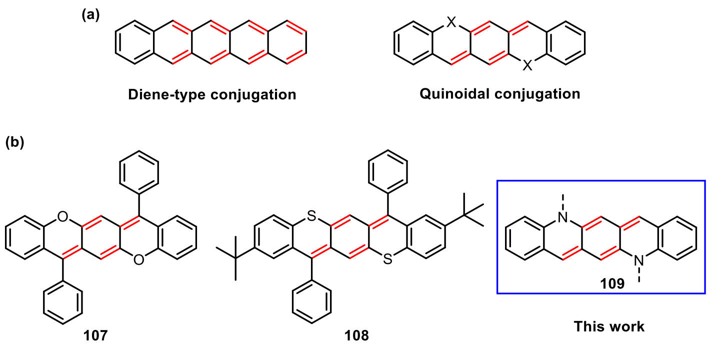

Figure 28. a) Structure patterns of Diene-like conjugation and Quinoidal conjugation; b) Chemical structures of **107**, **108**, and **109**.

Chi et al. investigated sulfur- and oxygen-embedded quinoidal conjugated acene analogues, **107** and **108** (see Figure 28).[129-131] They demonstrated that their dications display properties similar to those of the acenes with similar length, but for the larger representatives these dications are — contrary to the isoelectronic acenes themselves — isolable, stable and can be characterized. In this contribution, we extend this concept to *N*-heterocycles.

Herein we describe the synthesis and characterization of novel *N,N'*-diaryldiazapentacenes in their neutral, radical cation, and closed-shell dication states, spectroscopically matching the dianion, radical anion, and neutral **TAP**.[71]

4.2 Synthesis of Neutral Compounds, Radical Cations, and Dications of 7,14-Dimesityl-5,12-Dihydro-5,12-Diaryldiaza-pentacenes

Starting from quinacridone, copper catalyzed *N*-arylation with different 4-iodoarenes gave **QA-tBu**, **-OMe**, and **-CF$_3$** in excellent yields. A double nucleophilic addition reaction of the organolithium compound formed from bromomesitylene and *n*-BuLi followed by treatment with $SnCl_2$ in THF furnished three **Quino**-structures in 32-39% yield. Oxidation with $AgSbF_6$ (1 eq.) gave the monocations **Quino**s$^{+\cdot}$ as the dark brown solids. To obtain the dications **Quino**s^{2+}, the stronger oxidant $NO^+PF_6^-$ is employed.

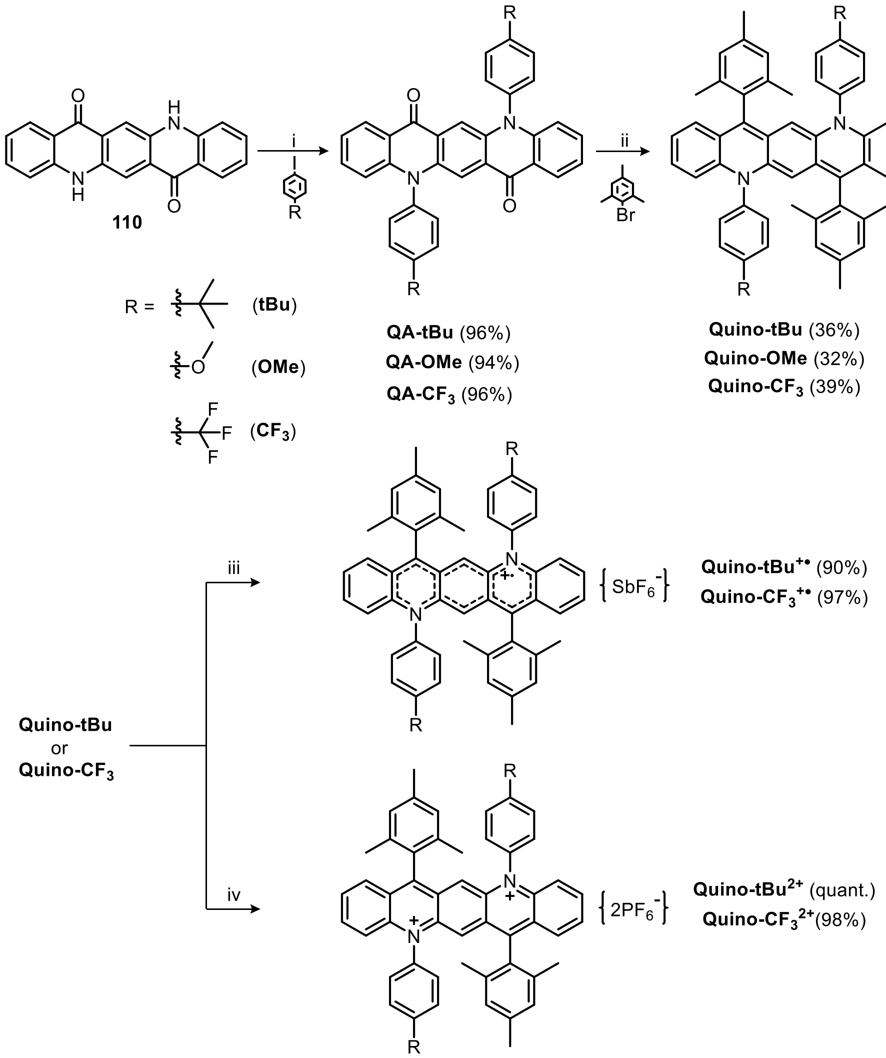

Scheme 18. Synthetic details towards nitrogen-embeded quinodial pentacenes and their corresponding radical cations and dications. i) 2,2,6,6-Tetramethyl-3,5-heptanedione, K_2CO_3, CuI, DMF, 146 ℃, 36 h; ii) (a) *n*-BuLi, THF, -78 ℃ to r.t., 12 h; (b) $SnCl_2$, THF, r.t. 1 h iii) $AgSbF_6$, DCM, r.t., 12 h; iv) $NO^+PF_6^-$, DCM, r.t., 12 h. Adapted with permission of ref. 120 © 2020, Wiley-VCH.

4.3 Results and Discussion

As shown in Figure 29, the **Quinos**$^{+\cdot}$ display intense electron spin resonance (ESR) spectra without fine-structures (g_e = 2.0017).

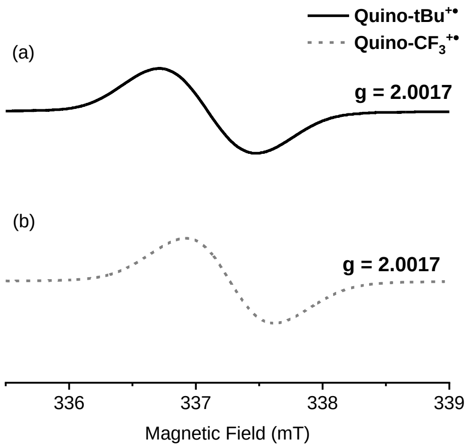

Figure 29. ESR spectra of a) **Quino-tBu**$^{+\cdot}$ and b) **Quino-CF$_3$**$^{+\cdot}$ recorded in DCM at r.t.. Adapted with permission of ref. 120 © 2020, Wiley-VCH.

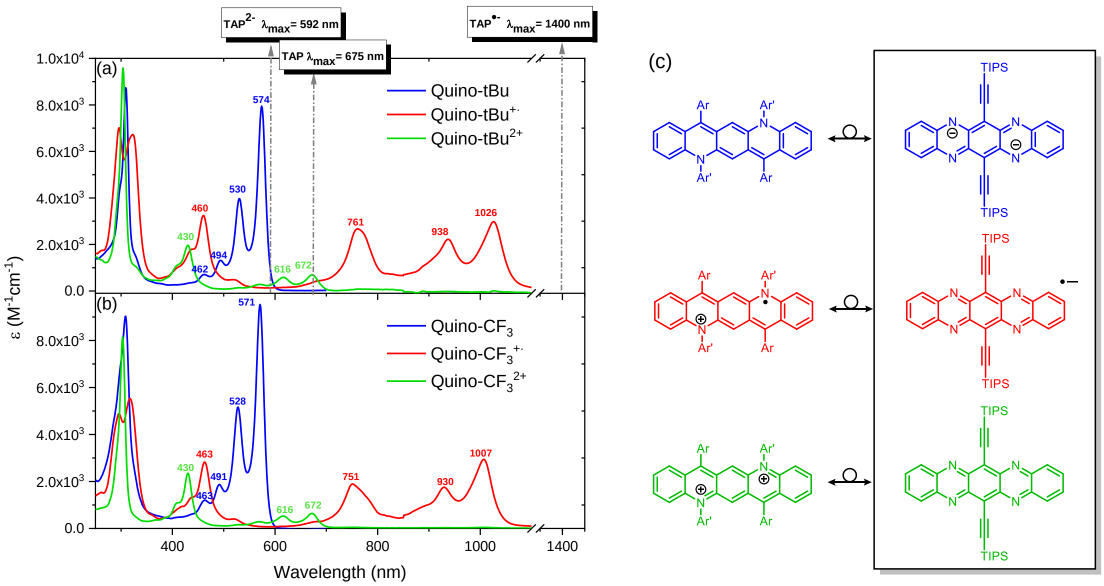

Figure 30. Absorption spectra of a) **Quino-tBu**, **Quino-tBu**$^{+\cdot}$, and **Quino-tBu**$^{2+}$ (dotted arrows: maximum absorptions of **TAP**, **TAP**$^{\cdot-}$, and **TAP**$^{2-}$); b) **Quino-CF$_3$**, **Quino-CF$_3$**$^{+\cdot}$, and **Quino-CF$_3$**$^{2+}$ measured in DCM; c) Comparison of the electronic properties of **Quino**s and of **TAP**. Adapted with permission of ref. 120 © 2020, Wiley-VCH.

Figure 30a and 30b display the UV-vis spectra of the three oxidation states of **Quino-tBu** and **Quino-CF$_3$**. They are very similar, as expected. The neutral **Quino-tBu** displays an absorption spectrum with a maximum at 574 nm. Upon oxidation into the radical cation, a large red-shift to 1026 nm is observed. The dication on the other hand displays an absorption spectrum with a λ_{max} of 672 nm. These spectra resemble the UV-vis spectra that are observed for other azaacenes but in the sequence dianion-radical anion-neutral species (cf. absorption maxima sketched for **TAP** in Figure 30a). Apparently, these species are isoelectronic (see Figure 30c; **Quino/TAP^{2-}** 24 e$^-$, **Quino$^{+\cdot}$/TAP$^{-\cdot}$** 23 e$^-$, **Quino^{2+}/TAP** 22 e$^-$ per backbone).[132-134]

Table 4. Comparison of most significant single excitation contributions of the bright states (BS) for **Quino-CF$_3$** versus **TAP^{2-}**, **Quino-CF$_3^{+\cdot}$** versus **TAP^{1-}**, and **Quino-CF$_3^{2+}$** versus **TAP**. The molecular orbital (MO) numbers are indicated below the MO pictures, where the MO numbers in respective neutral specie are written in parentheses. The **Quino-CF$_3$** and **TAP** species were computed at G16 B3LYP/6-311G**/DCM and CAM-B3LYP/6-311++G**/THF level of theory,[135] respectively. Adapted with permission of ref. 120 © 2020, Wiley-VCH.

State	Most Significant Single Excitation Contribution					
	Quino-CF$_3$			TAP^{2-}		
BS1	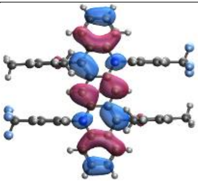 **HOMO** (HOMO)	→	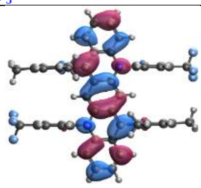 **LUMO** (LUMO)	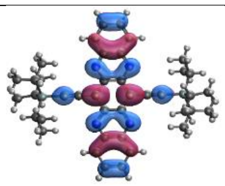 **HOMO** (LUMO)	→	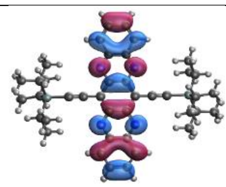 **LUMO** (LUMO+1)
	Quino-CF$_3^{+\cdot}$			TAP^{1-}		
BS1	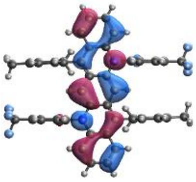 **HOMOβ** (HOMO-1)	→	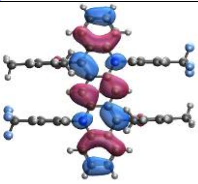 **LUMOβ** (HOMO)	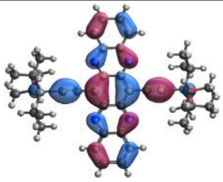 **HOMOβ** (HOMO)	→	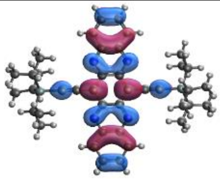 **LUMOβ** (LUMO)
BS2	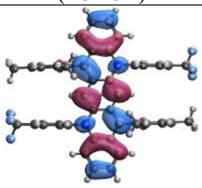 **HOMOα** (HOMO)	→	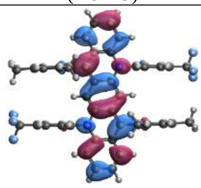 **LUMOα** (LUMO)	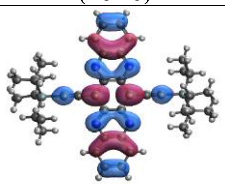 **HOMOα** (LUMO)	→	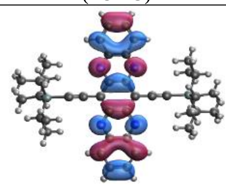 **LUMOα** (LUMO+1)
BS3	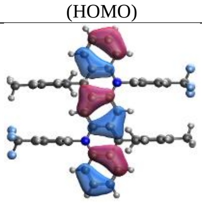 **HOMOβ-6** (HOMO-7)	→	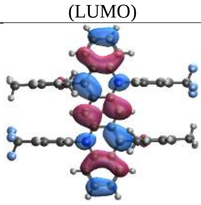 **LUMOβ** (HOMO)	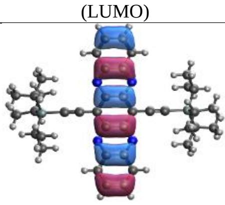 **HOMOβ-2** (HOMO-3)	→	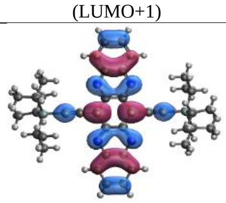 **LUMOβ** (LUMO)
	Quino-CF$_3^{2+}$			TAP		
BS1	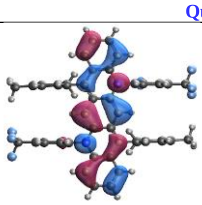 **HOMO-4** (HOMO-1)	→	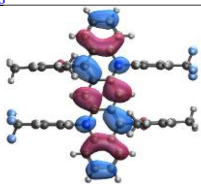 **LUMO** (HOMO)	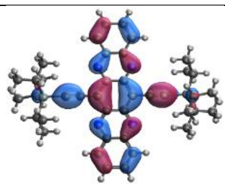 **HOMO** (HOMO)	→	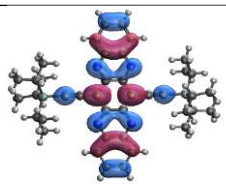 **LUMO** (LUMO)
BS2	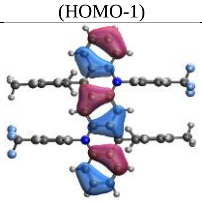 **HOMO-8** (HOMO-7)	→	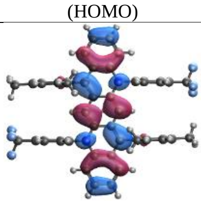 **LUMO** (HOMO)	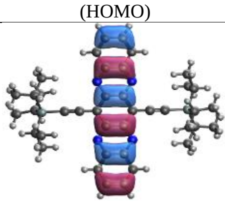 **HOMO-3** (HOMO-3)	→	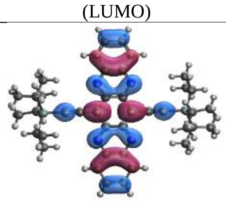 **LUMO** (LUMO)

Table 5. (TD)-DFT results at B3LYP/6-311G** level using a PCM model for DCM solvation for neutral, cationic, and dicationic **Quino-CF_3**.[135] Adapted with permission of ref. 120 © 2020, Wiley-VCH.

Molecules	Quino-CF_3				Quino-CF_3^+				Quino-CF_3^{2+}			
Ground State												
E	-2714.9418664				-2714.7860648				-2714.5917678			
IP	**0**				4.2396				9.5267			
E_{HOMO}	-4.353				-5.393 (α), -6.414 (β)				-7.437			
E_{LUMO}	-2.007				-3.145 (α), -4.124 (β)				-5.179			
$E_{H\text{-}L}$	2.346				2.247 (α), 2.597 (β)				2.258			
Excited State												
Bright state	**State**	**eV**	**nm**	**f**	**State**	**eV**	**nm**	**f**	**State**	**eV**	**nm**	**f**
BS1	**S1**	2.22	559	0.9445	**D1**	1.48	840	0.1263	**S5**	1.90	653	0.1055
Contribution	HOMO -> LUMO, 97%				HOMO-β -> LUMO-β, 79%				HOMO-4 -> LUMO, 79%			
BS2					**D2**	1.63	761	0.2554	**S12**	3.07	404	0.6858
Contribution					HOMO-α -> LUMO-α, 78%				HOMO-8 -> LUMO, 92%			
BS3					**D10**	2.83	437	0.3435				
Contribution					HOMO-β-6 -> LUMO-β, 78%							

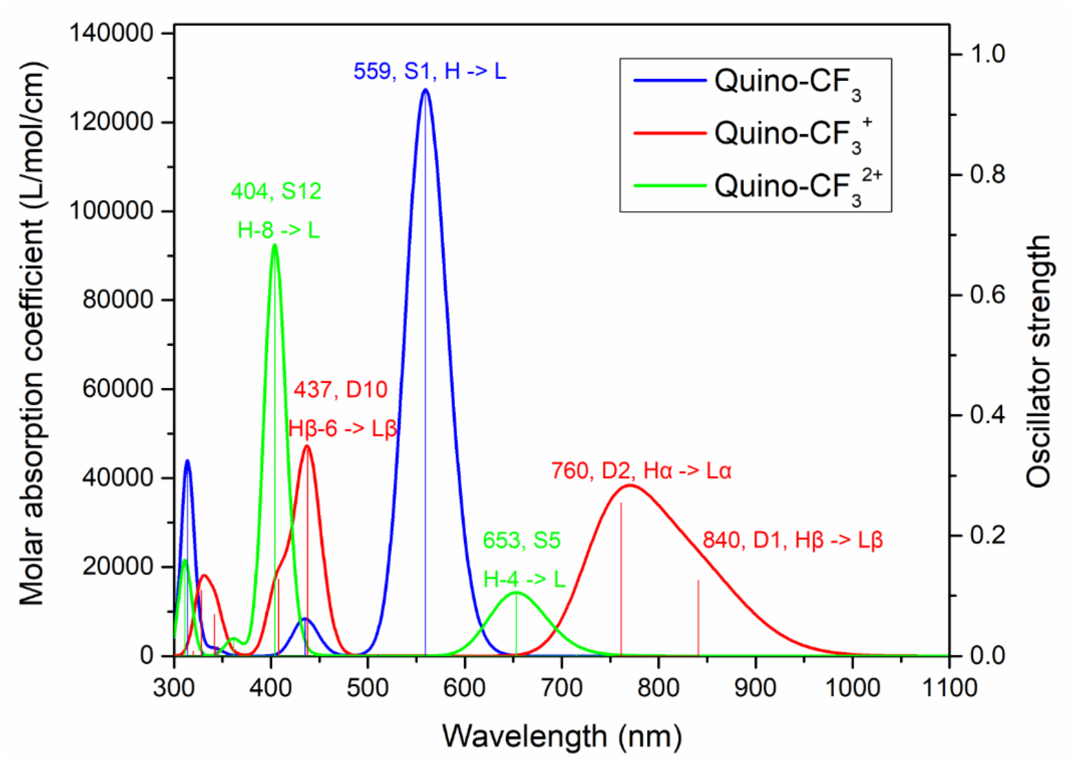

Figure 31. Simulated absorption spectra of neutral, cationic, and dicationic **Quino-CF_3** computed at TD-DFT/B3LYP/6-311G** level of theory.[135] All spectra were broadened using Gaussian functions with a full-width at half maximum of 0.2 eV. Adapted with permission of ref. 120 © 2020, Wiley-VCH.

To rationalize the experimental results, we performed quantum chemical calculations of the vertical excited states at TD-DFT/B3LYP/6-311G** level of theory. As can be seen from Figure 31, the simulated absorption spectra of the **Quino-CF_3** species are consistent with the experiments. The lowest electronic transition of **Quino-CF_3** is a HOMO->LUMO transition with the excitation energy of 2.22 eV located at 559 nm in the simulated absorption spectrum. Due to neglect of vibrational effects, the broadening of absorption bands is not reproduced. The lowest absorption band of **Quino-$CF_3^{+\cdot}$** is red-shifted to the near-infrared region with contributions from two electronic transitions of HOMOα->LUMOα and HOMOβ->LUMOβ character. Furthermore, the first bright state (BS1) of **Quino-CF$_3$$^{2+}$** lies in between those of **Quino-CF$_3$** and **Quino-CF$_3$$^{+\cdot}$** with a λ_{max} of 653 nm. Therefore, the first absorption band of **Quino-CF$_3$** is blue-shifted compared to that of its cationic and dicationic species. A similar blue-shift feature also exhibits in dianionic **TAP^{2-}**, when compared with **TAP** and **TAP$^{-\cdot}$**. Hence, the character of each vertical transition for **Quino-CF$_3$** and **TAP** is compared and shown in Table 4. It can be easily found that **Quino/TAP^{2-}**, **Quino$^{+\cdot}$/TAP$^{-\cdot}$**, and **Quino^{2+}/TAP** share common transition characters. For example, the most important contribution to the BS1 of **Quino-CF$_3$** is a HOMO to LUMO transition, the BS1 of **TAP^{2-}** is analogously also mainly a HOMO-LUMO transition with similar molecular orbital shapes. Thus, the resemblance of the peak position in the absorption spectra and the similar characteristics of the electronic transitions corroborate the isoelectronic properties of **Quino**/**TAP^{2-}**, **Quino$^{+\cdot}$/TAP$^{-\cdot}$**, and **Quino^{2+}**/**TAP**.

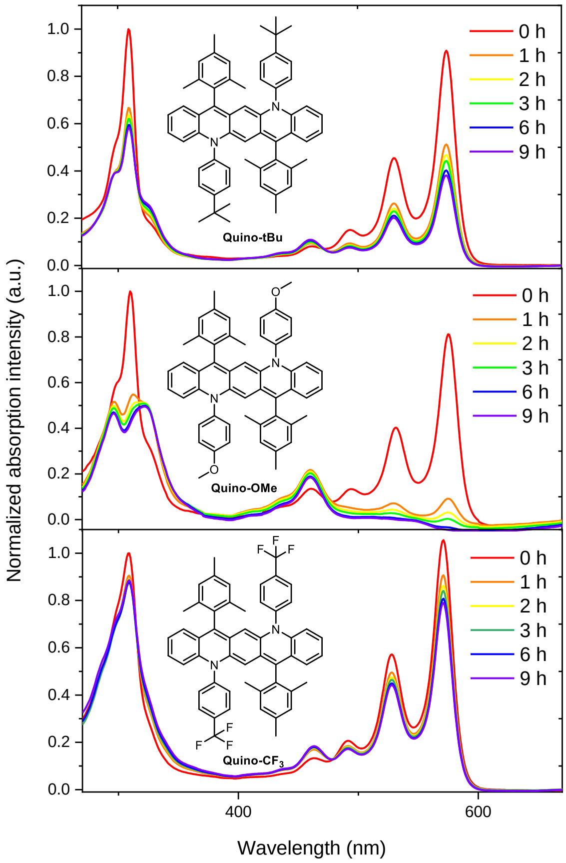

Figure 32. Time-dependent absorption spectra of **Quino-tBu**, **Quino-OMe**, and **Quino-CF$_3$** measured in DCM under ambient conditions. Adapted with permission of ref. 120 © 2020, Wiley-VCH.

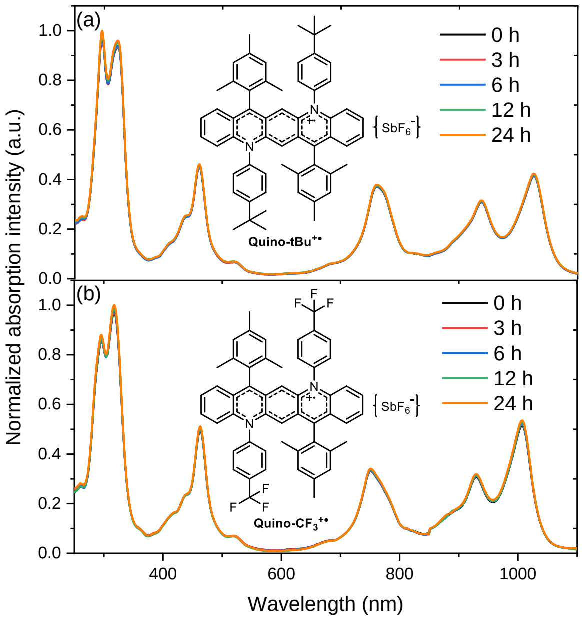

Figure 33. Time-dependent absorption spectra of a) **Quino-tBu**$^{+\bullet}$ and b) **Quino-CF$_3$**$^{+\bullet}$ measured in DCM under ambient conditions. Adapted with permission of ref. 120 © 2020, Wiley-VCH.

In addition, all three neutral **Quino** compounds are stable in the solid state. In DCM, under ambient conditions, the electron-rich **Quino-OMe** is the least stable (decomposition after 3 h, see Figure 32), while **Quino-CF$_3$** is much more persistent with around 20% absorption intensity loss after 9 h. Surprisingly, the **Quino**$^{+\cdot}$ species are stable and their absorption spectra (see Figure 33) in DCM remain unchanged under ambient conditions for at least 24 h.

The **Quino**-compounds are easily and reversibly oxidized at very similar potentials (see Figure 34). For **Quino-CF$_3$**, the first oxidation potential to the radical cation is located at -0.11 V and the second one to the dication is at +0.51 V (both vs. Fc/Fc$^+$). The more interesting experiment is the consecutive cyclovoltammetric reduction of the dications (example of **Quino-CF$_3$**$^{2+}$, see Figure 36). The first reduction potential of **Quino-CF$_3$**$^{2+}$ is at -0.28 V and the second one is at -0.83 V vs. Fc/Fc$^+$. This reduction is analogous to the reduction of **TAP** into the **TAP**$^{-\cdot}$ at -0.79 V and the second step is analogous to the reduction of **TAP**$^{-\cdot}$ into **TAP**$^{2-}$ (-1.23 V). As expected, the **Quino**$^{2+}$ species are more electron-accepting than the neutral compounds, in the case of the CF_3-species about 0.51 V. The second reduction is easier for the **Quino** series than for **TAP**, even if one starts from the radical cation ->neutral compound and for **TAP** from the radical anion -> dianion.

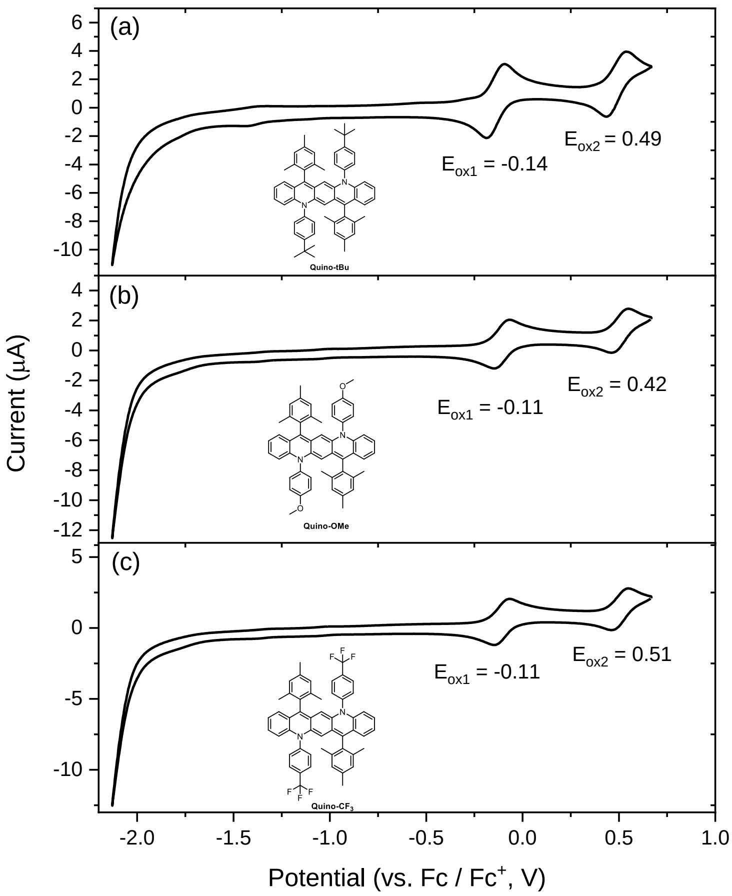

Figure 34. CVs of a) **Quino-tBu**, b) **Quino-OMe**, and c) **Quino-CF_3** using a gold working electrode, a platinum/titanium wire auxiliary electrode, and a silver wire reference electrode in degassed 0.1 M NBu_4PF_6 DCM solution. The electrode potential was externally calibrated by Fc/Fc^+ couple. Adapted with permission of ref. 120 © 2020, Wiley-VCH.

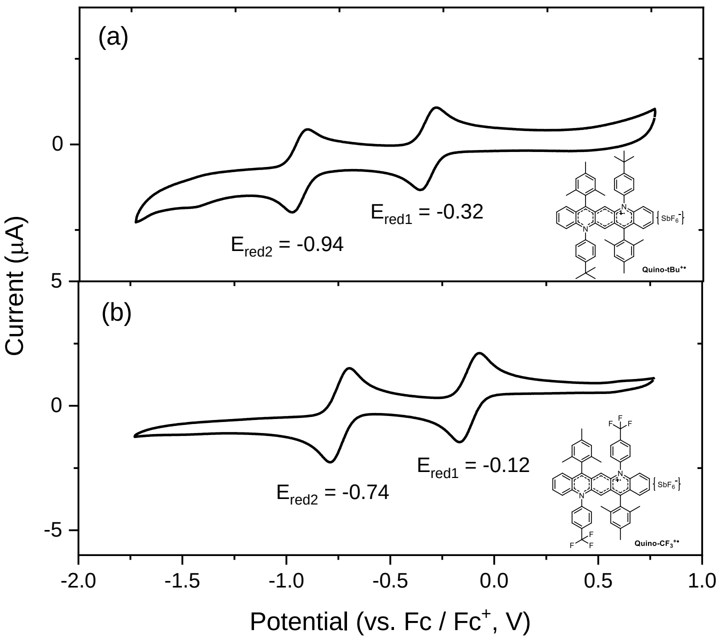

Figure 35. CVs of a) **Quino-tBu$^{+\cdot}$** and b) **Quino-$CF_3^{+\cdot}$** using a gold working electrode, a platinum/titanium wire auxiliary electrode, and a silver wire reference electrode in degassed 0.1 M NBu_4PF_6 DCM solution. The electrode potential was externally calibrated by Fc/Fc^+ couple. Adapted with permission of ref. 120 © 2020, Wiley-VCH.

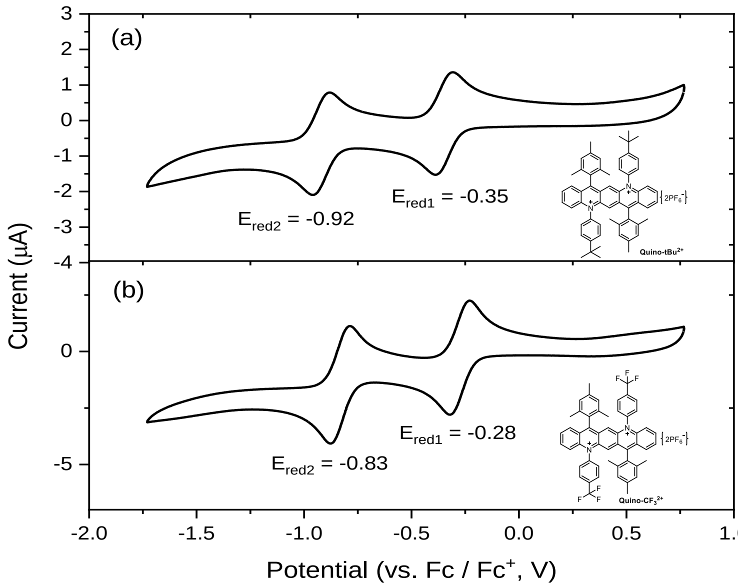

Figure 36. CVs of a) **Quino-tBu^{2+}** and b) **Quino-CF$_3$$^{2+}$** using a gold working electrode, a platinum/titanium wire auxiliary electrode, and a silver wire reference electrode in degassed 0.1 M NBu_4PF_6 DCM solution. The electrode potential was externally calibrated by Fc/Fc^+ couple. Adapted with permission of ref. 120 © 2020, Wiley-VCH.

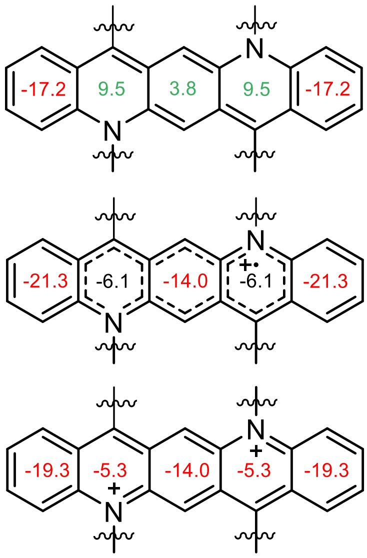

Figure 37. NICS(1)$_{zz}$ values of **Quino-CF$_3$** (top), **Quino-CF$_3$$^{+\cdot}$** (middle), and **Quino-CF$_3$$^{2+}$** (bottom) calculated at B3LYP/6-311G** level employing a PCM model for DCM solution.[135] Adapted with permission of ref. 120 © 2020, Wiley-VCH.

This facile oxidation is a testament to the formation of an aromatic system, i.e. **Quino-CF$_3$$^{2+}$**. To shed further light on this issue we performed nucleus-independent chemical shift (NICS) calculations (see Figure 37). In the neutral **Quino-CF$_3$**, NICS-values of the three interior rings are positive with the maximum value up to +9.5, yet smaller than those reported for the formally antiaromatic ring in *N,N'*-dihydrotetrazapentacene (+23, NICS (0)$_{zz}$).[136, 137] Upon monooxidation, the overall aromaticity of the system increases, and all the rings now display negative NICS-values, with the outer ones and the middle one being more aromatic than the formal pyridine-like ones. Further oxidation to **Quino-CF$_3$$^{2+}$** results in a fully aromatic system with large negative NICS values. The ^{1}H-NMR spectra of **Quino-CF$_3$** and **Quino-CF$_3$$^{2+}$** also support this conclusion. As shown in Figure 38, all the peaks of **Quino-CF$_3$$^{2+}$** are largely downfield-shifted, which indicates the formation of a more aromatic compound.

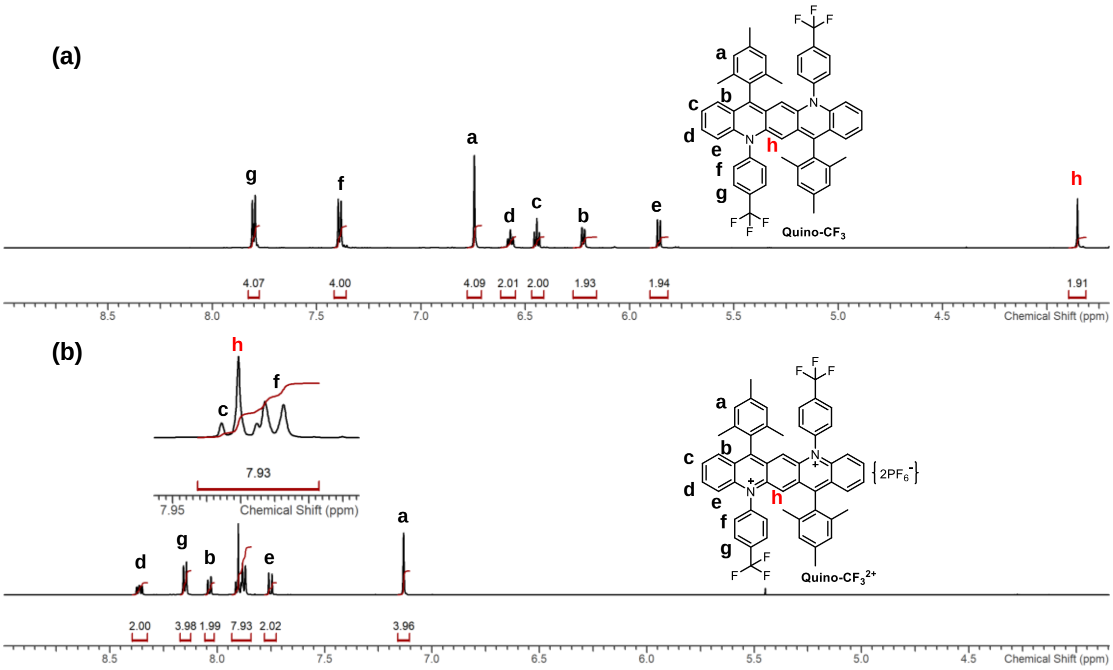

Figure 38. H[1] nuclear magnetic resonance (NMR) spectra of a) **Quino-CF$_3$** and b) **Quino-CF$_3$$^{2+}$** in aromatic region. Adapted with permission of ref. 120 © 2020, Wiley-VCH.

We obtained single crystalline specimens of **Quino-CF$_3$** and its radical cation by slow evaporation of THF and acetone respectively. Figure 39 displays the ORTEP and the bond distances of the neutral and the radical cation of **Quino-CF$_3$**. The neutral specimen displays a significant bond alternation, in accordance with the DFT-optimized geometry, that strongly suggests quinoidal character, as expected from the simple resonance structures. The quinoidal character decreases when going from the neutral compound to the radical cation, as expected. In the calculated structures (see Figure 39) this is also observed.

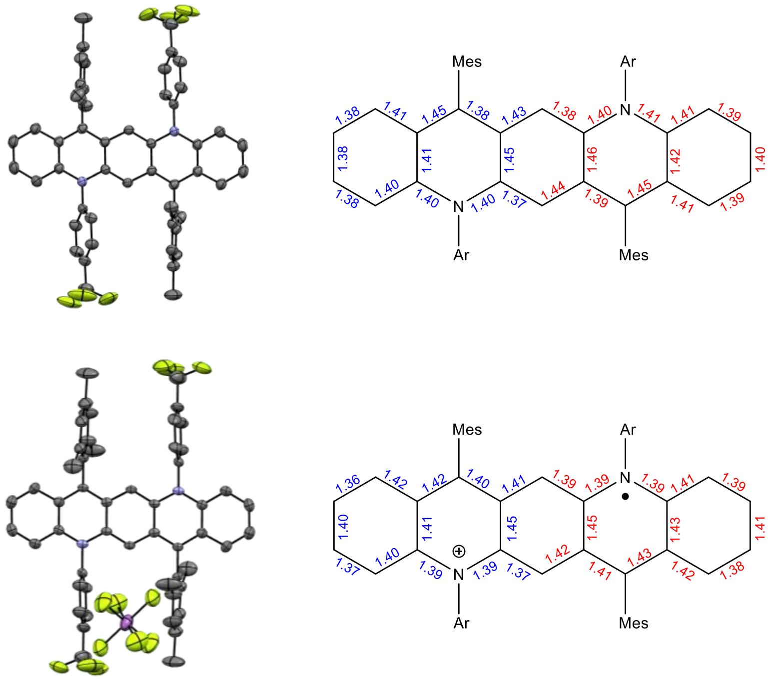

Figure 39. Single crystal structures and bond lengths (blue: derived from the crystal structures; red: calculated at the DFT/B3LYP/6-31+G** level of theory[135]) of neutral **Quino-CF_3** compound (top) and its radical cation (bottom). Adapted with permission of ref. 120 © 2020, Wiley-VCH.

4.4 Conclusion

The structural spectroscopic and quantum chemical data for the **Quino**s and their radical cations and dications display a significant resemblance to the data collected for the series of **TAP** dianion, radical anion and **TAP** as neutral compound. The resemblance is the most striking if one looks at the spectroscopic data, and while the **TAP** dianion does not feature a distinct quinoidal structure, **Quino**s do so. Yet the spectra are very similar. More remarkable is that the **TAP** radical anion and the **Quino** radical cations display red shifted spectra similar to each other suggesting an extensive isoelectronic relationship (see Figure 30). Over all, we prepared the neutral, *N,N'*-diaryldiazapentacenes and showed that they behave as neutral analogues of the known dianions of the diazapentacenes. They are easily oxidized and the radical cation is environmentally stable. In the future we will prepare *N,N'*-diaryldiazapentacenes with tailored packing behavior that should function as attractive “Ersatz”-tetraazapentacenes.[138]

Chapter 5. Synthesis and Characterization of Stable *N,N'*-Diarylated Dihydrodiazaacene Radical Cations

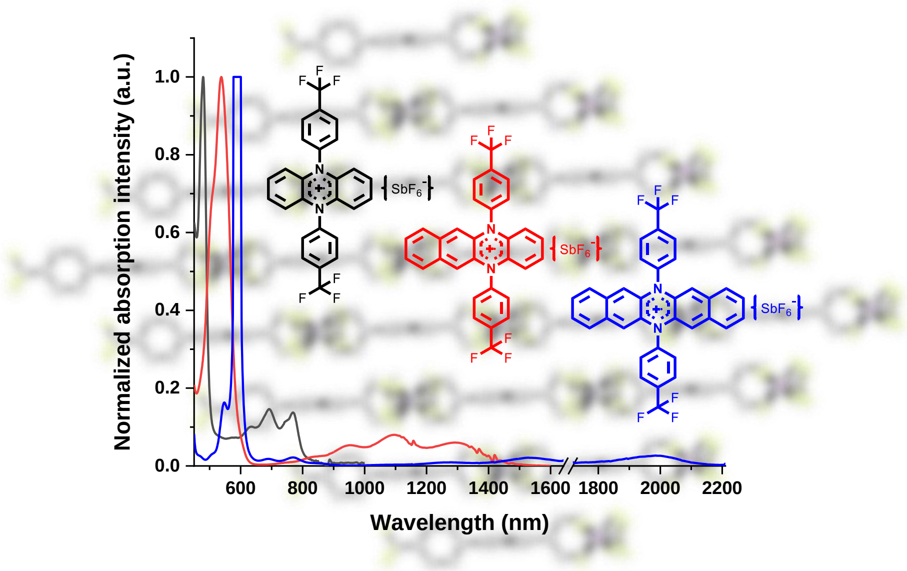

Figure 40. Chemical structures and normalized absorption spectra of *N,N'*-diarylated dihydrodiazaacene radical cations (**DDAs**$^{+}$).

5.1 Introduction and Research Purpose

Acene-based radicals,[61, 139-141] with open-shell electronic characteristics, exhibit particular electronic, magnetic, and optical properties, which have potential applications in spintronics,[142, 143] organic electronics,[144-147] organic superconductors,[148-150] and energy storage devices.[151, 152] The prerequisite for the applications of acene-based radicals is stability, since they are fairly reactive and easily form closed-shell compounds by oxidation, dimerization, and disproportionation.[61] At present, only a few stable acene-based radicals have been exploited and characterized successfully.

TAP is a state-of-the-art n-type semiconductor with the electron mobilities up to 10 $cm^2V^{-1}s^{-1}$ in OFETs.[73] In 2016, Marder and coworkers reported the synthesis of the radical anion **TAP**$^{-\cdot}$ (see Scheme 19)[70] by reducing **TAP** with one equivalent of potassium anthracenide. **TAP**$^{-\cdot}$ is stable in Et_2O solution under air for several hours. Later, our group reported an improved synthetic approach for **Br$_4$TAP** and then further reduced it to the radical anion **Br$_4$TAP**$^{-\cdot}$ (see Scheme 19)[72] employing a potassium anthracenide as well. **Br$_4$TAP**$^{-\cdot}$ is stable in dry Et_2O under air for at least several weeks. Recently, we described the preparation and characterization of the novel *N,N'*-diaryldiazapentacenes **Quino-CF$_3$** and radical cation **Quino-CF$_3$**$^{+\cdot}$ (see Scheme 19).[120] Surprisingly, the neutral **Quino-CF$_3$** is unstable in DCM with around 20% absorption intensity loss after 9 h in ambient surroundings, where **Quino-CF$_3$**$^{+\cdot}$ is so stable that its absorption spectra remain unchanged for at least 24 h under the same conditions. In this contribution, we continue to exploit novel acene-based radical ions, and a sequence of stable *N,N'*-dihydroazaacene-based radical cations were synthesized and well characterized.

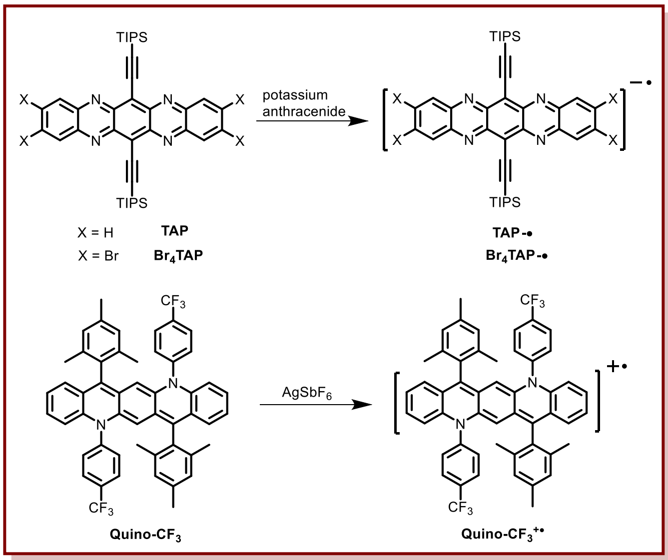

Scheme 19. Preparation of **TAP**$^{-\cdot}$,[70] **Br$_4$TAP**$^{-\cdot}$,[72] and **Quino-CF$_3$**$^{+\cdot}$ [120].

5.2 Synthesis of *N,N'*-Diarylated Dihydrodiazaacenes and Their Radical Cations

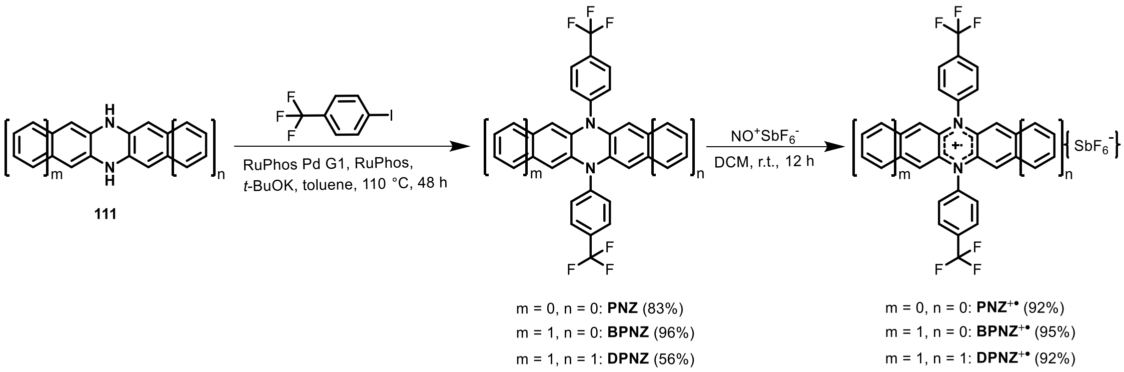

Scheme 20. Synthetic route to *N,N'*-diarylated dihydrodiazaacenes (**DDAs**) and their corresponding radical cations (**DDAs**$^{+\cdot}$).

As outlined in Scheme 20, **PNZ**, **BPNZ**, and **DPNZ** were prepared by the Buchwald-Hartwig amination of 4-iodobenzotrifluoride and *N,N'*-dihydroazaacenes employing a palladium catalyst under N_2 atmosphere. Treating **PNZ**, **BPNZ**, and **DPNZ** with 1 eq. $NO^+PF_6^-$ respectively furnished **PNZ**$^{+\cdot}$, **BPNZ**$^{+\cdot}$, and **DPNZ**$^{+\cdot}$ in excellent yields of 92-95%, while further oxidation of the three radical cations using excess equivalents of $NO^+PF_6^-$ failed to form the corresponding dications.

5.3 Results and Discussion

Figure 41 shows the EPR spectra of **DDAs**$^{+\cdot}$ in DCM. **PNZ**$^{+\cdot}$ and **DPNZ**$^{+\cdot}$ display the intense doublets with the g-values of 2.0022 and 2.0021 respectively, whereas **BPNZ**$^{+\cdot}$ exhibits a defined triplet spectrum with a g-value of 2.0019.

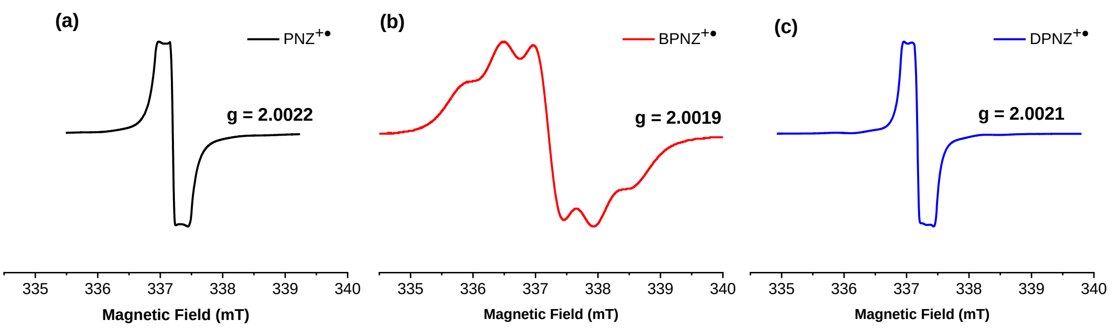

Figure 41. EPR spectra of (a) **PNZ**$^{+\cdot}$, (b) **BPNZ**$^{+\cdot}$, and (c) **DPNZ**$^{+\cdot}$ recorded in DCM under ambient conditions.

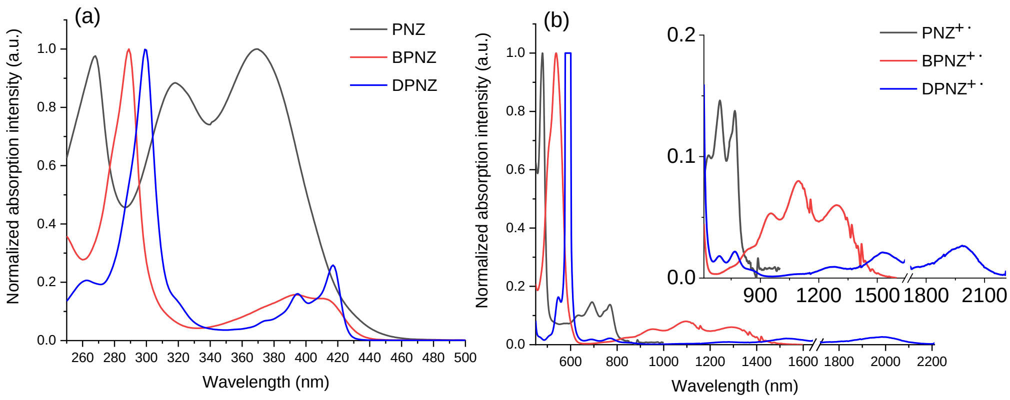

Figure 42. Normalized absorption spectra of (a) **DDA**s and (b) their radical cations measured in DCM. (Notice: The characteristic absorption (from 1200 nm to 2200 nm) intensity of **DPNZ**$^{+\cdot}$ is extremely weak, thus a high concentration solution was measured to obtain a good absorption spectrum without disturbing noise. However, the intensity of the absorption peak at around 590 nm was beyond measurement range under this concentration. As a consequence, there is a platform, rather than a peak at around 590 nm.)

UV-vis absorption spectra of **DDA**s and their radical cations in DCM were measured, and TD-DFT calculations of the vertical excited states were further employed to gain insight into their electronic transitions. As expected, **PNZ** displays the most hypsochromic absorption with a maximum absorption peak (λ_{max}) at 369 nm (see Figure 42a), a result of the shortest azaacene backbone in comparison to those of **BPNZ** and **DPNZ**. The absorption spectra of **BPNZ** and **DPNZ** are quite similar, exhibiting the λ_{max}s at 409 and 417 nm respectively. Upon oxidation into the corresponding radical cations, bathochromic-shifted absorption spectra are observed (see Figure 42b). **PNZ**$^{+\cdot}$ displays the most blue-shifted characteristic absorption band with the three peaks at 635, 692, and 769 nm, and the absorption band of **BPNZ**$^{+\cdot}$ peaks at 955, 1095, and 1291 nm, while **DPNZ**$^{+\cdot}$ exhibits the most red-shifted characteristic absorption band with the peaks at 1281, 1527, and 1986 nm. The significant characteristic absorption differences of the radical cation species indicate that the length of azaacene backbones defines their spectroscopic properties. The results are consistent with the TD-DFT calculations (see Figure 43 and Table 7). The simulated absorption spectra of **PNZ**$^{+\cdot}$, **BPNZ**$^{+\cdot}$, and **DPNZ**$^{+\cdot}$ display the λ_{max}s at 673, 1166, and 1839 nm respectively, which are mainly contributed by the HOMO (β) -> LUMO (β) transitions. In addition, Figure 44 shows the absorption intensity of the radical cation species as a function of time in DCM. All of the three radical cations are fairly stable and their absorption spectra remain unchanged under ambient conditions for at least 24 h.

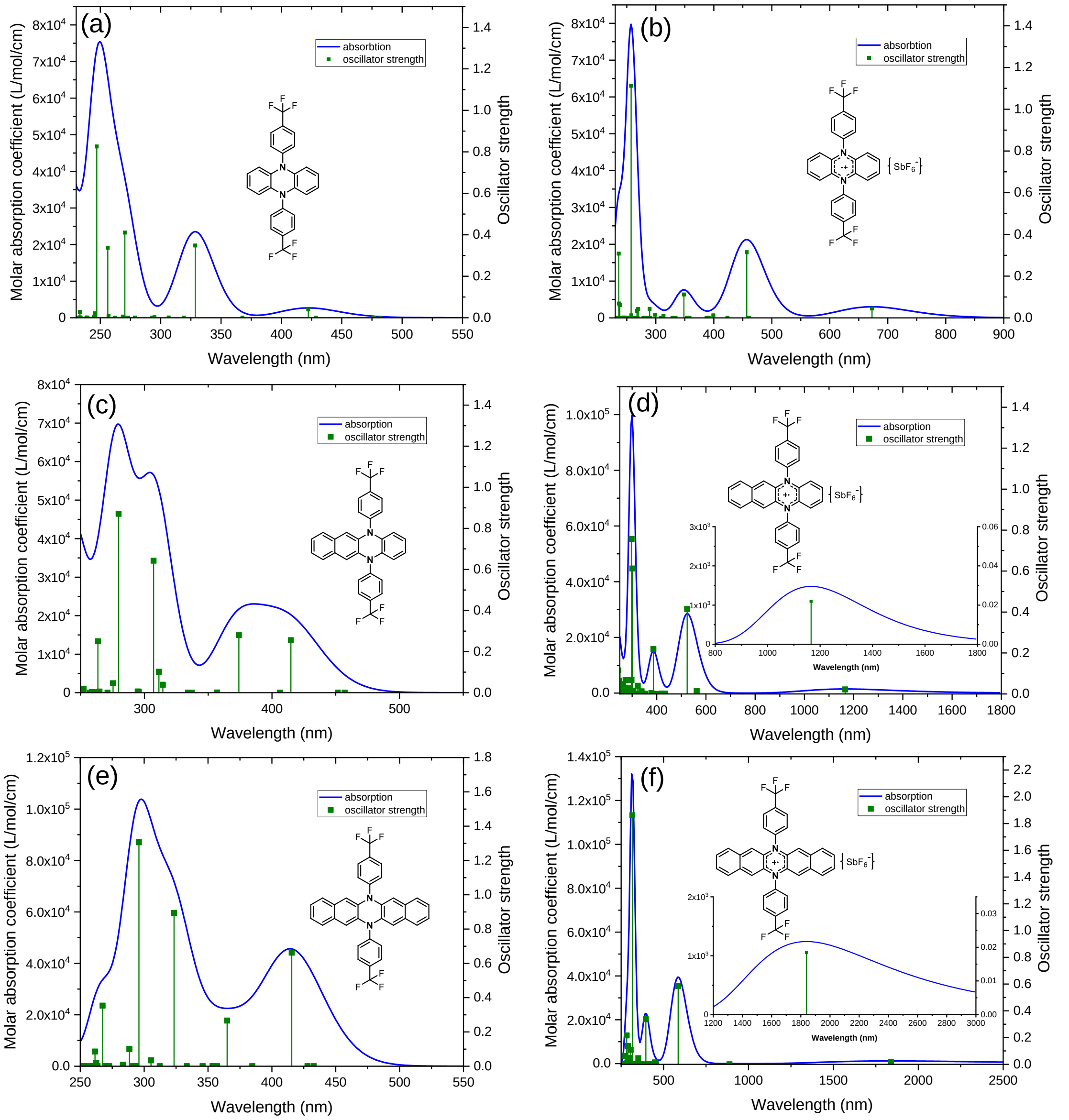

Figure 43. Simulated absorption spectra of a) **PNZ**; b) **PNZ**$^{+\cdot}$; c) **BPNZ**; d) **BPNZ**$^{+\cdot}$; e) **DPNZ**; f) **DPNZ**$^{+\cdot}$ calculated with Gaussian 16 at B3LYP/6-311++G**//DFT/B3LYP/6-311+G**/DCM level of theory.[135] The spectra were broadened using Gaussian functions with a full-width at half maximum of 0.2 eV.

Table 6. Photophysical, experimental and calculated electrochemical properties of **DDA**s and their radical cations.

Comp.	Abs [a] (nm)	E_{ox} [b] (V)	E_{red} [b] (V)	HOMO (eV) mes.[c]/cal.[d]	LUMO (eV) mes.[c]/cal.[d]	gap (eV) mes.[c]/ cal.[d]
PNZ	318, 369	0.06, 0.83	--	– 4.86/– 4.86	--/– 1.71	--/3.15
BPNZ	394, 409	0.51, 1.18	--	– 5.31/– 5.04	--/– 1.75	--/3.29
DPNZ	395, 417	0.26, 0.83	--	– 5.06/– 5.19	--/– 1.79	--/3.40
PNZ$^{+\cdot}$	635, 692, 769	0.14	– 0.63	--	--	0.77/--
BPNZ$^{+\cdot}$	955, 1095, 1291	0.21	– 0.46	--	--	0.67/--
DPNZ$^{+\cdot}$	1281, 1527, 1986	0.26	– 0.34	--	--	0.60/--

[a] Absorption peaks in DCM. [b] Oxidation and reduction potentials measured in CV using ferrocene/ferrocenium as the reference redox system and internal standard (−4.8 eV). [c] Calculated from CV measurements (E_{HOMO} = –4.80 eV – E_{ox} (0/+); E_{LUMO} = –4.80 eV – E_{red} (0/–); E_{gap} = E_{ox} (0/+) – E_{red} (0/–)). [d] Calculated by Gaussian 16 B3LYP/6-311++G**//DFT/B3LYP/6-311+G**.

Table 7. Selected TD-DFT (Gaussian 16 B3LYP/6-311++G**//DFT/B3LYP/6-311+G**/DCM)[135] calculated energies, oscillator strengths, and compositions of major electronic transitions of **DDAs** and their radical cations.

Comp.	Abs. (nm)	Osc. Strengths (f)	Major Transition Contributions
PNZ	329	0.3481	HOMO -> L+5 (69.1%)
	422	0.0398	HOMO -> L+2 (70.4%)
BPNZ	307	0.6425	H-1 -> L+3 (68.4%)
	374	0.2805	HOMO -> L+4 (68.9%)
	415	0.2552	HOMO -> L+2 (69.1%)
DPNZ	323	0.8932	H-1 -> L+3 (69.3%)
	365	0.2662	HOMO -> L+1 (69.7%)
	416	0.6623	HOMO -> L+1 (69.0%)
PNZ$^{+\cdot}$	349	0.1120	HOMO (α) -> L+3 (α) (94.3%)
	457	0.3146	H-1 (β) -> LUMO (β) (97.8%)
	673	0.0448	HOMO (β) -> LUMO (β) (99.0%)
BPNZ$^{+\cdot}$	387	0.2190	HOMO (α) -> LUMO (α) (92.6%)
	524	0.4145	H-1 (β) -> LUMO (β) (98.7%)
	1166	0.0219	HOMO (β) -> LUMO (β) (99.1%)
DPNZ$^{+\cdot}$	395	0.3366	HOMO (α) -> LUMO (α) (94.7%)
	586	0.5862	H-2 (β) -> LUMO (β) (99.0%)
	1839	0.0184	HOMO (β) -> LUMO (β) (99.5%)

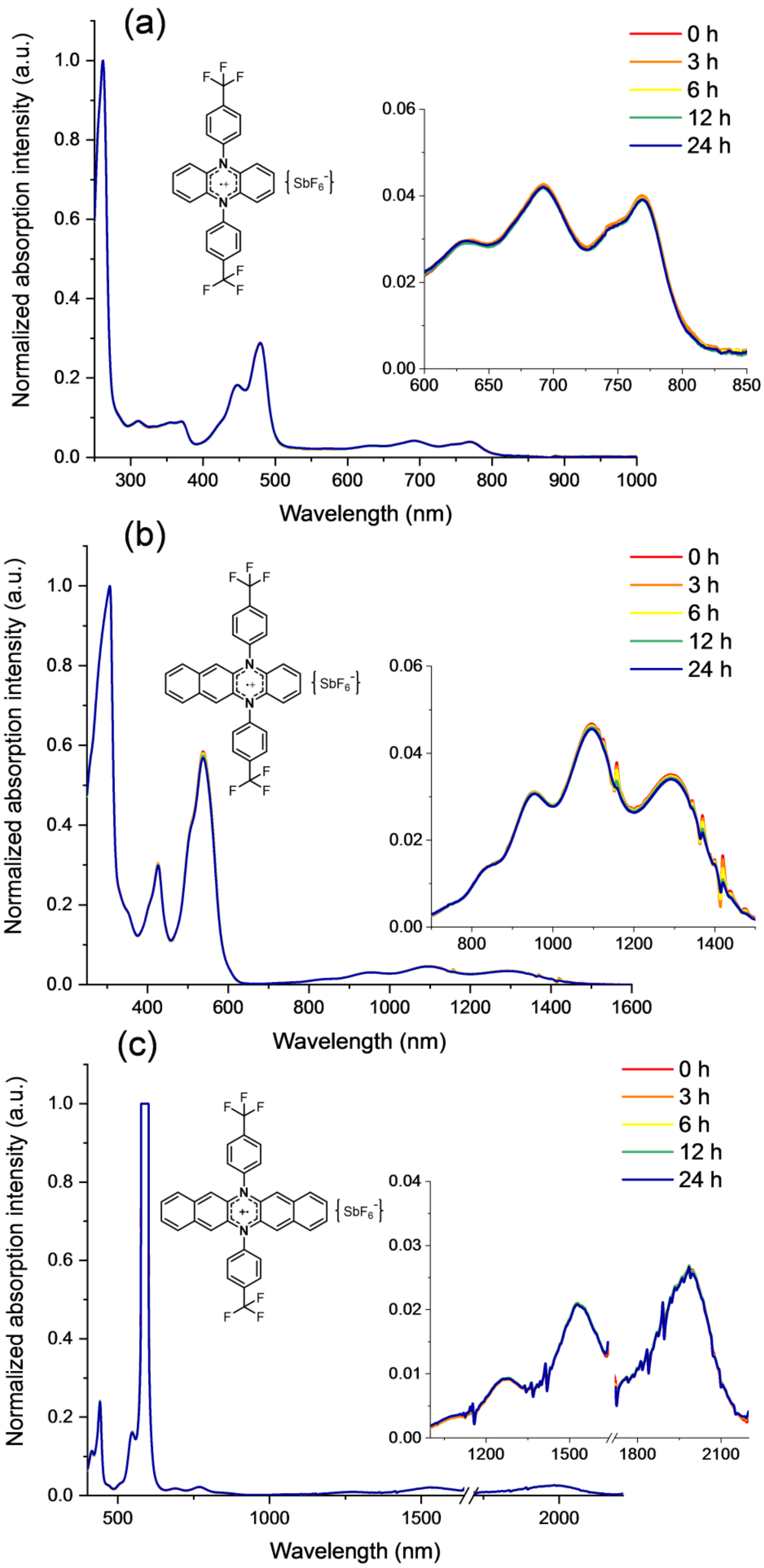

Figure 44. Normalized time-dependent absorption spectra of a) **PNZ**$^{+\cdot}$; b) **BPNZ**$^{+\cdot}$; c) **DPNZ**$^{+\cdot}$ measured in DCM.

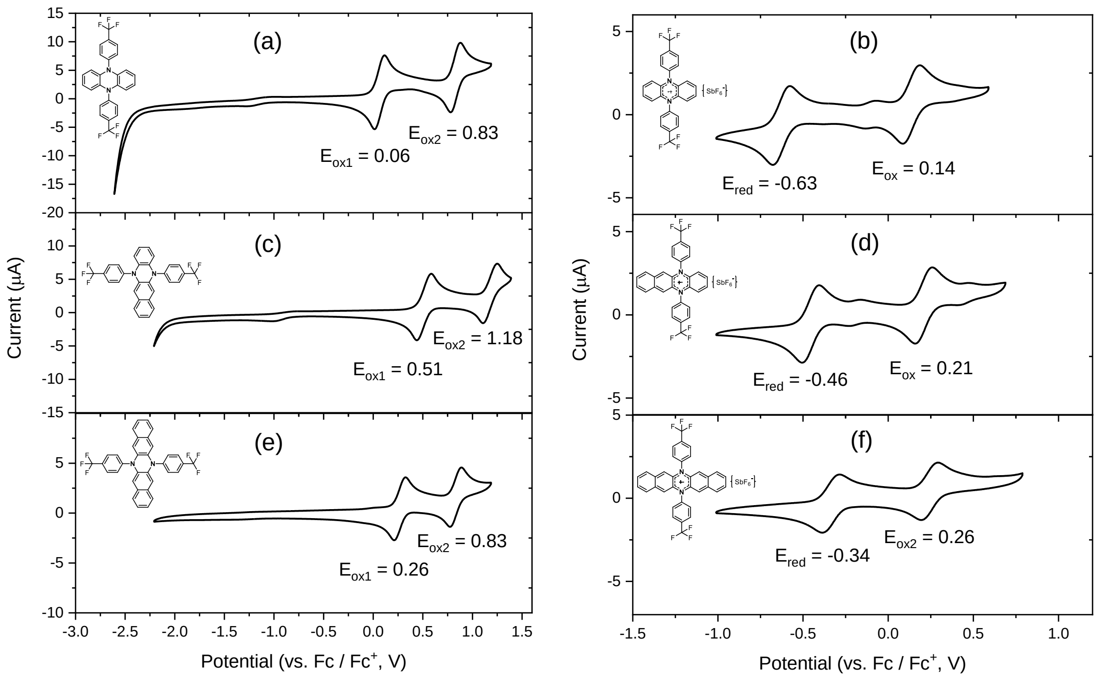

Figure 45. CVs of a) **PNZ**; b) **PNZ**$^{+\cdot}$; c) **BPNZ**; d) **BPNZ**$^{+\cdot}$; e) **DPNZ**; f) **DPNZ**$^{+\cdot}$ using a glass-carbon working electrode, a platinum/titanium wire auxiliary electrode, and a silver wire reference electrode in degassed 0.1 M NBu_4PF_6 DCM solution. The electrode potential was externally calibrated by Fc/Fc^+ couple.

The cyclic voltammograms (CVs) of **DDA**s and their radical cations are shown in Figure 45. As expected, all the three neutral species exhibit two reversible oxidation waves, attributed to the formation of their radical cations and dications respectively. **PNZ** and **DPNZ** oxidize to their radical cations easily with the first oxidation potentials at 0.06 V and 0.26 V (versus Fc/Fc^+) respectively, whereas **BPNZ** is the most stable with the first and second oxidation potentials at 0.51 V and 1.18 V (versus Fc/Fc^+). Unfortunately, the reduction waves of the neutral species are not observed, indicating they are difficult to be reduced due to the electron-rich 4n π-electron *N,N'*-dihydroazacene nuclei. More interesting is the CVs of the radical cation species, which display a reversible oxidation wave and a reversible reduction wave, attributed to the generation of the corresponding dications and neutral compounds respectively. From **PNZ**$^{+\cdot}$ to **DPNZ**$^{+\cdot}$, the oxidation potentials increase from 0.14 V to 0.26 V, while the absolute values of reduction pontentials decrease from 0.63 V to 0.34 V. The radical cationic species become much more difficult to oxidize and easier to reduce due to the extension of the π-conjugated systems.

NICS(1)$_{zz}$ calculations[137, 153] were performed to study the aromaticity of the neutral compounds and their radical cations. For the neutral compounds, the NICS-values of the inner *N,N'*-dihydropyrazine (see Figure 46) are positive, all the values surpassing +19.8, indicating their strong antiaromaticity. The values decrease from **PNZ** to **DPNZ** due to continually increased π-conjugation of the azaacene backbones. On the contrary, the NICS-values of peripheral benzene rings are negative, they are aromatic. Upon oxidation, the overall aromaticity of the azaacenes increases dramatically, and both the rings of **BPNZ**$^{+\cdot}$ and **DPNZ**$^{+\cdot}$ now are aromatic, with the NICS-values of *N,N'*-dihydropyrazine rings decreasing to -2.02 and -4.55 respectively.

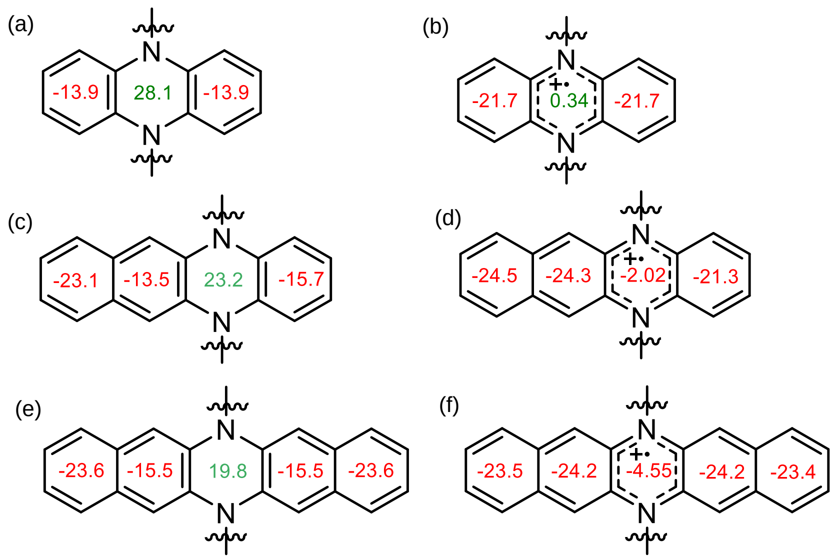

Figure 46. NICS(1)$_{zz}$ values of a) **PNZ**; b) **PNZ**$^{+\cdot}$; c) **BPNZ**; d) **BPNZ**$^{+\cdot}$; e) **DPNZ**; f) **DPNZ**$^{+\cdot}$ calculated with Gaussian 16 at B3LYP/6-311++G**//DFT/B3LYP/6-311+G** level of theory.[135]

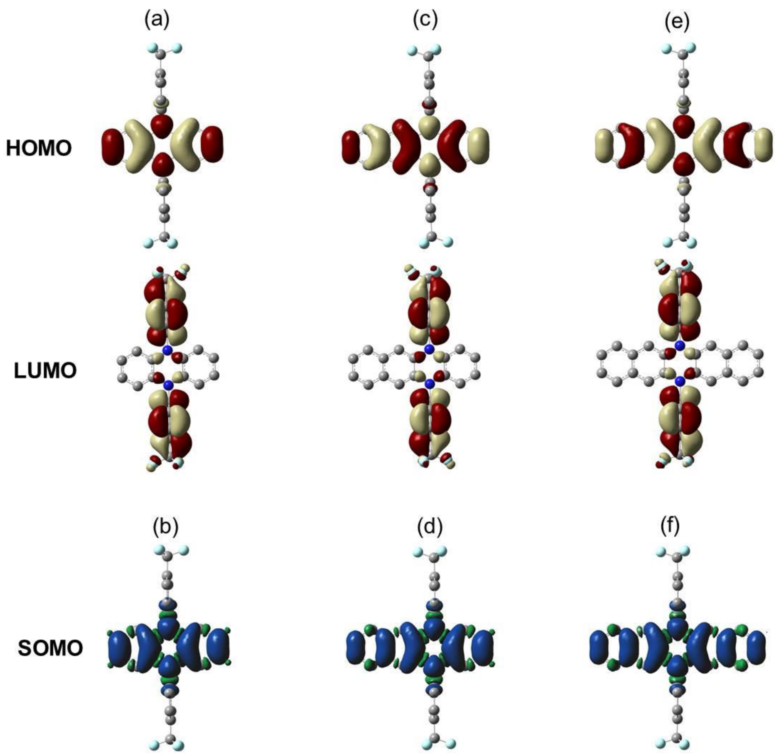

Figure 47. HOMOs and LUMOs (top) of a) **PNZ**; c) **BPNZ**; e) **DPNZ** calculated at DFT/B3LYP/6-311++G**//DFT/B3LYP/6-311+G** level of theory. Spin-density distributions (bottom) of b) **PNZ**$^{+\cdot}$; d) **BPNZ**$^{+\cdot}$; f) **DPNZ**$^{+\cdot}$ calculated at DFT/UB3LYP/6-311++G** //DFT/B3LYP/6-311+G** level of theory.[135]

Figure 47 shows the FMOs of **DDA**s and **DDA**s$^{+\bullet}$. Surprisingly, for the neutral species, their HOMOs are distributed over the whole dihydrodiazaacene nuclei, while the LUMOs are mainly located on the electron-withdrawing *para*-trifluoroaryl side groups, different from aryl-substituted acenes such as azarubrenes,[77] whose HOMOs and LUMOs are all distributed on the acene backbones. For **DDA**s$^{+\bullet}$, their SOMOs (singly occupied molecular orbitals) are mostly distributed on the dihydrodiazaacene cores, as expected.

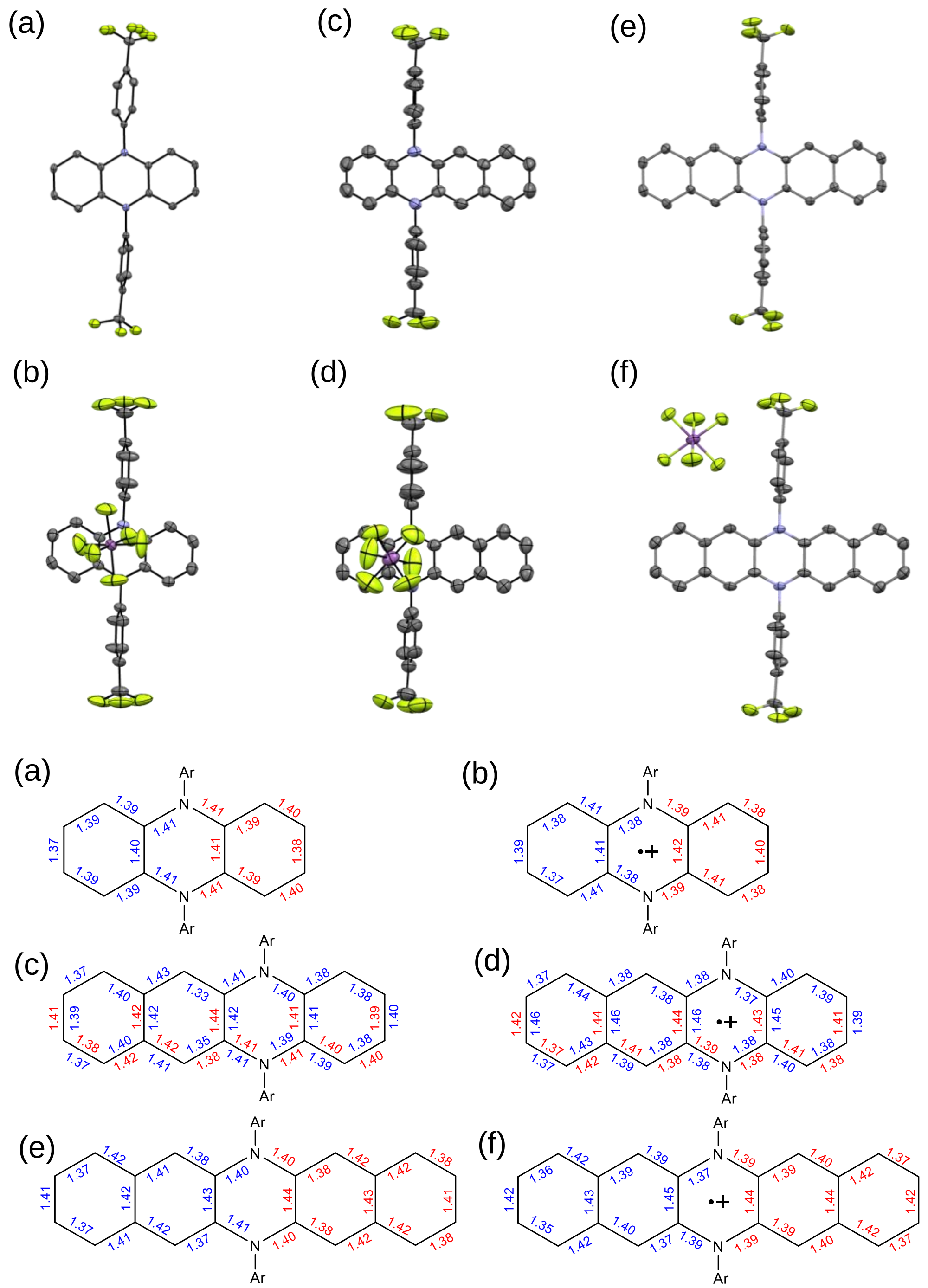

Figure 48. Single crystal structures (top) and bond lengths (bottom, blue: derived from the crystal structures; red: calculated at the DFT/B3LYP/6-311+G** level of theory[135]) of a) **PNZ**; b) **PNZ**$^{+\bullet}$; c) **BPNZ**; d) **BPNZ**$^{+\bullet}$; e) **DPNZ**; f) **DPNZ**$^{+\bullet}$.

We obtained single crystals of neutral **DDA**s for XRD analysis by slow evaporation of the saturated solutions of DCM under ambient conditions. The single crystals of **PNZ**$^{+\cdot}$, **BPNZ**$^{+\cdot}$, and **DPNZ**$^{+\cdot}$ were also grown successfully by slow evaporation of acetone solutions under air. For all the six compounds, their *N,N'*-dihydrodiazaacene backbones are planar (see Figure 48), with the *para*-trifluoroaryl side groups almost orthogonal to the azaacene backbones. Upon monooxidation, the neutral specimens display the more pronounced bond length alternations, which are in accordance with the DFT calculations. Noticeably, for the radical cation species, C-N bond lengths in *N,N'*-dihydropyrazine rings are shorter compared to those of the neutral species, which indicates stronger conjugation between nitrogen atoms and the adjacent phenyl rings in the oxidized diazaacene backbones, consistent with the NICS(1)$_{zz}$ calculations that *N,N'*-dihydropyrazine rings of the radical cations are much more aromatic.

5.4 Conclusion

In conclusion, a series of *N,N'*-diarylated dihydroazaacenes, *viz* **PNZ**, **BPNZ**, and **DPNZ**, were synthesized through the Buchwald-Hartwig amination of aryl iodides with *N,N'*-dihydroazaacenes. Upon monooxidation of the neutral compounds, radical cations **PNZ**$^{+\cdot}$, **BPNZ**$^{+\cdot}$, and **DPNZ**$^{+\cdot}$ formed, and they are all stable in DCM for at least 24 h. In comparison with the neutral species, the radical cation species display the bathochromic-shifted absorption spectra with a λ_{max} of 769, 1291, and 1986 nm respectively. The alternation of bond lengths between the neutral compounds and their corresponding radical cations in single crystal structures, as well as the NICS(1)$_{zz}$ calculations, indicate the *N,N'*-dihydropyrazine rings of the radical cations to be less antiaromatic. The current findings validate a practical strategy to exploit stable radical cations based on *N,N'*-dihydropyrazine units. In the future, we would like to prepare more *N,N'*-dihydrodiazaacene radical cations with longer backbones, such as *N,N'*-dihydrodiazahexacene and *N,N'*-dihydrodiazapentacene radical cations.

Summary and Outlook

In Chapter 2, we described the synthesis and properties of diazarubrene **DAR** and tetraazarubrene **TAR** (see Figure 49). Though **DAR** and **TAR** are much more stable in solution compared to rubrene, they are still somewhat sensitive towards oxidation since introducing nitrogen atoms into the phenyl peripheries does not lower HOMO and LUMO energies of rubrene sufficiently. Given that the reactive sites of rubrenes are on the tetracene backbone, if electron-deficient units are introduced into the backbones, the stability of rubrene should be greatly improved. As a consequence, novel azarubrenes such as **115** (see Scheme 21) containing azatetracene backbones, are promising stable semiconductors, worthy to be prepared in the future. Besides, the replacement of hydrogen atoms by electron-withdrawing halogen atoms in the backbones is another efficient approach to exploit stable rubrene anologues. Herein, fluoro-, chloro-, and bromo-substituted molecular structures **121** in Scheme 21 are proposed to be synthesized.

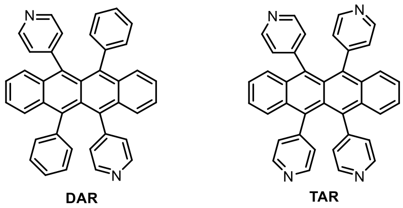

Figure 49. Chemical structures of **DAR** and **TAR**.

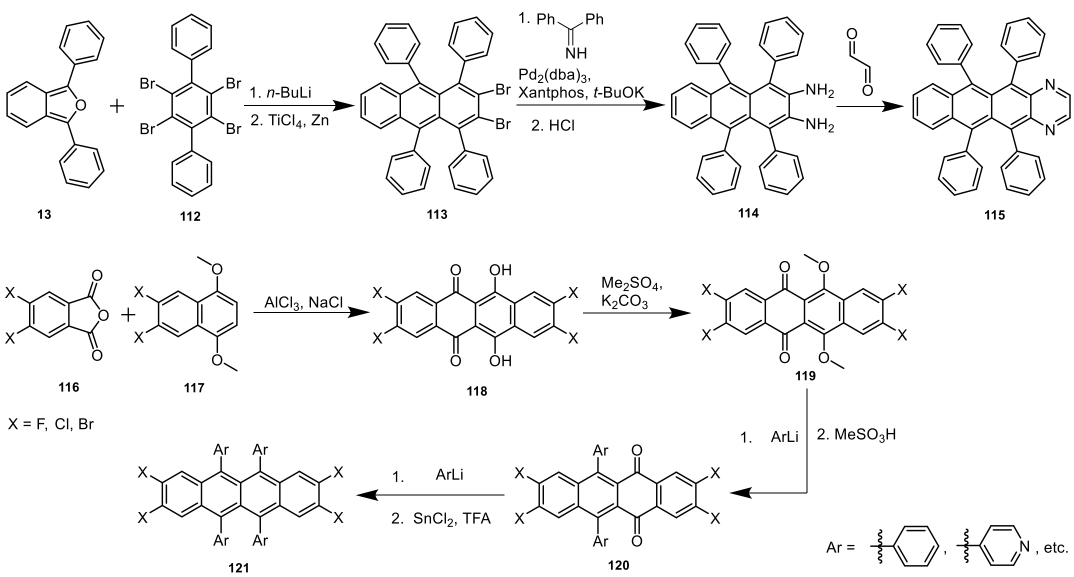

Scheme 21. Proposed synthetic route to target molecules **115** and **121**.

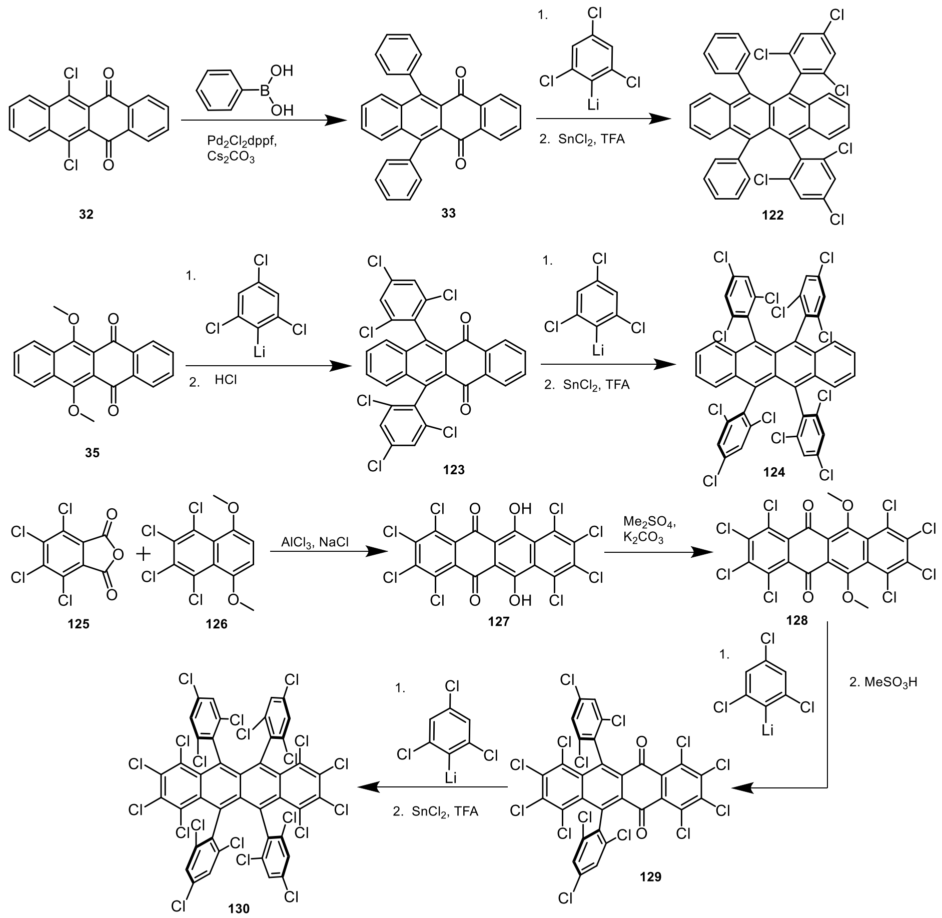

Scheme 22. Proposed synthetic route to target molecules **122**, **124**, and **130**.

Introducing chlorine atoms into acenes has been reported to be more effective to lower LUMO energies than that of fluorine, even if the latter has more electron-withdrawing ability, ascribed to the lack of a +M effect in the chloride substituents.[154] Chlorine-substituted semicondutors possess reduced reorganization energies and enhanced electron transfer integrals, thus exhibiting higher charge-transporting capabilities.[36] Hence, it’s of great interest to develop chloride-substituted rubrenes such as **122**, **124**, and **130** (see Scheme 22).

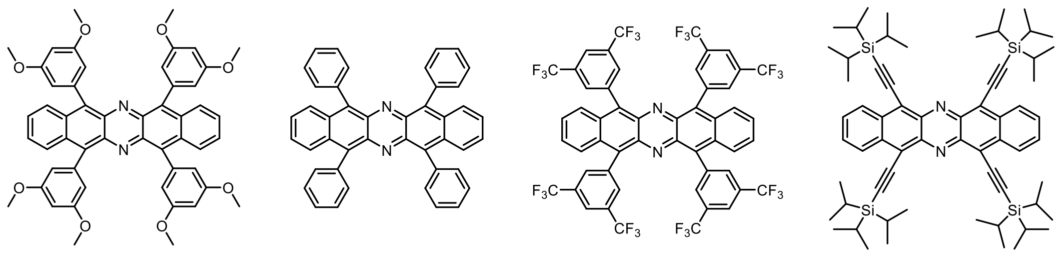

3a **3b** **3c** **3d**

Figure 49. Chemical structures of **3a-d**.

In Chapter 3, the stability, optoelectronic and electrochemical properties of 5,7,12,14-tetrafunctionalized diazapentacenes **3a-d** (see Figure 49) were investigated. Interestingly, **3a-c** underwent photooxidation in solution under ambient conditions, while **3d** displayed no sign of decomposition for 24 h, illustrating the alkynyl groups protect the diazapentacene backbone from oxidation. Hence, syntheses of stable 5,7,14,16-tetraalkynylized diazahexacene **140** and 7,9,16,18-tetraalkynylized diazaheptacene **141** (see Scheme 23) are of great interest.

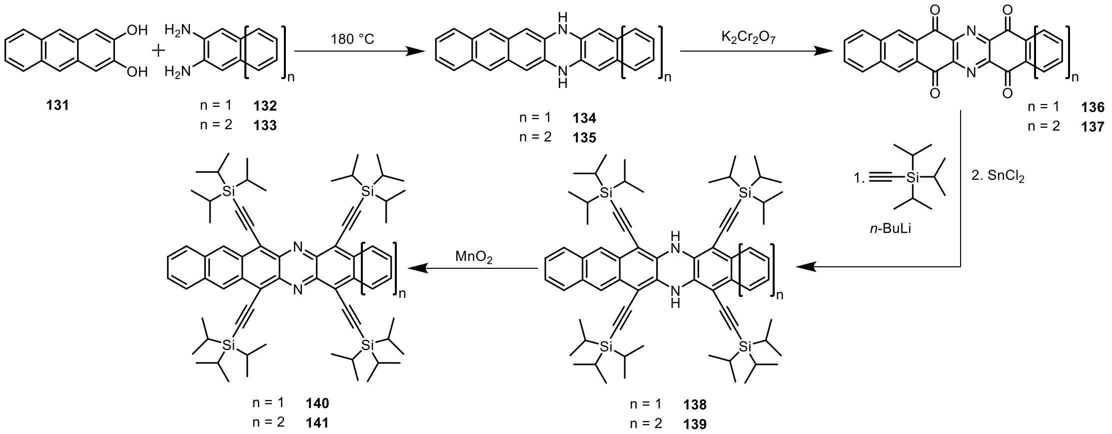

Scheme 23. Proposed synthetic route to target molecules **140** and **141**.

In Chapter 4, we reported a series of nitrogen-embeded quinodial pentacenes (**Quino**s, see Figure 50) and their radical cations (**Quino**s^{+}), as well as the dications (**Quino**s^{2+}). The **Quino**s are easily oxidized, while the **Quino**s$^{+\cdot}$ are environmentally stable. It is attractive to exploit neutral compounds **145**, monocations **146**, and dications **147** of 5,7,14,16-tetramesityl-9,18-dihydro-9,18-diaryldiazaheptacenes diazaheptacenes (see Scheme 24) in the future.

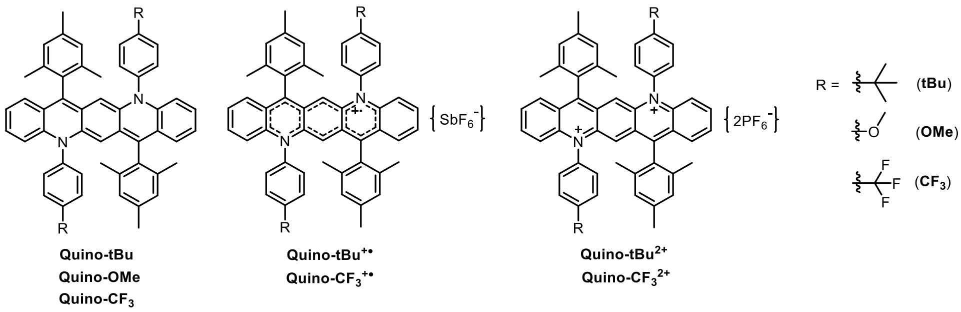

Figure 50. The neutral compounds, radical cations, and dications of 7,14-dimesityl-5,12-dihydro-5,12-diaryldiazapentacenes.

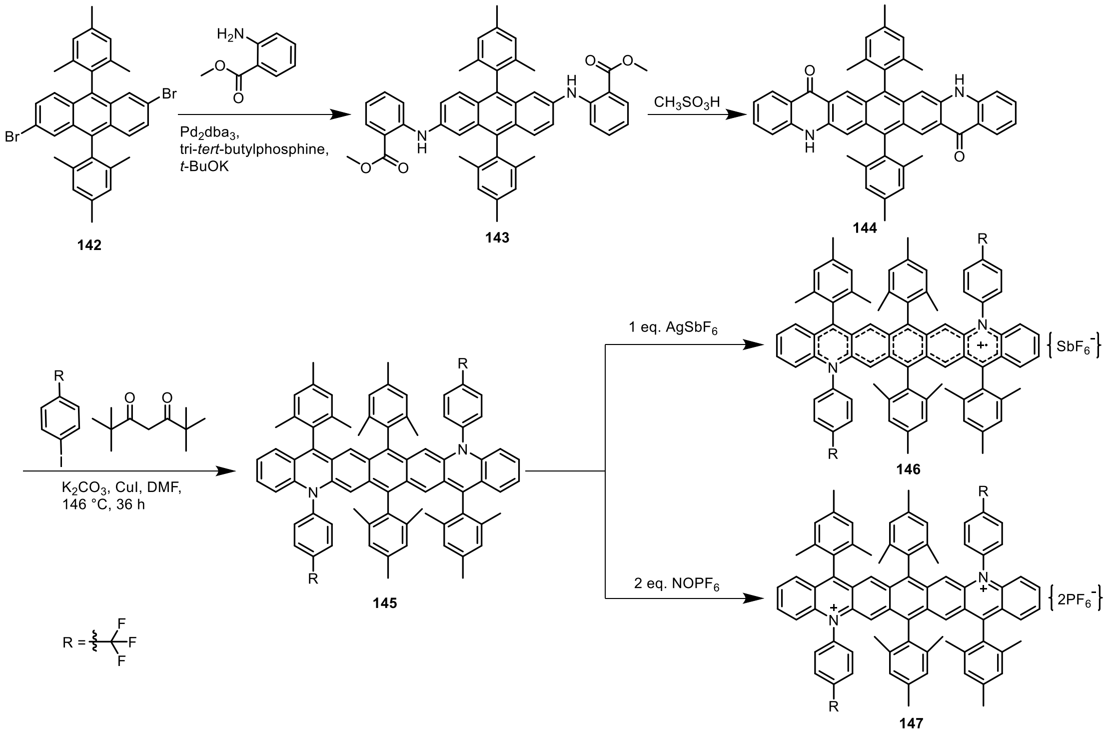

Scheme 24. Proposed synthetic route to target molecules **145**, **146**, and **147**.

In Chapter 5, we prepared the three stable radical cations (**PNZ**$^{+\cdot}$, **BPNZ**$^{+\cdot}$, and **DPNZ**$^{+\cdot}$; see Figure 50) and found that the length of *N,N'*-dihydroazaacene cores greatly influences their spectroscopic and aromatic properties. The radical cations exhibit tremendously absorption spectra in comparison with those of the neutral compounds. **PNZ**$^{+\cdot}$ displays the most blue-shifted characteristic absorption band with the three peaks at 635, 692, and 769 nm, and the absorption band of **BPNZ**$^{+\cdot}$ peaks at 955, 1095, and 1291 nm, while **DPNZ**$^{+\cdot}$ exhibits the most red-shifted characteristic absorption band with the peaks at 1281, 1527, and 1986 nm. Besides, the radical cations are much more aromatic than the corresponding neutral compounds. Therefore, it is attractive to further synthesize and characterize compounds **152** (see Scheme 25), which are of longer backbones.

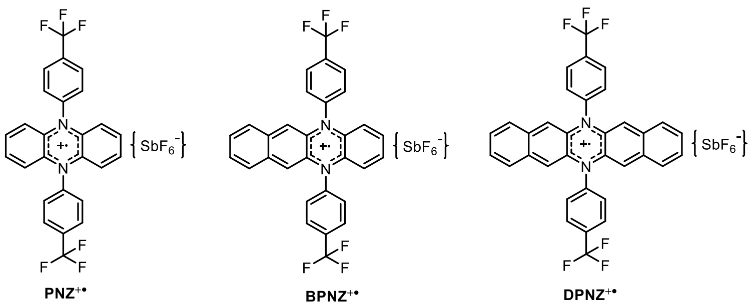

Figure 49. Chemical structures of **PNZ**$^{+\cdot}$, **BPNZ**$^{+\cdot}$, and **DPNZ**$^{+\cdot}$.

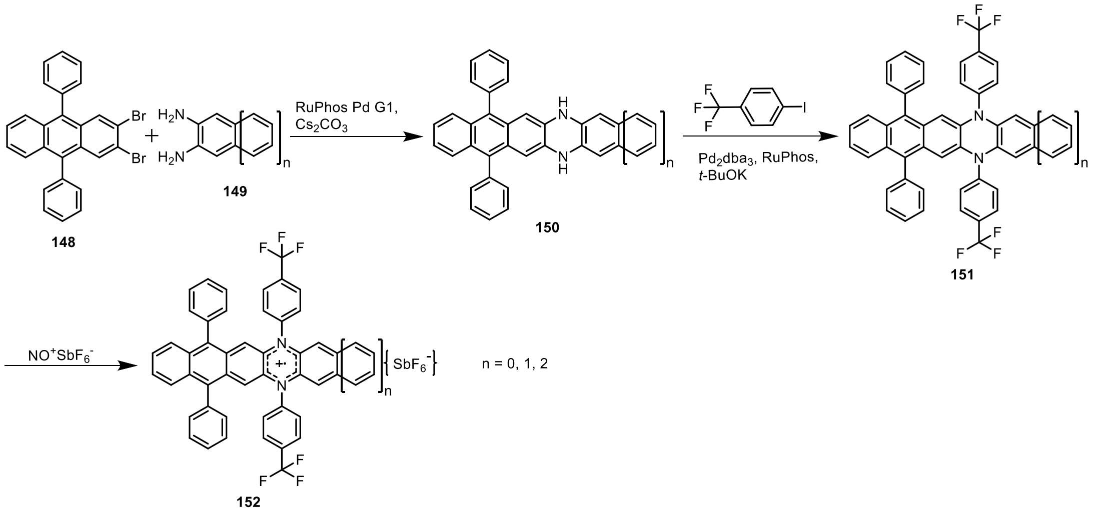

Scheme 25. Proposed synthetic route to target molecules **152**.

Chapter 6. Experimental Section

6.1 General Remarks

Chemicals were either purchased from the chemical store at the Organisch-Chemisches Institute of the University of Heidelberg or from commercial laboratory suppliers. Chemicals were purchased from Sigma-Aldrich, Abcr, TCI or Acros. Reagents were used without further purification unless otherwise noted.

Solvents were purchased from the store of the Theoretikum or chemical store at the Organisch-Chemisches Institute of the Heidelberg University and distilled prior use if necessary. All of the other absolute solvents were dried by an MB SPS-800 using drying columns.

Flash column chromatography was carried out using neutral silica gel S (0.032 mm-0.062 mm), purchased from Sigma Aldrich. Basic aluminum oxide, ranging 70-290 mesh (50-200 μm), was purchased from Sigma Aldrich and applied to separate the target molecules when necessary. As noted, Celite 545 (Fluka) was used for filtration.

Thin layer chromatography (TLC) was performed on Macherey & Nagel Polygram® SIL G/UV254 pre-coated plastic sheets. Components were visualized by observation under UV light (254 nm or 365 nm).

Gas chromatography-mass spectrometry (**GCMS**) chromatograms were recorded using a HP 5890 Series II Plus model, coupled with a HP 5972 Mass Selective Detector. As the capillary column, a HP 1 Crosslinked Methyl Silicone (25 m x 0.2 mm x 0.33 μm) was employed, with helium as carrier gas. The acquired data were analyzed using ACD/Labs Spectrus Processor 2012.

NMR spectra were recorded at r.t. on the following spectrometers: Bruker Avance III 300 (300 MHz), Bruker Avance III 400 (400 MHz), Bruker Avance III 500 (500 MHz) or Bruker Avance III 600 (600 MHz). Chemical shifts (δ) and coupling constants are reported in ppm and Hz, respectively, and are referenced to the peak of the residual protonated solvent.[155] Multiplicities are denoted at the centre of the signal as s (singlet), bs (broad singlet), d (doublet), bd (broad doublet), dd (doublet doublet), t (triplet), or m (multiplet).

High resolution mass spectra (HRMS) were obtained from electron impact (EI), electrospray ionization (ESI) or matrix-assisted laser desorption/ionization (MALDI) on a Bruker ApexQe hybrid 9.4 TFT-ICR-MS at the Organisch-Chemisches Institut der Universität Heidelberg.

Elemental analyses were carried out at the Organisch-Chemisches Institut der Universität Heidelberg.

IR spectra were recorded on a JASCO FT/IR-4100. Substances were applied as a film. The obtained data were processed with the software JASCO Spectra Manage II.

Melting points **(Mp**s**)** were determined in open glass capillaries with a Melting Point Apparatus MEL-TEMP (Electrothermal, Rochford, UK).

A**bsorption spectra** were recorded on a JASCO UV-VIS V-660 or JASCO UV-VIS V-670 and processed with the software JASCO Spectra Manage II. ASCII-files were exported and visualized by Origin.

Fluorescence spectra were recorded on a Jasco FP6500 spectrometer. Raw data were processed using JASCO Spectra Manage II. ASCII-files were exported and visualized with Origin.

Cylic Voltammetry experiments were carried out using a gold or glass carbon working electrode, a platinum/titanium wire auxiliary electrode, a silver wire reference electrode, a 0.1 M NBu_4PF_6 solution in degassed DCM, and ferrocene/ferrocenium as the reference redox system and internal standard (−4.8 eV).[156]

Crystal Structure Analysis was performed on Bruker Smart CCD or Bruker APEX diffractometers with Mo Kα radiation source (0.71073 Å), under direction of Dr. F. Rominger. Intensities were corrected for Lorentz and polarization effects; an empirical absorption correction was applied using SADABS based on the Laue symmetry of the reciprocal space. All structures were solved by direct methods and refined against F^2 with a Full-matrix least-squares algorithm using the SHELXTL (Version 2008/4) software package.

Device Fabrication Substrate modification: Si/SiO_2 substrates (300 nm) were modified by self-assembled monolayer of octadecyltrichlorosilane (OTS). Prior to functionalization substrates were cleaned in piranha solution. The process was carried out in a mixture of chloroform and *n*-hexane in a ratio of 1 : 4 and in the presence of OTS in relation to the volume of the mixture of 1 : 200. The substrates were kept in the solution for 30 min and then rinsed three times with chloroform in an ultrasonic cleaner and then dried under a nitrogen flux. Solvents (AR grade) and OTS were purchased from Sigma-Aldrich and used without further purification.

Thin film deposition: Both materials were deposited in the same conditions. Thin films of 50 nm (indication of quartz weight calibrated on pentacene) were thermally evaporated under high vacuum with the growth rate of 0.1 Å s^{-1} and substrate temperature of 60 ℃. Process was carried out in MBraun MBProVap-7 evaporation chamber (BioNanoPark in Lodz, Poland). Electrodes deposition: Transistors were prepared in top-contact/bottom gate configuration. The 50 nm thick source and drain electrodes were thermally evaporated under high vacuum with the growth rate of 1.0 nm s^{-1}. Silver electrodes were used. Ossila E325 Linear shadow source-drain masks with variable channel length from 10 µm to 30 µm and channel width of 1 mm were used.

Field effect measurements: OFET measurements were performed by using a Keithley 2634B source meter. Transfer characteristics were measured under a nitrogen atmosphere in the range of V_{GS} from 0 V to 80 V. The same range of changes was used for V_{DS} during output characteristics measurements. The charge carrier mobility was derived from transfer characteristics (|VDS = 80V|) in the saturation regime. For each sample twelve transistors were measured.

6.2 Synthesis Details and Analytical Data

6.2.1 Synthesis of Azarubrenes (Chapter 2)

4-((Trimethylsilyl)ethynyl)pyridine (**102**)[157] and 5,6,11,12-tetrachlorotetracene (**27**)[89] were synthesized according to the reported literatures.

1,1-Diphenyl-3-pyridyl-2-propyn-1-ol (**103**)

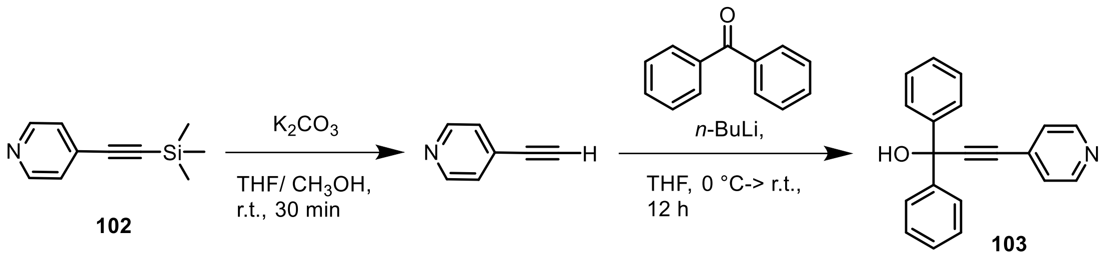

102 **103** 93%

A solution of **102** (4.92 g, 28.1 mmol, 1.00 eq.) in THF:CH_3OH (28:28 mL) was treated with K_2CO_3 (8.73 g, 63.2 mmol, 2.25 eq.). After 30 min of stirring at r.t., the mixture was filtered to remove inorganic salts and the solvent was evaporated under reduced pressure. Then the crude product was purified by a flash column chromatography (silica gel, petroleum ether (PE)/ethyl acetate (EE) = 5:1) to give a colorless solid. The fresh prepared 4-ethynylpridine (2.72 g, 26.3 mmol, 1.20 eq.) was dissolved into 32 mL dry THF, followed by adding *n*-BuLi (22.0 mmol, 8.78 mL, 2.50 M in hexane, 1.00 eq.) dropwise at -10 ℃. The solution was first stirred at -10 ℃ for 20 min and then at r.t. for 20 min. After that, benzophenone (4.00 g, 22.0 mmol, 1.00 eq.), dissolved in 32 mL THF, was added dropwise at r.t. and the mixture was stirred for 12 h. The mixture was quenched with water (8 mL) and dealt with a short column chromatography using THF as eluent. After evaporation of the solvent, the mixture was separated by a short column chromatography (silica gel, PE/EE = 5:1) to attain a white powder **103**. Yield: 5.85 g, 20.5 mmol, 93%, Rf = 0.35 (SiO_2, PE/EE = 1: 1). Mp: 183 ℃. ^{1}H-NMR ($CDCl_3$, 500 MHz, 298 K): δ = 8.55 (bs, 2H), 7.65 (d, *J*= 7.32 Hz, 4H), 7.40-7.34 (m, 6H), 7.33-7.29 (m, 2H), 3.55 (bs, 1H) ppm. ^{13}C{^{1}H} NMR ($CDCl_3$, 125 MHz, 298 K): δ = 149.3, 144.4, 131.1, 128.4, 128.0, 126.0, 125.8, 97.0, 84.2, 74.7 ppm. IR: $\tilde{\nu}$ = 3068, 2783, 1700, 1597, 1490, 1445, 1411, 1171, 1046, 996, 829, 753, 692, 643, 605, 552, 418 cm^{-1}. HRMS (ESI$^+$) m/z: [M+H]$^+$: calcd. for $C_{20}H_{16}NO$: 286.1226; found 286.1229 correct isotope distribution. Elemental analysis calcd. (%) for $C_{20}H_{16}NO$: C 84.19, H 5.30, N 4.91; found: C 84.05, H 5.48, N 4.82.

DAR

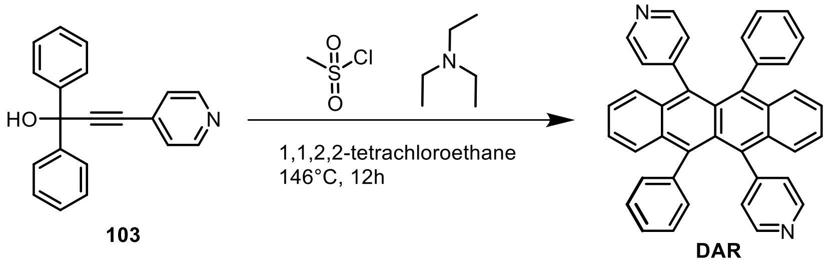

Under nitrogen atmosphere, **103** (0.20 g, 0.70 mmol, 1.00 eq.) was dissolved in 6 mL 1,1,2,2-tetrachloroethane and the solution was cooled to 0 ℃. Anhydrous TEA (0.20 mL) and MesCl (0.25 g, 98%, 2.10 mmol, 3.00 eq.) were added to this solution and stirred for 1 h at 0 ℃. Then it was heated to 146 ℃ and stirred for 5 h. After removal of the solvent through reduced pressure distillation, the mixture was first purified using a SiO_2 column chromatography (DCM/EE = 10:1), followed by an alumina column chromatography (DCM/ EE = 3:1). Then the crude product was recrystallized by methanol and hexane to obtain **DAR** as a red powder. Yield: 0.26 g, 0.05 mmol, 14%. Rf = 0.20 (SiO_2, DCM/EE = 1:1). Mp: 338 ℃ (decomposition). ^{1}H-NMR (cyclohexane-d_{12}, 300 MHz, 300 K): δ = 8.28-8.19 (m, 4H), 7.46-7.37 (m, 2H), 7.31-7.25 (m, 2H), 7.16-7.11 (m, 2H), 7.06-6.69 (m, 8H), 6.86-6.76 (m, 4H), 6.67-6.60 (m, 4H) ppm. IR: $\tilde{\nu}$ = 3060, 3027, 1581, 1396, 1068, 1024, 817, 757, 692, 586, 514, 460 cm^{-1}. HRMS (EI^+): m/z: $[M]^+$: calcd. for $C_{40}H_{26}N_2^+$: 534.2096; found 534.2081 correct isotope distribution.

DARO2

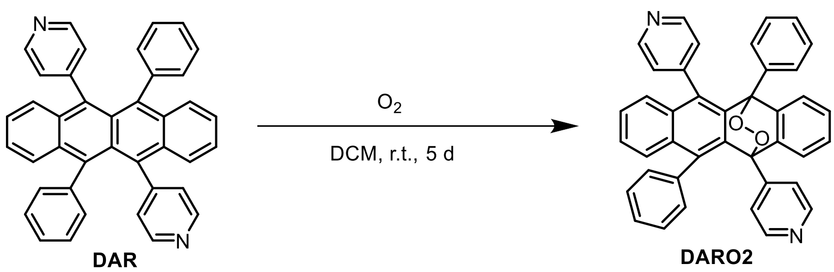

DAR (0.03 g, 0.06 mmol) was dissolved in 30 mL DCM and stirred at r.t. for 5 d. The solvent was removed under reduced pressure and the crude product was recrystallized by DCM to attain **DARO2** as a colorless powder. Yield: 0.03 g, 0.05 mmol, 83%. Rf = 0.20 (SiO_2, DCM/ EE = 1:1). Mp: 207 ℃. ^{1}H-NMR (CD_2Cl_2, 600 MHz, 295 K): δ = 8.45 (bs, 1H), 8.27 (bs, *2*H), 8.12 (bs, 1H), 7.54-7.38 (m, 3H), 7.36-7.32 (m, 1H), 7.31-7.13 (m, 12H), 7.12-7.08 (bd, *J*= 3.85 Hz, 1H), 7.07-6.96 (m, 2H), 6.92-6.87 (m, 1H), 6.74-6.96 (d, *J*= 7.70 Hz, 1H), 6.61-6.53

(bd, *J*= 4.13 Hz, 1H) ppm. $^{13}C\{^{1}H\}$ NMR (CD_2Cl_2, 150 MHz, 295 K): δ = 149.8, 148.7, 148.4, 147.1, 142.7, 140.0, 139.3, 138.2, 137.0, 134.9, 133.9, 133.8, 133.6, 133.2, 132.6, 132.2, 131.9, 128.8, 128.8, 128.5, 128.4, 128.0, 127.7, 127.5, 127.2, 127.1, 127.0, 126.9, 125.3, 124.6 ppm. IR: $\tilde{\nu}$ = 3041, 2927, 1589, 1463, 1411, 1270, 1184, 1051, 914, 821, 765, 730, 696, 605, 566 cm^{-1}. HRMS (ESI^+) m/z: $[M+H]^+$: calcd. for $C_{40}H_{27}N_2O_2^+$: 567.2067; found 567.2061; m/z: $[M+Na]^+$: calcd. for $C_{40}H_{26}N_2O_2Na^+$: 589.1886; found 589.1880 correct isotope distribution.

TAR

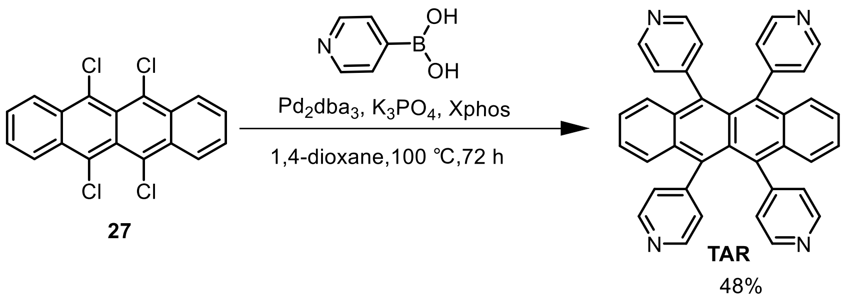

Under nitrogen atmosphere, **27** (0.20 g, 0.55 mmol, 1.00 eq.), 4-pyridinylboronic acid (0.48 g, 90%, 3.50 mmol, 6.40 eq.), Pd_2dba_3 (0.04 g, 0.04 mmol, 0.07 eq.) and XPhos (0.08 g, 0.16 mmol, 0.28 eq.) were added into a 50 mL flask. 16 mL 1,4-dioxane and 4 mL potassium phosphate solution (1.02 g, 4.80 mmol, 8.80 eq., 1.20 M) were degassed for 20 min and added into the flask. The resulting mixture was stirred at 100 ˚C for 72 h. The crude product was extracted with 50 mL DCM and washed three times with 50 mL water. After evaporation of the solvent under reduced pressure, the solid was purified by column chromatography (DCM/ CH_3OH = 40: 1 → 10: 1) to attain **TAR** as a red powder. Yield: 0.14 g, 0.26 mmol, 48%. Rf = 0.30 (SiO_2, DCM/CH_3OH = 10:1). Mp: 338 ℃. ^{1}H-NMR (THF-d_8, 500 MHz, 298 K): δ = 8.38-8.25 (m, 8H), 7.43-7.29 (m, 4H), 7.28-7.16 (m, 4H), 6.94-6.80 (m, 8H) ppm. $^{13}C\{^{1}H\}$ NMR (THF-d_8, 125 MHz, 298 K): δ = 150.1, 149.5, 135.8, 130.7, 128.4, 127.1, 126.7 ppm. IR: $\tilde{\nu}$ = 3031, 1936, 1589, 1540, 1467, 1403, 1209, 1064, 981, 817, 746, 582, 518, 460 cm^{-1}. HR-MS (EI^+): m/z: $[M]^+$: calcd. for $C_{38}H_{24}N_4$: 536.2001; found 536.2002 correct isotope distribution.

TARO2

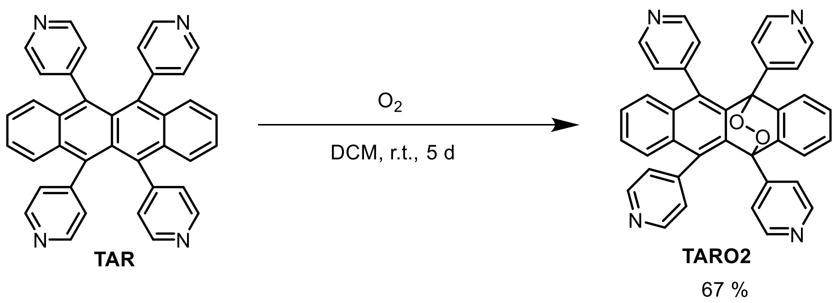

TAR (0.03 g, 0.06 mmol) was dissolved in 30 mL DCM and stirred at r.t. for 5 d. The solvent was removed under reduced pressure and the crude product was recrystallized by DCM to attain **TARO2** as a colorless powder. Yield: 0.02 g, 0.04 mmol, 67%. Rf = 0.30 (SiO_2, DCM/CH_3OH = 10:1). Mp: 220 ℃. ^{1}H-NMR (CD_2Cl_2, 300 MHz, 300 K): δ = 8.56 (d, J=5.0, 2H), 8.34 (s, 4H), 8.15 (d, J=4.9, 2H), 7.40-7.26 (m, 10H), 7.18 (d, J=3.8, 2H), 7.09 (dd, J=6.6, 3.3, 2H), 6.64 (d, J=3.7, 2H) ppm. ^{13}C{^{1}H} NMR (CD_2Cl_2, 150 MHz, 300 K): δ = 150.1, 149.2, 148.7, 146.3, 141.8, 138.3, 134.2, 133.4, 132.2, 128.8, 127.7, 127.0, 126.9, 124.7, 83.9 ppm. IR: $\tilde{\nu}$ = 3423, 3035, 2911, 1712, 1592, 1407, 1197, 973, 914, 821, 757, 727, 605, 566 cm^{-1}. HRMS (ESI$^+$) m/z: $[M+H]^+$: calcd. for $C_{38}H_{25}N_4O_2^+$: 569.1972; found 569.1973; m/z: $[M+Na]^+$: calcd. for $C_{38}H_{24}N_4O_2Na^+$: 591.1792; found 591.1793 correct isotope distribution.

6.2.2 Synthesis of 5,7,12,14-Tetrafunctionalized Diazapentacenes (Chapter 3)

5,7,12,14-Tetrabromo-6,13-dihydro-6,13-diazapentacene (**104**) was synthesized according to the literature procedures.[113]

General Synthesis Procedure for **3a-3c**:

104 (200 mg, 0.33 mmol), arylboronic acid (8.00 eq.), $Pd(PPh_3)_4$ (76.0 mg, 65.8 µmol, 0.20 eq.), and K_2CO_3 (462 mg, 3.34 mmol, 10.0 eq.) were added into the flask under N_2. 1,4-Dioxane (16 mL) and water (4 mL) were purged with N_2 for 20 min and then added into the flask. The resulting mixture was stirred at 70 ˚C for 4 days. After cooling to r.t., a pale green precipitate formed. It was collected by filtration and washed with water and ethanol. The crude product was dissolved in DCM (20 mL), followed by treatment with MnO_2 (872 mg, 10.0 mmol, 30.0 eq.) at r.t. for 6 h.

5,7,12,14-Tetra(3,5-dimethoxylphenyl)-6,13-diazapentacene (**3a**)

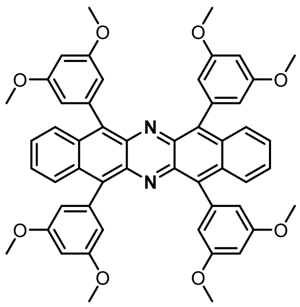

3,5-Dimethoxylphenylboronic acid (487 mg, 2.56 mmol, 8.00 eq.) was employed. After reaction, DCM was evaporated under reduced pressure and the crude product was purified by flash column chromatography (SiO_2, EE) to give a dark green solid. Further washing with PE gave pure **3a**. Yield: 146 mg, 0.18 mmol, 53%. Mp: > 400 ℃ (decomposition). ^{1}H-NMR ($CDCl_3$, 500 MHz, 295 K): δ = 8.15-7.98 (m, 4H), 7.42-7.32 (m, 4H), 6.67-6.47 (m, 12H), 3.78-3.66 (m, 24H) ppm. ^{13}C{^{1}H} NMR ($CDCl_3$, 126 MHz, 295 K): δ = 160.2, 138.1, 133.2, 127.8, 127.2, 110.2, 100.2, 55.4 ppm. IR: $\tilde{\nu}$ = 3073, 2993, 2932, 2829, 1594, 1449, 1206, 1137, 1057, 757 cm^{-1}. MS (MALDI) m/z: $[M]^+$: calcd. for $C_{52}H_{44}N_2O_8$: 824.9300; found 825.3180; correct isotope distribution.

5,7,12,14-Tetraphenyl-6,13-diazapentacene (**3b**)

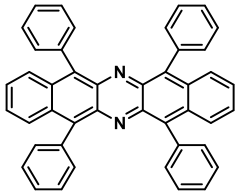

Phenylboronic acid (326 mg, 2.56 mmol, 8.00 eq) was employed. After reaction, DCM was evaporated under reduced pressure and the crude product was purified by flash column chromatography (SiO_2, DCM) to give a dark green solid. Subsequent washing with EE gave pure **3b**. Yield: 116 mg, 0.20 mmol, 59%. Mp: > 400 ℃ (decomposition). ^{1}H-NMR (CD_2Cl_2, 600 MHz, 295 K): δ = 8.00-7.94 (m, 4H), 7.50-7.46 (m, 8H), 7.45-7.40 (m, 12H), 7.33-7.29 (m, 4H) ppm. $^{13}C\{^{1}H\}$ NMR (CD_2Cl_2, 151 MHz, 295 K): δ = 138.9, 138.8, 137.4, 133.2, 132.8, 128.1, 128.0, 127.5, 126.7 ppm. IR: $\tilde{\nu}$ = 3080, 3053, 3023, 1730, 1434, 1392, 761, 697, 476 cm^{-1}. MS (ESI) m/z: $[M+H]^+$: calcd. for $C_{44}H_{29}N^+$: 585.7300; found 585.2330; m/z: $[M+Na]^+$: calcd. for $C_{44}H_{28}N_2Na^+$: 607.7118; found 607.2149; correct isotope distribution.

5,7,12,14-Tetra(3,5-bis(trifluoromethyl)phenyl)-6,13-diazapentacene (**3c**)

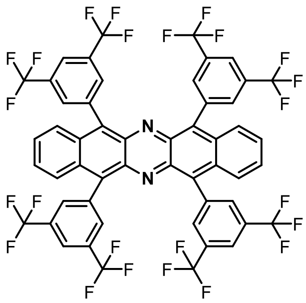

3,5-Bis(trifluoromethyl)phenylboronic acid (690 mg, 2.56 mmol, 8.00 eq.) was employed. After reaction, DCM was evaporated under reduced pressure and the crude product was purified by a flash column chromatography (silica gel, PE/DCM = 3:1) to give a dark green solid. Washed by PE, pure **3c** was obtained. Yield: 298 mg, 0.26 mmol, 79%. Mp: > 400 ℃ (decomposition). ^{1}H-NMR (CD_2Cl_2, 600 MHz, 295 K): δ = 8.00-7.97 (m, 4H), 7.86-7.84 (m, 8H), 7.80-7.76 (m, 4H), 7.49-7.45 (m, 4H) ppm. $^{13}C\{^{1}H\}$ NMR (CD_2Cl_2, 126 MHz, 295 K): δ = 139.0, 138.7, 136.5, 133.7, 132.5, 131.6, 128.7, 127.0, 124.8, 123.0, 122.2, 121.2 ppm. IR: $\tilde{\nu}$ = 2920, 2844, 1609, 1502, 1263, 1008, 974, 826, 552 cm^{-1}. MS (MALDI) m/z: $[M]^+$: calcd. for $C_{52}H_{20}N_2F_{24}$: 1128.7007; found 1128.1257; correct isotope distribution.

6.2.3 Synthesis of Neutral Compounds, Radical Cations, and Dications of 7,14-Dimesityl-5,12-Dihydro-5,12-Diaryldiaza-pentacenes (Chapter 4)

The radical cations and dications are synthesized in glove box under N_2.

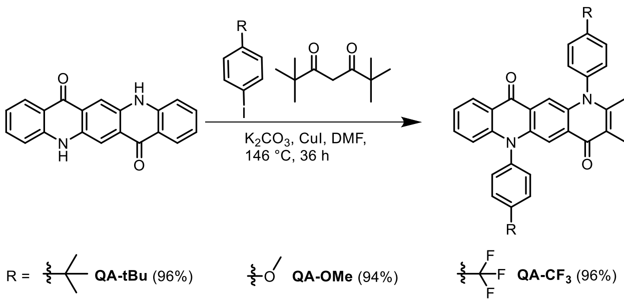

General procedure: Quinacridone (200 mg, 0.64 mmol, 1.00 eq.), 4-iodoarenes (2.56 mmol, 4.00 eq.), K_2CO_3 (354 mg, 2.56 mmol, 4.00 eq.), copper(I) iodide (48.8 mg, 0.26 mmol, 0.40 eq.), 2,2,6,6-tetramethyl-3,5-heptanedione (94.4 mg, 0.51 mmol, 0.80 eq.) and 20 mL dimethyl formamide (DMF) were added into a 100 mL flask under N_2. The mixture was stirred and heated to 146 ℃ for 36 h. After that, the mixture was allowed to cool to r.t. and an orange solid precipitated. The precipitate was filtered and then washed by water and ethanol.

N,N'-Bis(4-tert-butylphenyl)quinacridone (**QA-tBu**)

4-*tert*-Butyliodobenzene (666 mg, 2.56 mmol, 4.00 eq.) was used and **QA-tBu** was obtained as an orange powder. Yield: 354 mg, 0.62 mmol, 96%. Mp: > 400 ℃ (decomposition). ^{1}H-NMR (CD_2Cl_2, 400 MHz, 295 K): δ = 8.44-8.38 (m, 2H), 8.01-7.96 (m, 2H), 7.83-7.79 (m, 4H), 7.55-7.48 (m, 2H), 7.40-7.36 (m, 4H), 7.24-7.18 (m, 2H), 6.84-6.78 (m, 2H), 1.52 (s, 18H) ppm. ^{13}C{^{1}H} NMR (CD_2Cl_2, 100 MHz, 295 K): δ = 178.3, 153.7, 144.6, 138.5, 136.7, 134.3, 130.0, 128.9, 127.6, 126.1, 121.6, 121.2, 117.5, 115.4, 35.6, 31.8 ppm. IR: $\tilde{\nu}$ = 2953, 1630, 1602, 1481, 1435, 1286, 900, 755, 560, 490 cm^{-1}. MS (MALDI) m/z: [M]$^+$: calcd. for $C_{40}H_{36}N_2O_2$: 576.278; found 576.306 correct isotope distribution.

N,N'-Bis(4-methoxylphenyl)quinacridone (**QA-OMe**)

4-Methoxyliodobenzene (599 mg, 2.56 mmol, 4.00 eq.) was used and **QA-OMe** was obtained as an orange powder. Yield: 316 mg, 0.60 mmol, 94%. Mp: > 400 ℃ (decomposition). ^{1}H-NMR (CD_2Cl_2, 600 MHz, 295 K): δ = 8.45-8.37 (m, 2H), 8.00-7.96 (s, 2H), 7.56-7.51 (m, 2H), 7.38-7.35 (m, 4H), 7.31-7.27 (m, 4H), 7.25-7.18 (m, 2H), 6.89-6.82 (m, 2H), 4.03-3.98 (s, 6H) ppm. ^{13}C{^{1}H} NMR (CD_2Cl_2, 151 MHz, 295 K): δ = 178.3, 161.0, 144.7, 138.6, 134.3, 131.8, 131.6, 127.5, 126.0, 121.5, 121.1, 117.4, 116.9, 115.3, 56.3 ppm. IR: $\tilde{\nu}$ = 2962, 2913, 2863, 1525, 1312, 738, 571 cm^{-1}. MS (MALDI) m/z: $[M]^+$: calcd. for $C_{34}H_{24}N_2O_4$: 524.576; found 524.204 correct isotope distribution.

N,N'-Bis(4-trifluoromethylphenyl)quinacridone (**QA-CF$_3$**)

4-Trifluoromethyliodobenzene (697 mg, 2.56 mmol, 4.00 eq.) was used and **QA-CF$_3$** was obtained as an orange powder. Yield: 370 mg, 0.62 mmol, 96%. Mp: > 400 ℃ (decomposition). ^{1}H-NMR (CD_2Cl_2, 400 MHz, 295 K): δ = 8.40-8.29 (m, 2H), 8.13-8.04 (m, 4H), 7.91-7.83 (s, 2H), 7.70-7.64 (m, 4H), 7.57-7.51 (m, 2H), 7.27-7.17 (m, 2H), 6.78-6.67 (m, 2H) ppm. ^{13}C{^{1}H} NMR (CD_2Cl_2, 151 MHz, 295 K): δ = 177.9, 143.9, 142.8, 138.0, 134.7, 131.7, 129.3, 127.8, 126.0, 122.2, 121.2, 117.0, 115.1 ppm. IR: $\tilde{\nu}$ = 3084, 2943, 1609, 1483, 1320, 1096, 1062, 754, 609 cm^{-1}. HRMS (MALDI) m/z: $[M]^+$: calcd. for $C_{34}H_{18}F_6N_2O_2$: 600.5204; found 601.1353 correct isotope distribution.

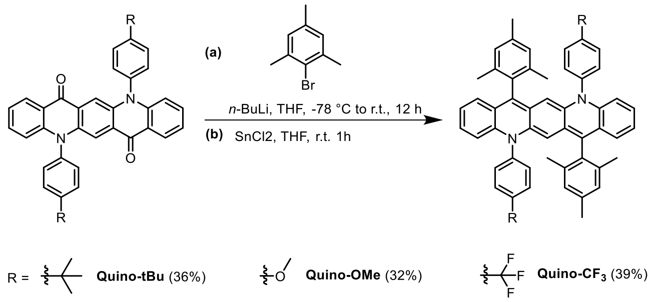

General procedure: 2-Bromomesitylene (552 mg, 0.42 mL, 2.77 mmol, 8.00 eq.) was dissolved in 20 mL dry THF under protection of N_2. *n*-BuLi (0.83 mL, 2.08 mmol, 2.5 M, 6.00 eq.) was added dropwise at -78 ℃. Three hours later, *N,N'*-diphenylquinacridone derivatives (0.35 mmol, 1.00 eq.) were added and the temperature was allowed to increase to r.t.. After stirring for another 12 h, the reaction was quenched by 1 mL water fllowed by adding $SnCl_2$ (3.61 g, 19.0 mmol, 50.0 eq.) into the flask directly. After that, the mixture was stirred at r.t. for 1 h. The mixture was poured into 100 mL ethanol and a red precipitate appeared. The precipitate was filtered and washed by water and ethanol.

7,14-Dimesityl-5,12-dihydro-5,12-bis(4-tert-butylphenyl)diazapentacene (**Quino-tBu**)

QA-tBu (200 mg, 0.35 mmol, 1.00 eq.) was used and **Quino-tBu** was obtained as a red powder. Yield: 97.9 mg, 0.13 mmol, 36%. Mp: > 400 ℃ (decomposition). ^{1}H-NMR (THF-d_8, 600 MHz, 295 K): δ = 7.55-7.47 (m, 4H), 7.06-7.03 (m, 4H), 6.75-6.72 (s, 4H), 6.52-6.47 (m, 2H), 7.37-6.32 (m, 2H), 6.07-6.02 (m, 2H), 5.88-5.83 (m, 2H), 4.15-4.10 (s, 2H), 2.24-2.20 (s, 6H), 1.99-1.93 (s, 12H), 1.38-1.34 (s, 18H) ppm. ^{13}C{^{1}H} NMR (THF-d_8, 150 MHz, 295 K): δ = 151.9, 144.2, 141.5, 137.7, 137.4, 136.3, 133.4, 131.6, 129.6, 128.7, 128.2, 126.5, 126.0, 123.4, 122.7, 121.4, 113.8, 35.1, 31.6, 21.3, 19.7 ppm. IR: $\tilde{\nu}$ = 2962, 2913, 2863, 1525, 1312, 738, 571 cm^{-1}. HRMS (MALDI) m/z: [M]$^+$: calcd. for $C_{58}H_{58}N_2$: 782.4600; found 782.4604 correct isotope distribution.

7,14-Dimesityl-5,12-dihydro-5,12-bis(4-methoxylphenyl)diazapentacene (**Quino-OMe**)

QA-OMe (184 mg, 0.35 mmol, 1.00 eq.) was used and **Quino-OMe** was obtained as a red powder. Yield: 81.9 mg, 0.11 mmol, 32%. Mp: > 400 ℃ (decomposition). ^{1}H-NMR (THF-d_8, 300 MHz, 300 K): δ = 7.01-6.94 (m, 8H), 6.77-6.73 (m, 4H), 6.56-6.48 (s, 2H), 6.42-6.34 (m, 2H), 6.23-6.14 (m, 2H), 6.00-5.91 (m, 2H), 3.87-3.85 (s, 2H), 3.85-3.82 (s, 6H), 2.28-2.24 (s, 6H), 1.97-1.92 (s, 12H) ppm. ^{13}C{^{1}H} NMR (THF-d_8, 101 MHz, 295 K): δ = 160.5, 144.8, 141.9, 137.6, 136.9, 133.7, 133.1, 132.0, 131.4, 128.8, 126.8, 126.2, 123.8, 121.7, 116.7, 114.0, 96.6, 55.8, 21.1, 19.9 ppm. IR: $\tilde{\nu}$ = 2913, 2852, 1506, 1324, 1236, 830, 738, 548 cm^{-1}. HRMS (MALDI) m/z: [M]$^+$: calcd. for $C_{52}H_{46}N_2O_2$: 730.3559; found 730.3572 correct isotope distribution.

7,14-Dimesityl-5,12-dihydro-5,12-bis(4-trifluoromethylphenyl)diazapentacene (**Quino-CF_3**)

QA-CF_3 (210 mg, 0.35 mmol, 1.00 eq.) was used and **Quino-CF_3** was obtained as a red powder. Yield: 110 mg, 0.14 mmol, 39%. Mp: > 400 ℃ (decomposition). ^{1}H-NMR (THF-d_8, 600 MHz, 295 K): δ = 7.84-7.78 (m, 4H), 7.43-7.36 (m, 4H), 6.77-6.71 (m, 4H), 6.60-6.52 (m, 2H), 6.48-6.41 (m, 2H), 6.27-6.18 (m, 2H), 5.89-5.81 (m, 2H), 3.89-3.79 (m, 2H), 2.24-2.21 (s, 6H), 1.96-1.93 (s, 12H) ppm. $^{13}C\{^1H\}$ NMR (THF-d_8, 151 MHz, 295 K): δ = 144.2, 144.1, 141.0, 137.4, 133.1, 131.9, 131.4, 131.2, 131.0, 129.0, 128.9, 126.8, 126.6, 126.0, 124.2, 123.8, 122.3, 113.8, 96.7, 21.0, 19.8 ppm. IR: $\tilde{\nu}$ = 3423, 3035, 2911, 1712, 1592, 1407, 1197, 973, 914, 821, 757, 727, 605, 566 cm^{-1}. HRMS (MALDI) m/z: [M]$^+$: calcd. for $C_{52}H_{40}F_6N_2$: 806.3096; found 806.3099 correct isotope distribution.

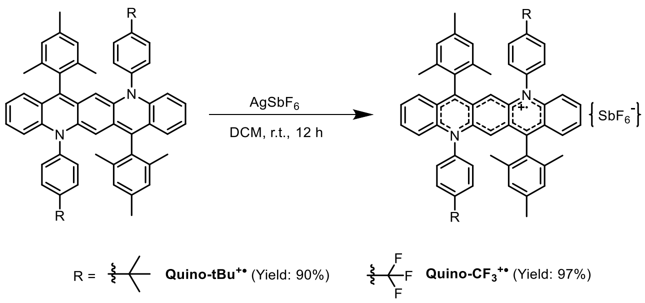

General procedure: To a stirring solution of **Quino-tBu** or **Quino-CF$_3$** (63.9 µmol, 1.00 eq.) in 10 mL DCM, $AgSbF_6$ (22.0 mg, 63.9 µmol, 1.00 eq.) in 1 mL CH_3CN solution was added dropwise and the reaction mixture was stirred for 12 h at r.t.. After that, the mixture was filtered and the solvent was removed under vacuum to give the radical cations without further purification.

Quino-tBu$^{+\bullet}$

Quino-tBu (50.0 mg, 63.9 µmol, 1.00 eq.) was used and **Quino-tBu$^{+\bullet}$** was obtained as a dark brown powder. Yield: 58.5 mg, 57.5 µmol, 90%. IR: $\tilde{\nu}$ = 3057, 2958, 2917, 2867, 1556, 1385, 1248, 1160, 761, 643, 564, 503 cm^{-1}.

Quino-CF$_3^{+\bullet}$

Quino-CF$_3$ (50.6 mg, 63.9 µmol, 1.00 eq.) was used and **Quino-CF$_3^{+\bullet}$** was obtained as a dark brown powder. Yield: 64.6 mg, 62.0 µmol, 97%. IR: $\tilde{\nu}$ = 3065, 2924, 2852, 1560, 1316, 1248, 1062, 1160, 746, 643 cm^{-1}.

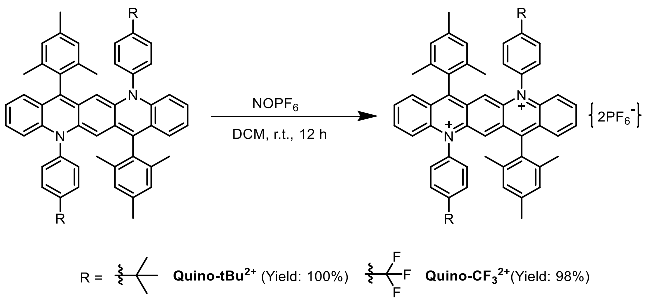

General procedure: To a stirring solution of **Quino-tBu** or **Quino-CF_3** (63.9 μmol, 1.00 eq.) in 10 mL DCM, $NOPF_6$ (22.3 mg, 128 μmol, 2.00 eq.) in 1 mL CH_3CN solution was added dropwise and the reaction mixture was stirred for 12 h at r.t.. After that, the mixture was filtered and the solvent was removed under vacuum to give the dications without further purification.

Quino-tBu^{2+}

Quino-tBu (50 mg, 63.9 μmol, 1.00 eq.) was used and **Quino-tBu^{2+}** was obtained as a deep green solid. Yield: 68.5 mg, 63.8 μmol, 100%. ^{1}H-NMR (acetonitrile-d_3, 600 MHz, 295 K): δ = 8.33-8.28 (m, 2H), 8.26-8.22 (m, 2H), 7.87-7.81 (m, 8H), 7.71-7.68 (m, 2H), 7.60-7.55 (m, 4H), 7.16-7.12 (m, 4H), 2.47-2.39 (s, 6H), 1.78-1.71 (m, 12H), 1.51-1.48 (s, 6H) ppm. ^{13}C{^{1}H} NMR (acetonitrile-d_3, 151 MHz, 295 K): δ = 167.1, 157.1, 147.5, 144.5, 141.9, 138.0, 137.3, 134.9, 130.8, 130.4, 129.8, 129.3, 129.2, 129.1, 128.2, 123.4, 121.5, 36.0, 31.6, 21.8, 20.3 ppm. IR: $\tilde{\nu}$ = 2958, 2920, 2867, 1609, 1533, 826, 765, 560 cm^{-1}.

Quino-CF_3^{2+}

Quino-CF_3 (51.6 mg, 63.9 μmol, 1.00 eq.) was used and **Quino-CF_3^{2+}** was obtained as a deep green solid. Yield: 68.7 mg, 62.6 μmol, 98%. ^{1}H-NMR (acetonitrile-d_3, 600 MHz, 295 K): δ = 8.40-8.32 (m, 2H), 8.20-8.11 (m, 4H), 8.07-8.01 (m, 2H), 7.94-7.83 (m, 8H), 7.79-7.72 (m, 2H), 7.13 (s, 4H), 2.45-2.42 (m, 6H), 1.76-1.71 (m, 12H) ppm. ^{13}C{^{1}H} NMR (acetonitrile-d_3, 151 MHz, 295 K): δ = 168.5, 147.5, 145.7, 142.8, 140.9, 137.8, 137.7, 134.9, 131.4, 131.2, 130.5, 130.0, 129.6, 129.4, 127.7, 125.8, 124.0, 123.2, 121.6, 21.5, 20.6 ppm. IR: $\tilde{\nu}$ = 3095, 2920, 2852, 1316, 1065, 830, 552 cm^{-1}.

6.2.4 Synthesis of Stable *N,N'*-Diarylated Dihydrodiazaacenes and Their Radical Cations (Chapter 5)

The radical cations are synthesized in glove box under N_2. 5,10-Di(4-trifluoromethylphenyl) 5,10-dihydrophenazine (**PNZ**),[158] 5,12-dihydrobenzo[b]phenazine,[159] and 6,13-dihydro-dibenzo[b,i]phenazine[160] were synthesized according to the reported literatures.

General procedure (**GP1**): To a stirring solution of *N*,*N'*-disubstituted dihydrophenazine (1.00 eq.) in 15 mL DCM, $NO^+SbF_6^-$ (1.05 eq.) in 1.5 mL CH_3CN solution was added dropwise and the reaction mixture was stirred for 12 h at r.t.. After that, the mixture was filtered and the solvent was removed under reduced pressure to give the corresponding radical cations.

General procedure (**GP2**): Dihydrophenazine (1.00 eq.), 4-iodobenzotrifluoride (4.00 eq.), RuPhos Pd G1 (0.05 eq.), *t*-BuOK (6.00 eq.), and RuPhos (0.10 eq.) were added into 100 mL flask under N_2. After bubbled with a flow of N_2 for 30 min, 20 mL of toluene was added into the abovementioned flask. The mixture was allowed to heated to 100 ℃ and stirred for 36 h. Thereafter, the solution was filtered through a silica pad with EE, and then concentrated under reduced pressure.

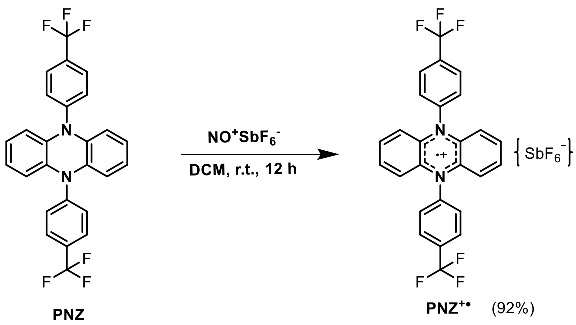

PNZ$^{+\bullet}$

PNZ (50.0 mg, 106 μmol) was used with **GP1**, and **PNZ$^{+\bullet}$** was obtained as a deep green solid. Yield: 69.1 mg, 97.8 μmol, 92%. IR: $\tilde{\nu}$ = 3086, 2920, 2851, 1604, 1559, 1466, 1319, 1060, 649 cm^{-1}.

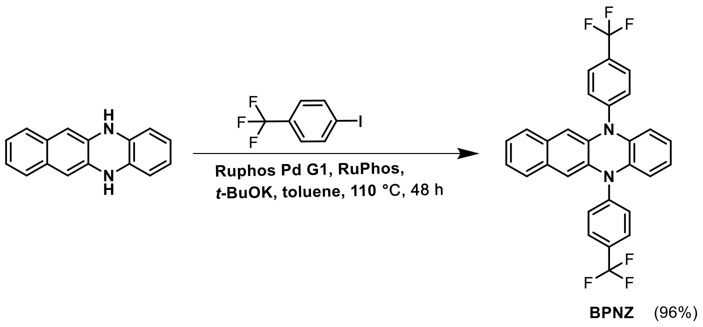

5,12-Di(4-trifluoromethylphenyl)-5,12-dihydrobenzo[b]phenazine (**BPNZ**)

5,12-Dihydrobenzo[b]phenazine (500 mg, 2.15 mmol), 4-iodobenzotrifluoride (2.34 g, 8.61 mmol), RuPhos Pd G1 (88.0 mg, 108 µmol), *t*-BuOK (1.45 g, 12.9 mmol), and RuPhos (100 mg, 215 µmol) were used with **GP2**. The crude product was washed by PE and a faint yellow solid was obtained. Yield: 1.08 g, 2.07 mmol, 96%. Mp: 305 °C. ^{1}H-NMR (CD_2Cl_2, 600 MHz, 295 K): δ = 8.05-7.92 (m, 4H), 7.66-7.60 (m, 4H), 7.09-7.03 (m, 2H), 7.00-6.95 (m, 2H), 6.42-6.33 (m, 2H), 5.85-5.80 (s, 2H), 5.75-5.67 (m, 2H) ppm. ^{13}C {^{1}H} NMR (CD_2Cl_2, 151 MHz, 295 K): δ = 143.7, 136.6, 134.7, 132.5, 131.0, 129.3, 126.0, 125.5, 124.7, 123.7, 121.6, 113.4, 108.0 ppm. IR: $\tilde{\nu}$ = 3059, 1475, 1332, 1120, 1060, 843, 732 cm^{-1}. MS (MALDI) m/z: $[M]^+$: calcd. for $C_{30}H_{18}N_2F_6$: 520.478; found 520.098; correct isotope distribution.

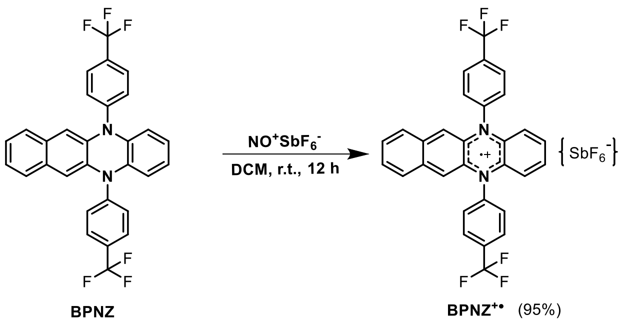

$BPNZ^{+\bullet}$

BPNZ (50.0 mg, 96.1 µmol) and $NO^+SbF_6^-$ (26.8 mg, 101 µmol) were used with **GP1**, and **$BPNZ^{+\bullet}$** was obtained as a dark red solid. Yield: 69.0 mg, 91.3 µmol, 95%. IR: $\tilde{\nu}$ = 3063, 2980, 2915, 1600, 1435, 1323, 1065, 645 cm^{-1}.

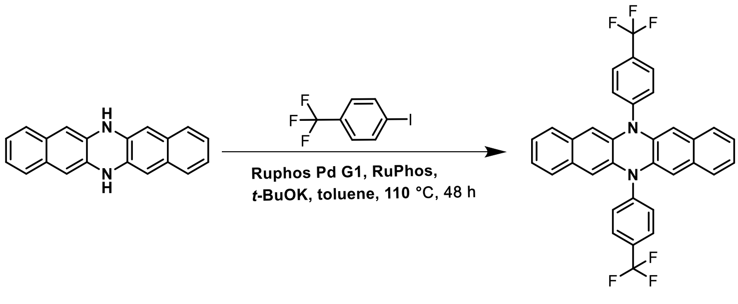

6,13-Di(4-trifluoromethylphenyl)-6,13-dihydrodibenzo[b,i]phenazine (**DPNZ**)

6,13-Dihydrodibenzo[b,i]phenazine (200 mg, 703 μmol), 4-iodobenzotrifluoride (765 mg, 2.81 mmol), RuPhos Pd G1 (28.7 mg, 35.2 μmol), *t*-BuOK (474 mg, 4.22 mmol), and RuPhos (32.8 mg, 70.3 μmol) were used with **GP2**. After having a column chromatography (silica gel, DCM), the residue was washed by PE to give a yellow solid. Yield: 226 mg, 395 μmol, 56%. Mp: > 400 ℃ (decomposition). ^{1}H-NMR (CD_2Cl_2, 400 MHz, 295 K): δ = 8.10-8.01 (m, 4H), 7.74-7.67 (m, 4H), 7.18-7.12 (m, 4H), 7.06-6.99 (m, 4H), 6.02-5.97 (s, 4H) ppm. ^{13}C {^{1}H} NMR (CD_2Cl_2, 151 MHz, 295 K): δ = 143.7, 136.6, 134.7, 132.5, 131.0, 129.3, 126.0, 125.5, 124.7, 123.7, 121.6, 113.4, 108.0 ppm. IR: $\tilde{\nu}$ = 3059, 1614, 1457, 1305, 1129, 1060, 843, 746 cm^{-1}. MS (MALDI) m/z: $[M]^+$: calcd. for $C_{30}H_{18}N_2F_6$: 520.478; found 520.098; correct isotope distribution.

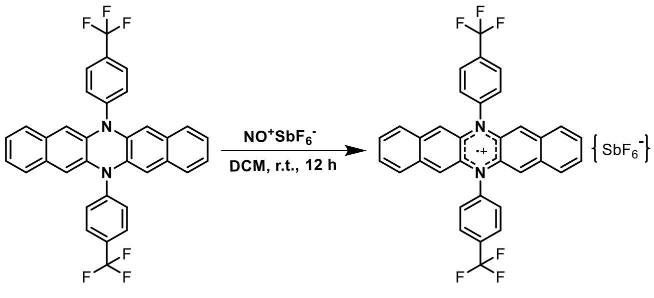

DPNZ$^{+\bullet}$

DPNZ (50.0 mg, 87.6 μmol) and $NO^+SbF_6^-$ (25.6 mg, 96.4 μmol) were used with **GP1**, and **DPNZ$^{+\bullet}$** was obtained as a brown solid. Yield: 65.0 mg, 80.6 μmol, 92%. IR: $\tilde{\nu}$ = 3054, 2925, 2856, 2754, 1591, 1314, 1055, 645 cm^{-1}.

6.3 NMR Spectra

6.3.1 NMR spectra (Chapter 2)

^{1}H-NMR and $^{13}C\{^{1}H\}$ NMR of 1,1-diphenyl-3-pyridyl-2-propyn-1-ol

OriginalDateForRelativeTime	2017-07-20T19:31:06			*Multiplets Integrals Sum*	14.84	*Number of Nuclei*	15 H's
Acquisition Time (sec)	3.2768	*Comment*	Z810701 0032 (PA BBI 500S2 H-BB-D-05 Z)	*D*	0.1	*D1*	0.1
DE	6.5	*DS*	2	*Date*	20 Jul 2017 19:31:06	*Date Stamp*	20 Jul 2017 19:31:06
File Name	\\bunz22\Mitarbeiter\Gaozhan XIE\03 analytics\01-NMR\d170720ubxgz024\1\fid			*Frequency (MHz)*	500.1300	*GB*	0
INSTRUM	<spect>	*LB*	0.3	*NS*	2048	*Nucleus*	1H
Number of Transients	2048						
Origin	spect	*Original Points Count*	49152	*Owner*	ns	*PC*	1
PROBHD	<Z810701 0032 (PA BBI 500S2 H-BB-D-05 Z)>			*PULPROG*	<zg30>	*Points Count*	65536
Pulse Sequence	zg30						
Receiver Gain	287.00	*SF*	500.130048920708	*SFO1*	500.13250065		
SI	65536	*SSB*	0	*SW(cyclical) (Hz)*	15000.00	*SWH*	15000
Solvent	CHLOROFORM-d						
Spectrum Offset (Hz)	2488.2749	*Spectrum Type*	standard	*Sweep Width (Hz)*	14999.77	*TD*	98304
TD0	256						
TE	298.0033	*Temperature (degree C)*	25.003	*UNC1*	<1H>	*WDW*	1

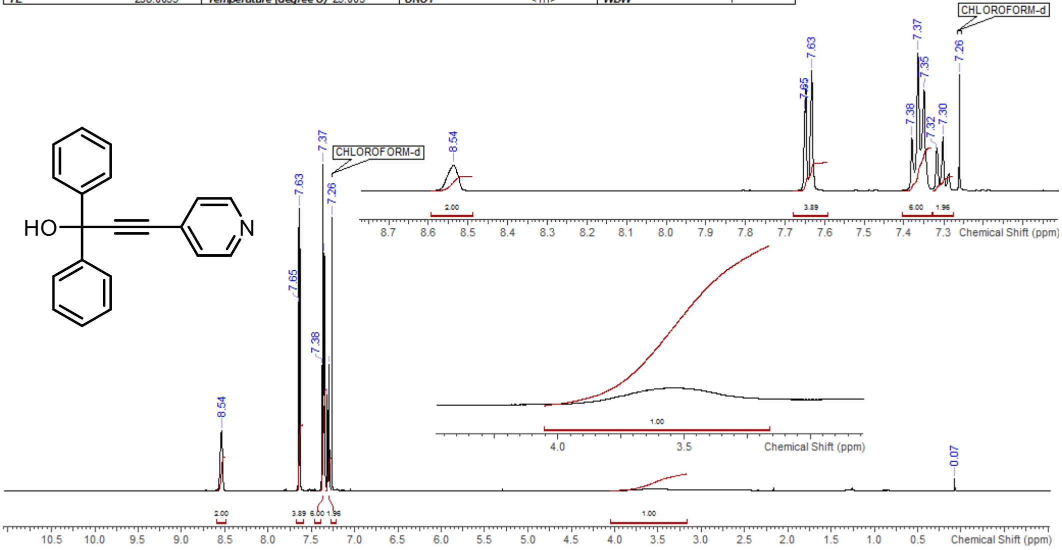

Acquisition Time (sec)	1.7302	*Comment*	Z810701_0032 (PA BBI 500S2 H-BB-D-05 Z)	*D*	1.5	*D1*	1.5
DE	20	*DS*	4	*Date*	20 Jul 2017 23:19:26	*Date Stamp*	20 Jul 2017 23:19:26
File Name	\\bunz22\Mitarbeiter\Gaozhan XIE\03_analytics\01-NMR\d170720ubxgz024\2\PDATA\1\1r			*Frequency (MHz)*	125.7578	*GB*	0
INSTRUM	<spect>	*LB*	0.5	*NS*	4096	*Nucleus*	13C
Number of Transients	4096						
Origin	spect	*Original Points Count*	65536	*Owner*	ns	*PC*	1.4
PROBHD	<Z810701_0032 (PA BBI 500S2 H-BB-D-05 Z)>			*PULPROG*	<zgpg30>	*Points Count*	65536
Pulse Sequence	zgpg30						
Receiver Gain	2050.00	*SF*	125.757789	*SFO1*	125.77162235679	*SI*	65536
SSB	0	*SW(cyclical) (Hz)*	37878.79	*SWH*	37878.7878787879	*Solvent*	CHLOROFORM-d
Spectrum Offset (Hz)	13830.6719	*Spectrum Type*	standard	*Sweep Width (Hz)*	37878.21	*TD*	131072
TD0	512						
TE	298.0268	*Temperature (degree C)*	25.027	*UNC1*	<13C>	*WDW*	1

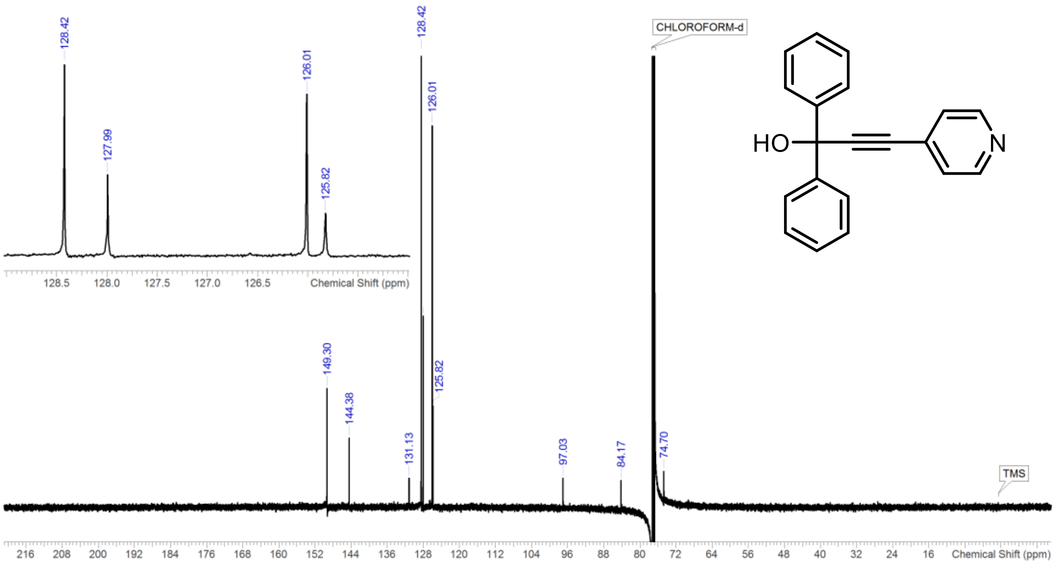

^{1}H-NMR and ^{13}C{^{1}H} NMR of **DAR**

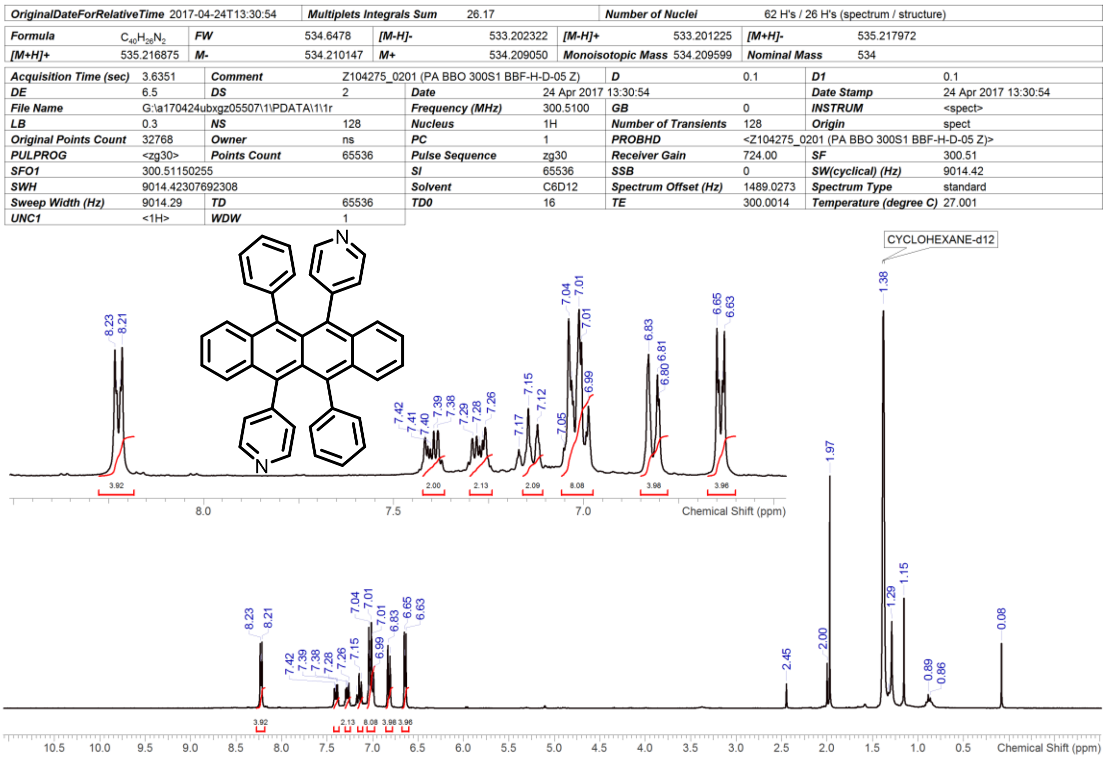

Because **DAR** can be oxidized easily, there is still a little amount of **DARO2** in final product after recrystallization. Fortunately, the solubility of **DAR** is quite better than that of **DARO2** in cyclohexane-d$_{12}$ so that we can get unambiguous ^{1}H-NMR spectrum of **DAR** in this deuterated solvent. However, the dissolved amount of **DAR** is not sufficient enough to reach the requirement of ^{13}C{^{1}H} NMR measurement.

[1]H-NMR and [13]C{[1]H} NMR of **DARO2**

OriginalDateForRelativeTime	2017-07-07T21:10:32			***Multiplets Integrals Sum***	22.80	***Number of Nuclei***	24 H's		
Acquisition Time (sec)	3.6351	***Comment***	XGZO 055	***D***	0.1	***D1***	0.1	***DE***	12
DS	2	***Date***	07 Jul 2017 21:10:32			***Date Stamp***	07 Jul 2017 21:10:32		
File Name	\\bunz22\Mitarbeiter\Gaozhan XIE\03_analytics\01-NMR\e170707ubxgz055-oxidized\2\fid					***Frequency (MHz)***	600.2438	***GB***	0
INSTRUM	<spect>	***LB***	0.3	***NS***	128	***Nucleus***	1H	***Number of Transients***	128
Origin	spect	***Original Points Count***	65536	***Owner***	ns	***PC***	1		
PROBHD	<Z132808_0001 (CP QCI 600S3 H/P/C-N-D-05 Z LT)>					***PULPROG***	<zg30>	***Points Count***	65536
Pulse Sequence	zg30	***Receiver Gain***	15.35	***SF***	600.243829	***SFO1***	600.246830219145		
SI	65536	***SSB***	0	***SW(cyclical) (Hz)***	18028.85	***SWH***	18028.8461538462		
Solvent	DICHLOROMETHANE-d2			***Spectrum Offset (Hz)***	2807.9971	***Spectrum Type***	standard	***Sweep Width (Hz)***	18028.57
TD	131072	***TD0***	16	***TE***	294.9497	***Temperature (degree C)***	21.950	***UNC1***	<1H>
WDW	1								

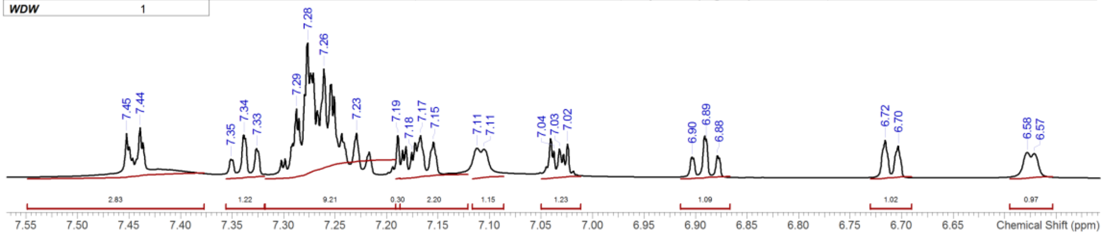

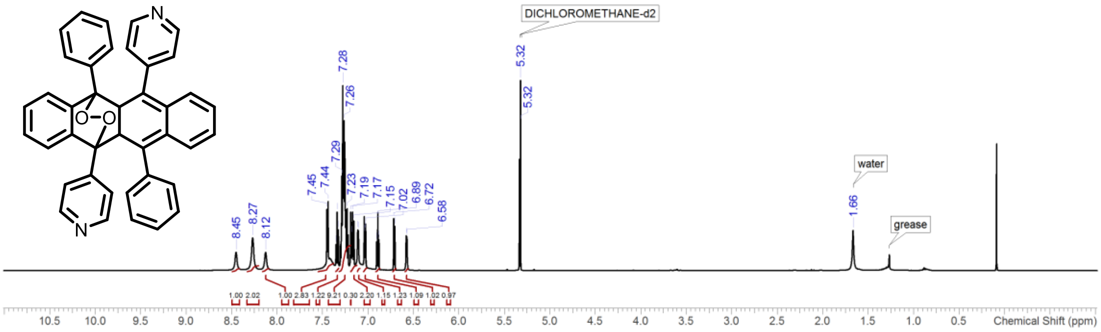

Acquisition Time (sec)	1.0795	***Comment***	XGZO 055	***D***	0.03	***D1***	2	***DE***	18
DS	4	***Date***	07 Jul 2017 21:01:22			***Date Stamp***	07 Jul 2017 21:01:22		
File Name	C:\Users\bunz\Application Data\SSH\temp\1\PDATA\1\1r					***Frequency (MHz)***	150.9314	***GB***	0
INSTRUM	<spect>	***LB***	1	***NS***	4096	***Nucleus***	13C	***Number of Transients***	4096
Origin	spect	***Original Points Count***	49066	***Owner***	ns	***PC***	1.4		
PROBHD	<Z132808_0001 (CP QCI 600S3 H/P/C-N-D-05 Z LT)>					***PULPROG***	<zgpg30>	***Points Count***	65536
Pulse Sequence	zgpg30	***Receiver Gain***	2050.00	***SF***	150.931431	***SFO1***	150.94803345741		
SI	65536	***SSB***	0	***SW(cyclical) (Hz)***	45454.55	***SWH***	45454.5454545455		
Solvent	DICHLOROMETHANE-d2			***Spectrum Offset (Hz)***	16626.6035	***Spectrum Type***	standard	***Sweep Width (Hz)***	45453.85
TD	98132	***TD0***	512	***TE***	294.9497	***Temperature (degree C)***	21.950	***UNC1***	<13C>
WDW	1								

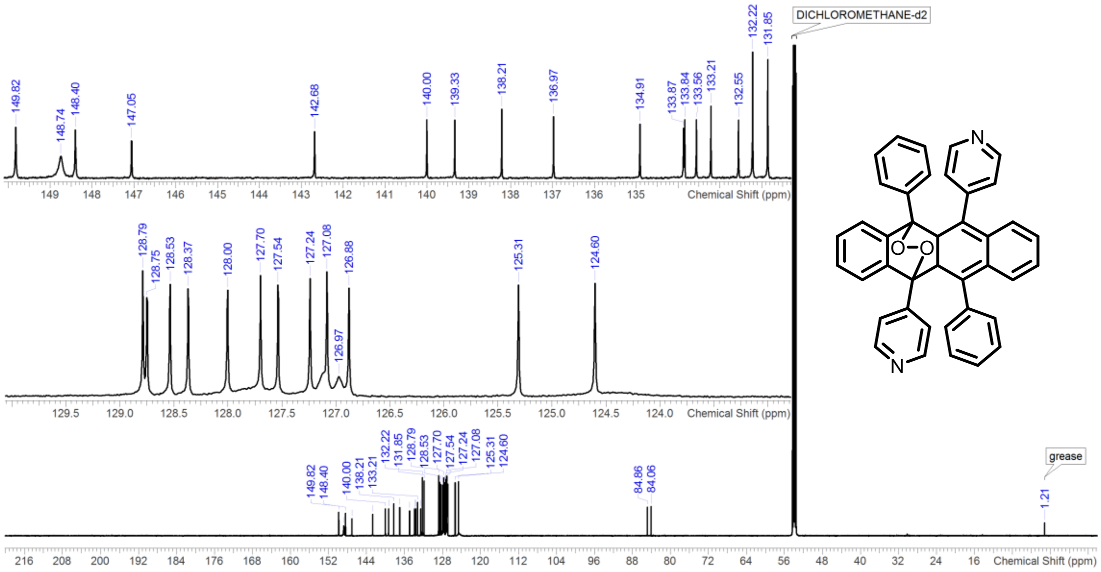

^{1}H-NMR and ^{13}C{^{1}H} NMR of **TAR**

OriginalDateForRelativeTime	2017-12-06T00:07:28	**Multiplets Integrals Sum**	24.25	**Number of Nuclei**	37 H's

Acquisition Time (sec)	3.2768	**Comment**	Z810701_0032 (PA BBI 500S2 H-BB-D-05 Z)			**D**	0.1	**D1**	0.1
DE	6.5	**DS**	2	**Date**	06 Dec 2017 00:07:28			**Date Stamp**	06 Dec 2017 00:07:28
File Name	\\bunz22\Mitarbeiter\Gaozhan XIE\03_analytics\01-NMR\d171205ubxgzTAR\1\PDATA\1\1r					**Frequency (MHz)**	500.1299	**GB**	0
INSTRUM	<spect>	**LB**	0.3	**NS**	1024	**Nucleus**	1H	**Number of Transients**	1024
Origin	spect	**Original Points Count**	49152	**Owner**	ns	**PC**	1		
PROBHD	<Z810701_0032 (PA BBI 500S2 H-BB-D-05 Z)>			**PULPROG**	<zg30>	**Points Count**	65536	**Pulse Sequence**	zg30
Receiver Gain	256.00	**SF**	500.129953368799			**SFO1**	500.13250065		
SI	65536	**SSB**	0	**SW(cyclical) (Hz)**	15000.00	**SWH**	15000	**Solvent**	THF
Spectrum Offset (Hz)	3411.5051	**Spectrum Type**	standard	**Sweep Width (Hz)**	14999.77	**TD**	98304	**TD0**	128
TE	298.0014	**Temperature (degree C)**	25.001	**UNC1**	<1H>	**WDW**	1		

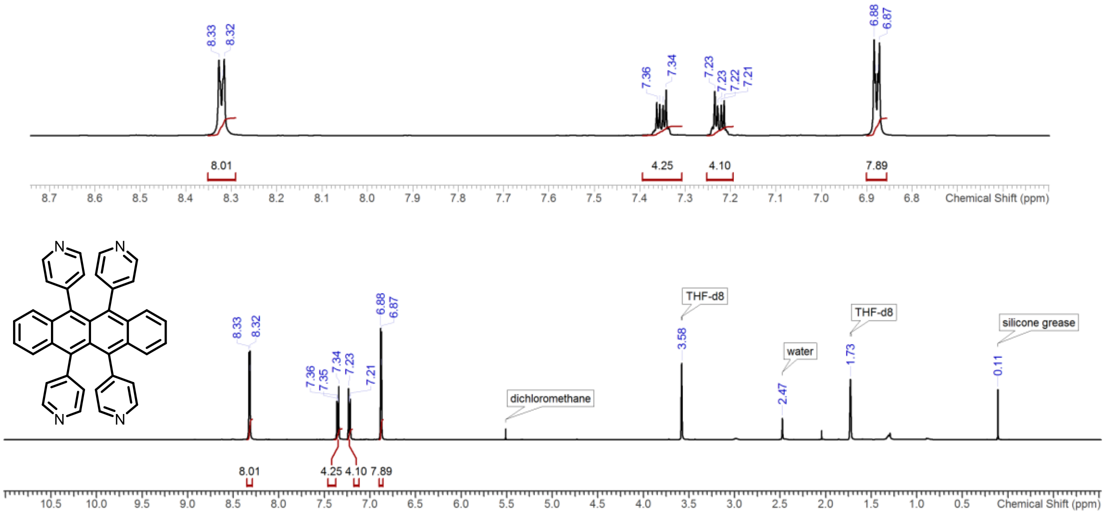

OriginalDateForRelativeTime	2017-12-06T02:01:26	**Multiplets Integrals Sum**	0.00	**Number of Nuclei**	4 C's

Acquisition Time (sec)	1.7302	**Comment**	Z810701_0032 (PA BBI 500S2 H-BB-D-05 Z)			**D**	1.5	**D1**	1.5
DE	20	**DS**	4	**Date**	06 Dec 2017 02:01:26			**Date Stamp**	06 Dec 2017 02:01:26
File Name	\\bunz22\Mitarbeiter\Gaozhan XIE\03_analytics\01-NMR\d171205ubxgzTAR\2\PDATA\1\1r					**Frequency (MHz)**	125.7578	**GB**	0
INSTRUM	<spect>	**LB**	0.5	**NS**	2048	**Nucleus**	13C	**Number of Transients**	2048
Origin	spect	**Original Points Count**	65536	**Owner**	ns	**PC**	1.4		
PROBHD	<Z810701_0032 (PA BBI 500S2 H-BB-D-05 Z)>			**PULPROG**	<zgpg30>	**Points Count**	65536	**Pulse Sequence**	zgpg30
Receiver Gain	2050.00	**SF**	125.757789	**SFO1**	125.77162235679			**SI**	65536
SSB	0	**SW(cyclical) (Hz)**	37878.79	**SWH**	37878.7878787879			**Solvent**	THF
Spectrum Offset (Hz)	14197.8975	**Spectrum Type**	standard	**Sweep Width (Hz)**	37878.21	**TD**	131072	**TD0**	256
TE	298.0056	**Temperature (degree C)**	25.006	**UNC1**	<13C>	**WDW**	1		

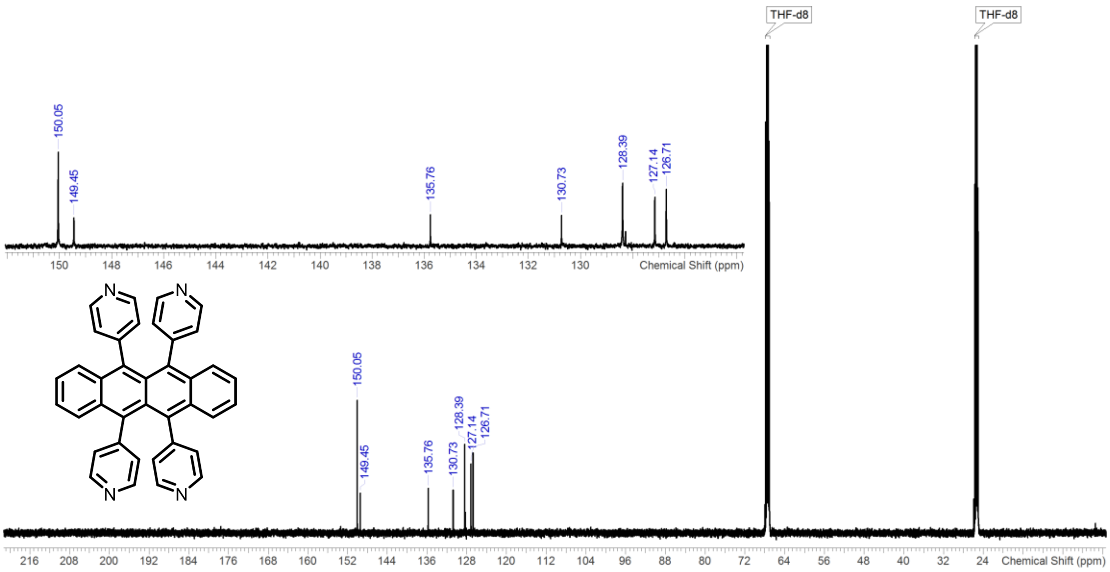

[1]H-NMR and [13]C{[1]H} NMR of **TARO2**

Acquisition Time (sec)	3.6351	*Comment*	Z104275_0201 (PA BBO 300S1 BBF-H-D-05 Z)			*D*	0.1	*D1*	0.1
DE	6.5	*DS*	2	*Date*	16 Jun 2017 20:08:50				
Date Stamp	16 Jun 2017 20:08:50								
File Name	\\bunz22\Mitarbeiter\Gaozhan XIE\03_analytics\01-NMR\Rubren paper\a170616ubxgz084white\1\PDATA\1\1r							*Frequency (MHz)*	300.5100
GB	0	*INSTRUM*	<spect>	*LB*	0.3	*NS*	128	*Nucleus*	1H
Number of Transients	128	*Origin*	spect	*Original Points Count*	32768	*Owner*	ns	*PC*	1
PROBHD	<Z104275_0201 (PA BBO 300S1 BBF-H-D-05 Z)>			*PULPROG*	<zg30>	*Points Count*	65536	*Pulse Sequence*	zg30
Receiver Gain	1030.00	*SF*	300.510036133872			*SFO1*	300.51150255	*SI*	65536
SSB	0	*SW(cyclical) (Hz)*	9014.42	*SWH*	9014.42307692308				
Solvent	DICHLOROMETHANE-d2			*Spectrum Offset (Hz)*	1491.0892	*Spectrum Type*	standard	*Sweep Width (Hz)*	9014.29
TD	65536	*TD0*	16	*TE*	299.9984	*Temperature (degree C)*	26.998	*UNC1*	<1H>
WDW	1								

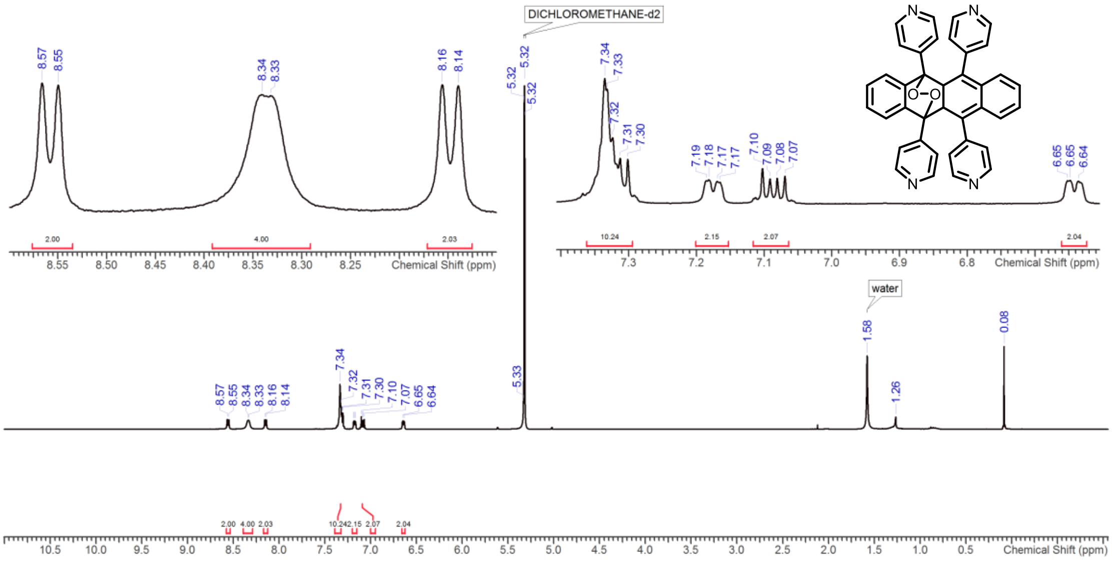

OriginalDateForRelativeTime	2017-07-21T21:43:52			*Multiplets Integrals Sum*	0.00	*Number of Nuclei*	0 C's

Acquisition Time (sec)	1.0795	*Comment*	XG 084	*D*	0.03	*D1*	2	*DE*	18
DS	4	*Date*	21 Jul 2017 21:43:52			*Date Stamp*	21 Jul 2017 21:43:52		
File Name	\\bunz22\Mitarbeiter\Gaozhan XIE\03_analytics\01-NMR\e170721ubxg.084-oxidization\1\PDATA\1\1r							*Frequency (MHz)*	150.9314
GB	0	*INSTRUM*	<spect>	*LB*	1	*NS*	4096	*Nucleus*	13C
Number of Transients	4096	*Origin*	spect	*Original Points Count*	49066	*Owner*	ns	*PC*	1.4
PROBHD	<Z132808_0001 (CP QCI 600S3 H/P/C-N-D-05 Z LT)>			*PULPROG*	<zgpg30>	*Points Count*	65536	*Pulse Sequence*	zgpg30
Receiver Gain	2050.00	*SF*	150.931431	*SFO1*	150.94803345741			*SI*	65536
SSB	0	*SW(cyclical) (Hz)*	45454.55	*SWH*	45454.5454545455				
Solvent	DICHLOROMETHANE-d2			*Spectrum Offset (Hz)*	16642.1660	*Spectrum Type*	standard	*Sweep Width (Hz)*	45453.85
TD	98132	*TD0*	512	*TE*	294.9489	*Temperature (degree C)*	21.949	*UNC1*	<13C>
WDW	1								

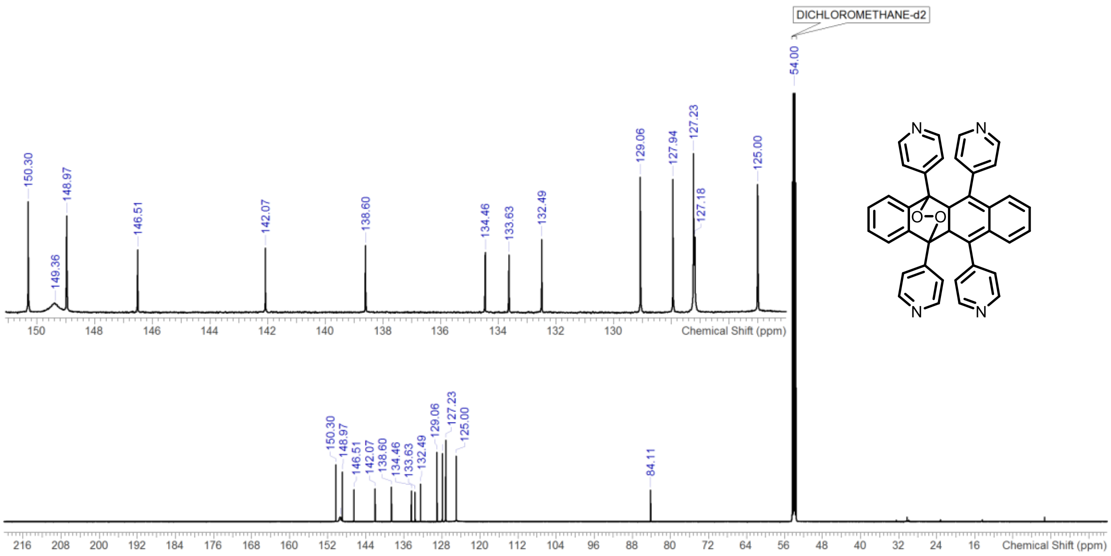

6.3.2 NMR spectra (Chapter 3)

^{1}H-NMR and ^{13}C{^{1}H} NMR of **3a**

Acquisition Time (sec)	3.2768	***Comment***	Z810701_0032 (PA BBI 500S2 H-BB-D-05 Z)			***D***	0.1	***D1***	0.1
DE	6.5	***DS***	2	***Date***	29 Oct 2018 16:57:12			***Date Stamp***	29 Oct 2018 16:57:12
File Name	C:\Users\bunz\Application Data\SSH\temp\1\PDATA\1\1r					***Frequency (MHz)***	500.1301	***GB***	0
INSTRUM	<spect>	***LB***	0.3	***NS***	512	***Nucleus***	1H	***Number of Transients***	512
Origin	spect	***Original Points Count***	49152	***Owner***	ns	***PC***	1		
PROBHD	<Z810701_0032 (PA BBI 500S2 H-BB-D-05 Z)>			***PULPROG***	<zg30>	***Points Count***	65536	***Pulse Sequence***	zg30
Receiver Gain	322.00	***SF***	500.130050707952			***SFO1***	500.13250065		
SI	65536	***SSB***	0	***SW(cyclical) (Hz)***	15000.00	***SWH***	15000	***Solvent***	CHLOROFORM-d
Spectrum Offset (Hz)	2488.5029	***Spectrum Type***	standard	***Sweep Width (Hz)***	14999.77	***TD***	98304	***TD0***	64
TE	294.9941	***Temperature (degree C)***	21.994	***UNC1***	<1H>	***WDW***	1		

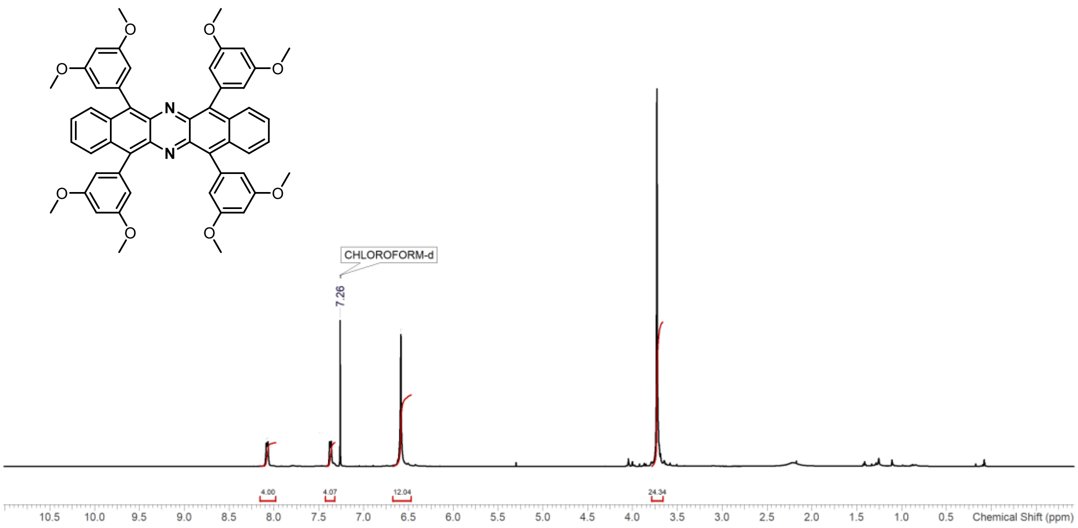

Acquisition Time (sec)	1.7302	***Comment***	Z810701_0032 (PA BBI 500S2 H-BB-D-05 Z)			***D***	1.5	***D1***	1.5
DE	20	***DS***	4	***Date***	29 Oct 2018 21:49:10			***Date Stamp***	29 Oct 2018 21:49:10
File Name	C:\Users\bunz\Application Data\SSH\temp\2\PDATA\1\1r					***Frequency (MHz)***	125.7578	***GB***	0
INSTRUM	<spect>	***LB***	0.5	***NS***	3200	***Nucleus***	13C	***Number of Transients***	3200
Origin	spect	***Original Points Count***	65536	***Owner***	ns	***PC***	1.4		
PROBHD	<Z810701_0032 (PA BBI 500S2 H-BB-D-05 Z)>			***PULPROG***	<zgpg30>	***Points Count***	65536	***Pulse Sequence***	zgpg30
Receiver Gain	2050.00	***SF***	125.757789	***SFO1***	125.77162235679			***SI***	65536
SSB	0	***SW(cyclical) (Hz)***	37878.79	***SWH***	37878.7878787879			***Solvent***	CHLOROFORM-d
Spectrum Offset (Hz)	13850.2148	***Spectrum Type***	standard	***Sweep Width (Hz)***	37878.21	***TD***	131072	***TD0***	400
TE	295.0027	***Temperature (degree C)***	22.003	***UNC1***	<13C>	***WDW***	1		

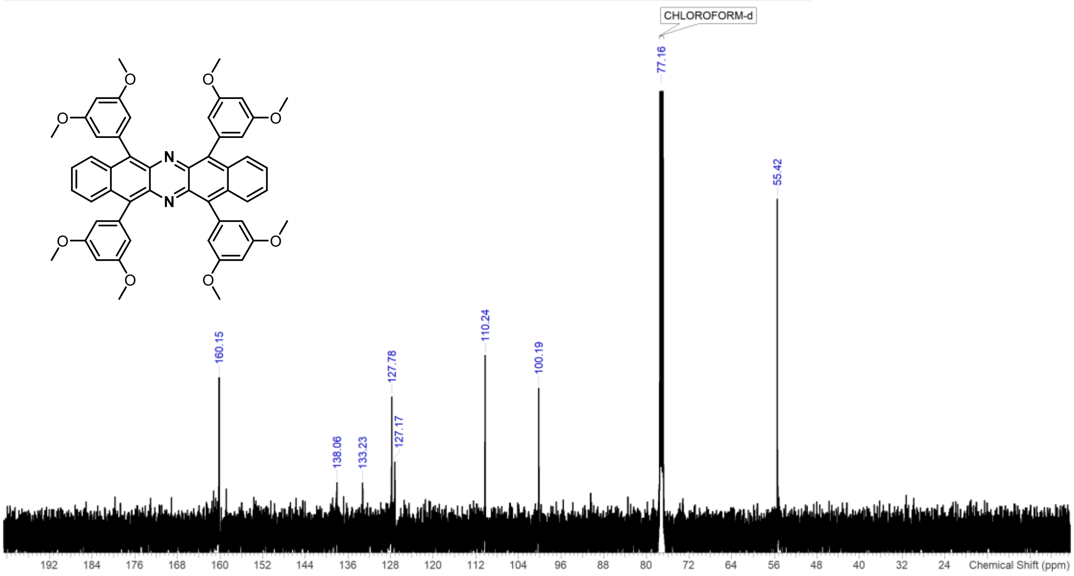

^{1}H-NMR and $^{13}C\{^{1}H\}$ NMR of **3b**

Multiplets Integrals Sum	28.29	Number of Nuclei	28 H's

Acquisition Time (sec)	3.6351	Comment	GZ 273	D	0.1	D1	0.1	DE	12
DS	2	Date	13 Apr 2019 21:57:39			Date Stamp	13 Apr 2019 21:57:39		
File Name	\\bunz22\Mitarbeiter\Gaozhan XIE\03_analytics\01-NMR\nmr02\e190412ubgz.273\2\PDATA\1\1r					Frequency (MHz)	600.2438	GB	0
INSTRUM	<spect>	LB	0.3	NS	128	Nucleus	1H	Number of Transients	128
Origin	spect	Original Points Count	65536	Owner	ns	PC	1		
PROBHD	<Z132808_0001 (CP QCI 600S3 H/P/C-N-D-05 Z LT)>					PULPROG	<zg30>	Points Count	65536
Pulse Sequence	zg30	Receiver Gain	16.84	SF	600.243829	SFO1	600.246830219145		
SI	65536	SSB	0	SW(cyclical) (Hz)	18028.85	SWH	18028.8461538462		
Solvent	DICHLOROMETHANE-d2			Spectrum Offset (Hz)	2807.2170	Spectrum Type	standard	Sweep Width (Hz)	18028.57
TD	131072	TD0	16	TE	295.0002	Temperature (degree C)	22.000	UNC1	<1H>
WDW	1								

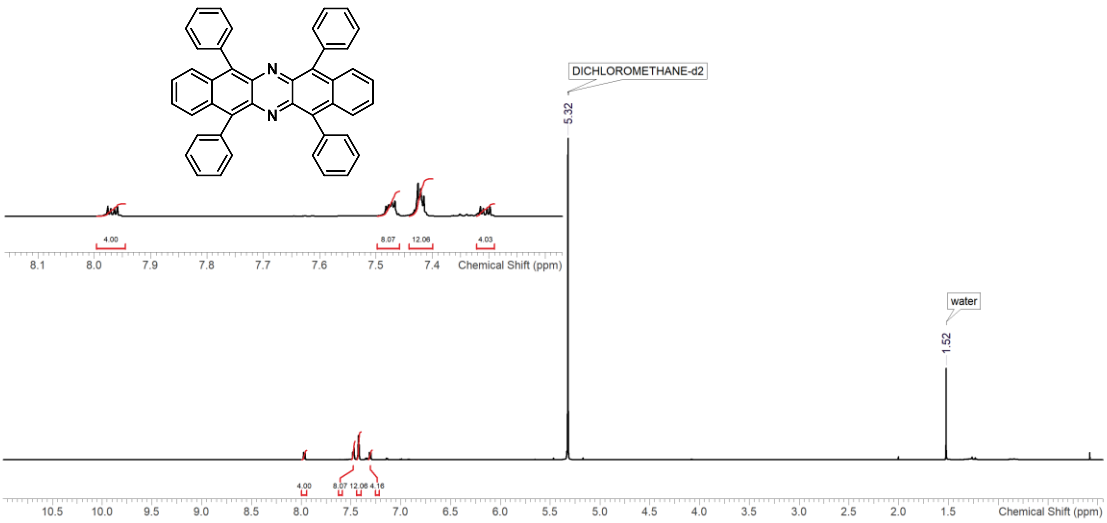

Multiplets Integrals Sum	0.00	Number of Nuclei	0 C's

Acquisition Time (sec)	1.0795	Comment	GZ 273	D	0.03	D1	2	DE	18
DS	4	Date	13 Apr 2019 21:48:39			Date Stamp	13 Apr 2019 21:48:39		
File Name	\\bunz22\Mitarbeiter\Gaozhan XIE\03_analytics\01-NMR\nmr02\e190412ubgz.273\1\PDATA\1\1r					Frequency (MHz)	150.9314	GB	0
INSTRUM	<spect>	LB	1	NS	3200	Nucleus	13C	Number of Transients	3200
Origin	spect	Original Points Count	49066	Owner	ns	PC	1.4		
PROBHD	<Z132808_0001 (CP QCI 600S3 H/P/C-N-D-05 Z LT)>			PULPROG	<zgpg30>	Points Count	65536	Pulse Sequence	zgpg30
Receiver Gain	2050.00	SF	150.931431	SFO1	150.94803345741			SI	65536
SSB	0	SW(cyclical) (Hz)	45454.55	SWH	45454.5454545455				
Solvent	DICHLOROMETHANE-d2			Spectrum Offset (Hz)	16644.2480	Spectrum Type	standard	Sweep Width (Hz)	45453.85
TD	98132	TD0	400	TE	295.0001	Temperature (degree C)	22.000	UNC1	<13C>
WDW	1								

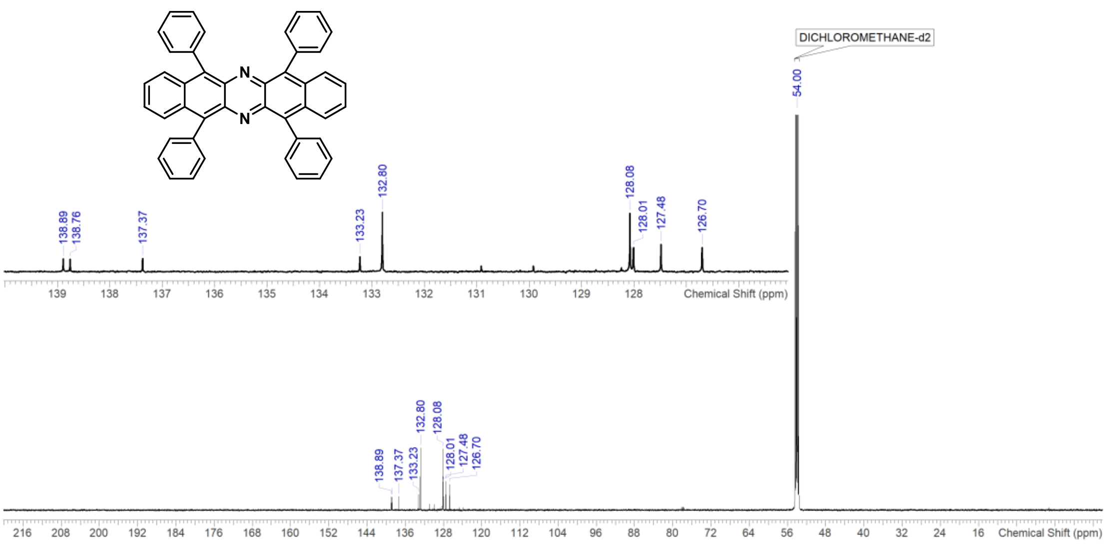

^{1}H-NMR and $^{13}C\{^{1}H\}$ NMR of **3c**

Multiplets Integrals Sum	19.81	Number of Nuclei	20 H's

Acquisition Time (sec)	3.6351	Comment	GZ 399	D	0.1	D1	0.1	DE	12
DS	2	Date	25 Apr 2019 02:14:00			Date Stamp	25 Apr 2019 02:14:00		
File Name	\\bunz22\Mitarbeiter\Gaozhan XIE\03_analytics\01-NMR\nmr02\e190424ubgz.399\2\PDATA\1\1r					Frequency (MHz)	600.2438	GB	0
INSTRUM	<spect>	LB	0.3	NS	128	Nucleus	1H	Number of Transients	128
Origin	spect	Original Points Count	65536	Owner	ns	PC	1		
PROBHD	<Z132808_0001 (CP QCI 600S3 H/P/C-N-D-05 Z LT)>					PULPROG	<zg30>	Points Count	65536
Pulse Sequence	zg30	Receiver Gain	16.84	SF	600.243829	SFO1	600.246830219145		
SI	65536	SSB	0	SW(cyclical) (Hz)	18028.85	SWH	18028.8461538462		
Solvent	DICHLOROMETHANE-d2			Spectrum Offset (Hz)	2807.2170	Spectrum Type	standard	Sweep Width (Hz)	18028.57
TD	131072	TD0	16	TE	294.9995	Temperature (degree C)	22.000	UNC1	<1H>
WDW	1								

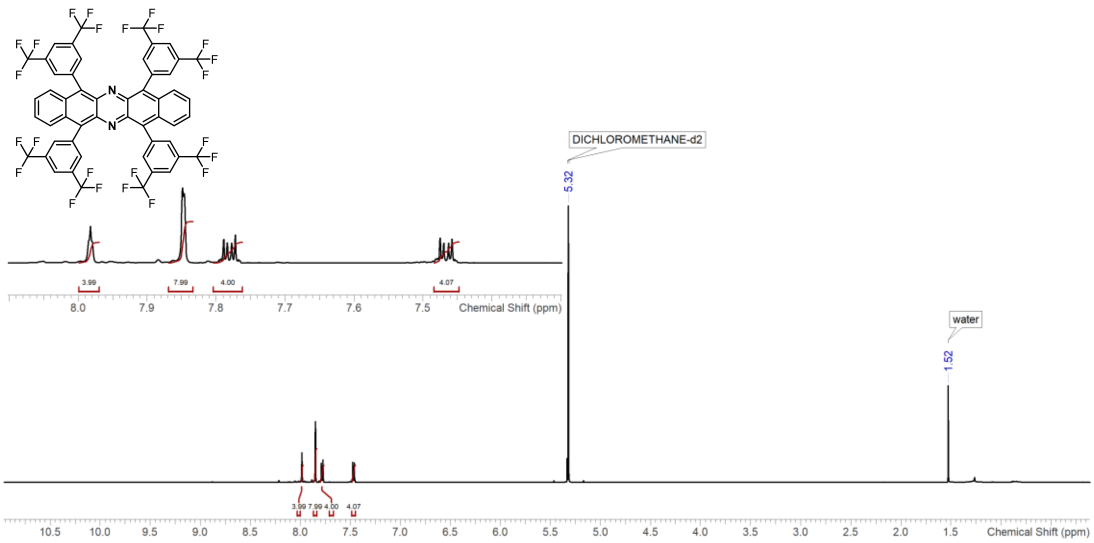

Multiplets Integrals Sum	0.00	Number of Nuclei	0 C's

Acquisition Time (sec)	1.0795	Comment	GZ 399	D	0.03	D1	2	DE	18
DS	4	Date	30 Apr 2019 18:58:38			Date Stamp	30 Apr 2019 18:58:38		
File Name	\\bunz22\Mitarbeiter\Gaozhan XIE\03_analytics\01-NMR\nmr02\e190430ubgz.399\1\PDATA\1\1r					Frequency (MHz)	150.9314	GB	0
INSTRUM	<spect>	LB	1	NS	4096	Nucleus	13C	Number of Transients	4096
Origin	spect	Original Points Count	49066	Owner	ns	PC	1.4		
PROBHD	<Z132808_0001 (CP QCI 600S3 H/P/C-N-D-05 Z LT)>			PULPROG	<zgpg30>	Points Count	65536	Pulse Sequence	zgpg30
Receiver Gain	2050.00	SF	150.931431	SFO1	150.94803345741			SI	65536
SSB	0	SW(cyclical) (Hz)	45454.55	SWH	45454.5454545455				
Solvent	DICHLOROMETHANE-d2			Spectrum Offset (Hz)	16644.9277	Spectrum Type	standard	Sweep Width (Hz)	45453.85
TD	98132	TD0	512	TE	294.9996	Temperature (degree C)	22.000	UNC1	<13C>
WDW	1								

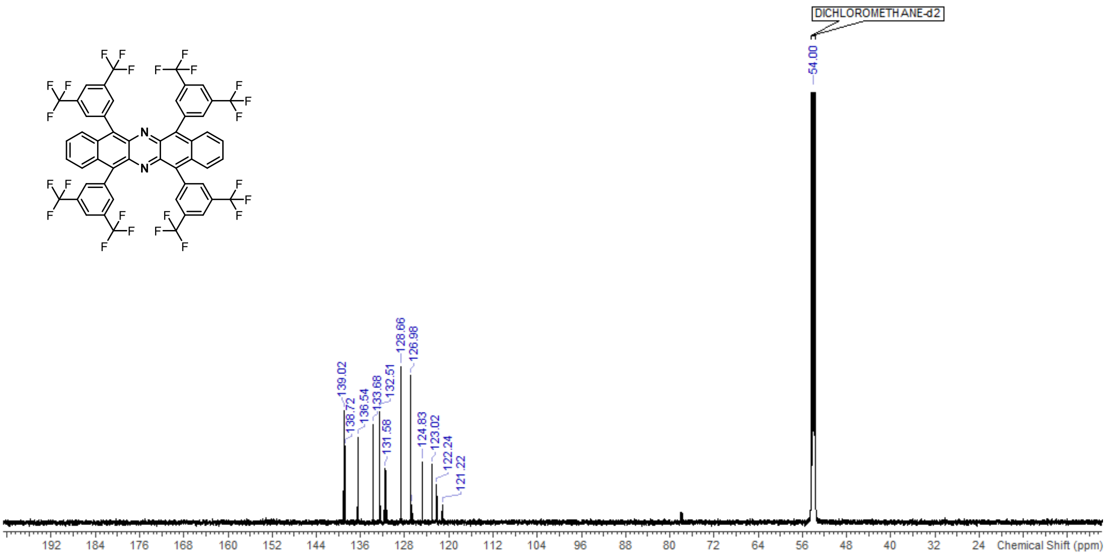

6.3.3 NMR spectra (Chapter 4)

^{1}H-NMR and ^{13}C{^{1}H} NMR of **QA-tBu**

Multiplets Integrals Sum	37.05	***Number of Nuclei***	66 H's

Acquisition Time (sec)	2.7263	***Comment***	GZ 359	***D***	0.5	***D1***	0.5	***DE***	10
DS	2	***Date***	27 Mar 2019 23:33:43			***Date Stamp***	27 Mar 2019 23:33:43		
File Name	C:\Users\bunz\Application Data\SSH\temp\c190327ubgz.359\2\PDATA\1\1r					***Frequency (MHz)***	400.3300	***GB***	0
INSTRUM	<spect>	***LB***	0.3	***NS***	128	***Nucleus***	1H	***Number of Transients***	128
Origin	spect	***Original Points Count***	32768	***Owner***	ns	***PC***	1		
PROBHD	<Z130030_0004 (CPP BBO 400S1 BB-H&F-D-05 LT)>					***PULPROG***	<zg30>	***Points Count***	65536
Pulse Sequence	zg30	***Receiver Gain***	724.00	***SF***	400.33004886814			***SFO1***	400.3320009
SI	65536	***SSB***	0	***SW(cyclical) (Hz)***	12019.23	***SWH***	12019.2307692308		
Solvent	DICHLOROMETHANE-d2			***Spectrum Offset (Hz)***	1985.5005	***Spectrum Type***	standard	***Sweep Width (Hz)***	12019.05
TD	65536	***TD0***	16	***TE***	294.999	***Temperature (degree C)***	21.999	***UNC1***	<1H>
WDW	1								

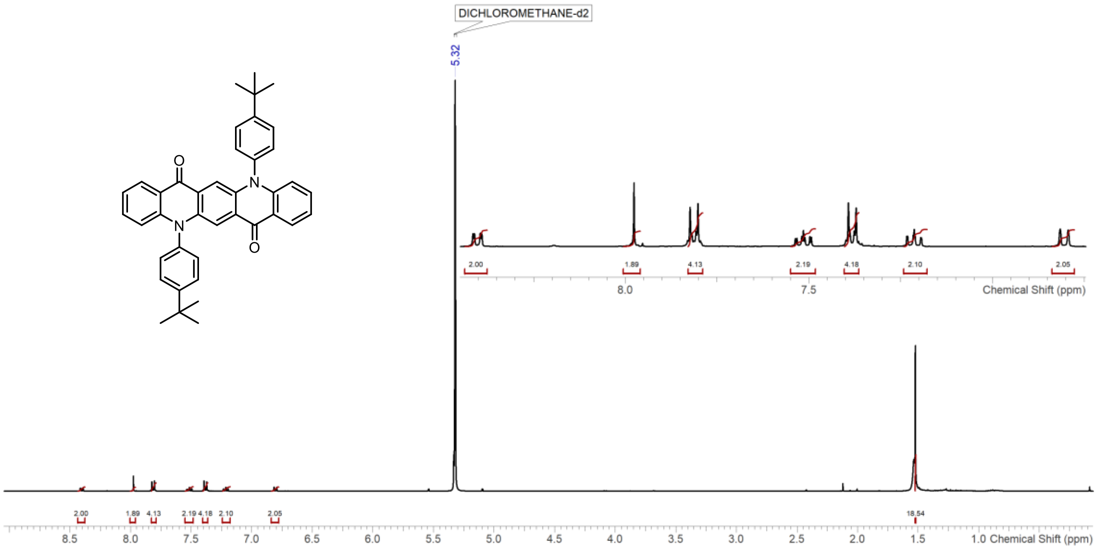

Multiplets Integrals Sum	0.00	***Number of Nuclei***	0 C's

Acquisition Time (sec)	1.5897	***Comment***	GZ 359	***D***	1.5	***D1***	1.5	***DE***	18
DS	2	***Date***	27 Mar 2019 23:25:52			***Date Stamp***	27 Mar 2019 23:25:52		
File Name	\\bunz22\Mitarbeiter\Gaozhan XIE\03_analytics\01-NMR\nmr02\c190327ubgz.359\1\PDATA\1\1r					***Frequency (MHz)***	100.6631	***GB***	0
INSTRUM	<spect>	***LB***	1	***NS***	4096	***Nucleus***	13C	***Number of Transients***	4096
Origin	spect	***Original Points Count***	49066	***Owner***	ns	***PC***	1.4		
PROBHD	<Z130030_0004 (CPP BBO 400S1 BB-H&F-D-05 LT)>			***PULPROG***	<zgpg30>	***Points Count***	65536	***Pulse Sequence***	zgpg30
Receiver Gain	2050.00	***SF***	100.663059	***SFO1***	100.67413193649			***SI***	65536
SSB	0	***SW(cyclical) (Hz)***	30864.20	***SWH***	30864.1975308642				
Solvent	DICHLOROMETHANE-d2			***Spectrum Offset (Hz)***	11135.0059	***Spectrum Type***	standard	***Sweep Width (Hz)***	30863.73
TD	98132	***TD0***	512	***TE***	295.0014	***Temperature (degree C)***	22.001	***UNC1***	<13C>
WDW	1								

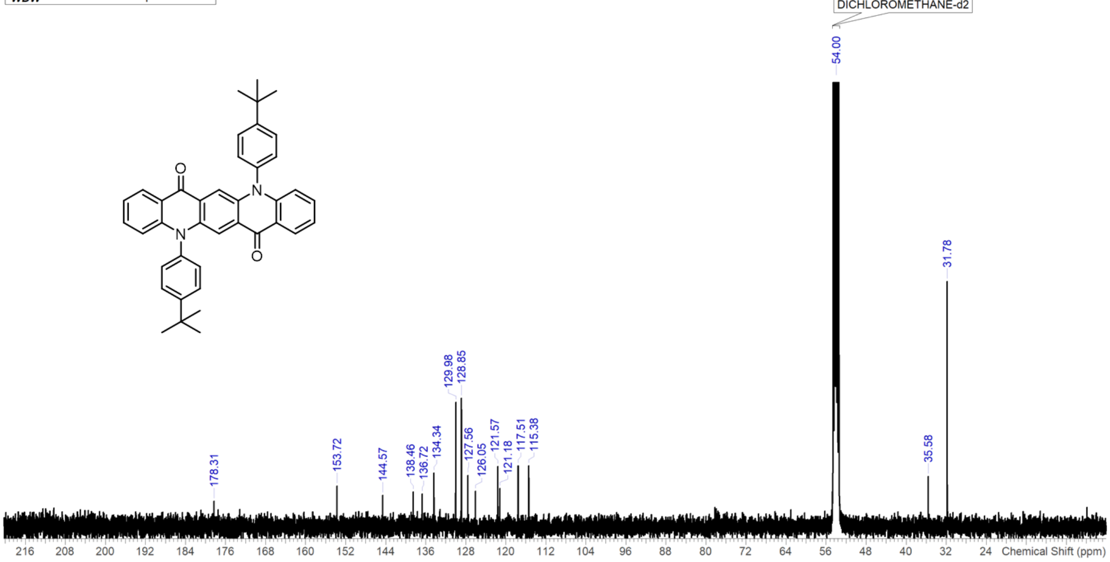

^{1}H-NMR and ^{13}C{^{1}H} NMR of **QA-OMe**

Multiplets Integrals Sum	81.87	Number of Nuclei	86 H's

Acquisition Time (sec)	3.6351	**Comment**	GZ 376	**D**	0.1	**D1**	0.1	**DE**	12
DS	2	**Date**	13 Mar 2019 19:19:45			**Date Stamp**	13 Mar 2019 19:19:45		
File Name	\\bunz22\Mitarbeiter\Gaozhan XIE\03_analytics\01-NMR\nmr02\e190313ubgz.376\2\PDATA\1\1r					**Frequency (MHz)**	600.2438	**GB**	0
INSTRUM	<spect>	**LB**	0.3	**NS**	80	**Nucleus**	1H	**Number of Transients**	80
Origin	spect	**Original Points Count**	65536	**Owner**	ns	**PC**	1		
PROBHD	<Z132808_0001 (CP QCI 600S3 H/P/C-N-D-05 Z LT)>					**PULPROG**	<zg30>	**Points Count**	65536
Pulse Sequence	zg30	**Receiver Gain**	15.35	**SF**	600.243829	**SFO1**	600.246830219145		
SI	65536	**SSB**	0	**SW(cyclical) (Hz)**	18028.85	**SWH**	18028.8461538462		
Solvent	DICHLOROMETHANE-d2			**Spectrum Offset (Hz)**	2806.3765	**Spectrum Type**	standard	**Sweep Width (Hz)**	18028.57
TD	131072	**TD0**	10	**TE**	295.0004	**Temperature (degree C)**	22.000	**UNC1**	<1H>
WDW	1								

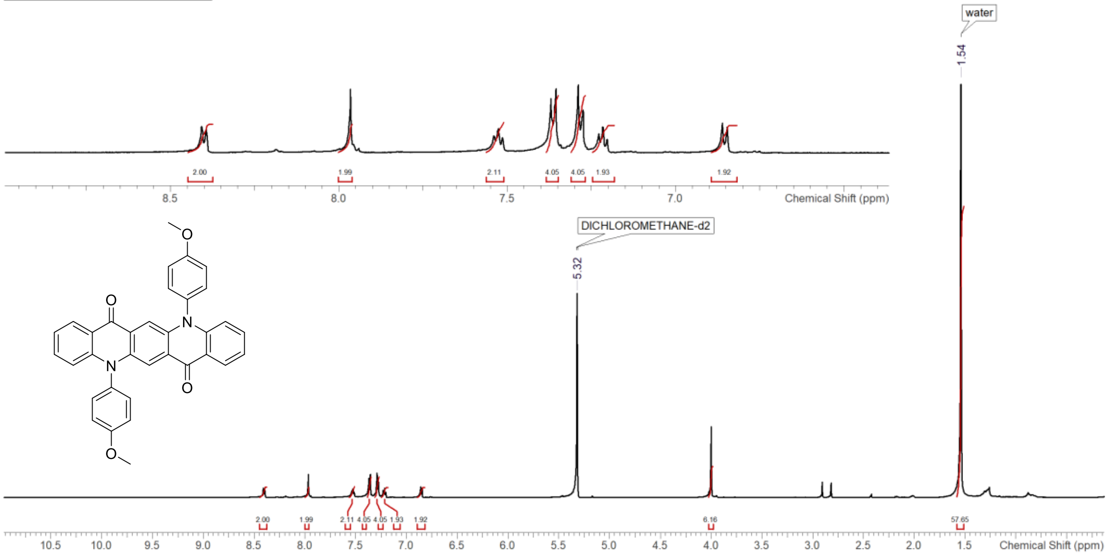

Multiplets Integrals Sum	0.00	Number of Nuclei	0 C's

Acquisition Time (sec)	1.0795	**Comment**	GZ 376	**D**	0.03	**D1**	2	**DE**	18
DS	4	**Date**	13 Mar 2019 19:13:31			**Date Stamp**	13 Mar 2019 19:13:31		
File Name	\\bunz22\Mitarbeiter\Gaozhan XIE\03_analytics\01-NMR\nmr02\e190313ubgz.376\1\PDATA\1\1r					**Frequency (MHz)**	150.9314	**GB**	0
INSTRUM	<spect>	**LB**	1	**NS**	3200	**Nucleus**	13C	**Number of Transients**	3200
Origin	spect	**Original Points Count**	49066	**Owner**	ns	**PC**	1.4		
PROBHD	<Z132808_0001 (CP QCI 600S3 H/P/C-N-D-05 Z LT)>			**PULPROG**	<zgpg30>	**Points Count**	65536	**Pulse Sequence**	zgpg30
Receiver Gain	2050.00	**SF**	150.931431	**SFO1**	150.94803345741			**SI**	65536
SSB	0	**SW(cyclical) (Hz)**	45454.55	**SWH**	45454.5454545455				
Solvent	DICHLOROMETHANE-d2			**Spectrum Offset (Hz)**	16643.5547	**Spectrum Type**	standard	**Sweep Width (Hz)**	45453.85
TD	98132	**TD0**	400	**TE**	294.9997	**Temperature (degree C)**	22.000	**UNC1**	<13C>
WDW	1								

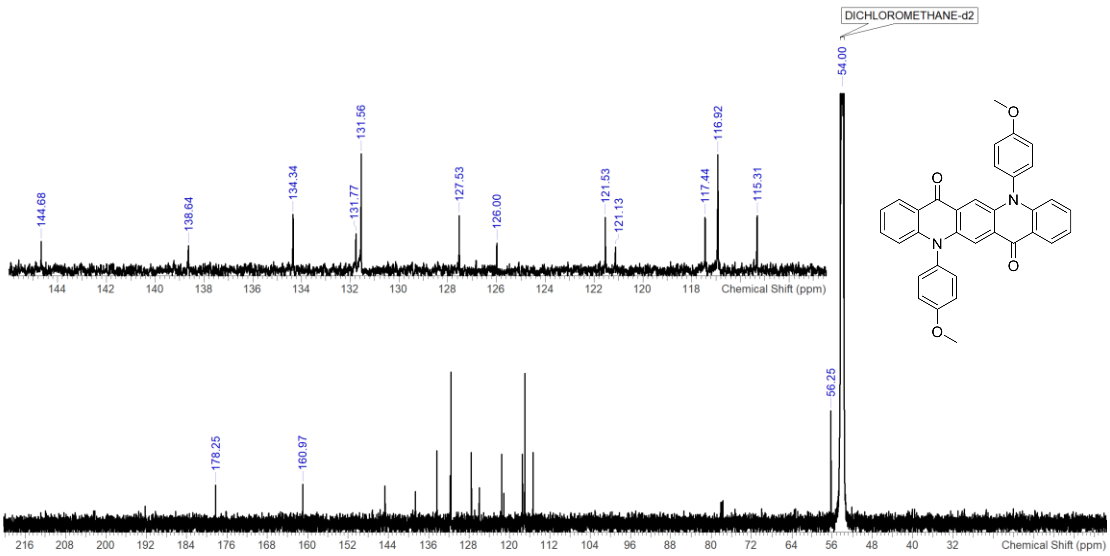

^{1}H-NMR and $^{13}C\{^{1}H\}$ NMR of **QA-CF$_3$**

Multiplets Integrals Sum	17.82	Number of Nuclei	32 H's

Acquisition Time (sec)	2.7263	Comment	GZ 386	D	0.5	D1	0.5	DE	10
DS	2	Date	02 Apr 2019 19:17:32			Date Stamp	02 Apr 2019 19:17:32		
File Name	\\bunz22\Mitarbeiter\Gaozhan XIE\03_analytics\01-NMR\nmr02\c190402ubgz.386\2\PDATA\1\1r					Frequency (MHz)	400.3300	GB	0
INSTRUM	<spect>	LB	0.3	NS	128	Nucleus	1H	Number of Transients	128
Origin	spect	Original Points Count	32768	Owner	ns	PC	1		
PROBHD	<Z130030_0004 (CPP BBO 400S1 BB-H&F-D-05 LT)>					PULPROG	<zg30>	Points Count	65536
Pulse Sequence	zg30	Receiver Gain	645.00	SF	400.33004918049			SFO1	400.3320009
SI	65536	SSB	0	SW(cyclical) (Hz)	12019.23	SWH	12019.2307692308		
Solvent	DICHLOROMETHANE-d2			Spectrum Offset (Hz)	1985.5085	Spectrum Type	standard	Sweep Width (Hz)	12019.05
TD	65536	TD0	16	TE	294.9981	Temperature (degree C)	21.998	UNC1	<1H>
WDW	1								

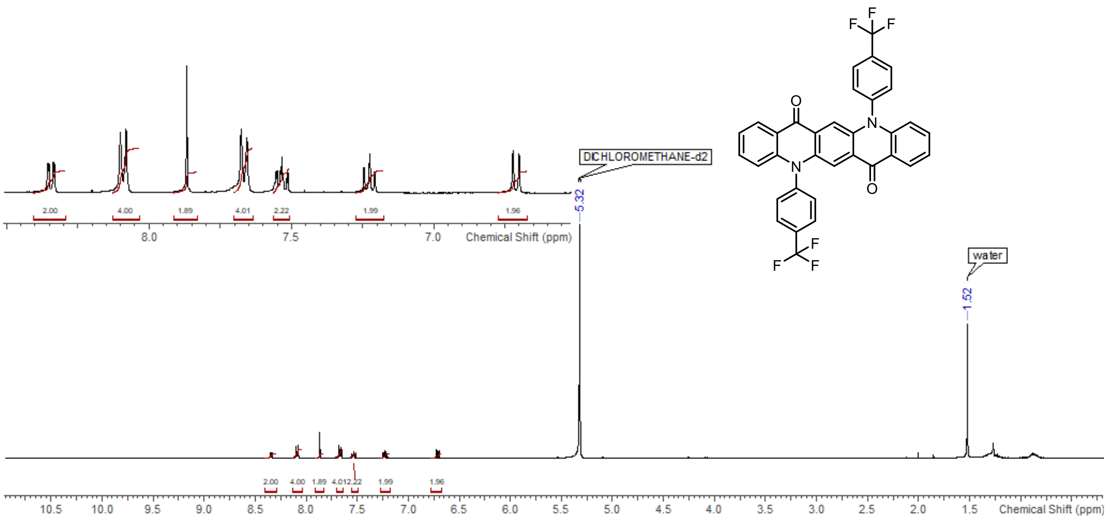

Multiplets Integrals Sum	0.00	Number of Nuclei	0 C's

Acquisition Time (sec)	1.5897	Comment	GZ 386	D	1.5	D1	1.5	DE	18
DS	2	Date	02 Apr 2019 19:09:41			Date Stamp	02 Apr 2019 19:09:41		
File Name	\\bunz22\Mitarbeiter\Gaozhan XIE\03_analytics\01-NMR\nmr02\c190402ubgz.386\1\PDATA\1\1r					Frequency (MHz)	100.6631	GB	0
INSTRUM	<spect>	LB	1	NS	4096	Nucleus	13C	Number of Transients	4096
Origin	spect	Original Points Count	49066	Owner	ns	PC	1.4		
PROBHD	<Z130030_0004 (CPP BBO 400S1 BB-H&F-D-05 LT)>			PULPROG	<zgpg30>	Points Count	65536	Pulse Sequence	zgpg30
Receiver Gain	1620.00	SF	100.663059	SFO1	100.67413193649			SI	65536
SSB	0	SW(cyclical) (Hz)	30864.20	SWH	30864.1975308642				
Solvent	DICHLOROMETHANE-d2			Spectrum Offset (Hz)	11134.5430	Spectrum Type	standard	Sweep Width (Hz)	30863.73
TD	98132	TD0	512	TE	294.999	Temperature (degree C)	21.999	UNC1	<13C>
WDW	1								

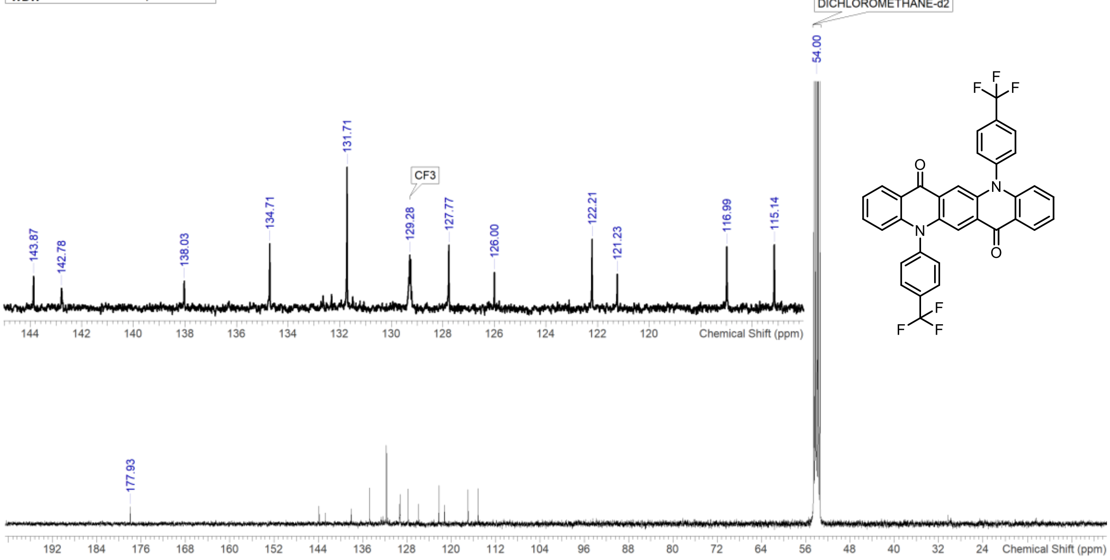

^{1}H-NMR and ^{13}C{^{1}H} NMR of **Quino-tBu**

Acquisition Time (sec)	3.6351	**Comment**	GZ 369	**D**	0.1	**D1**	0.1	**DE**	12
DS	2	**Date**	04 Mar 2019 17:11:44			**Date Stamp**	04 Mar 2019 17:11:44		
File Name	\\bunz22\Mitarbeiter\Gaozhan XIE\03_analytics\01-NMR\nmr02\e190304ubgz.369\2\PDATA\1\1r							**Frequency (MHz)**	600.2438
GB	0	**INSTRUM**	<spect>	**LB**	0.3	**NS**	128	**Nucleus**	1H
Number of Transients	128	**Origin**	spect	**Original Points Count**	65536	**Owner**	ns	**PC**	1
PROBHD	<Z132808_0001 (CP QCI 600S3 H/P/C-N-D-05 Z LT)>					**PULPROG**	<zg30>	**Points Count**	65536
Pulse Sequence	zg30	**Receiver Gain**	13.85	**SF**	600.243829	**SFO1**	600.246830219145		
SI	65536	**SSB**	0	**SW(cyclical) (Hz)**	18028.85	**SWH**	18028.8461538462		
Solvent	THF	**Spectrum Offset (Hz)**	2809.0774	**Spectrum Type**	standard	**Sweep Width (Hz)**	18028.57	**TD**	131072
TD0	16	**TE**	295.0003	**Temperature (degree C)**	22.000	**UNC1**	<1H>	**WDW**	1

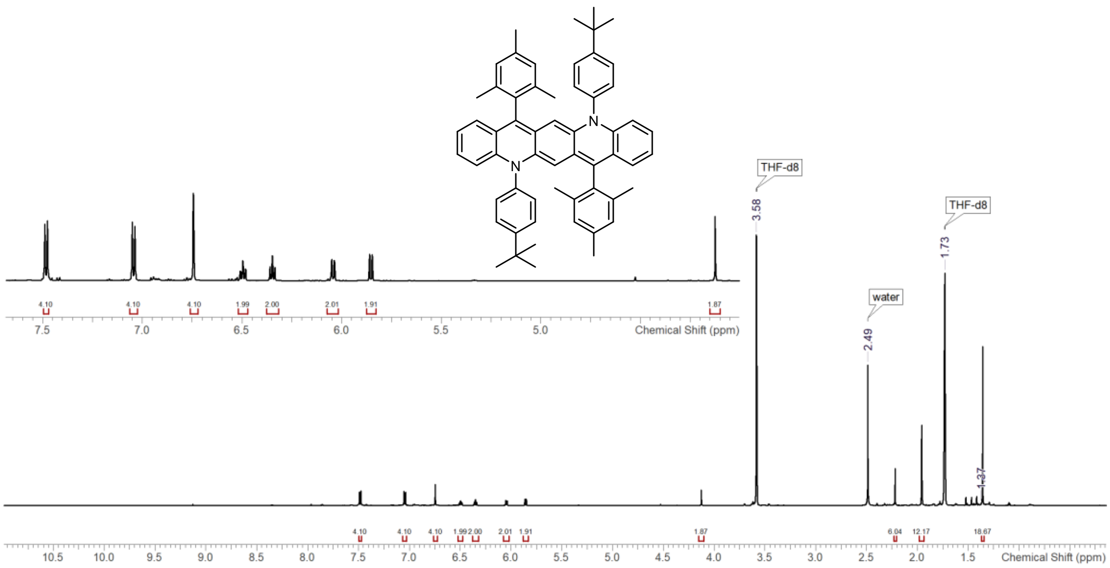

Multiplets Integrals Sum	0.00	**Number of Nuclei**	0 C's

Acquisition Time (sec)	1.0795	**Comment**	GZ 369	**D**	0.03	**D1**	2	**DE**	18
DS	4	**Date**	04 Mar 2019 17:02:37			**Date Stamp**	04 Mar 2019 17:02:37		
File Name	\\bunz22\Mitarbeiter\Gaozhan XIE\03_analytics\01-NMR\nmr02\e190304ubgz.369\1\PDATA\1\1r					**Frequency (MHz)**	150.9314	**GB**	0
INSTRUM	<spect>	**LB**	1	**NS**	4096	**Nucleus**	13C	**Number of Transients**	4096
Origin	spect	**Original Points Count**	49066	**Owner**	ns	**PC**	1.4		
PROBHD	<Z132808_0001 (CP QCI 600S3 H/P/C-N-D-05 Z LT)>					**PULPROG**	<zgpg30>	**Points Count**	65536
Pulse Sequence	zgpg30	**Receiver Gain**	2050.00	**SF**	150.931431	**SFO1**	150.94803345741		
SI	65536	**SSB**	0	**SW(cyclical) (Hz)**	45454.55	**SWH**	45454.5454545455		
Solvent	THF	**Spectrum Offset (Hz)**	16678.6387	**Spectrum Type**	standard	**Sweep Width (Hz)**	45453.85	**TD**	98132
TD0	512	**TE**	294.9989	**Temperature (degree C)**	21.999	**UNC1**	<13C>	**WDW**	1

User Notes	GZ 369

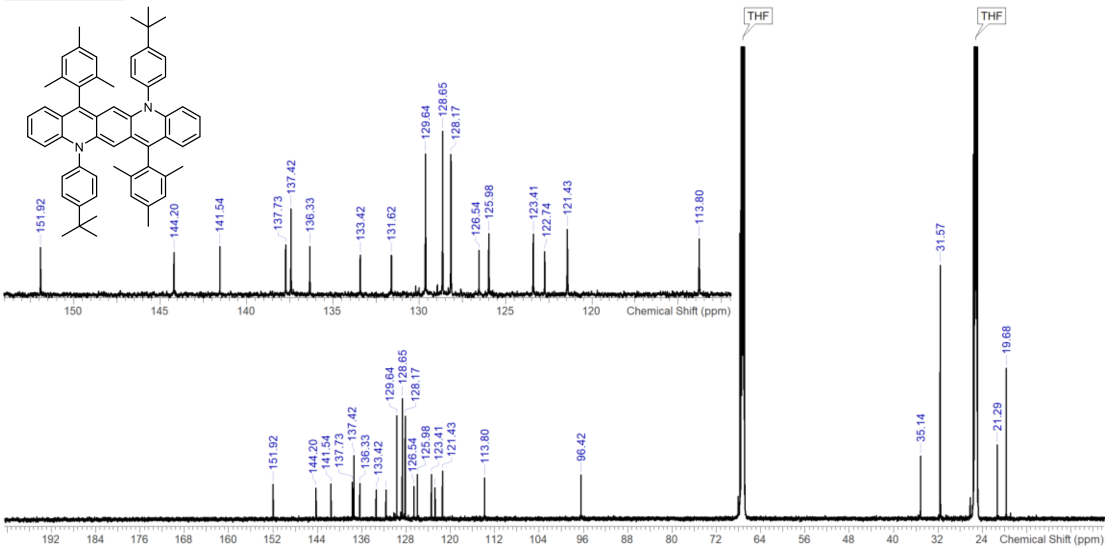

^{1}H-NMR and ^{13}C{^{1}H} NMR of **Quino-OMe**

Multiplets Integrals Sum	45.71	Number of Nuclei	47 H's

Acquisition Time (sec)	3.6351	Comment	Z104275_0201 (PA BBO 300S1 BBF-H-D-05 Z)			D	0.1	D1	0.1
DE	6.5	DS	2	Date	15 May 2019 01:03:45			Date Stamp	15 May 2019 01:03:45
File Name	\\bunz22\Mitarbeiter\Gaozhan XIE\03_analytics\01-NMR\nmr02\a190514ubxgz378\1\PDATA\1\1r					Frequency (MHz)	300.5100	GB	0
INSTRUM	<spect>	LB	0.3	NS	128	Nucleus	1H	Number of Transients	128
Origin	spect	Original Points Count	32768	Owner	ns	PC	1		
PROBHD	<Z104275_0201 (PA BBO 300S1 BBF-H-D-05 Z)>			PULPROG	<zg30>	Points Count	65536	Pulse Sequence	zg30
Receiver Gain	724.00	SF	300.510043559377			SFO1	300.51150255		
SI	65536	SSB	0	SW(cyclical) (Hz)	9014.42	SWH	9014.42307692308		
Solvent	THF	Spectrum Offset (Hz)	1492.0177	Spectrum Type	standard	Sweep Width (Hz)	9014.29	TD	65536
TD0	16	TE	300.0031	Temperature (degree C)	27.003	UNC1	<1H>	WDW	1

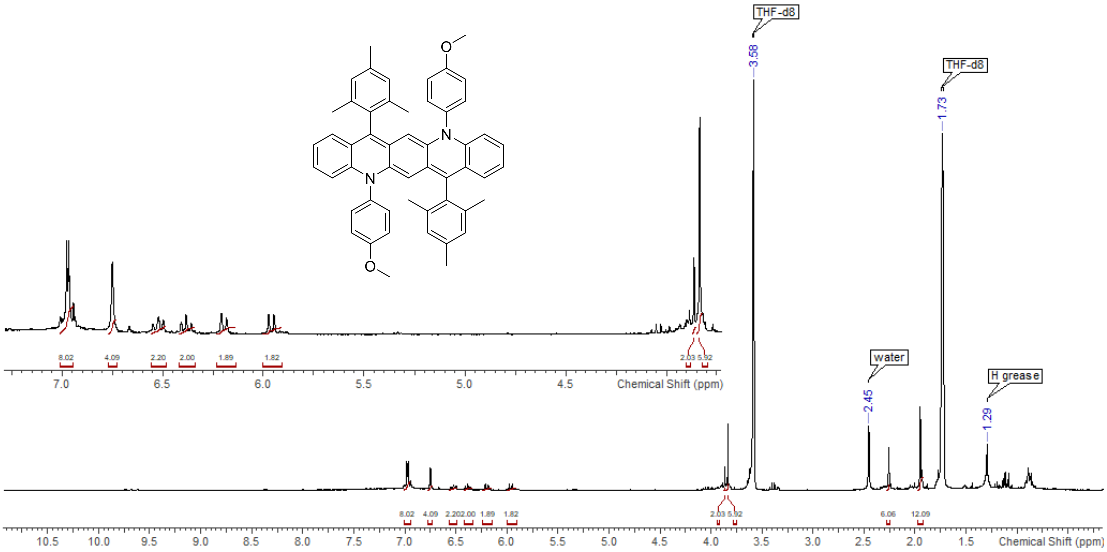

Multiplets Integrals Sum	0.00	Number of Nuclei	0 C's

Acquisition Time (sec)	1.5897	Comment	GZ 378	D	1.5	D1	1.5	DE	18
DS	2	Date	29 Mar 2019 05:20:49			Date Stamp	29 Mar 2019 05:20:49		
File Name	\\bunz22\Mitarbeiter\Gaozhan XIE\03_analytics\01-NMR\nmr02\c190328ubgz.378\1\PDATA\1\1r					Frequency (MHz)	100.6631	GB	0
INSTRUM	<spect>	LB	1	NS	4096	Nucleus	13C	Number of Transients	4096
Origin	spect	Original Points Count	49066	Owner	ns	PC	1.4		
PROBHD	<Z130030_0004 (CPP BBO 400S1 BB-H&F-D-05 LT)>					PULPROG	<zgpg30>	Points Count	65536
Pulse Sequence	zgpg30	Receiver Gain	2050.00	SF	100.663059	SFO1	100.67413193649		
SI	65536	SSB	0	SW(cyclical) (Hz)	30864.20	SWH	30864.1975308642		
Solvent	THF	Spectrum Offset (Hz)	11177.6270	Spectrum Type	standard	Sweep Width (Hz)	30863.73	TD	98132
TD0	512	TE	295.0005	Temperature (degree C)	22.000	UNC1	<13C>	WDW	1

User Notes	GZ 378

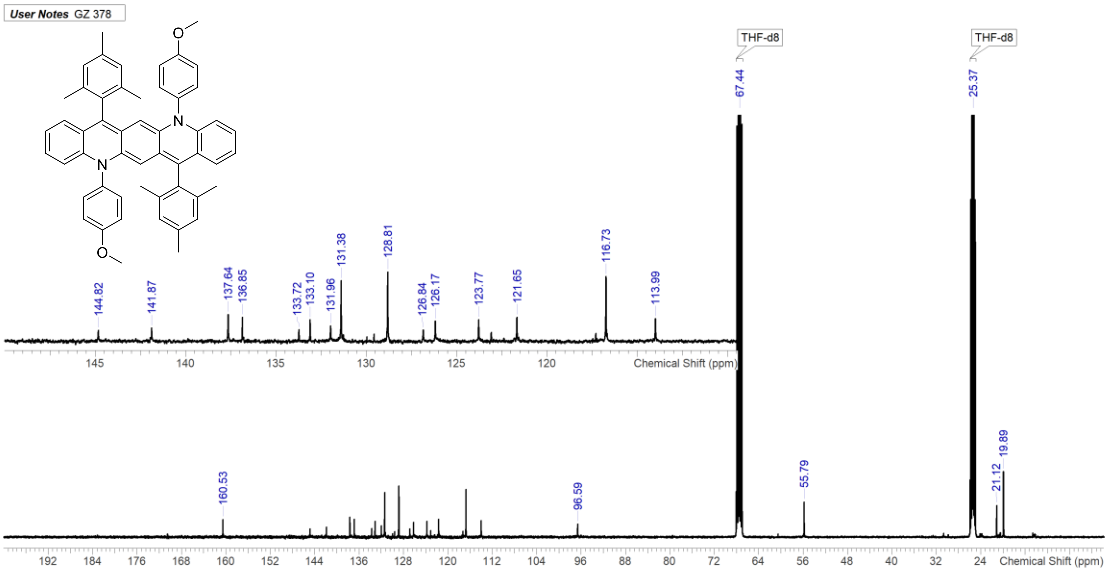

[1]H-NMR and [13]C{[1]H} NMR of **Quino-CF_3**

Multiplets Integrals Sum	39.87	Number of Nuclei	40 H's

Acquisition Time (sec)	3.6351	Comment	GZ 388	D	0.1	D1	0.1	DE	12
DS	2	Date	07 Apr 2019 17:45:36			Date Stamp	07 Apr 2019 17:45:36		
File Name	\\bunz22\Mitarbeiter\Gaozhan XIE\03_analytics\01-NMR\nmr02\e190405ubgz.388\2\PDATA\1\1r					Frequency (MHz)	600.2440	GB	0
INSTRUM	<spect>	LB	0.3	NS	128	Nucleus	1H	Number of Transients	128
Origin	spect	Original Points Count	65536	Owner	ns	PC	1		
PROBHD	<Z132808_0001 (CP QCI 600S3 H/P/C-N-D-05 Z LT)>					PULPROG	<zg30>	Points Count	65536
Pulse Sequence	zg30	Receiver Gain	15.35	SF	600.243944334864			SFO1	600.246830219145
SI	65536	SSB	0	SW(cyclical) (Hz)	18028.85	SWH	18028.8461538462		
Solvent	THF	Spectrum Offset (Hz)	3924.3643	Spectrum Type	standard	Sweep Width (Hz)	18028.57	TD	131072
TD0	16	TE	295.0005	Temperature (degree C)	22.000	UNC1	<1H>	WDW	1

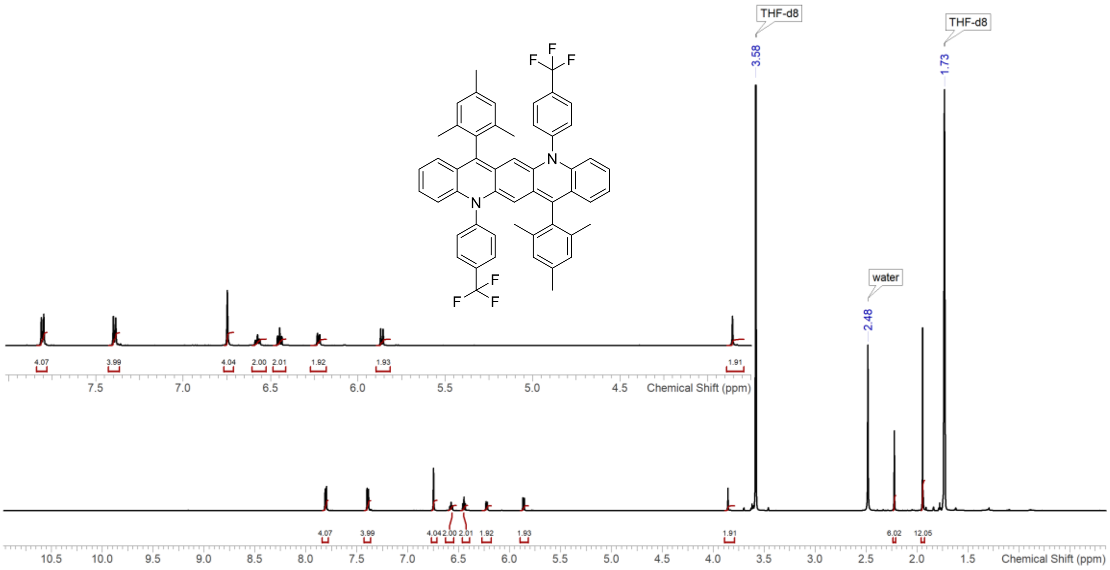

Multiplets Integrals Sum	0.00	Number of Nuclei	0 C's

Acquisition Time (sec)	1.0795	Comment	GZ 388	D	0.03	D1	2	DE	18
DS	4	Date	07 Apr 2019 17:36:36			Date Stamp	07 Apr 2019 17:36:36		
File Name	\\bunz22\Mitarbeiter\Gaozhan XIE\03_analytics\01-NMR\nmr02\e190405ubgz.388\1\PDATA\1\1r					Frequency (MHz)	150.9314	GB	0
INSTRUM	<spect>	LB	1	NS	4096	Nucleus	13C	Number of Transients	4096
Origin	spect	Original Points Count	49066	Owner	ns	PC	1.4		
PROBHD	<Z132808_0001 (CP QCI 600S3 H/P/C-N-D-05 Z LT)>					PULPROG	<zgpg30>	Points Count	65536
Pulse Sequence	zgpg30	Receiver Gain	2050.00	SF	150.931431	SFO1	150.94803345741		
SI	65536	SSB	0	SW(cyclical) (Hz)	45454.55	SWH	45454.5454545455		
Solvent	THF	Spectrum Offset (Hz)	16995.7363	Spectrum Type	standard	Sweep Width (Hz)	45453.85	TD	98132
TD0	512	TE	295.0006	Temperature (degree C)	22.001	UNC1	<13C>	WDW	1

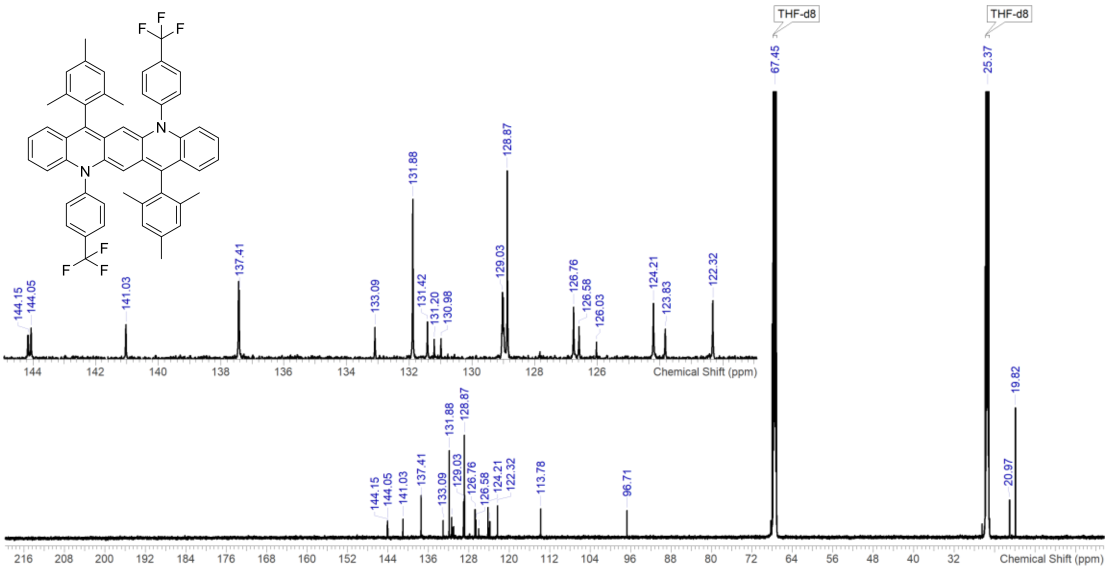

^{1}H, ^{1}H COSY and ^{1}H, ^{1}H ROESY of **Quino-CF$_3$**

Acquisition Time (sec)	(0.2908, 0.0364)	*Comment*	Graf COSYGPSW THF /opt/topspin oci 42
Date	21 May 2019 15:16:00		
File Name	\\bunz22\Mitarbeiter\Gaozhan XIE\03_analytics\01-NMR\nmr02\c190528ubgz.388\40019\PDATA\1\2rr		
Frequency (MHz)	(399.8900, 399.8900)	*Nucleus*	(1H, 1H)
Number of Transients	1	*Origin*	spect
Original Points Count	(1024, 128)	*Owner*	auto
Points Count	(1024, 1024)	*Pulse Sequence*	cosygpppqf
Solvent	THF	*Spectrum Type*	COSY
Sweep Width (Hz)	(3517.69, 3517.69)	*Temperature (degree C)*	22.148
Title	Graf COSYGPSW THF /opt/topspin oci 42		

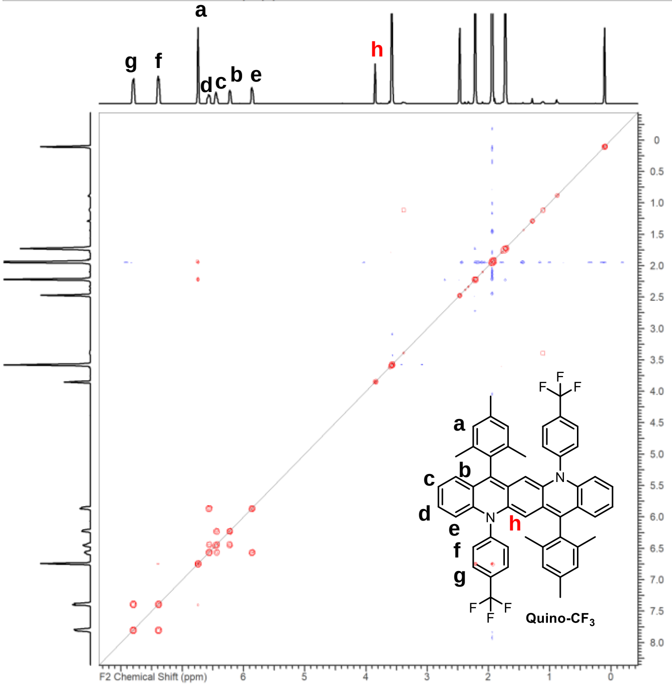

Acquisition Time (sec)	(0.2556, 0.0319)	*Comment*	GZ 388	*Date*	20 May 2019 01:23:14
File Name	\\bunz22\Mitarbeiter\Gaozhan XIE\03_analytics\01-NMR\nmr02\c190516ubgz.388\3\PDATA\1\2rr				
Frequency (MHz)	(400.1800, 400.1800)			*Nucleus*	(1H, 1H)
Number of Transients	16	*Origin*	spect	*Original Points Count*	(2048, 256)
Owner	ns	*Points Count*	(2048, 2048)	*Pulse Sequence*	roesyetgp.2
Solvent	THF	*Spectrum Type*	ROESY	*Sweep Width (Hz)*	(8008.91, 8008.91)
Temperature (degree C)	21.998	*Title*	GZ 388		

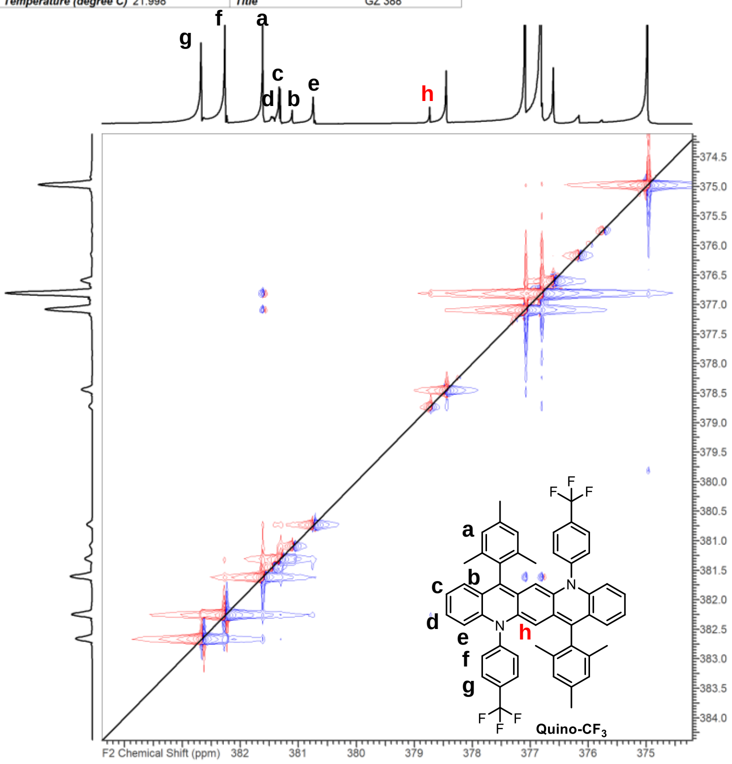

^{1}H, ^{19}F NOESY and ^{1}H, ^{19}F COSY of **Quino-CF_3**

Acquisition Time (sec)	(0.2561, 0.0021)	***Comment***	Graf A_19F_HOESY THF /opt/topspin oci 42
Date	21 May 2019 15:45:06		
File Name	\\bunz22\Mitarbeiter\Gaozhan XIE\03_analytics\01-NMR\nmr02\c190528ubgz.388\40021\PDATA\1\2rr		
Frequency (MHz)	(399.8900, 376.2726)	***Nucleus***	(1H, 19F)
Number of Transients	8	***Origin***	spect
Original Points Count	(1024, 64)	***Owner***	auto
Points Count	(1024, 512)	***Pulse Sequence***	hoesyph
Solvent	THF	***Spectrum Type***	NOESY
Sweep Width (Hz)	(3993.96, 30061.65)	***Temperature (degree C)***	22.148
Title	Graf A_19F_HOESY THF /opt/topspin oci 42		

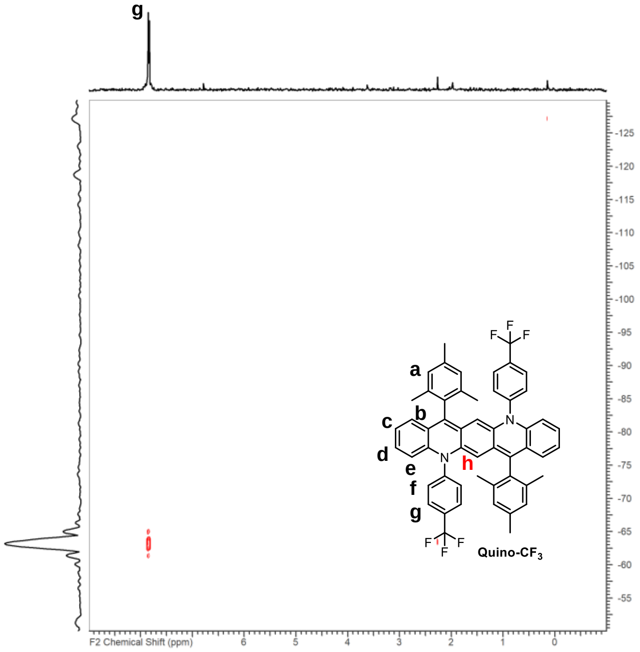

Acquisition Time (sec)	(0.2135, 0.0057)	***Comment***	Graf A_19F_hetCOSY THF /opt/topspin oci 42
Date	22 May 2019 09:57:36		
File Name	\\bunz22\Mitarbeiter\Gaozhan XIE\03_analytics\01-NMR\nmr02\c190528ubgz.388\40022\PDATA\1\2rr		
Frequency (MHz)	(399.8900, 376.2726)	***Nucleus***	(1H, 19F)
Number of Transients	8	***Origin***	spect
Original Points Count	(1024, 128)	***Owner***	auto
Points Count	(2048, 1024)	***Pulse Sequence***	cosygphfqfqn.jg
Solvent	THF	***Spectrum Type***	COSY
Sweep Width (Hz)	(4793.06, 22602.34)	***Temperature (degree C)***	22.148
Title	Graf A_19F_hetCOSY THF /opt/topspin oci 42		

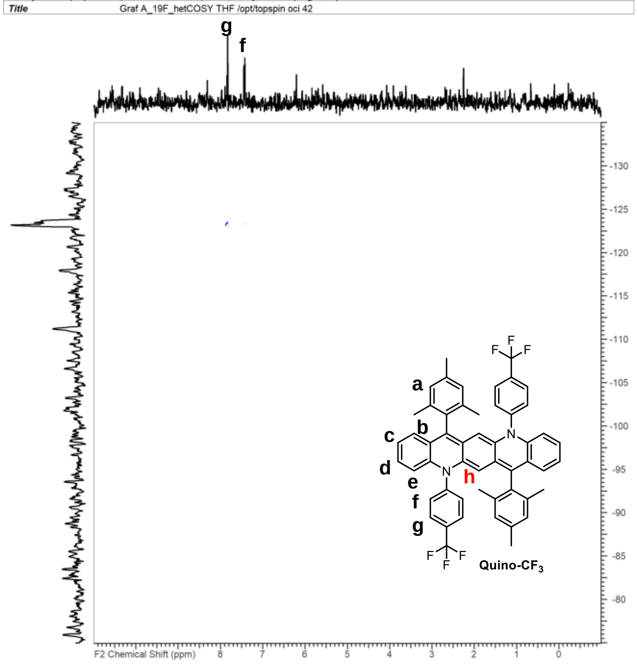

^{1}H-NMR and ^{13}C{^{1}H} NMR of **Quino-tBu^{2+}**

Multiplets Integrals Sum	57.91	Number of Nuclei	58 H's

Acquisition Time (sec)	3.6351	Comment	GZ 389	D	0.1	D1	0.1	DE	12
DS	2	Date	15 Apr 2019 02:20:46			Date Stamp	15 Apr 2019 02:20:46		
File Name	\\bunz22\Mitarbeiter\Gaozhan XIE\03_analytics\01-NMR\nmr02\e190412ubgz.389\2\PDATA\1\1r					Frequency (MHz)	600.2438	GB	0
INSTRUM	<spect>	LB	0.3	NS	128	Nucleus	1H	Number of Transients	128
Origin	spect	Original Points Count	65536	Owner	ns	PC	1		
PROBHD	<Z132808_0001 (CP QCI 600S3 H/P/C-N-D-05 Z LT)>					PULPROG	<zg30>	Points Count	65536
Pulse Sequence	zg30	Receiver Gain	15.35	SF	600.243829	SFO1	600.246830219145		
SI	65536	SSB	0	SW(cyclical) (Hz)	18028.85	SWH	18028.8461538462		
Solvent	ACETONITRILE-d3			Spectrum Offset (Hz)	2812.9792	Spectrum Type	standard	Sweep Width (Hz)	18028.57
TD	131072	TD0	16	TE	294.9998	Temperature (degree C)	22.000	UNC1	<1H>
WDW	1								

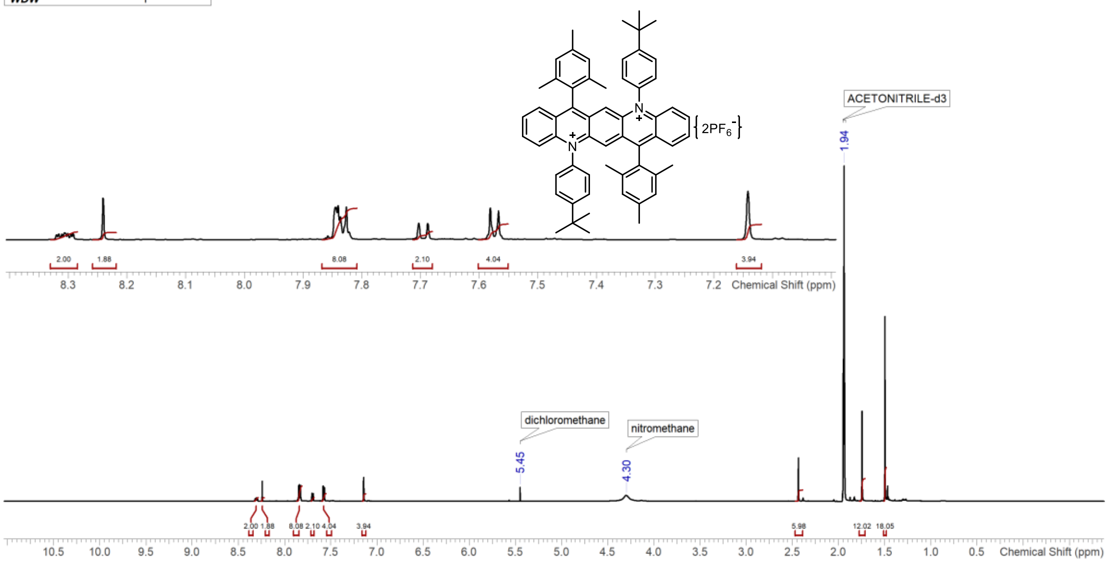

Multiplets Integrals Sum	0.00	Number of Nuclei	0 C's

Acquisition Time (sec)	1.0795	Comment	GZ 389	D	0.03	D1	2	DE	18
DS	4	Date	15 Apr 2019 02:11:46			Date Stamp	15 Apr 2019 02:11:46		
File Name	\\bunz22\Mitarbeiter\Gaozhan XIE\03_analytics\01-NMR\nmr02\e190412ubgz.389\1\PDATA\1\1r					Frequency (MHz)	150.9314	GB	0
INSTRUM	<spect>	LB	1	NS	4096	Nucleus	13C	Number of Transients	4096
Origin	spect	Original Points Count	49066	Owner	ns	PC	1.4		
PROBHD	<Z132808_0001 (CP QCI 600S3 H/P/C-N-D-05 Z LT)>			PULPROG	<zgpg30>	Points Count	65536	Pulse Sequence	zgpg30
Receiver Gain	2050.00	SF	150.931431	SFO1	150.94803345741			SI	65536
SSB	0	SW(cyclical) (Hz)	45454.55	SWH	45454.5454545455			Solvent	ACETONITRILE-d3
Spectrum Offset (Hz)	16718.0684	Spectrum Type	standard	Sweep Width (Hz)	45453.85	TD	98132	TD0	512
TE	294.9991	Temperature (degree C)	21.999	UNC1	<13C>	WDW	1		

User Notes	GZ 389

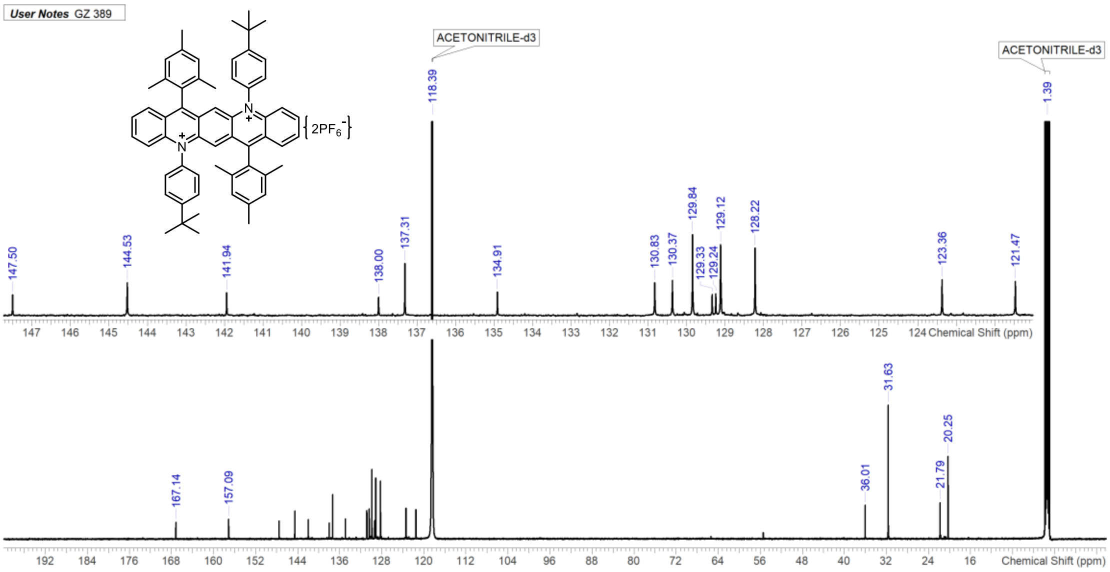

^{1}H-NMR and ^{13}C{^{1}H} NMR of **Quino-CF$_3$$^{2+}$**

Multiplets Integrals Sum	39.97	Number of Nuclei	40 H's

Acquisition Time (sec)	3.6351	Comment	GZ 397	D	0.1	D1	0.1	DE	12
DS	2	Date	18 Apr 2019 13:21:21			Date Stamp	18 Apr 2019 13:21:21		
File Name	\\bunz22\Mitarbeiter\Gaozhan XIE\03_analytics\01-NMR\nmr02\e190418ubgz.397\2\PDATA\1\1r					Frequency (MHz)	600.2438	GB	0
INSTRUM	<spect>	LB	0.3	NS	128	Nucleus	1H	Number of Transients	128
Origin	spect	Original Points Count	65536	Owner	ns	PC	1		
PROBHD	<Z132808_0001 (CP QCI 600S3 H/P/C-N-D-05 Z LT)>					PULPROG	<zg30>	Points Count	65536
Pulse Sequence	zg30	Receiver Gain	15.35	SF	600.243829	SFO1	600.246830219145		
SI	65536	SSB	0	SW(cyclical) (Hz)	18028.85	SWH	18028.8461538462		
Solvent	ACETONITRILE-d3			Spectrum Offset (Hz)	2813.2793	Spectrum Type	standard	Sweep Width (Hz)	18028.57
TD	131072	TD0	16	TE	295.0009	Temperature (degree C)	22.001	UNC1	<1H>
WDW	1								

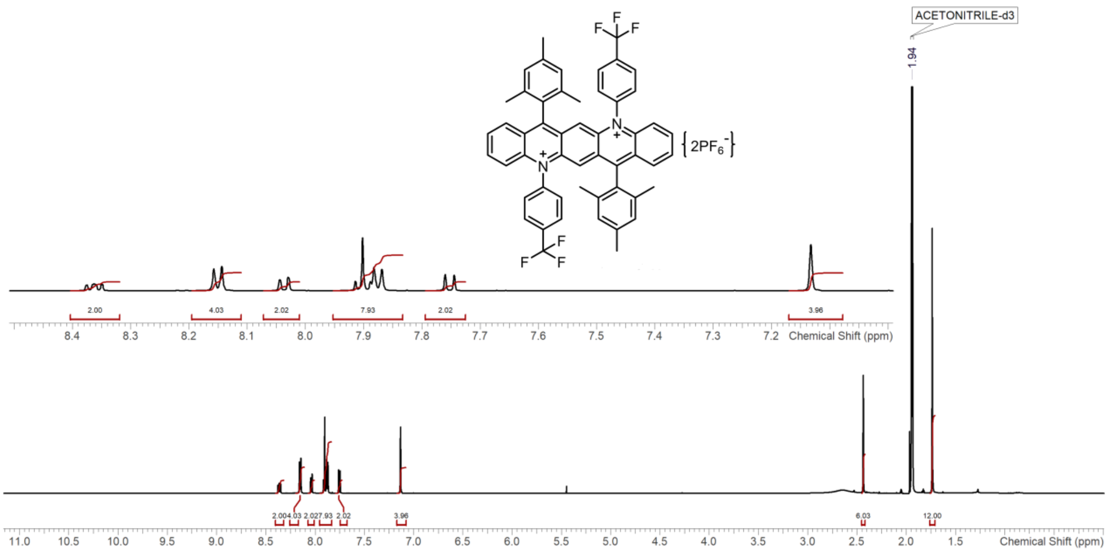

Multiplets Integrals Sum	0.00	Number of Nuclei	0 C's

Acquisition Time (sec)	1.0795	Comment	GZ 397	D	0.03	D1	2	DE	18
DS	4	Date	18 Apr 2019 13:12:19			Date Stamp	18 Apr 2019 13:12:19		
File Name	\\bunz22\Mitarbeiter\Gaozhan XIE\03_analytics\01-NMR\nmr02\e190418ubgz.397\1\PDATA\1\1r					Frequency (MHz)	150.9314	GB	0
INSTRUM	<spect>	LB	1	NS	4096	Nucleus	13C	Number of Transients	4096
Origin	spect	Original Points Count	49066	Owner	ns	PC	1.4		
PROBHD	<Z132808_0001 (CP QCI 600S3 H/P/C-N-D-05 Z LT)>			PULPROG	<zgpg30>	Points Count	65536	Pulse Sequence	zgpg30
Receiver Gain	2050.00	SF	150.931431	SFO1	150.94803345741			SI	65536
SSB	0	SW(cyclical) (Hz)	45454.55	SWH	45454.5454545455			Solvent	ACETONITRILE-d3
Spectrum Offset (Hz)	16763.7422	Spectrum Type	standard	Sweep Width (Hz)	45453.85	TD	98132	TD0	512
TE	294.9997	Temperature (degree C)	22.000	UNC1	<13C>	WDW	1		

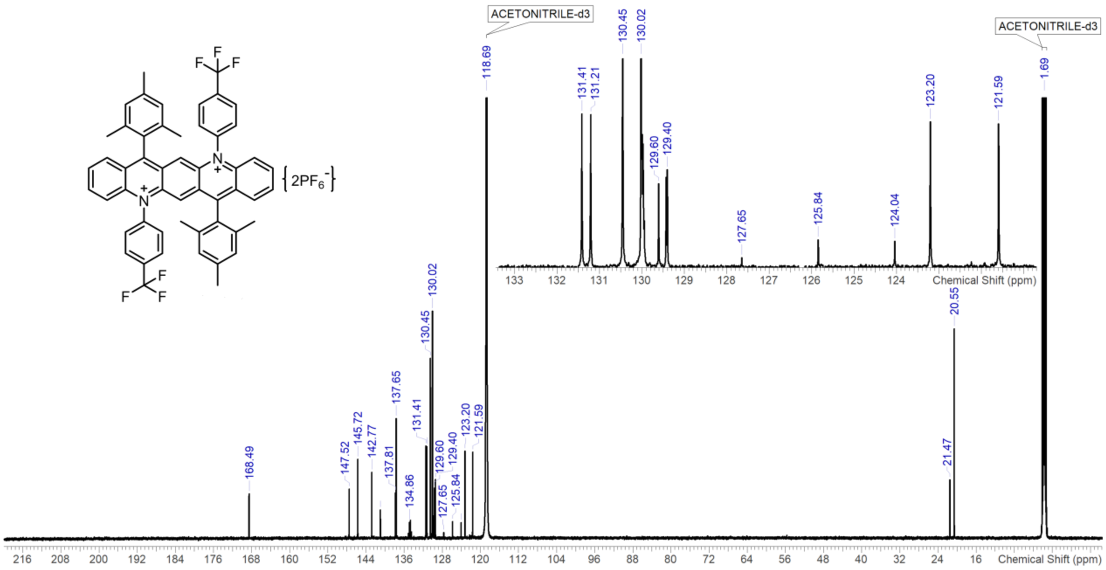

^1H, ^1H COSY and ^1H, ^1H ROESY of **Quino-CF$_3^{2+}$**

Acquisition Time (sec)	(0.2272, 0.0284)	*Comment*	GZ 397	*Date*	30 Apr 2019 20:16:16
File Name	\\bunz22\Mitarbeiter\Gaozhan XIE\03_analytics\01-NMR\nmr02\e190430ubqz.397\2\PDATA\1\2rr				
Frequency (MHz)	(600.2438, 600.2438)			*Nucleus*	(1H, 1H)
Number of Transients	8	*Origin*	spect	*Original Points Count*	(2048, 256)
Owner	ns	*Points Count*	(2048, 2048)	*Pulse Sequence*	cosygpmfppqf
Solvent	ACETONITRILE-d3			*Spectrum Type*	COSY
Sweep Width (Hz)	(9010.02, 9004.61)	*Temperature (degree C)*	22.000	*Title*	GZ 397

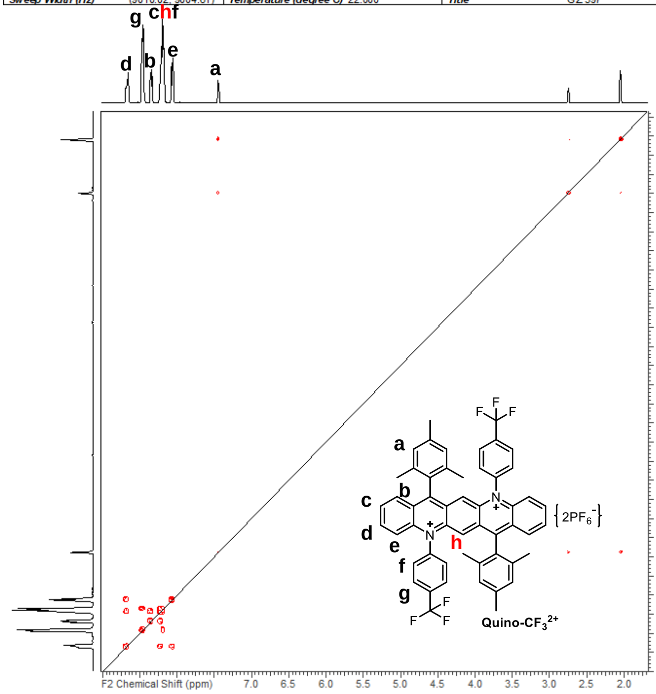

Acquisition Time (sec)	(0.1136, 0.0284)	*Comment*	GZ 397	*Date*	30 Apr 2019 23:19:28
File Name	\\bunz22\Mitarbeiter\Gaozhan XIE\03_analytics\01-NMR\nmr02\e190430ubqz.397\3\PDATA\1\2rr				
Frequency (MHz)	(600.2438, 600.2438)			*Nucleus*	(1H, 1H)
Number of Transients	16	*Origin*	spect	*Original Points Count*	(1024, 256)
Owner	ns	*Points Count*	(2048, 1024)	*Pulse Sequence*	roesyadjsph.jq
Solvent	ACETONITRILE-d3			*Spectrum Type*	ROESY
Sweep Width (Hz)	(9010.02, 9000.21)	*Temperature (degree C)*	21.999	*Title*	GZ 397

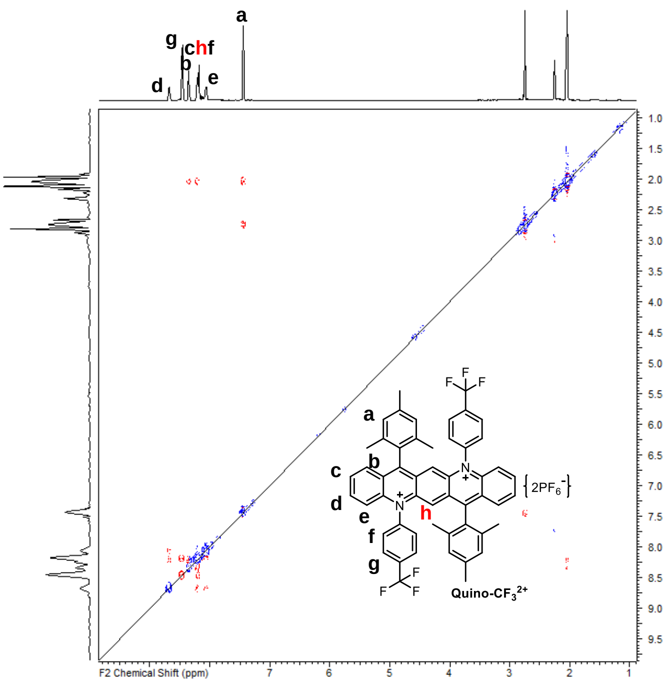

^{1}H, ^{15}N HMBC of **Quino-CF$_3$$^{2+}$**

Acquisition Time (sec)	(0.1704, 0.0052)	***Comment***	GZ 397	***Constant (Hz)***	8.0
Date	07 May 2019 23:07:22				
File Name	\\bunz22\Mitarbeiter\Gaozhan XIE\03_analytics\01-NMR\nmr02\c190507ubgz.397\2\PDATA\1\2rr				
Frequency (MHz)	(400.3300, 40.5651)			***Nucleus***	(1H, 15N)
Number of Transients	128	***Origin***	spect	***Original Points Count***	(1024, 128)
Owner	ns	***Points Count***	(2048, 2048)	***Pulse Sequence***	hmbcgpndqf
Solvent	ACETONITRILE-d3			***Spectrum Type***	HMBC
Sweep Width (Hz)	(6006.68, 24378.33)			***Temperature (degree C)***	21.999
Title	GZ 397				

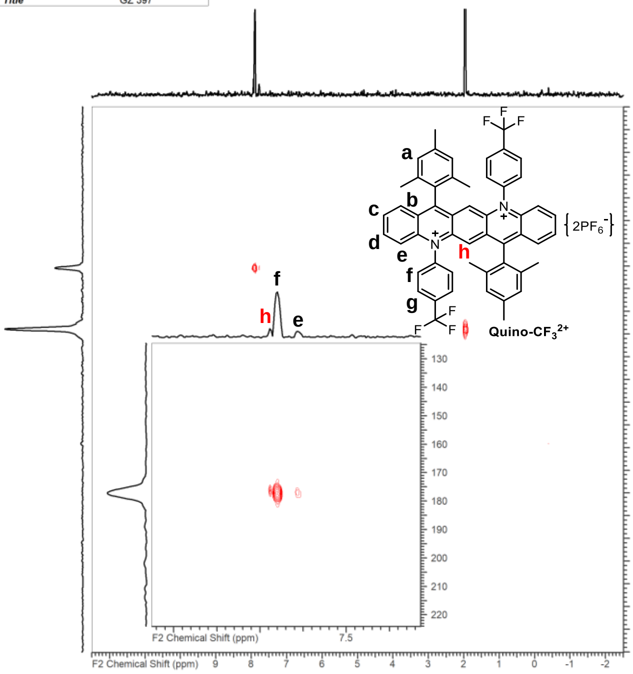

6.3.4 NMR spectra (Chapter 5)

^{1}H-NMR and ^{13}C{^{1}H} NMR of **BPNZ**

Multiplets Integrals Sum	18.07	***Number of Nuclei***	18 H's

Acquisition Time (sec)	3.6351	***Comment***	GZ 475	***D***	0.1	***D1***	0.1	***DE***	12
DS	2	***Date***	07 Oct 2019 14:25:26			***Date Stamp***	07 Oct 2019 14:25:26		
File Name	\\bunz22\Mitarbeiter\Gaozhan XIE\03_analytics\01-NMR\nmr-biradical01\e191007ubgz.475\2\PDATA\1\1r							***Frequency (MHz)***	600.2438
GB	0	***INSTRUM***	<spect>	***LB***	0.3	***NS***	128	***Nucleus***	1H
Number of Transients	128	***Origin***	spect	***Original Points Count***	65536	***Owner***	ns	***PC***	1
PROBHD	<Z132808_0001 (CP QCI 600S3 H/P/C-N-D-05 Z LT)>			***PULPROG***	<zg30>	***Points Count***	65536	***Pulse Sequence***	zg30
Receiver Gain	15.35	***SF***	600.243829	***SFO1***	600.246830219145			***SI***	65536
SSB	0	***SW(cyclical) (Hz)***	18028.85	***SWH***	18028.8461538462				
Solvent	DICHLOROMETHANE-d2			***Spectrum Offset (Hz)***	2807.2170	***Spectrum Type***	standard	***Sweep Width (Hz)***	18028.57
TD	131072	***TD0***	16	***TE***	295.0004	***Temperature (degree C)***	22.000	***UNC1***	<1H>
WDW	1								

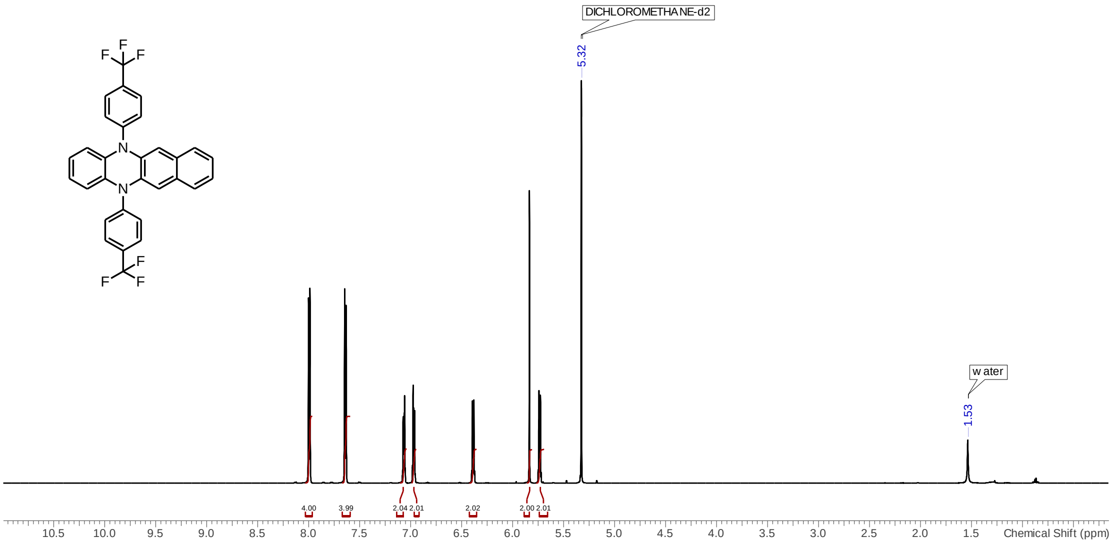

Multiplets Integrals Sum	0.00	***Number of Nuclei***	0 C's

Acquisition Time (sec)	1.0795	***Comment***	GZ 475	***D***	0.03	***D1***	2	***DE***	18
DS	4	***Date***	07 Oct 2019 14:16:15			***Date Stamp***	07 Oct 2019 14:16:15		
File Name	\\bunz22\Mitarbeiter\Gaozhan XIE\03_analytics\01-NMR\nmr-biradical01\e191007ubgz.475\1\PDATA\1\1r							***Frequency (MHz)***	150.9314
GB	0	***INSTRUM***	<spect>	***LB***	1	***NS***	3160	***Nucleus***	13C
Number of Transients	3160	***Origin***	spect	***Original Points Count***	49066	***Owner***	ns	***PC***	1.4
PROBHD	<Z132808_0001 (CP QCI 600S3 H/P/C-N-D-05 Z LT)>			***PULPROG***	<zgpg30>	***Points Count***	65536	***Pulse Sequence***	zgpg30
Receiver Gain	2050.00	***SF***	150.931431	***SFO1***	150.94803345741			***SI***	65536
SSB	0	***SW(cyclical) (Hz)***	45454.55	***SWH***	45454.5454545455				
Solvent	DICHLOROMETHANE-d2			***Spectrum Offset (Hz)***	16644.2480	***Spectrum Type***	standard	***Sweep Width (Hz)***	45453.85
TD	98132	***TD0***	512	***TE***	294.9991	***Temperature (degree C)***	21.999	***UNC1***	<13C>
WDW	1								

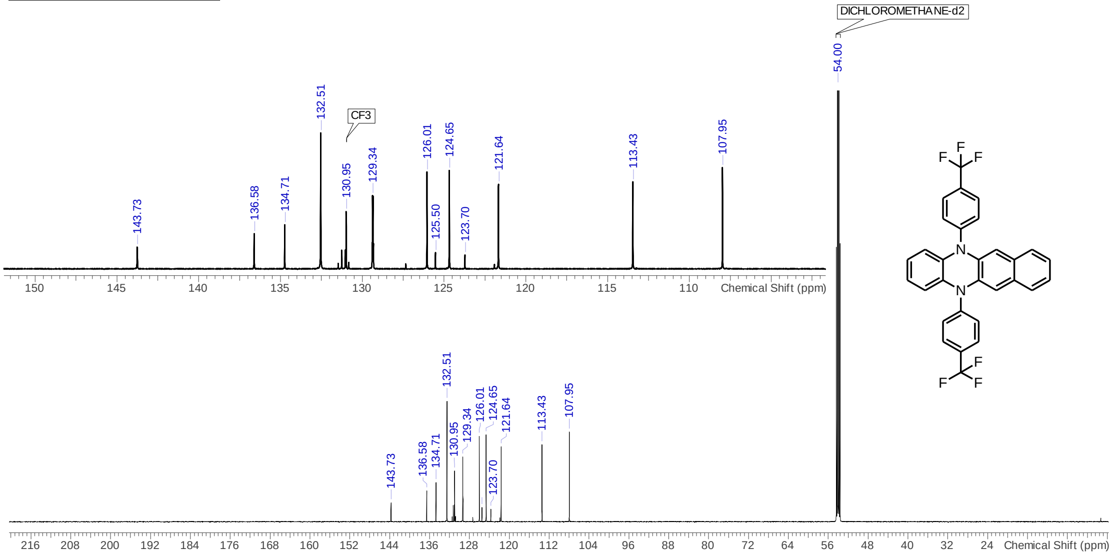

^{1}H, ^{1}H COSY and ^{1}H, ^{1}H ROESY of **BPNZ**

Acquisition Time (sec)	(0.2272, 0.0284)	Comment	GZ 475	Date	07 Oct 2019 15:28:56
File Name	\\bunz22\Mitarbeiter\Gaozhan XIE\03_analytics\01-NMR\nmr-biradical01\e191007ubgz.475\3\PDATA\1\2rr				
Frequency (MHz)	(600.2438, 600.2438)			Nucleus	(1H, 1H)
Number of Transients	8	Origin	spect	Original Points Count	(2048, 256)
Owner	ns	Points Count	(2048, 2048)	Pulse Sequence	cosygpmfppqf
Solvent	DICHLOROMETHANE-d2			Spectrum Type	COSY
Sweep Width (Hz)	(9010.02, 9004.61)	Temperature (degree C)	22.001	Title	GZ 475

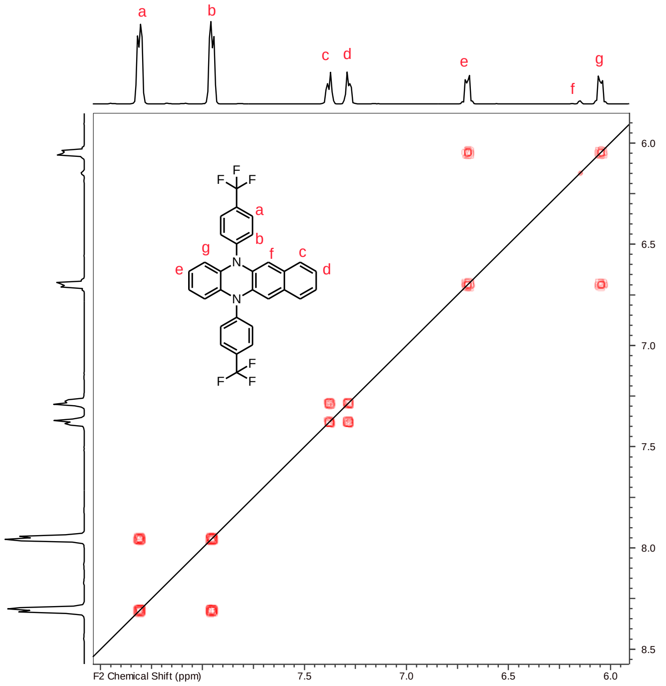

Acquisition Time (sec)	(0.1136, 0.0284)	Comment	GZ 475	Date	07 Oct 2019 18:31:50
File Name	\\bunz22\Mitarbeiter\Gaozhan XIE\03_analytics\01-NMR\nmr-biradical01\e191007ubgz.475\4\PDATA\1\2rr				
Frequency (MHz)	(600.2438, 600.2438)			Nucleus	(1H, 1H)
Number of Transients	16	Origin	spect	Original Points Count	(1024, 256)
Owner	ns	Points Count	(2048, 1024)	Pulse Sequence	noesygpphpp
Solvent	DICHLOROMETHANE-d2			Spectrum Type	NOESY
Sweep Width (Hz)	(9010.02, 9000.21)	Temperature (degree C)	22.001	Title	GZ 475

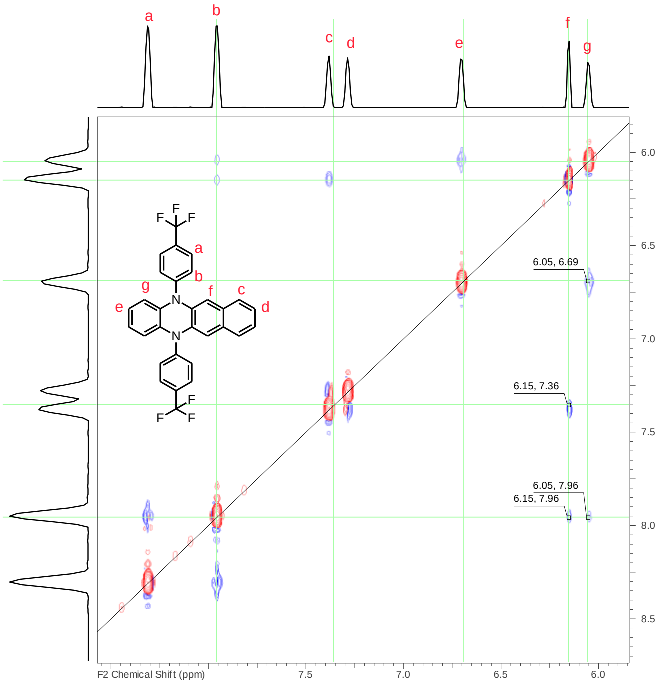

^{1}H-NMR and ^{13}C{^{1}H} NMR of **DPNZ**

Multiplets Integrals Sum	20.13	**Number of Nuclei**	30 H's

Acquisition Time (sec)	2.7263	**Comment**	GZ 446	**D**	0.5	**D1**	0.5	**DE**	10
DS	2	**Date**	10 Oct 2019 18:50:17			**Date Stamp**	10 Oct 2019 18:50:17		
File Name	\\bunz22\Mitarbeiter\Gaozhan XIE\03_analytics\01-NMR\nmr-biradical01\c191010ubgz.446\2\PDATA\1\1r							**Frequency (MHz)**	400.3300
GB	0	**INSTRUM**	<spect>	**LB**	0.3	**NS**	128	**Nucleus**	1H
Number of Transients	128	**Origin**	spect	**Original Points Count**	32768	**Owner**	ns	**PC**	1
PROBHD	<Z130030_0004 (CPP BBO 400S1 BB-H&F-D-05 LT)>			**PULPROG**	<zg30>	**Points Count**	65536	**Pulse Sequence**	zg30
Receiver Gain	812.00	**SF**	400.330049193387			**SFO1**	400.3320009	**SI**	65536
SSB	0	**SW(cyclical) (Hz)**	12019.23	**SWH**	12019.2307692308				
Solvent	DICHLOROMETHANE-d2			**Spectrum Offset (Hz)**	1985.4963	**Spectrum Type**	standard	**Sweep Width (Hz)**	12019.05
TD	65536	**TD0**	16	**TE**	295.0004	**Temperature (degree C)**	22.000	**UNC1**	<1H>
WDW	1								

User Notes	GZ 446

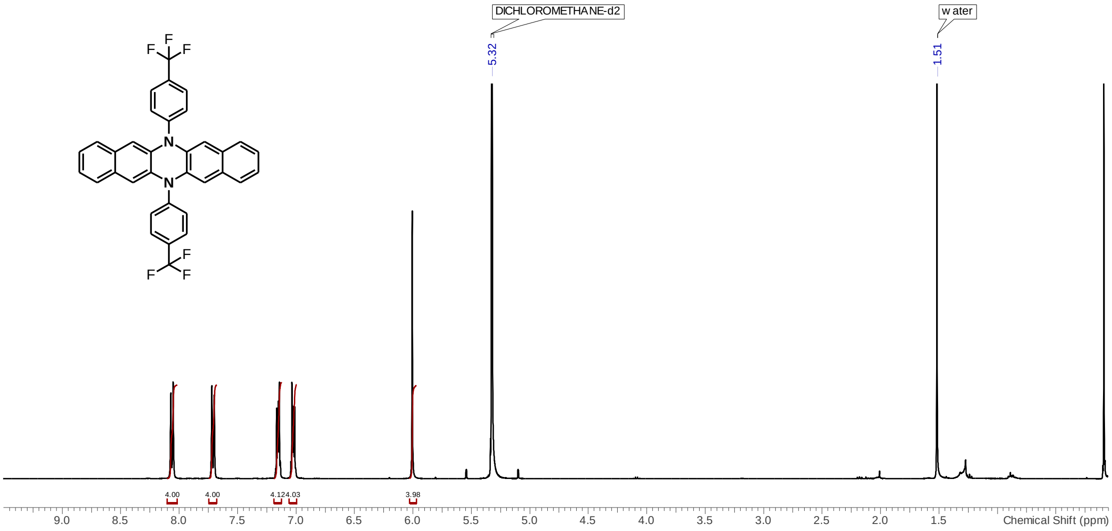

Multiplets Integrals Sum	0.00	**Number of Nuclei**	0 C's

Acquisition Time (sec)	1.5897	**Comment**	GZ 446	**D**	1.5	**D1**	1.5	**DE**	18
DS	2	**Date**	10 Oct 2019 18:42:25			**Date Stamp**	10 Oct 2019 18:42:25		
File Name	\\bunz22\Mitarbeiter\Gaozhan XIE\03_analytics\01-NMR\nmr-biradical01\c191010ubgz.446\1\PDATA\1\1r							**Frequency (MHz)**	100.6631
GB	0	**INSTRUM**	<spect>	**LB**	1	**NS**	4096	**Nucleus**	13C
Number of Transients	4096	**Origin**	spect	**Original Points Count**	49066	**Owner**	ns	**PC**	1.4
PROBHD	<Z130030_0004 (CPP BBO 400S1 BB-H&F-D-05 LT)>			**PULPROG**	<zgpg30>	**Points Count**	65536	**Pulse Sequence**	zgpg30
Receiver Gain	2050.00	**SF**	100.663059	**SFO1**	100.67413193649			**SI**	65536
SSB	0	**SW(cyclical) (Hz)**	30864.20	**SWH**	30864.1975308642				
Solvent	DICHLOROMETHANE-d2			**Spectrum Offset (Hz)**	11135.0059	**Spectrum Type**	standard	**Sweep Width (Hz)**	30863.73
TD	98132	**TD0**	512	**TE**	295.0007	**Temperature (degree C)**	22.001	**UNC1**	<13C>
WDW	1								

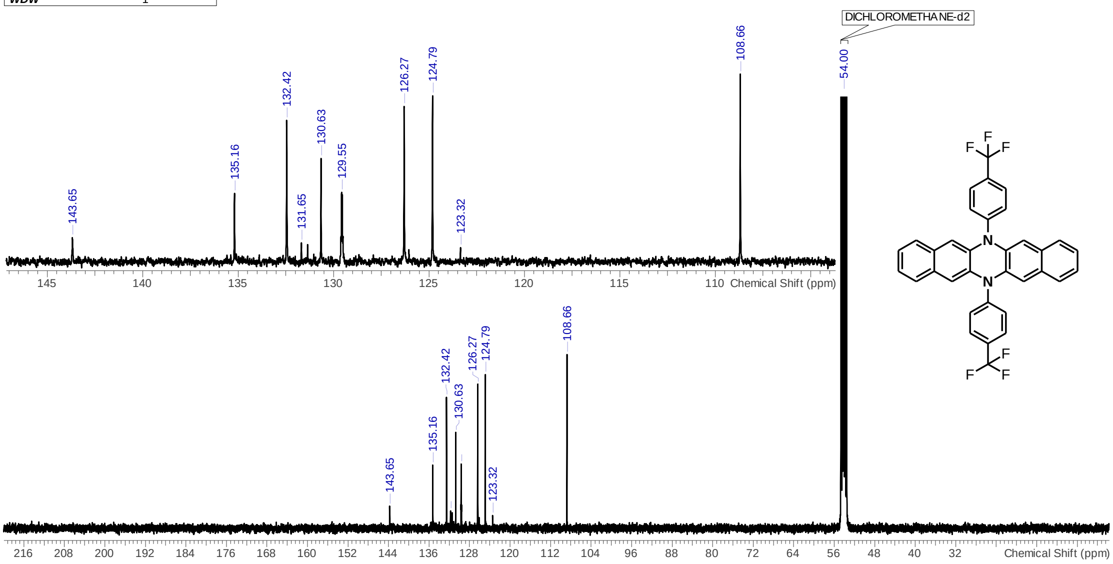

^{1}H, ^{1}H COSY and ^{1}H, ^{1}H ROESY of **DPNZ**

Acquisition Time (sec)	(0.3408, 0.0426)	*Comment*	GZ 446	*Date*	10 Oct 2019 19:14:22
File Name	\\bunz22\Mitarbeiter\Gaozhan XIE\03_analytics\01-NMR\nmr-biradical01\c191010ubgz.446\3\PDATA\1\2rr				
Frequency (MHz)	(400.3300, 400.3300)			*Nucleus*	(1H, 1H)
Number of Transients	8	*Origin*	spect	*Original Points Count*	(2048, 256)
Owner	ns	*Points Count*	(2048, 2048)	*Pulse Sequence*	cosygpmfppqf
Solvent	DICHLOROMETHANE-d2			*Spectrum Type*	COSY
Sweep Width (Hz)	(6006.68, 6006.68)	*Temperature (degree C)*	22.000	*Title*	GZ 446

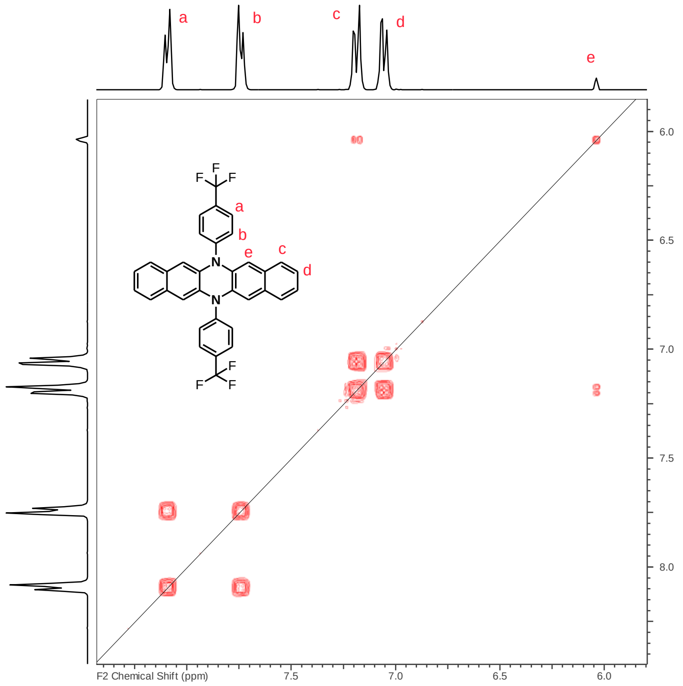

Acquisition Time (sec)	(0.3408, 0.0426)	*Comment*	GZ 446	*Date*	11 Oct 2019 08:01:30
File Name	\\bunz22\Mitarbeiter\Gaozhan XIE\03_analytics\01-NMR\nmr-biradical01\c191010ubgz.446\4\PDATA\1\2rr				
Frequency (MHz)	(400.3300, 400.3300)			*Nucleus*	(1H, 1H)
Number of Transients	16	*Origin*	spect	*Original Points Count*	(2048, 256)
Owner	ns	*Points Count*	(2048, 2048)	*Pulse Sequence*	roesyetgp.2
Solvent	DICHLOROMETHANE-d2			*Spectrum Type*	ROESY
Sweep Width (Hz)	(6006.68, 6006.68)	*Temperature (degree C)*	22.000	*Title*	GZ 446

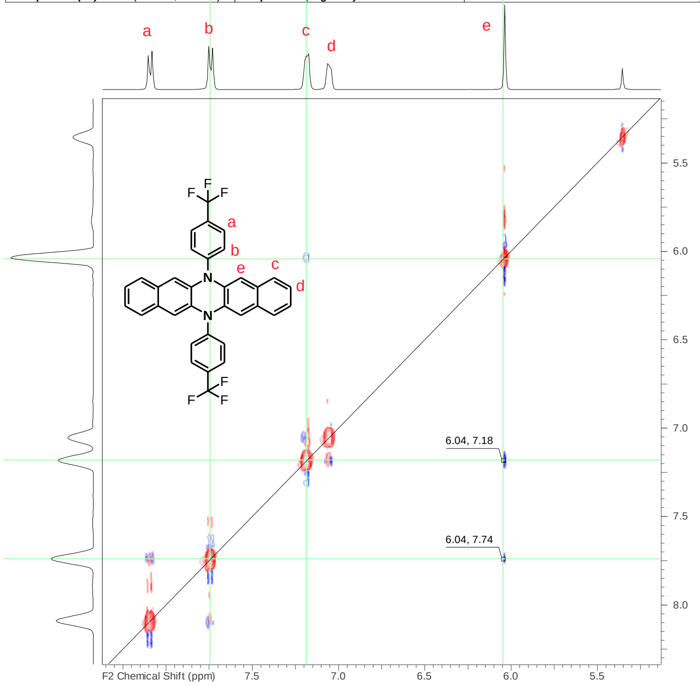

6.4 CV Spectra

Rubrene with ferrocene (a):

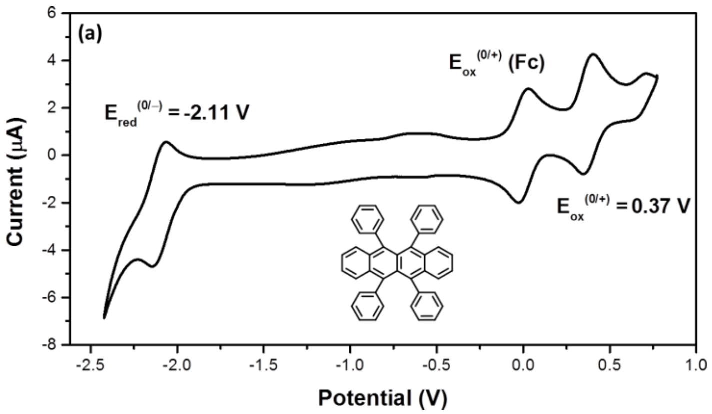

DAR with ferrocene (b):

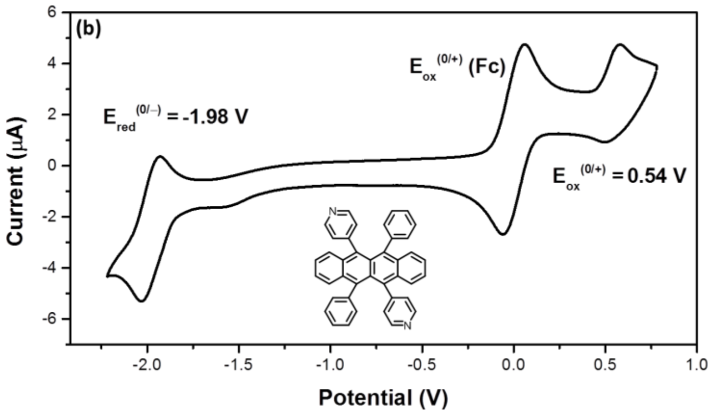

TAR with ferrocene (c):

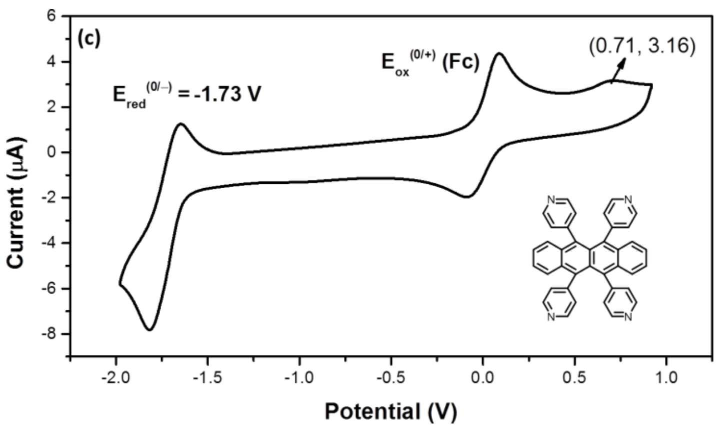

CVs of a) **3a**, b) **3b**, c) **3c**, and d) **3d** with ferrocene:

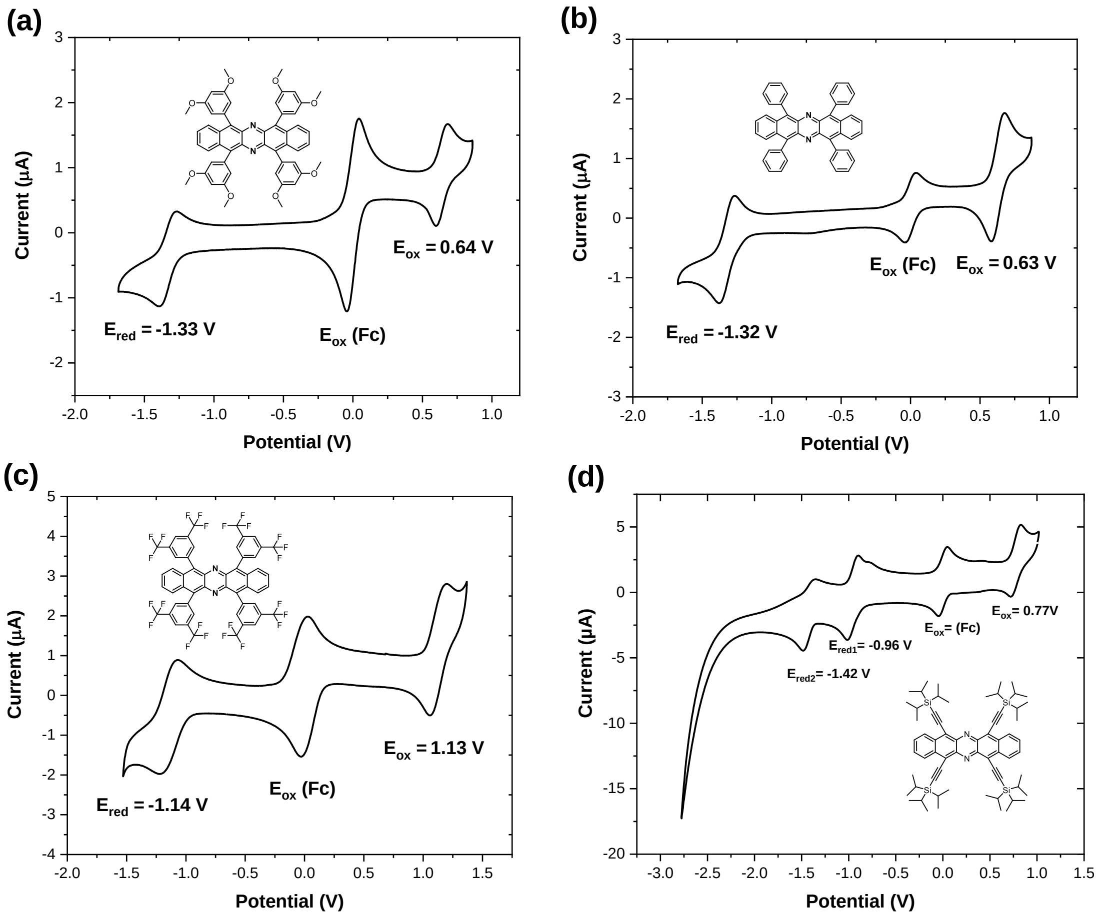

6.5 Single Crystal Structure Data

DAR

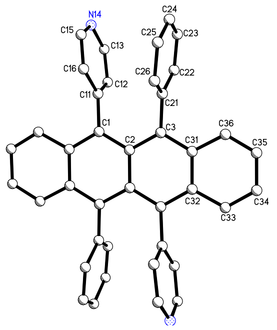

Identification code	gxi2	
Empirical formula	$C_{40}H_{26}N_2$	
Formula weight	534.63	
Temperature	100(2) K	
Wavelength	1.54178 Å	
Crystal system	triclinic	
Space group	$P\bar{1}$	
Z	1	
Unit cell dimensions	a = 7.0727(7) Å	α = 90.402(7) deg.
	b = 8.2696(8) Å	β =106.039(7) deg.
	c = 11.8550(10) Å	γ = 97.605(8) deg.
Volume	659.84(11) $Å^3$	
Density (calculated)	1.35 g/cm^3	
Absorption coefficient	0.60 mm^{-1}	
Crystal shape	irregular	
Crystal size	0.070 x 0.064 x 0.045 mm^3	
Crystal colour	red	
Theta range for data collection	3.9 to 61.8 deg.	
Index ranges	$-7 \le h \le 7$, $-9 \le k \le 9$, $-13 \le l \le 13$	
Reflections collected	7917	
Independent reflections	1985 (R(int) = 0.0387)	
Observed reflections	998 ($I > 2\sigma(I)$)	
Absorption correction	Semi-empirical from equivalents	
Max. and min. transmission	1.72 and 0.61	
Refinement method	Full-matrix least-squares on F^2	
Data/restraints/parameters	7917 / 0 / 191	
Goodness-of-fit on F^2	0.79	
Final R indices (I>2sigma(I))	R1 = 0.041, wR2 = 0.086	
Largest diff. peak and hole	0.31 and -0.37 $eÅ^{-3}$	

DARO2

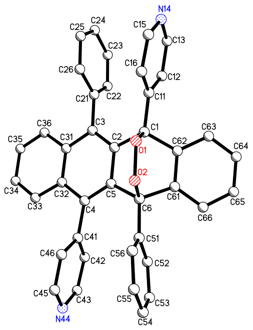

Identification code	gxi1	
Empirical formula	$C_{40}H_{26}N_2O_2$	
Formula weight	566.63	
Temperature	200(2) K	
Wavelength	0.71073 Å	
Crystal system	monoclinic	
Space group	$P2_1/n$	
Z	4	
Unit cell dimensions	a = 13.9299(7) Å	α = 90 deg.
	b = 11.2010(5) Å	β = 96.8662(14) deg.
	c = 18.2839(9) Å	γ = 90 deg.
Volume	2832.4(2) $Å^3$	
Density (calculated)	1.33 g/cm^3	
Absorption coefficient	0.08 mm^{-1}	
Crystal shape	irregular	
Crystal size	0.146 x 0.105 x 0.067 mm^3	
Crystal colour	yellow	
Theta range for data collection	1.7 to 25.1 deg.	
Index ranges	$-16\leq h\leq 16$, $-13\leq k\leq 13$, $-21\leq l\leq 21$	
Reflections collected	26610	
Independent reflections	5024 (R(int) = 0.0392)	
Observed reflections	3757 ($I > 2\sigma(I)$)	
Absorption correction	Semi-empirical from equivalents	
Max. and min. transmission	0.96 and 0.92	
Refinement method	Full-matrix least-squares on F^2	
Data/restraints/parameters	5024 / 0 / 397	
Goodness-of-fit on F^2	1.06	
Final R indices (I>2sigma(I))	R1 = 0.042, wR2 = 0.101	
Largest diff. peak and hole	0.17 and -0.21 $eÅ^{-3}$	

TAR

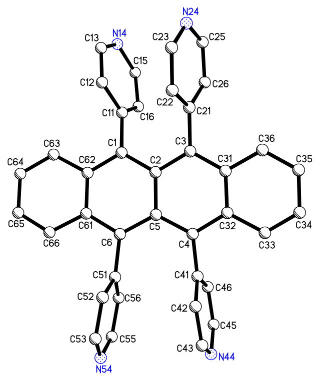

Identification code	gxi5	
Empirical formula	$C_{42}H_{32}N_4O$	
Formula weight	608.71	
Temperature	100(2) K	
Wavelength	1.54178 Å	
Crystal system	triclinic	
Space group	P $\bar{1}$	
Z	4	
Unit cell dimensions	a = 7.7635(16) Å	α = 97.536(17) deg.
	b = 18.657(4) Å	β = 90.005(17) deg.
	c = 21.765(5) Å	γ = 100.929(17) deg.
Volume	3067.7(12) Å^3	
Density (calculated)	1.32 g/cm^3	
Absorption coefficient	0.62 mm^{-1}	
Crystal shape	plate	
Crystal size	0.184 x 0.142 x 0.022 mm^3	
Crystal colour	red	
Theta range for data collection	3.4 to 63.2 deg.	
Index ranges	$-8\le h\le 4$, $-20\le k\le 21$, $-24\le l\le 24$	
Reflections collected	31146	
Independent reflections	9492 (R(int) = 0.1020)	
Observed reflections	5709 ($I > 2\sigma(I)$)	
Absorption correction	Semi-empirical from equivalents	
Max. and min. transmission	1.97 and 0.58	
Refinement method	Full-matrix least-squares on F^2	
Data/restraints/parameters	9492 / 1664 / 892	
Goodness-of-fit on F^2	1.08	
Final R indices (I>2sigma(I))	R1 = 0.111, wR2 = 0.263	
Largest diff. peak and hole	0.44 and -0.37 eÅ^{-3}	

TARO2

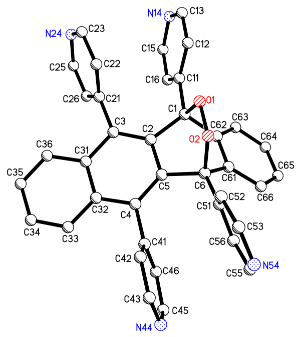

Identification code	gxi3sq	
Empirical formula	$C_{38}H_{24}N_4O_2$	
Formula weight	568.61	
Temperature	200(2) K	
Wavelength	0.71073 Å	
Crystal system	tetragonal	
Space group	P4/n	
Z	16	
Unit cell dimensions	a = 29.9853(18) Å	α = 90 deg.
	b = 29.9853(18) Å	β = 90 deg.
	c = 14.2542(9) Å	γ = 90 deg.
Volume	12816.2(17) $Å^3$	
Density (calculated)	1.18 g/cm^3	
Absorption coefficient	0.07 mm^{-1}	
Crystal shape	plate	
Crystal size	0.15 x 0.10 x 0.03 mm^3	
Crystal colour	colourless	
Theta range for data collection	1.0 to 20.4 deg.	
Index ranges	$-29 \leq h \leq 29$, $-29 \leq k \leq 29$, $-13 \leq l \leq 13$	
Reflections collected	52616	
Independent reflections	6330 (R(int) = 0.1772)	
Observed reflections	3410 ($I > 2\sigma(I)$)	
Absorption correction	Semi-empirical from equivalents	
Max. and min. transmission	0.96 and 0.91	
Refinement method	Full-matrix least-squares on F^2	
Data/restraints/parameters	6330 / 780 / 793	
Goodness-of-fit on F^2	1.04	
Final R indices (I>2sigma(I))	R1 = 0.070, wR2 = 0.177	
Largest diff. peak and hole	0.30 and -0.33 $eÅ^{-3}$	

3a

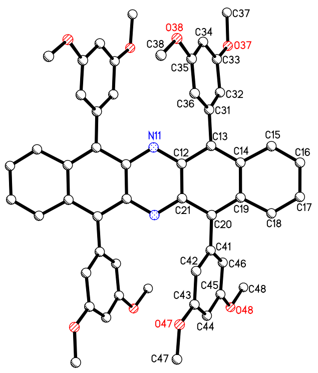

Identification code	gxi8	
Empirical formula	$C_{60}H_{60}N_2O_{10}$	
Formula weight	969.10	
Temperature	110(2) K	
Wavelength	1.54178 Å	
Crystal system	monoclinic	
Space group	$P2_1/n$	
Z	2	
Unit cell dimensions	a = 12.0746(6) Å	α = 90 deg.
	b = 8.6963(3) Å	β =101.040(4) deg.
	c = 24.0293(12) Å	γ = 90 deg.
Volume	2476.5(2) $Å^3$	
Density (calculated)	1.30 g/cm^3	
Absorption coefficient	0.71 mm^{-1}	
Crystal shape	brick	
Crystal size	0.162 x 0.065 x 0.057 mm^3	
Crystal colour	green	
Theta range for data collection	4.5 to 62.1 deg.	
Index ranges	$-13 \le h \le 12$, $-9 \le k \le 9$, $-27 \le l \le 16$	
Reflections collected	12244	
Independent reflections	3763 (R(int) = 0.0196)	
Observed reflections	3214 ($I > 2\sigma(I)$)	
Absorption correction	Semi-empirical from equivalents	
Max. and min. transmission	2.21 and 0.57	
Refinement method	Full-matrix least-squares on F^2	
Data/restraints/parameters	3763 / 236 / 375	
Goodness-of-fit on F^2	1.03	
Final R indices (I>2sigma(I))	R1 = 0.037, wR2 = 0.094	
Largest diff. peak and hole	0.25 and -0.27 $eÅ^{-3}$	

3c

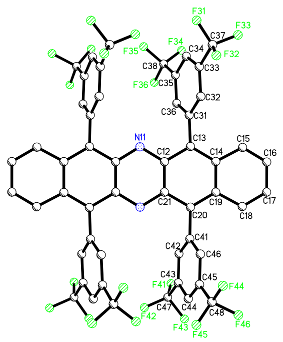

Identification code	gxi16	
Empirical formula	$C_{52}H_{20}F_{24}N_2$	
Formula weight	1128.70	
Temperature	200(2) K	
Wavelength	1.54178 Å	
Crystal system	monoclinic	
Space group	$P2_1/n$	
Z	2	
Unit cell dimensions	a = 12.859(3) Å	α = 90 deg.
	b = 7.9086(16) Å	β = 103.83(3) deg.
	c = 23.298(5) Å	γ = 90 deg.
Volume	2300.8(8) $Å^3$	
Density (calculated)	1.63 g/cm^3	
Absorption coefficient	1.48 mm^{-1}	
Crystal shape	plank	
Crystal size	0.126 x 0.041 x 0.015 mm^3	
Crystal colour	blue	
Theta range for data collection	3.9 to 57.9 deg.	
Index ranges	$-12 \le h \le 14, -6 \le k \le 8, -25 \le l \le 24$	
Reflections collected	11891	
Independent reflections	3181 (R(int) = 0.0731)	
Observed reflections	1842 ($I > 2\sigma(I)$)	
Absorption correction	Semi-empirical from equivalents	
Max. and min. transmission	1.49 and 0.61	
Refinement method	Full-matrix least-squares on F^2	
Data/restraints/parameters	3181 / 1316 / 464	
Goodness-of-fit on F^2	1.04	
Final R indices (I>2sigma(I))	R1 = 0.053, wR2 = 0.097	
Largest diff. peak and hole	0.19 and -0.24 $eÅ^{-3}$	

Quino-tBu

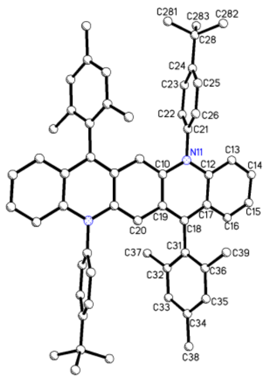

Identification code	gxi14	
Empirical formula	$C_{58}H_{58}N_2$	
Formula weight	783.06	
Temperature	200(2) K	
Wavelength	1.54178 Å	
Crystal system	monoclinic	
Space group	$P2_1/n$	
Z	2	
Unit cell dimensions	a = 9.4682(3) Å	α = 90 deg.
	b = 13.7037(3) Å	β = 97.603(3) deg.
	c = 17.4850(6) Å	γ = 90 deg.
Volume	2248.72(12) $Å^3$	
Density (calculated)	1.16 g/cm^3	
Absorption coefficient	0.50 mm^{-1}	
Crystal shape	plank	
Crystal size	0.076 x 0.075 x 0.045 mm^3	
Crystal colour	purple	
Theta range for data collection	5.1 to 72.1 deg.	
Index ranges	$-11 \leq h \leq 10$, $-16 \leq k \leq 7$, $-19 \leq l \leq 21$	
Reflections collected	15084	
Independent reflections	4319 (R(int) = 0.0229)	
Observed reflections	3192 ($I > 2\sigma(I)$)	
Absorption correction	Semi-empirical from equivalents	
Max. and min. transmission	1.33 and 0.69	
Refinement method	Full-matrix least-squares on F^2	
Data/restraints/parameters	4319 / 0 / 277	
Goodness-of-fit on F^2	1.03	
Final R indices (I>2sigma(I))	R1 = 0.049, wR2 = 0.118	
Largest diff. peak and hole	0.26 and -0.19 $eÅ^{-3}$	

Quino-CF_3

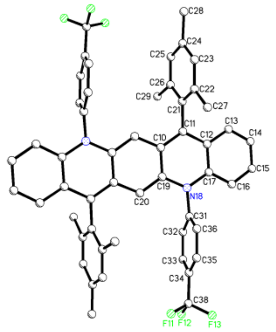

Identification code	gxi12	
Empirical formula	$C_{52}H_{40}F_6N_2$	
Formula weight	806.86	
Temperature	200(2) K	
Wavelength	1.54178 Å	
Crystal system	triclinic	
Space group	$P\bar{1}$	
Z	2	
Unit cell dimensions	a = 12.8417(4) Å	α = 78.588(3) deg.
	b = 13.0652(4) Å	β = 67.275(2) deg.
	c = 15.1490(5) Å	γ = 61.268(2) deg.
Volume	2055.50(12) $Å^3$	
Density (calculated)	1.30 g/cm^3	
Absorption coefficient	0.78 mm^{-1}	
Crystal shape	plank	
Crystal size	0.219 x 0.048 x 0.028 mm^3	
Crystal colour	red	
Theta range for data collection	3.2 to 69.6 deg.	
Index ranges	$-15 \le h \le 15$, $-15 \le k \le 13$, $-16 \le l \le 18$	
Reflections collected	19919	
Independent reflections	7408 (R(int) = 0.0194)	
Observed reflections	5644 ($I > 2\sigma(I)$)	
Absorption correction	Semi-empirical from equivalents	
Max. and min. transmission	1.43 and 0.64	
Refinement method	Full-matrix least-squares on F^2	
Data/restraints/parameters	7408 / 297 / 573	
Goodness-of-fit on F^2	1.04	
Final R indices (I>2sigma(I))	R1 = 0.049, wR2 = 0.117	
Largest diff. peak and hole	0.24 and -0.30 $eÅ^{-3}$	

Quino-$CF_3^{+\bullet}$

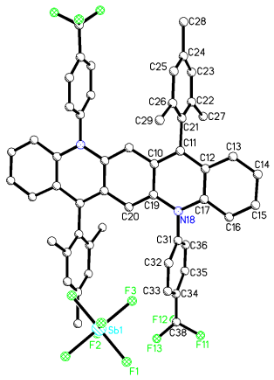

Identification code	gxi13
Empirical formula	$C_{55}H_{46}F_{12}N_2OSb$
Formula weight	1100.69
Temperature	200(2) K
Wavelength	0.71073 Å
Crystal system	orthorhombic
Space group	Pccn
Z	4
Unit cell dimensions	a = 20.8537(6) Å α = 90 deg.
	b = 15.2043(4) Å β = 90 deg.
	c = 15.7519(5) Å γ = 90 deg.
Volume	4994.4(3) $Å^3$
Density (calculated)	1.46 g/cm^3
Absorption coefficient	0.64 mm^{-1}
Crystal shape	plank
Crystal size	0.159 x 0.070 x 0.026 mm^3
Crystal colour	brown
Theta range for data collection	1.7 to 25.1 deg.
Index ranges	$-24 \leq h \leq 24$, $-18 \leq k \leq 18$, $-18 \leq l \leq 18$
Reflections collected	58204
Independent reflections	4427 (R(int) = 0.0926)
Observed reflections	2585 ($I > 2\sigma(I)$)
Absorption correction	Semi-empirical from equivalents
Max. and min. transmission	0.96 and 0.88
Refinement method	Full-matrix least-squares on F^2
Data/restraints/parameters	4427 / 96 / 340
Goodness-of-fit on F^2	1.03
Final R indices (I>2sigma(I))	R1 = 0.055, wR2 = 0.143
Largest diff. peak and hole	0.70 and -0.55 $eÅ^{-3}$

PNZ$^{+\bullet}$

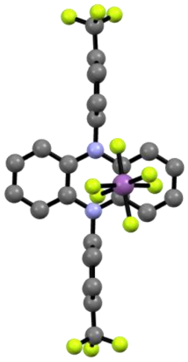

Identification code	gxi24	
Empirical formula	$C_{27}H_{18}Cl_2F_{12}N_2Sb$	
Formula weight	791.08	
Temperature	200(2) K	
Wavelength	0.71073 Å	
Crystal system	monoclinic	
Space group	C2/c	
Z	4	
Unit cell dimensions	a = 15.7925(10) Å	α = 90 deg.
	b = 23.3446(15) Å	β = 92.9869(19) deg.
	c = 8.0504(5) Å	γ = 90 deg.
Volume	2963.9(3) $Å^3$	
Density (calculated)	1.77 g/cm^3	
Absorption coefficient	1.21 mm^{-1}	
Crystal shape	plate	
Crystal size	0.132 x 0.111 x 0.022 mm^3	
Crystal colour	green	
Theta range for data collection	1.6 to 30.5 deg.	
Index ranges	$-22\leq h\leq 22$, $-31\leq k\leq 33$, $-11\leq l\leq 11$	
Reflections collected	18810	
Independent reflections	4530 (R(int) = 0.0270)	
Observed reflections	3811 ($I > 2\sigma(I)$)	
Absorption correction	Semi-empirical from equivalents	
Max. and min. transmission	0.96 and 0.89	
Refinement method	Full-matrix least-squares on F^2	
Data/restraints/parameters	4530 / 8 / 213	
Goodness-of-fit on F^2	1.06	
Final R indices (I>2sigma(I))	R1 = 0.038, wR2 = 0.094	
Largest diff. peak and hole	0.57 and -0.51 $eÅ^{-3}$	

BPNZ

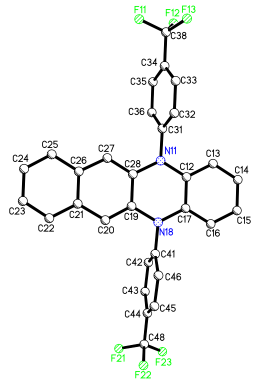

Identification code	gxi20	
Empirical formula	$C_{30}H_{18}F_6N_2$	
Formula weight	520.46	
Temperature	200(2) K	
Wavelength	1.54178 Å	
Crystal system	monoclinic	
Space group	$P2_1$	
Z	4	
Unit cell dimensions	a = 13.0758(11) Å	α = 90 deg.
	b = 9.4675(6) Å	β =100.142(6) deg.
	c = 19.5081(13) Å	γ = 90 deg.
Volume	2377.3(3) $Å^3$	
Density (calculated)	1.45 g/cm^3	
Absorption coefficient	1.02 mm^{-1}	
Crystal shape	?	
Crystal size	0.097 x 0.068 x 0.042 mm^3	
Crystal colour	pale yellow	
Theta range for data collection	3.4 to 57.9 deg.	
Index ranges	$-14 \le h \le 14$, $-10 \le k \le 10$, $-12 \le l \le 21$	
Reflections collected	16536	
Independent reflections	6204 (R(int) = 0.0565)	
Observed reflections	3445 ($I > 2\sigma(I)$)	
Absorption correction	Semi-empirical from equivalents	
Max. and min. transmission	1.42 and 0.71	
Refinement method	Full-matrix least-squares on F^2	
Data/restraints/parameters	6204 / 835 / 711	
Goodness-of-fit on F^2	0.99	
Final R indices (I>2sigma(I))	R1 = 0.096, wR2 = 0.231	
Absolute structure parameter	0.2(2)	
Largest diff. peak and hole	0.58 and -0.37 $eÅ^{-3}$	

BPNZ$^{+\bullet}$

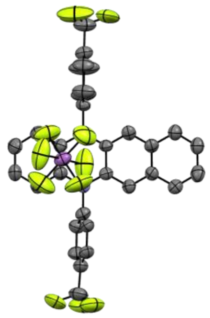

Identification code	gxi22	
Empirical formula	$C_{31.50}H_{21}F_{12}N_2O_{0.50}Sb$	
Formula weight	785.25	
Temperature	200(2) K	
Wavelength	1.54178 Å	
Crystal system	orthorhombic	
Space group	Aba2	
Z	8	
Unit cell dimensions	a = 46.518(4) Å	α = 90 deg.
	b = 16.4075(15) Å	β = 90 deg.
	c = 8.0281(6) Å	γ = 90 deg.
Volume	6127.4(9) $Å^3$	
Density (calculated)	1.70 g/cm^3	
Absorption coefficient	8.07 mm^{-1}	
Crystal shape	plate	
Crystal size	0.125 x 0.071 x 0.020 mm^3	
Crystal colour	orange	
Theta range for data collection	5.7 to 63.7 deg.	
Index ranges	$-52 \leq h \leq 54$, $-18 \leq k \leq 8$, $-8 \leq l \leq 9$	
Reflections collected	9129	
Independent reflections	4182 (R(int) = 0.0895)	
Observed reflections	2513 ($I > 2\sigma(I)$)	
Absorption correction	Semi-empirical from equivalents	
Max. and min. transmission	3.60 and 0.62	
Refinement method	Full-matrix least-squares on F^2	
Data/restraints/parameters	4182 / 1062 / 481	
Goodness-of-fit on F^2	0.97	
Final R indices (I>2sigma(I))	R1 = 0.070, wR2 = 0.170	
Absolute structure parameter	0.00(2)	
Largest diff. peak and hole	0.49 and -0.87 $eÅ^{-3}$	

DBPNZ

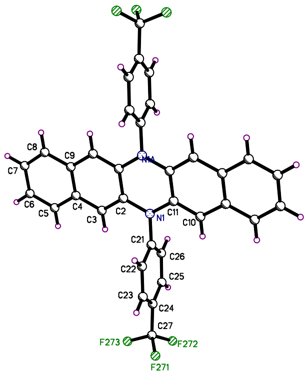

Identification code	gxi17	
Empirical formula	$C_{34}H_{20}F_6N_2$	
Formula weight	570.52	
Temperature	200(2) K	
Wavelength	0.71073 Å	
Crystal system	Monoclinic	
Space group	$P2_1/c$	
Z	2	
Unit cell dimensions	a = 13.0273(7) Å	α = 90 deg.
	b = 9.5645(5) Å	β = 96.985(1) deg.
	c = 10.6532(6) Å	γ = 90 deg.
Volume	1317.53(12) Å^3	
Density (calculated)	1.44 g/cm^3	
Absorption coefficient	0.11 mm^{-1}	
Crystal shape	brick	
Crystal size	0.132 x 0.072 x 0.053 mm^3	
Crystal colour	yellow	
Theta range for data collection	1.6 to 31.5 deg.	
Index ranges	$-19 \le h \le 18$, $-14 \le k \le 13$, $-15 \le l \le 15$	
Reflections collected	18491	
Independent reflections	4357 (R(int) = 0.0567)	
Observed reflections	2592 (I > 2\s(I))	
Absorption correction	Semi-empirical from equivalents	
Refinement method	Full-matrix least-squares on F^2	
Data/restraints/parameters	4357 / 0 / 190	
Goodness-of-fit on F^2	1.03	
Final R indices ($I>2\sigma(I)$)	R1 = 0.061, wR2 = 0.148	
Largest diff. peak and hole	0.44 and -0.41 eÅ^{-3}	

DBPNZ$^{+\bullet}$

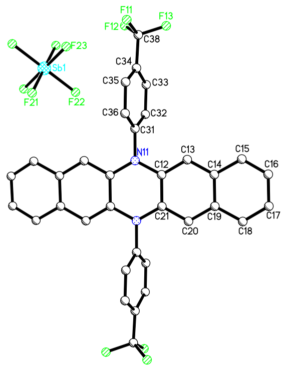

Identification code	gxi18	
Empirical formula	$C_{34}H_{20}F_{12}N_2Sb$	
Formula weight	806.27	
Temperature	200(2) K	
Wavelength	1.54178 Å	
Crystal system	triclinic	
Space group	$P\bar{1}$	
Z	1	
Unit cell dimensions	a = 8.4529(8) Å	α = 97.542(8) deg.
	b = 8.4694(8) Å	β = 91.735(8) deg.
	c = 11.8279(13) Å	γ = 113.939(7) deg.
Volume	763.97(14) $Å^3$	
Density (calculated)	1.75 g/cm^3	
Absorption coefficient	8.10 mm^{-1}	
Crystal shape	plate	
Crystal size	0.077 x 0.060 x 0.012 mm^3	
Crystal colour	violet	
Theta range for data collection	3.8 to 67.0 deg.	
Index ranges	$-10 \le h \le 5$, $-9 \le k \le 10$, $-14 \le l \le 13$	
Reflections collected	6402	
Independent reflections	2603 (R(int) = 0.0397)	
Observed reflections	2086 ($I > 2\sigma(I)$)	
Absorption correction	Semi-empirical from equivalents	
Max. and min. transmission	1.41 and 0.67	
Refinement method	Full-matrix least-squares on F^2	
Data/restraints/parameters	2603 / 79 / 251	
Goodness-of-fit on F^2	1.15	
Final R indices (I>2sigma(I))	R1 = 0.048, wR2 = 0.094	
Largest diff. peak and hole	0.74 and -0.86 $eÅ^{-3}$	

References

[1] M. Mas-Torrent, C. Rovira, *Chem. Rev.* **2011**, *111*, 4833-4856.

[2] C. Wang, H. Dong, W. Hu, Y. Liu, D. Zhu, *Chem. Rev.* **2012**, *112*, 2208-2267.

[3] H. Dong, X. Fu, J. Liu, Z. Wang, W. Hu, *Adv. Mater.* **2013**, *25*, 6158-6183.

[4] H. Sirringhaus, *Adv. Mater.* **2014**, *26*, 1319-1335.

[5] H. Li, W. Shi, J. Song, H.-J. Jang, J. Dailey, J. Yu, H. E. Katz, *Chem. Rev.* **2018**, *119*, 3-35.

[6] J. T. Quinn, J. Zhu, X. Li, J. Wang, Y. Li, *J. Mater. Chem. C* **2017**, *5*, 8654-8681.

[7] G. Schweicher, G. Garbay, R. Jouclas, F. Vibert, F. Devaux, Y. H. Geerts, *Adv. Mater.* **2020**, *32*, 1905909.

[8] B. Schmaltz, T. Weil, K. Müllen, *Adv. Mater.* **2009**, *21*, 1067-1078.

[9] K.-J. Baeg, G.-T. Bae, Y.-Y. Noh, *ACS Appl. Mater. Interfaces* **2013**, *5*, 5804-5810.

[10] L. A. Majewski, R. Schroeder, M. Grell, *Adv. Funct. Mater.* **2005**, *15*, 1017-1022.

[11] J. Takeya, M. Yamagishi, Y. Tominari, R. Hirahara, Y. Nakazawa, T. Nishikawa, T. Kawase, T. Shimoda, S. Ogawa, *Appl. Phys. Lett.* **2007**, *90*, 102120.

[12] D. Gundlach, J. Nichols, L. Zhou, T. N. Jackson, *Appl. Phys. Lett.* **2002**, *80*, 2925-2927.

[13] M. Halik, H. Klauk, U. Zschieschang, G. Schmid, S. Ponomarenko, S. Kirchmeyer, W. Weber, *Adv. Mater.* **2003**, *15*, 917-922.

[14] J. E. Anthony, D. L. Eaton, S. R. Parkin, *Org. Lett.* **2002**, *4*, 15-18.

[15] T. Izawa, E. Miyazaki, K. Takimiya, *Adv. Mater.* **2008**, *20*, 3388-3392.

[16] S. Miao, A. L. Appleton, N. Berger, S. Barlow, S. R. Marder, K. I. Hardcastle, U. H. Bunz, *Chem. Eur. J.* **2009**, *15*, 4990-4993.

[17] T. He, M. Stolte, F. Würthner, *Adv. Mater.* **2013**, *25*, 6951-6955.

[18] R. d. Schmidt, J. H. Oh, Y.-S. Sun, M. Deppisch, A.-M. Krause, K. Radacki, H. Braunschweig, M. Könemann, P. Erk, Z. Bao, *J. Am. Chem. Soc.* **2009**, *131*, 6215-6228.

[19] X. Gao, Y. Hu, *J. Mater. Chem. C* **2014**, *2*, 3099-3117.

[20] X. Zhao, X. Zhan, *Chem. Soc. Rev.* **2011**, *40*, 3728-3743.

[21] J. E. Anthony, A. Facchetti, M. Heeney, S. R. Marder, X. Zhan, *Adv. Mater.* **2010**, *22*, 3876-3892.

[22] J. Zaumseil, H. Sirringhaus, *Chem. Rev.* **2007**, *107*, 1296-1323.

[23] A. Aleshin, J. Lee, S. Chu, J. Kim, Y. Park, *Appl. Phys. Lett.* **2004**, *84*, 5383-5385.

[24] C. Reese, M. E. Roberts, S. R. Parkin, Z. Bao, *Appl. Phys. Lett.* **2009**, *94*, 202101.

[25] T. W. Kelley, D. V. Muyres, P. F. Baude, T. P. Smith, T. D. Jones, *Mater. Res. Soc. Symp. Proc.* **2003**, *771*, 169.

[26] J. Han, X. Liu, Y. Li, Z. Lou, M. Yi, H. Kong, J. Luo, *Org. Chem. Front.* **2019**, *6*, 2839-2843.

[27] D. Sparfel, F. Gobert, J. Rigaudy, *Tetrahedron* **1980**, *36*, 2225-2235.

[28] O. Berg, E. L. Chronister, T. Yamashita, G. W. Scott, R. M. Sweet, J. Calabrese, *J. Phys. Chem. A* **1999**, *103*, 2451-2459.

[29] J. E. Anthony, J. S. Brooks, D. L. Eaton, S. R. Parkin, *J. Am. Chem. Soc.* **2001**, *123*, 9482-9483.

[30] U. H. Bunz, *Chem. Eur. J.* **2009**, *15*, 6780-6789.

[31] U. H. Bunz, J. U. Engelhart, B. D. Lindner, M. Schaffroth, *Angew. Chem. Int. Ed.* **2013**, *52*, 3810-3821.

[32] U. H. Bunz, *Acc. Chem. Res.* **2015**, *48*, 1676-1686.

[33] Q. Miao, *Adv. Mater.* **2014**, *26*, 5541-5549.

[34] D. Liu, X. Xu, Y. Su, Z. He, J. Xu, Q. Miao, *Angew. Chem. Int. Ed.* **2013**, *52*, 6222-6227.

[35] Z. Liang, Q. Tang, J. Xu, Q. Miao, *Adv. Mater.* **2011**, *23*, 1535-1539.

[36] M. Chu, J. X. Fan, S. Yang, D. Liu, C. F. Ng, H. Dong, A. M. Ren, Q. Miao, *Adv. Mater.* **2018**, *30*, 1803467.

[37] J. U. Engelhart, F. Paulus, M. Schaffroth, V. Vasilenko, O. Tverskoy, F. Rominger, U. H. Bunz, *J. Org. Chem.* **2016**, *81*, 1198-1205.

[38] D. A. da Silva Filho, E. G. Kim, J. L. Brédas, *Adv. Mater.* **2005**, *17*, 1072-1076.

[39] C. Wang, H. Dong, L. Jiang, W. Hu, *Chem. Soc. Rev.* **2018**, *47*, 422-500.

[40] L. Huang, Q. Liao, Q. Shi, H. Fu, J. Ma, J. Yao, *J. Mater. Chem.* **2010**, *20*, 159-166.

[41] R. Zeis, C. Besnard, T. Siegrist, C. Schlockermann, X. Chi, C. Kloc, *Chem. Mater.* **2006**, *18*, 244-248.

[42] V. Podzorov, E. Menard, A. Borissov, V. Kiryukhin, J. A. Rogers, M. Gershenson, *Phys. Rev. Lett.* **2004**, *93*, 086602.

[43] D. Braga, A. Jaafari, L. Miozzo, M. Moret, S. Rizzato, A. Papagni, A. Yassar, *Eur. J. Org. Chem.* **2011**, *2011*, 4160-4169.

[44] J. A. Dodge, J. Bain, A. R. Chamberlin, *J. Org. Chem.* **1990**, *55*, 4190-4198.

[45] J. T. Ly, S. A. Lopez, J. B. Lin, J. J. Kim, H. Lee, E. K. Burnett, L. Zhang, A. Aspuru-Guzik, K. Houk, A. L. Briseno, *J. Mater. Chem. C* **2018**, *6*, 3757-3761.

[46] S. Uttiya, L. Miozzo, E. Fumagalli, S. Bergantin, R. Ruffo, M. Parravicini, A. Papagni, M. Moret, A. Sassella, *J. Mater. Chem. C* **2014**, *2*, 4147-4155.

[47] Y.-S. Wu, T.-H. Liu, H.-H. Chen, C. H. Chen, *Thin Solid Films* **2006**, *496*, 626-630.

[48] X. Ren, M. J. Bruzek, D. A. Hanifi, A. Schulzetenberg, Y. Wu, C. H. Kim, Z. Zhang, J. E. Johns, A. Salleo, S. Fratini, *Adv. Electron. Mater.* **2017**, *3*, 1700018.

[49] M. Mamada, H. Katagiri, T. Sakanoue, S. Tokito, *Cryst. Growth Des.* **2015**, *15*, 442-448.

[50] W. A. Ogden, S. Ghosh, M. J. Bruzek, K. A. McGarry, L. Balhorn, V. Young Jr, L. J. Purvis, S. E. Wegwerth, Z. Zhang, N. A. Serratore, *Cryst. Growth Des.* **2017**, *17*, 643-658.

[51] Z. Zhang, W. A. Ogden, V. G. Young, C. J. Douglas, *Chem. Commun.* **2016**, *52*, 8127-8130.

[52] X. Gu, B. Shan, Z. He, Q. Miao, *ChemPlusChem* **2017**, *82*, 1034-1038.

[53] K. Kitamura, K. Asahina, Y. Nagai, H. Sugiyama, H. Uekusa, T. Hamura, *Chem. Eur. J.* **2018**, *24*, 14034-14038.

[54] I. Kaur, W. Jia, R. P. Kopreski, S. Selvarasah, M. R. Dokmeci, C. Pramanik, N. E. McGruer, G. P. Miller, *J. Am. Chem. Soc.* **2008**, *130*, 16274-16286.

[55] D. Maulding, B. G. Roberts, *J. Org. Chem.* **1969**, *34*, 1734-1736.

[56] Y. Huang, E. Egap, *Polym. J.* **2018**, *50*, 603-614.

[57] Y. Teki, *Chem. Eur. J.* **2020**, *26*, 980-996.

[58] K. Nakahara, S. Iwasa, M. Satoh, Y. Morioka, J. Iriyama, M. Suguro, E. Hasegawa, *Chem. Phys. Lett.* **2002**, *359*, 351-354.

[59] H. Nishide, S. Iwasa, Y.-J. Pu, T. Suga, K. Nakahara, M. Satoh, *Electrochim. Acta* **2004**, *50*, 827-831.

[60] T. Janoschka, N. Martin, U. Martin, C. Friebe, S. Morgenstern, H. Hiller, M. D. Hager, U. S. Schubert, *Nature* **2015**, *527*, 78-81.

[61] K. Kato, A. Osuka, *Angew. Chem. Int. Ed.* **2019**, *131*, 9074-9082.

[62] M. Ballester, J. Riera-Figueras, J. Castaner, C. Badfa, J. M. Monso, *J. Am. Chem. Soc.* **1971**, *93*, 2215-2225.

[63] K. Kato, W. Cha, J. Oh, K. Furukawa, H. Yorimitsu, D. Kim, A. Osuka, *Angew. Chem. Int. Ed.* **2016**, *55*, 8711-8714.

[64] T. Kobashi, D. Sakamaki, S. Seki, *Angew. Chem. Int. Ed.* **2016**, *55*, 8634-8638.

[65] D. Rottschäfer, B. Neumann, H. G. Stammler, M. van Gastel, D. M. Andrada, R. S. Ghadwal, *Angew. Chem. Int. Ed.* **2018**, *57*, 4765-4768.

[66] Y. Kawanaka, A. Shimizu, T. Shinada, R. Tanaka, Y. Teki, *Angew. Chem. Int. Ed.* **2013**, *52*, 6643-6647.

[67] A. Shimizu, A. Ito, Y. Teki, *Chem. Commun.* **2016**, *52*, 2889-2892.

[68] Z. Zeng, Y. M. Sung, N. Bao, D. Tan, R. Lee, J. L. Zafra, B. S. Lee, M. Ishida, J. Ding, J. T. López Navarrete, *J. Am. Chem. Soc.* **2012**, *134*, 14513-14525.

[69] Y. Tian, K. Uchida, H. Kurata, Y. Hirao, T. Nishiuchi, T. Kubo, *J. Am. Chem. Soc.* **2014**, *136*, 12784-12793.

[70] L. Ji, M. Haehnel, I. Krummenacher, P. Biegger, F. L. Geyer, O. Tverskoy, M. Schaffroth, J. Han, A. Dreuw, T. B. Marder, *Angew. Chem. Int. Ed.* **2016**, *55*, 10498-10501.

[71] L. Ji, A. Friedrich, I. Krummenacher, A. Eichhorn, H. Braunschweig, M. Moos, S. Hahn, F. L. Geyer, O. Tverskoy, J. Han, *J. Am. Chem. Soc.* **2017**, *139*, 15968-15976.

[72] H. Reiss, L. Ji, J. Han, S. Koser, O. Tverskoy, J. Freudenberg, F. Hinkel, M. Moos, A. Friedrich, I. Krummenacher, *Angew. Chem. Int. Ed.* **2018**, *57*, 9543-9547.

[73] X. Xu, Y. Yao, B. Shan, X. Gu, D. Liu, J. Liu, J. Xu, N. Zhao, W. Hu, Q. Miao, *Adv. Mater.* **2016**, *28*, 5276-5283.

[74] M. Fahlman, A. Crispin, X. Crispin, S. Henze, M. P. de Jong, W. Osikowicz, C. Tengstedt, W. R. Salaneck, *J. Phys. Condens. Matter* **2007**, *19*, 183202.

[75] C. M. Wehrmann, R. T. Charlton, M. S. Chen, *J. Am. Chem. Soc.* **2019**, *141*, 3240-3248.

[76] M. Imran, C. M. Wehrmann, M. S. Chen, *J. Am. Chem. Soc.* **2020**, *142*, 38-43.

[77] G. Xie, S. Hahn, F. Rominger, J. Freudenberg, U. H. Bunz, *Chem. Commun.* **2018**, *54*, 7593-7596.

[78] V. C. Sundar, J. Zaumseil, V. Podzorov, E. Menard, R. L. Willett, T. Someya, M. E. Gershenson, J. A. Rogers, *Science* **2004**, *303*, 1644-1646.

[79] A. Molinari, I. Gutiérez, I. N. Hulea, S. Russo, A. F. Morpurgo, *Appl. Phys. Lett.* **2007**, *90*, 212103.

[80] T. K. Mullenbach, K. A. McGarry, W. A. Luhman, C. J. Douglas, R. J. Holmes, *Adv. Mater.* **2013**, *25*, 3689-3693.

[81] K. Miyata, Y. Kurashige, K. Watanabe, T. Sugimoto, S. Takahashi, S. Tanaka, J. Takeya, T. Yanai, Y. Matsumoto, *Nat. Chem.* **2017**, *9*, 983.

[82] I. Breen, R. Tempelaar, L. A. Bizimana, B. Kloss, D. R. Reichman, D. B. Turner, *J. Am. Chem. Soc.* **2017**, *139*, 11745-11751.

[83] O. Mitrofanov, D. V. Lang, C. Kloc, J. M. Wikberg, T. Siegrist, W.-Y. So, M. Sergent, A. P. Ramirez, *Phys. Rev. Lett.* **2006**, *97*, 166601.

[84] E. Fumagalli, L. Raimondo, L. Silvestri, M. Moret, A. Sassella, M. Campione, *Chem. Mater.* **2011**, *23*, 3246-3253.

[85] Y. Sakamoto, T. Suzuki, *J. Org. Chem.* **2017**, *82*, 8111-8116.

[86] F. Anger, T. Breuer, A. Ruff, M. Klues, A. Gerlach, R. Scholz, S. Ludwigs, G. Witte, F. Schreiber, *J. Phys. Chem. C* **2016**, *120*, 5515-5522.

[87] J. U. Engelhart, O. Tverskoy, U. H. Bunz, *J. Am. Chem. Soc.* **2014**, *136*, 15166-15169.

[88] U. H. Bunz, *Pure Appl. Chem.* **2010**, *82*, 953-968.

[89] X. Chi, D. Li, H. Zhang, Y. Chen, V. Garcia, C. Garcia, T. Siegrist, *Org. Electron.* **2008**, *9*, 234-240.

[90] D. Pappo, T. Mejuch, O. Reany, E. Solel, M. Gurram, E. Keinan, *Org. Lett.* **2009**, *11*, 1063-1066.

[91] M. Liu, S.-J. Su, M.-C. Jung, Y. Qi, W.-M. Zhao, J. Kido, *Chem. Mater.* **2012**, *24*, 3817-3827.

[92] X. Gu, W. A. Luhman, E. Yagodkin, R. J. Holmes, C. J. Douglas, *Org. Lett.* **2012**, *14*, 1390-1393.

[93] M. J. Frisch, G. W. Trucks, H. B. Schlegel, G. E. Scuseria, M. A. Robb, J. R. Cheeseman, I. G. Scalmani, V. Barone, B. Mennucci, G. A. Petersson, H. Nakatsuji, M. Caricato, X. Li, H. P. Hratchian, A. F. Izmaylov, J. Bloino, G. Zheng, J. L. Sonnenberg, M. Hada, M. Ehara, K. Toyota, R. Fukuda, J. Hasegawa, M. Ishida, T. Nakajima, Y. Honda, O. Kitao, H. Nakai, T. Vreven, J. A. Jr. Montgomery, J. E. Peralta, F. Ogliaro, M. J. Bearpark, J. Heyd, E. N. Brothers, K. Kudin, V. N. Staroverov, R. Kobayashi, J. Normand, K. Raghavachari, A. P. Rendell, J. C. Burant, S. S. Iyengar, J. Tomasi, M. Cossi, N. Rega, N. J. Millam, M. Klene, J. E. Knox, J. B. Cross, V. Bakken, C. Adamo, J. Jaramillo, R. Gomperts, R. E. Stratmann, O. Yazyev, A. J. Austin, R. Cammi, C. Pomelli, J. W. Ochterski, R. L. Martin, K. Morokuma, V. G. Zakrzewski, G. A. Voth, P. Salvador, J. J. Dannenberg, S. Dapprich, A. D. Daniels, O. Farkas, J. B. Foresman, J. V. Ortiz, D. J. Cioslowski, D. Fox, *J. Gaussian 09*, Gaussian. Inc.: Wallingford, CT, **2009**.

[94] M. A. Spackman, D. Jayatilaka, *CrystEngComm* **2009**, *11*, 19-32.

[95] S. Bergantin, M. Moret, *Cryst. Growth Des.* **2012**, *12*, 6035-6041.

[96] S. Bergantin, M. Moret, G. Buth, F. P. Fabbiani, *J. Phys. Chem. C* **2014**, *118*, 13476-13483.

[97] G. Xie, M. Hauschild, H. Hoffmann, L. Ahrens, F. Rominger, M. Borkowski, T. Marszalek, J. Freudenberg, M. Kivala, U. H. Bunz, *Chem. Eur. J.* **2020**, *26*, 799-803.

[98] U. H. Bunz, J. Freudenberg, *Acc. Chem. Res.* **2019**, *52*, 1575-1587.

[99] B. Kohl, F. Rominger, M. Mastalerz, *Angew. Chem. Int. Ed.* **2015**, *127*, 6149-6154.

[100] B.-L. Hu, C. An, M. Wagner, G. Ivanova, A. Ivanova, M. Baumgarten, *J. Am. Chem. Soc.* **2019**, *141*, 5130-5134.

[101] Q. Miao, *Synlett* **2012**, *2012*, 326-336.

[102] U. H. Bunz, J. U. Engelhart, *Chem. Eur. J.* **2016**, *22*, 4680-4689.

[103] F. Paulus, J. U. Engelhart, P. E. Hopkinson, C. Schimpf, A. Leineweber, H. Sirringhaus, Y. Vaynzof, U. H. Bunz, *J. Mater. Chem. C* **2016**, *4*, 1194-1200.

[104] J. U. Engelhart, B. D. Lindner, M. Schaffroth, D. Schrempp, O. Tverskoy, U. H. Bunz, *Chem. Eur. J.* **2015**, *21*, 8121-8129.

[105] Z. Wang, Z. Wang, Y. Zhou, P. Gu, G. Liu, K. Zhao, L. Nie, Q. Zeng, J. Zhang, Y. Li, *J. Mater. Chem. C* **2018**, *6*, 3628-3633.

[106] Q. Miao, X. Chi, S. Xiao, R. Zeis, M. Lefenfeld, T. Siegrist, M. L. Steigerwald, C. Nuckolls, *J. Am. Chem. Soc.* **2006**, *128*, 1340-1345.

[107] B.-B. Jang, S. H. Lee, Z. H. Kafafi, *Chem. Mater.* **2006**, *18*, 449-457.

[108] J. Lu, D. M. Ho, N. J. Vogelaar, C. M. Kraml, R. A. Pascal, *J. Am. Chem. Soc.* **2004**, *126*, 11168-11169.

[109] W. Fan, T. Winands, N. L. Doltsinis, Y. Li, Z. Wang, *Angew. Chem. Int. Ed.* **2017**, *129*, 15575-15579.

[110] Z. Chen, Y. Ni, Y. Zhi, F. Wen, Z. Zhou, Y. Wei, W. Zhu, Z. Liu, *Angew. Chem. Int. Ed.* **2018**, *57*, 12549-12553.

[111] R. G. Clevenger, B. Kumar, E. M. Menuey, G. H. Lee, D. Patterson, K. V. Kilway, *Chem. Eur. J.* **2018**, *24*, 243-250.

[112] Y. Xiao, J. T. Mague, R. H. Schmehl, F. M. Haque, R. A. Pascal Jr, *Angew. Chem. Int. Ed.* **2019**, *131*, 2857-2859.

[113] X.-Y. Wang, F.-D. Zhuang, R.-B. Wang, X.-C. Wang, X.-Y. Cao, J.-Y. Wang, J. Pei, *J. Am. Chem. Soc.* **2014**, *136*, 3764-3767.

[114] J. E. Anthony, *Chem. Rev.* **2006**, *106*, 5028-5048.

[115] S. H. Etschel, J. T. Margraf, A. Y. Amin, F. Hampel, C. M. Jäger, T. Clark, M. Halik, R. R. Tykwinski, *Chem. Commun.* **2013**, *49*, 6725-6727.

[116] J. N. Wilson, U. H. Bunz, *J. Am. Chem. Soc.* **2005**, *127*, 4124-4125.

[117] J. J. Hoff, L. Zhu, Y. Dong, T. Albers, P. J. Steel, X. Cui, Y. Wen, I. Lebedyeva, S. Miao, *RSC Adv.* **2016**, *6*, 86824-86828.

[118] A. V. Lunchev, S. A. Morris, R. Ganguly, A. C. Grimsdale, *Chem. Eur. J.* **2019**, *25*, 1819-1823.

[119] C.-L. Song, C.-B. Ma, F. Yang, W.-J. Zeng, H.-L. Zhang, X. Gong, *Org. Lett.* **2011**, *13*, 2880-2883.

[120] G. Xie, V. Brosius, J. Han, F. Rominger, A. Dreuw, J. Freudenberg, U. H. Bunz, *Chem. Eur. J.* **2020**, *26*, 160-164.

[121] B. Kohl, F. Rominger, M. Mastalerz, *Org. Lett.* **2014**, *16*, 704-707.

[122] L. Ueberricke, D. Holub, J. Kranz, F. Rominger, M. Elstner, M. Mastalerz, *Chem. Eur. J.* **2019**, *25*, 11121-11134.

[123] C. Wang, J. Zhang, G. Long, N. Aratani, H. Yamada, Y. Zhao, Q. Zhang, *Angew. Chem. Int. Ed.* **2015**, *54*, 6292-6296.

[124] Z. Wang, P. Gu, G. Liu, H. Yao, Y. Wu, Y. Li, G. Rakesh, J. Zhu, H. Fu, Q. Zhang, *Chem. Commun.* **2017**, *53*, 7772-7775.

[125] Z. Liang, Q. Tang, R. Mao, D. Liu, J. Xu, Q. Miao, *Adv. Mater.* **2011**, *23*, 5514-5518.

[126] Q. Tang, J. Liu, H. S. Chan, Q. Miao, *Chem. Eur. J.* **2009**, *15*, 3965-3969.

[127] J. Fleischhauer, S. Zahn, R. Beckert, U. W. Grummt, E. Birckner, H. Görls, *Chem. Eur. J.* **2012**, *18*, 4549-4557.

[128] G. A. Zissimou, A. Kourtellaris, P. A. Koutentis, *J. Org. Chem.* **2018**, *83*, 4754-4761.

[129] S. Dong, T. Y. Gopalakrishna, Y. Han, H. Phan, T. Tao, Y. Ni, G. Liu, C. Chi, *J. Am. Chem. Soc.* **2019**, *141*, 62-66.

[130] Y. Chen, H. Kueh, T. Y. Gopalakrishna, S. Dong, Y. Han, C. Chi, *Org. Lett.* **2019**, *21*, 3127-3130.

[131] X. L. Shi, C. Y. Chi, *Top. Curr. Chem.* **2017**, *375*, 68.

[132] R. Mondal, C. Tönshoff, D. Khon, D. C. Neckers, H. F. Bettinger, *J. Am. Chem. Soc.* **2009**, *131*, 14281-14289.

[133] B. Shen, T. Geiger, R. Einholz, F. Reicherter, S. Schundelmeier, C. C. Maichle-Mössmer, B. Speiser, H. F. Bettinger, *J. Org. Chem.* **2018**, *83*, 3149-3158.

[134] R. Einholz, H. F. Bettinger, *Angew. Chem. Int. Ed.* **2013**, *52*, 9818-9820.

[135] Gaussian 16, Revision B.01, M. J. Frisch, G. W. Trucks, H. B. Schlegel, G. E. Scuseria, M. A. Robb, J. R. Cheeseman, G. Scalmani, V. Barone, G. A. Petersson, H. Nakatsuji, X. Li, M. Caricato, A. V. Marenich, J. Bloino, B. G. Janesko, R. Gomperts, B. Mennucci, H. P. Hratchian, J. V. Ortiz, A. F. Izmaylov, J. L. Sonnenberg, D. Williams-Young, F. Ding, F. Lipparini, F. Egidi, J. Goings, B. Peng, A. Petrone, T. Henderson, D. Ranasinghe, V. G. Zakrzewski, J. Gao, N. Rega, G. Zheng, W. Liang, M. Hada, M. Ehara, K. Toyota, R. Fukuda, J. Hasegawa, M. Ishida, T. Nakajima, Y. Honda, O. Kitao, H. Nakai, T. Vreven, K. Throssell, J. A. Montgomery, Jr., J. E. Peralta, F. Ogliaro, M. J. Bearpark, J. J. Heyd, E. N. Brothers, K. N. Kudin, V. N. Staroverov, T. A. Keith, R. Kobayashi, J. Normand, K. Raghavachari, A. P. Rendell, J. C. Burant, S. S. Iyengar, J. Tomasi, M. Cossi, J. M. Millam, M. Klene, C. Adamo, R. Cammi, J. W. Ochterski, R. L. Martin, K. Morokuma, O. Farkas, J. B. Foresman, D. J. Fox, Gaussian, Inc., Wallingford CT, **2016**.

[136] J. I. Wu, C. S. Wannere, Y. Mo, P. v. R. Schleyer, U. H. Bunz, *J. Org. Chem.* **2009**, *74*, 4343-4349.

[137] Z. Chen, C. S. Wannere, C. Corminboeuf, R. Puchta, P. V. R. Schleyer, *Chem. Rev.* **2005**, *105*, 3842-3888.

[138] Q. Miao, T.-Q. Nguyen, T. Someya, G. B. Blanchet, C. Nuckolls, *J. Am. Chem. Soc.* **2003**, *125*, 10284-10287.

[139] C. Sato, S. Suzuki, M. Kozaki, K. Okada, *Org. Lett.* **2016**, *18*, 1052-1055.

[140] L. Ji, S. Hahn, P. Biegger, H. Reiss, J. Han, A. Friedrich, I. Krummenacher, H. Braunschweig, M. Moos, J. Freudenberg, C. Lambert, A. Dreuw, T. B. Marder, U. H. F. Bunz, *Chem. Eur. J.* **2019**, *25*, 9840-9845.

[141] S. Dong, T. S. Herng, T. Y. Gopalakrishna, H. Phan, Z. L. Lim, P. Hu, R. D. Webster, J. Ding, C. Chi, *Angew. Chem. Int. Ed.* **2016**, *55*, 9316-9320.

[142] S. Sanvito, *Chem. Soc. Rev.* **2011**, *40*, 3336-3355.

[143] Z. Sun, Q. Ye, C. Chi, J. Wu, *Chem. Soc. Rev.* **2012**, *41*, 7857-7889.

[144] T. Kusamoto, H. Nishihara, *Nature* **2018**, *563*, 480-481.

[145] Q. Peng, A. Obolda, M. Zhang, F. Li, *Angew. Chem. Int. Ed.* **2015**, *54*, 7091-7095.

[146] Y. Gao, W. Xu, H. Ma, A. Obolda, W. Yan, S. Dong, M. Zhang, F. Li, *Chem. Mater.* **2017**, *29*, 6733-6739.

[147] Y. Zheng, M. S. Miao, G. Dantelle, N. D. Eisenmenger, G. Wu, I. Yavuz, M. L. Chabinyc, K. N. Houk, F. Wudl, *Adv. Mater.* **2015**, *27*, 1718-1723.

[148] S. Pal, M. Itkis, F. Tham, R. Reed, R. Oakley, R. Haddon, *Science* **2005**, *309*, 281-284.

[149] S. K. Pal, M. E. Itkis, F. S. Tham, R. W. Reed, R. T. Oakley, B. Donnadieu, R. C. Haddon, *J. Am. Chem. Soc.* **2007**, *129*, 7163-7174.

[150] M. Xue, T. Cao, D. Wang, Y. Wu, H. Yang, X. Dong, J. He, F. Li, G. Chen, *Sci. Rep.* **2012**, *2*, 389.

[151] S. Muench, A. Wild, C. Friebe, B. Häupler, T. Janoschka, U. S. Schubert, *Chem. Rev.* **2016**, *116*, 9438-9484.

[152] T. B. Schon, B. T. McAllister, P.-F. Li, D. S. Seferos, *Chem. Soc. Rev.* **2016**, *45*, 6345-6404.

[153] M. Müller, S. Koser, O. Tverskoy, F. Rominger, J. Freudenberg, U. H. Bunz, *Chem. Eur. J.* **2019**, *25*, 6082-6086.

[154] M. L. Tang, J. H. Oh, A. D. Reichardt, Z. Bao, *J. Am. Chem. Soc.* **2009**, *131*, 3733-3740.

[155] G. R. Fulmer, A. J. Miller, N. H. Sherden, H. E. Gottlieb, A. Nudelman, B. M. Stoltz, J. E. Bercaw, K. I. Goldberg, *Organometallics* **2010**, *29*, 2176-2179.

[156] C. M. Cardona, W. Li, A. E. Kaifer, D. Stockdale, G. C. Bazan, *Adv. Mater.* **2011**, *23*, 2367-2371.

[157] F. Hinderer, U. H. Bunz, *Chem. Eur. J.* **2013**, *19*, 8490-8496.

[158] J. P. Cole, C. R. Federico, C.-H. Lim, G. M. Miyake, *Macromolecules* **2019**, *52*, 747-754.

[159] Q. Tang, Z. Liang, J. Liu, J. Xu, Q. Miao, *Chem. Commun.* **2010**, *46*, 2977-2979.

[160] D. Sakamaki, D. Kumano, E. Yashima, S. Seki, *Angew. Chem. Int. Ed.* **2015**, *54*, 5404-5407.

Eidesstattliche Versicherung gemäß § 8 der Promotionsordnung der Naturwissenschaftlich-Mathematischen Gesamtfakultät der Universität Heidelberg

Bei der eingereichten Dissertation zu dem Thema

"Synthesis and Characterization of Azaacenes and Stable Azaacene Radical Cations"

handelt es sich um meine eigenständig erbrachte Leistung.

Ich habe nur die angegebenen Quellen und Hilfsmittel benutzt und mich keiner unzulässigen Hilfe Dritter bedient. Insbesondere habe ich wörtlich oder sinngemäß aus anderen Werken übernommene Inhalte als solche kenntlich gemacht.

Die Arbeit oder Teile davon habe ich bislang nicht an einer Hochschule des In- oder Auslands als Bestandteil einer Prüfungs- oder Qualifikationsleistung vorgelegt.

Die Richtigkeit der vorstehenden Erklärung bestätige ich.

Die Bedeutung der eidesstaatlichen Versicherung und die strafrechtlichen Folgen einer unrichtigen oder unvollständigen eidesstattlichen Versicherung sind mir bekannt.

Ich versichere an Eides statt, dass ich nach bestem Wissen die reine Wahrheit erklärt und nichts verschwiegen

Ort und Datum

Unterschrift